



**HAL**  
open science

# Electrophysiological characterization of cerebello-hippocampal interaction in mice across behavioural states

Arturo Torres Herráez

► **To cite this version:**

Arturo Torres Herráez. Electrophysiological characterization of cerebello-hippocampal interaction in mice across behavioural states. Neuroscience. Sorbonne Université, 2019. English. NNT : 2019SORUS391 . tel-03145381

**HAL Id: tel-03145381**

**<https://theses.hal.science/tel-03145381>**

Submitted on 18 Feb 2021

**HAL** is a multi-disciplinary open access archive for the deposit and dissemination of scientific research documents, whether they are published or not. The documents may come from teaching and research institutions in France or abroad, or from public or private research centers.

L'archive ouverte pluridisciplinaire **HAL**, est destinée au dépôt et à la diffusion de documents scientifiques de niveau recherche, publiés ou non, émanant des établissements d'enseignement et de recherche français ou étrangers, des laboratoires publics ou privés.



# SORBONNE UNIVERSITÉ

Ecole Doctorale Cerveau Cognition Comportement

*Laboratoire Neurosciences Paris Seine, Equipe Cervelet Navigation et Mémoire*

## **ELECTROPHYSIOLOGICAL CHARACTERIZATION OF CEREBELLO-HIPPOCAMPAL INTERACTION IN MICE ACROSS BEHAVIOURAL STATES**

Par Arturo TORRES HERRÁEZ

Thèse de doctorat de Neurosciences  
Dirigée par Laure RONDI-REIG

Présentée et soutenue publiquement le 10 Septembre 2019,  
devant un jury composé de:

Dr Laure RONDI-REIG	Directeur de recherche, Paris	Directrice de thèse
Dr Philippe ISOPE	Directeur de recherche, Strasbourg	Rapporteur
Dr Bruno POU CET	Directeur de recherche, Marseille	Rapporteur
Pr Valérie EGO-STENGEL	Professeur, Gif-sur-Yvette	Examineur
Pr Matt W. JONES	Professor, Bristol	Examineur
Pr Marie VIDAILHET	Professeur des Universités-Praticien Hospitalier, Paris	Président de jury







## **ACKNOWLEDGEMENTS/AGRADECIMIENTOS**

There are so many things for which I am extremely grateful that this section will be as hard to condense as any other in this thesis. The last five years in Paris and the four that I have spent in this team have been one of the most enriching experiences in my life. Indeed, the person who leaves now this city to face new adventures in the Big Apple is not the same who arrived. I am stronger, more self-assured and a little bit more multilingual and many people are responsible for such changes and deserve a particular mention in here.

First I have to thank Laure Rondi Reig for the opportunity she offered me to join her lab for my PhD. She has been a dedicated and patient director. I have not always been an easy student as my organization skills are not particularly well developed, however, she has always been there to try to put the correct pace in to my sometimes wandering mind. I think thanks to that my PhD has been fruitful in both my formation and my production as researcher. The second mention is to Thomas Watson, he was the reason I joined the lab in the first place and he taught me almost everything I needed for arriving to this day with a thesis under my arm. He was not only a mentor but he became a friend, one of those friends that I know will be there forever despite of the distance. Of course, I have also to thank everyone in the CeZaMe team for the help, the support and for creating an environment which made really easy to get up everyday and go to work. This nice environment extends to the whole IBPS where I have met wonderful people and created that important network that gave me a great personal and professional input. In particular, I want to thank to everyone in the IBPS Doc and Postdoc Club, it was great to be part of it. Keep rowing mates! Apart from the IBPS, I have to thank to the ENP for the great opportunity that they gave me when they accepted me in their Graduate Program. Every single person working in there has been always friendly, helpful and supportive. It has been an honor to be part of it and I will be always grateful. Moreover, I have to thank to all my colleagues from my year, sharing the experience with you has made it even better.

I am going to switch language now as, both in Paris and in Madrid, a huge contribution to make this thesis possible came from amazing Spanish and Chilean people. Esta tesis y todo lo que soy se lo debo casi por entero a mi familia, ambas la que me vino dada y la que he elegido y por las que me siento la persona más afortunada en el mundo.

Madre, padre, no existen palabras para describir la gratitud que siento por la vida que me habéis dado, por el profundo amor que siempre he sentido de vuestra parte, por el apoyo incondicional, por el orgullo que he visto siempre en vuestra mirada y que me ha hecho sentir que podía ser lo que quisiera. El hecho de que me lanzase a hacer entrevistas en el extranjero cuando no sabía casi nada de inglés, el valor que me empujó a subirme a ese avión que me trajo a París, la fuerza para escribir esta tesis, todo es gracias a vosotros porque me habéis dado el mejor regalo que un hijo puede recibir, confianza y seguridad en mi

mismo. No solo eso, vuestra ansia de aprender y comprender aquello que desconocéis, vuestro desparpajo a la hora de enfrentar cualquiera que sea el reto, vuestra implicación y pasión por toda causa que consideréis justa de defender, todo ello ha sido una inspiración constante para mi. Os quiero muchísimo.

Rebeca, mi amor, no imaginas lo feliz que me hiciste al decidir emprender esta aventura conmigo pese a que pareciese, o mejor dicho fuese, una locura. Eres la persona más fuerte y valiente que conozco, nada te echa para atrás y la manera en la que enfrentas cada reto es inspiradora y me hace sentir tremendamente orgulloso. Tu has sido los cimientos que han permitido que construyésemos la maravillosa vida que hemos tenido en París y que me han sujetado en los momentos duros. Aunque a veces no haya sido la persona más comunicativa y parezca que me guardaba los problemas para mi quiero que sepas que el mero hecho de saber que al llegar a casa tu estarías allí, tu sola presencia, han sido siempre suficiente para liberarme de la carga y hacerme avanzar. Esta tesis es tan tuya como mía pues aunque no siempre lo hayas sabido has compartido siempre su peso. Estoy deseando seguir con nuestras aventuras, mi vida. Gracias por elegirme.

Y por supuesto otra parte de mi familia elegida, todos aquellos amigos que han estado ahí de una forma u otra en la casilla de salida, en el camino, en la meta y en el horizonte. Mariano, yo no sería quien soy si no me hubiese cruzado contigo hace tantos años ya. Fuiste una revelación y una revolución y por dejados que seamos y por mucho que haya kilómetros de por medio, siempre serás un hermano para mi. Pero es que realmente somos familia numerosa, porque Baños, Pableras, sois mis “brothers” y sin vosotros todo habría sido mucho más aburrido. Espero vivir muchas más noches de bar compartiendo copas, música, risas, mujeres y más a vuestro lado. Por otra parte, a la neurociencia llegué gracias a la maravillosa gente que me enseñó tanto (en el laboratorio y la cafetería) en mi paso por el departamento de Fisiología Animal de la Universidad Autónoma de Madrid y por ello les estoy muy agradecido. Igualmente, a todos los Neurosexys del Master que terminaron de demostrarme que había elegido bien mi camino, los congresos siempre van a ser mejores con vosotros. Finalmente, París no habría sido París sin los amigos que me han arropado aquí. Mil gracias a los “Jinto y Farlopa” y todos los que llegaron después. Y en especial a Inés, una “hija” inesperada con la que he compartido tanto cervezas como cerebelos, nunca una mudanza dio tanto de sí. Y para terminar, mi otro “hijo” hallado en París pero de proveniencia lejana, Sebastian. Tu amistad y la de Estefani son de las mejores cosas que me llevo de estos años y sé de verdad que son de las que se proyectan también hacia el horizonte. Ya sois para siempre nuestros amigos chilenos y vais a ser insustituibles.

## **RÉSUMÉ**

L'implication du cervelet dans la cognition et navigation spatiale a été récemment remarqué par l'équipe de Rondi Reig chez l'homme et dans modèles murines. Également, ces études suggèrent fortement que le cervelet interagit avec l'hippocampe dans un réseau fonctionnel. Cependant, à ce jour il nous manque d'informations relatives sur le substrat anatomique et les mécanismes physiologiques qui permettent cette interaction. Cette information est fondamentale pour comprendre le rôle du cervelet dans ces fonctions et il a constitué le sujet de ma thèse.

À cette fin, nous avons employé une combinaison de techniques comprenant le traçage anatomique trans-synaptique rétrograde avec le virus de la rage et des enregistrements électrophysiologiques extracellulaires simultanées dans le cervelet et l'hippocampe chez la souris engagé dans plusieurs comportements. Nous avons identifié trois régions dans le cortex cérébelleux qui projet à l'hippocampe par routes di- et tri-synaptiques: Crus I, lobule VI et le paraflocculus. De plus, nous avons trouvé une synchronisation dynamique entre l'activité oscillatoire enregistrée dans ces zones et celle de l'hippocampe dans la bande thêta, un mécanisme qui était auparavant associé à une interaction fonctionnelle. Plus précisément, nous avons constaté une augmentation significative de la cohérence Crus I-hippocampe pendant la consécution d'un comportement dirigé vers un but. Enfin, nous avons caractérisé la modulation de l'activité cérébelleuse et de la cohérence cérébello-hippocampique au cours du sommeil et avons trouvé une augmentation de la cohérence Crus I-hippocampe pendant le sommeil paradoxal en phase avec un rythme cérébelleux ultra-lent (<1Hz).

## **MOTS-CLÉS**

Cervelet

Hippocampe

Traçage anatomique trans-synaptique rétrograde

Électrophysiologie

Cohérence cérébello-hippocampique

Comportement dirigé vers un but

## **ABSTRACT**

The implication of the cerebellum in spatial cognition and spatial navigation has been recently highlighted both in humans and mice models by the team of Laure Rondi Reig. Similarly, these studies strongly suggested that the cerebellum interacts with the hippocampus in a functional network. However, to the date we lack information about the anatomical substrate for such interaction as well as the physiological mechanisms underlying it. This information is fundamental in order to fully understand the role of the cerebellum in these functions and it has been the main focus of my thesis.

To that aim, we have employed a combination of technical approaches including anatomical retrograde trans-synaptic tracing with rabies virus and multi-site extracellular electrophysiological recordings in the cerebellum and the hippocampus of behaving mice. We have identified three main cerebellar cortical areas projecting through di- and/or tri-synaptic pathways to the hippocampus: the Crus I, the lobule VI and the paraflocculus. Moreover, we have found dynamic theta coherence between the oscillatory activity recorded in these areas and that from the hippocampus, a mechanism that has been previously associated with functional interaction. Specifically, we have found a significant increase in the theta coherence between the Crus I and the hippocampus when the animals performed a goal directed behaviour. Finally, we have characterised the modulation of the cerebellar activity and the cerebello-hippocampal coherence across the sleep cycle and we have found increased Crus I-hippocampus theta coherence during REM sleep which is in phase with a cerebellar infra-slow (< 1Hz) rhythm.

## **KEYWORDS**

Cerebellum

Hippocampus

Anatomical retrograde trans-synaptic tracing

Electrophysiology

Cerebello-hippocampal coherence

Goal-directed behaviour

<b>INTRODUCTION</b> .....	13
<b>CHAPTER 1: The “Little Brain”: Basic organization, physiology and function</b> .....	17
<b>1.1 ANATOMO-FUNCTIONAL ORGANIZATION OF THE CEREBELLUM</b> .....	19
1.1.1 MAPS OF THE CEREBELLUM .....	19
1.1.1.1 Transversal organization .....	19
1.1.1.2 Longitudinal organization: zones and microzones .....	21
1.1.1.3 Zebrin II as another indicator of longitudinal band organization .....	22
1.1.2 FUNDAMENTAL CEREBELLAR CIRCUIT ARCHITECTURE .....	22
1.1.2.1 General organization .....	22
1.1.2.2 Purkinje cells: the core of the circuit .....	24
1.1.2.3 Granule cell layer: The input stage .....	26
<b>1.2 CEREBELLAR INFORMATION PROCESSING</b> .....	28
1.2.1 ORIGIN AND ORGANIZATION OF THE CEREBELLAR INPUTS .....	28
1.2.2 PHYSIOLOGICAL RELEVANCE OF THE ANATOMICAL MAPS .....	31
1.2.3 DEEP CEREBELLAR NUCLEI AND CEREBELLAR LOOPS .....	33
1.2.4 THE TARGETS OF THE CEREBELLUM .....	35
<b>1.3 INTEGRATION OF THE ELEMENTS IN TO THE CIRCUIT</b> .....	36
1.3.1 THE BEAM HYPOTHESIS .....	36
1.3.2 REVISITING THE MODELS FROM A PHYSIOLOGICAL PERSPECTIVE: PATCHES VERSUS BEAM .....	37
1.3.3 THE MARR-ALBUS-ITO THEORY .....	38
1.3.4 CONNECTING THE PATCHES .....	39
<b>1.4 INTEGRATION OF ACTIVITY PATTERNS AND SYNAPTIC PLASTICITIES IN TO THE     CEREBELLAR MODELS</b> .....	40
1.4.1 SPATIOTEMPORAL FIRING PATTERNS .....	40
1.4.2 READ-OUT OF THE CORTICAL ACTIVITY PATTERNS BY THE DEEP CEREBELLAR NUCLEI .....	42
1.4.3 OSCILLATIONS IN THE OLIVOCEREBELLAR SYSTEM .....	43
1.4.4 MULTIPLE PLASTICITY SITES IN THE CEREBELLAR CIRCUIT .....	46

CHAPTER 2: Cerebro-cerebellar loops: Beyond motor control .....	47
2.1. <b>ANATOMICAL SUBSTRATES FOR CEREBRO-CEREBELLAR LOOPS</b> .....	50
2.1.1.    PROJECTIONS FROM THE CEREBRUM TO THE CEREBELLUM .....	50
2.1.2.    PROJECTIONS FROM THE CEREBELLUM TO THE CEREBRUM .....	52
2.1.3.    CLOSED-LOOPS IN THE CEREBRO-CEREBELLAR PATHWAYS .....	54
2.2. <b>PHYSIOLOGICAL EVIDENCE FOR CEREBELLAR ENGAGEMENT IN NON-MOTOR             FUNCTIONS</b> .....	56
2.2.1.    FUNCTIONAL RELEVANCE OF THE ANATOMICAL PATHWAYS .....	56
2.2.2.    THE CEREBELLAR COGNITIVE AFFECTIVE SYNDROME IN HUMANS .....	59
2.2.3.    THE CEREBELLUM AS A GENERAL PREDICTOR FOR PSYCHIATRIC DISEASES .....	60
2.2.4.    THE ROLE OF THE CEREBELLUM IN SLEEP REGULATION AND SLEEP DISORDERS ....	61
CHAPTER 3: Evidence of cerebello-hippocampal interaction .....	63
3.1. <b>THE HIPPOCAMPUS AND SPATIAL COGNITION</b> .....	65
3.1.1.    FUNDAMENTAL ANATOMY OF THE HIPPOCAMPAL FORMATION .....	66
3.1.1.1    Fundamental hippocampal circuit .....	66
3.1.1.2    Topographical organization of the hippocampal formation .....	68
3.1.2.    SPATIAL ENCODING CELLS IN THE HIPPOCAMPAL FORMATION .....	70
3.1.3.    INFORMATION NEEDED TO CONSTRUCT SPATIAL COGNITIVE MAPS .....	73
3.2. <b>EVIDENCE OF CEREBELLO-HIPPOCAMPAL INTERACTION</b> .....	74
3.2.1    ANATOMICAL AND PHYSIOLOGICAL STUDIES SUPPORTING CEREBELLAR PROJECTIONS TO THE HIPPOCAMPUS .....	74
3.2.2    EARLY ANATOMICAL AND PHYSIOLOGICAL STUDIES SUPPORTING HIPPOCAMPAL PROJECTIONS TO THE CEREBELLUM .....	75
3.2.3    EVIDENCE FOR A CEREBELLAR ROLE IN SPATIAL NAVIGATION .....	76
<b>SCIENTIFIC QUESTION AND INTRODUCTION TO THE RESULTS</b> .....	79
<b>RESULTS</b> .....	81

CHAPTER 1: Anatomical and electrophysiological foundations of cerebello-hippocampal interaction.....	83
CHAPTER 2: Modulation of cerebellar oscillations and cerebello-hippocampal interaction across sleep states .....	141
<b>DISCUSSION</b> .....	165
1. TOPOGRAPHICAL ORGANIZATION OF CEREBELLAR PROJECTIONS TO THE HIPPOCAMPUS ....	167
2. MECHANISMS FOR CEREBELLO-HIPPOCAMPAL INTERACTION .....	172
3. CONCLUSIONS AND FUTURE PERSPECTIVES .....	176
<b>REFERENCES</b> .....	179
<b>APPENDIX</b> .....	211
1. INDEX OF FIGURES .....	213
2. RÉSUMÉ ÉTENDU EN FRANÇAIS .....	217



# **INTRODUCTION**



The cerebellum has been a main focus of study for neuroscientists for more than a century. It is noteworthy to mention that the father of modern neuroscience, Santiago Ramón y Cajal, chose the avian cerebellum as the subject of study for his first set of papers. Indeed, out of these pioneering works published between 1888 and 1890, the basis of our present knowledge on the anatomical organization of the cerebellum as well as some insights on its development and function were already established (see Sotelo, 2008 for a review about first Cajal's works). It was precisely the exquisite and highly repetitive organization of cerebellar circuitry that attracted Ramon y Cajal, whose drawings, with detailed cell morphologies accompanied by arrows suggesting the directionality of information flow, are still surprisingly up to date (**Figure 1**).

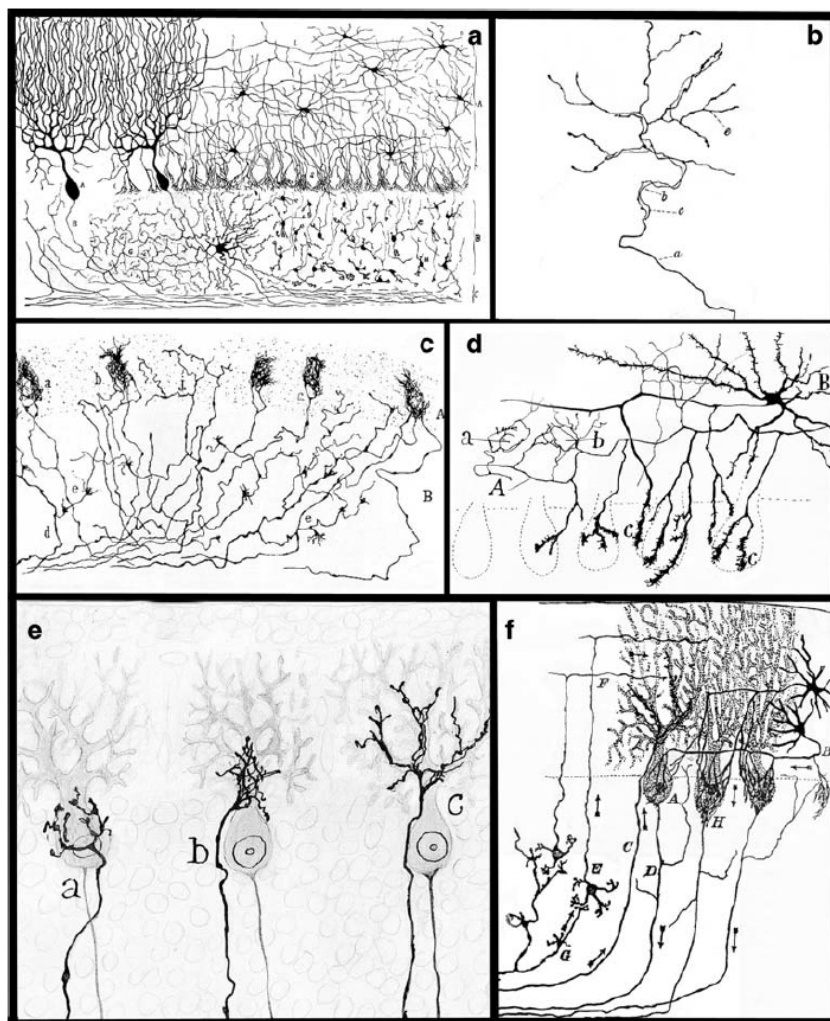


**Figure 1. Cajal's illustrations of his studies to unravel the circuitry of the cerebellum. a)** First drawing published in 1888 illustrating the three-layered cortex of the cerebellum and their containing neuronal types. **b)** Illustration of a climbing fibre under the name of "vertical fibres" published in 1889. **c)** Drawing of several ascending fibres emerging from white matter. **d)** Illustration of a basket cell. **e)** Schematic representation of the maturation of climbing fibre-Purkinje cell synapses. **f)** Figure showing the connections of the Purkinje cells and the direction of nerve impulses within the cerebellar circuit. (From Sotelo, 2008)

However, interest in the cerebellum started far before, in the early nineteenth century, and for a completely different reason: its functional link to motor control. The first lesion studies on cerebellar function were carried out by animal experimentalists like Flourens (1824) and Luciani (1891) and gave rise to the general conclusion that the cerebellum is implicated in the coordination and fine control of voluntary movements. Such conclusion was further extended and characterized by clinical studies on humans showing cerebellar deficits or lesions which associated these pathologies with three main symptoms: atonia, or lack of muscular tension; asthenia, or weakness in movements; and astasia, or inability to maintain continuity in a sequence of movements producing tremor or hesitation due to the imperfect fusion of muscular contractions (Holmes, 1917). These studies were highly influential and biased the cerebellar field towards the search for the physiological substrate for motor control.

Of course, major discoveries regarding cerebellar organization and function have been achieved during the last 120 years. New powerful technical approaches and improvements, such as electrophysiology, neuroanatomical tracing, immunohistochemistry, optogenetics and functional imaging have allowed contemporary neuroscientists to revisit some old hypotheses and dogmas, such as the homogeneity of the cerebellar circuit or its purely motor function, changing our perception about the cerebellum and largely increasing our knowledge about it. It is now clear, for instance, that the cerebellum is highly reciprocally interconnected with high associative areas of the brain like the prefrontal cortex (Kelly and Stick, 2003) and, in humans, it is involved in a plethora of non-motor functions such as language, affective processing, executive functions, working memory or spatial navigation (Ramnani, 2006; Schmahmann et al., 2009, 2010; Igloi et al., 2015).

During my PhD I have focussed my work on trying to better understand how the cerebellum integrates in a functional network with the hippocampus, a region heavily involved in spatial cognition and memory (Eichenbaum, 2000; Mosser et al., 2017). Along this introduction I will start describing the fundamental organization and physiology of the cerebellum, then I am going to focus on its role beyond motor control through its interaction with the cerebral cortex and, finally, I am going to specifically detail the current evidences supporting its interaction with the hippocampus.

**CHAPTER 1:**

**The “Little Brain”: Basic organization, physiology and function**



Cerebellum literally means “little brain” in Latin. This name probably derives from comparisons with the cerebrum (the “great brain”) in avian or mammalian brains, where the cerebellum clearly resembles the former in shape (it is also highly folded) but has a smaller size. This structure is part of the hindbrain and can be found in all vertebrates (except maybe in lampreys in which its presence is still under debate). Although much variability in shape and size relative to the rest of the brain is observed between monophyletic groups and even between species inside them, the fundamental architecture and organization of the cerebellum is evolutionary preserved (Butler and Hodos, 2005).

In this chapter I will briefly describe the cerebellar structure, connectivity and function under the prism of the most recent discoveries and theories, punctually emphasizing the contrast and controversies with more classical views.

### **1.1 ANATOMO-FUNCTIONAL ORGANIZATION OF THE CEREBELLUM:**

The cerebellum is composed of the cerebellar cortex and three pairs of deep cerebellar nuclei (bilaterally represented on both sides of the midline and embedded in the white matter; see **Figure 2A**) which, together with some vestibular nuclei, are the only output towards ascending and descending pathways. However, given its close anatomical and functional relationship, the inferior olivary complex, a group of nuclei in the medulla oblongata, which are the source of one of the main inputs to the cerebellum, is often considered in conjunction with the cerebellum as the olivocerebellar system (see Llinás, 2013).

#### **1.1.1 MAPS OF THE CEREBELLUM:**

The description and division of the cerebellar architecture has been a complicated issue in the field due to the different terminologies, the different criteria employed and a reductionist approach from each specific sub-field. However, substantial efforts has been made recently in order to integrate and conciliate all the information in to a general and more holistic view (for instance, see the review by Apps and Hawkes, 2009).

##### **1.1.1.1 Transversal organization**

The pronounced folding of the cerebellar cortex in the transversal axis gives clear anatomical landmarks to firstly subdivide it grossly in to three lobes based on their relative position in respect to the primary and posterolateral fissures: the anterior, posterior and flocculo-nodular lobes; and secondly in ten lobules (Larsell, 1970) (**Figure 2B**). The pattern of lobulation is under strong genetic control and is highly conserved across species (Larsell, 1970). However, their identity as potential functional units is not clear. While many studies of functional imaging in humans found restricted activation of specific lobules during different task (see Stoodley and Schmahmann, 2009), suggesting that they represent functional units, electrophysiological studies carried out in other species seemed to indicate that the anatomically delimited lobules are not

functional demarcations (see Apps and Hawkes, 2009). In fact, transversal regionalization is better established when studying the molecular expression patterns across development which allows identification of four main zones in mice that, indeed, don't correspond to specific lobules (Ozol et al., 1999): the anterior zone (AZ) corresponds to lobules I-V, the central zone (CZ) includes lobules VI and VII, the posterior zone (PZ) groups lobules VIII and IX, and the nodular zone (NZ) comprises lobule X (**Figure 2C**)

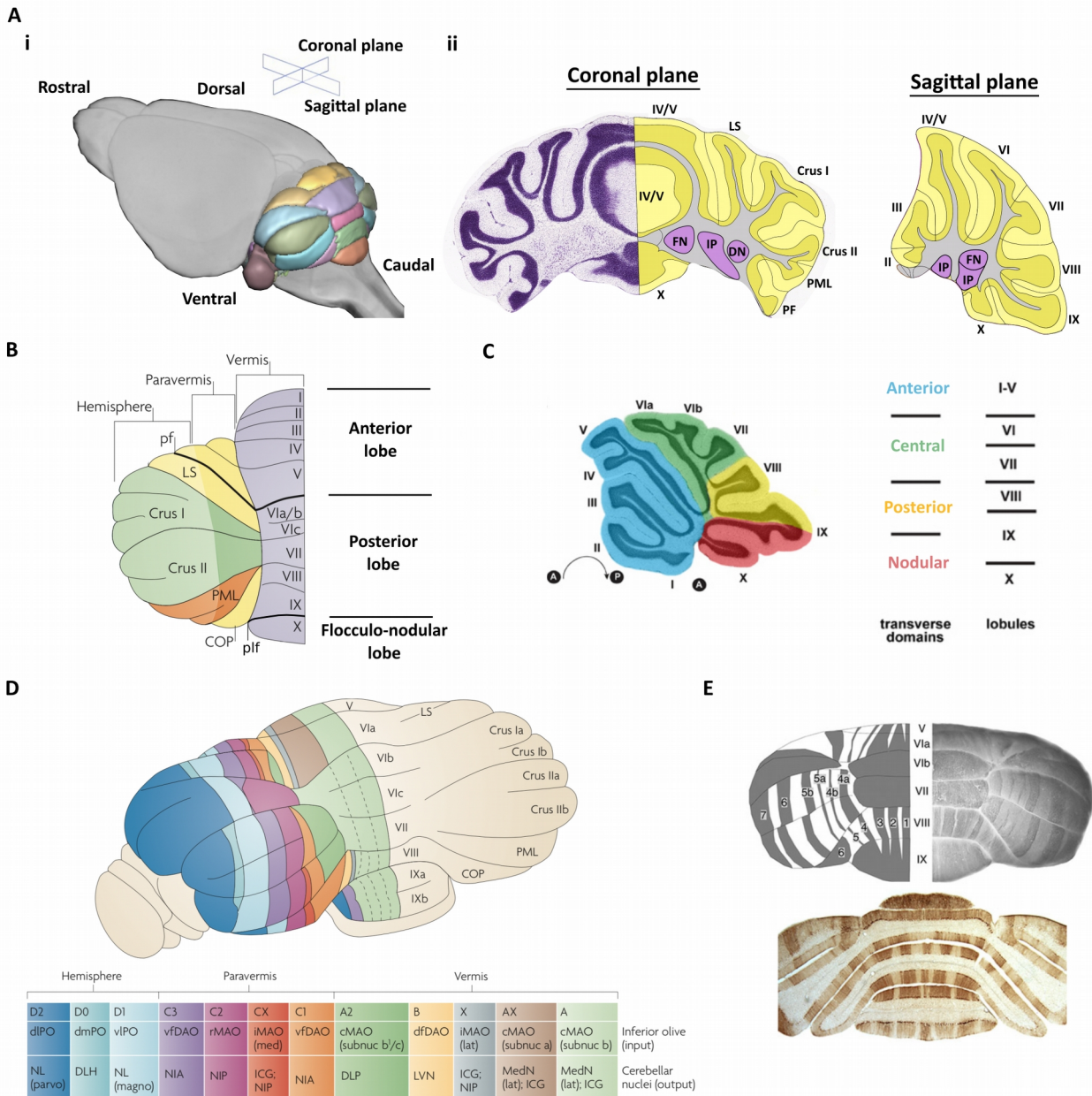


**Figure 2. Fundamental organization of the cerebellum.** **A, i)** Three dimensional reconstruction of the central nervous system of the mouse with the cerebellum coloured (Adapted from the Australian Mouse Brain Mapping Consortium). **ii)** Examples of a coronal and sagittal sections of the cerebellum. The cerebellar cortex appears in yellow (light for the molecular layer and dark for the granule cell layer), the white matter in grey and the deep cerebellar nuclei in purple. (Adapted from the Allen Mouse Brain Reference Atlas). **B)** Schematic representation of the unfolded cerebellum of the mouse showing the different lobes, lobules and longitudinal zones (Adapted from Apps and Hawkes, 2009). **C)** Sagittal section of the cerebellum divided by the main transverse

domains (Adapted from Reeber et al., 2013). **D**) Schematic representation of the modular organization of the cerebellum in the rat (top) and the specific inferior olivary inputs/cerebellar nuclei output pattern which defines them (bottom) (From Apps and Hawkes, 2009). **E**) Schematic (left) and whole mount (right) dorsal view of the Zebrin II staining banding pattern (top). The bands are also visible in a coronal section of the cerebellum (bottom) (From Hawkes, 2014). cMAO, caudal medial accessory olive; COP, copula pyramidis; dfDAO, dorsal fold of dorsal accessory olive; DLH, dorsolateral hump; DLP, dorsolateral protuberance of medial nucleus; dlPO, dorsal lamella of the principal olive; dmPO, dorsomedial subnucleus of the principal olive; DN, dentate nucleus (same as NL, lateral nucleus); FN, fastigial nucleus (same as MedN, medial nucleus); ICG, interstitial cell group; iMAO, intermediate medial accessory olive; IP, nucleus interpositus; LVN, lateral vestibular nucleus; LS, lobule Simplex; NIA, nucleus interpositus anterior; NIP, nucleus interpositus posterior; PML, paramedian lobule; PF, paraflocculus; rMAO, rostral medial accessory olive; vfDAO, ventral fold of dorsal accessory olive; vlPO, ventral lamella of the principal olive.

### 1.1.1.2 Longitudinal organization: zones and microzones

These transversal zones may relate to some functionally relevant organization but, such a correspondence is still poorly understood. Indeed, anatomical, physiological and behavioural studies support a longitudinal rather than transversal organization of the cerebellar cortex. A primary division, taking into account the outputs through specific deep cerebellar nuclei, differentiates three longitudinal regions running in the rostro-caudal axis (Jansen and Brodal, 1940) (**Figure 2B**): the vermis (or medial cerebellum), which projects to the fastigial nucleus located in a medial position; the paravermis (or pars intermedia), which routes through the nucleus interpositus; and the hemispheres (or lateral cerebellum), which projects to the lateral-most dentate nucleus. These longitudinal regions can be further subdivided when we include the patterning of olivary nuclei inputs. As mentioned above, the inferior olivary complex sends one of the main two inputs to the cerebellum, the climbing fibres, and the topographical organization of these inputs also follows a longitudinal pattern. Thus, specific olivary nuclei or even a specific sub-region of a nucleus project to particular parasagittal bands in the contralateral cerebellar cortex (Voogd and Bigare, 1980), which in turn projects to specific parts of the deep cerebellar nuclei. Moreover, later studies have shown that collaterals from the climbing fibres also contact the same deep cerebellar nucleus (Voogd and Bigaré, 1980) and those nuclear cells project back to the same region of the inferior olive (Chan-Palay, 1973). These anatomical complexes led to the division of the olivocerebellar circuits in different modules (**Figure 2D**) that have been found to be highly conserved across species and to serve as a useful framework in studying functional compartments (Cerminara and Apps, 2010; Ruigrok, 2010). Further subdivision of these anatomically defined modules into narrower functional units or “microzones” (Oscarsson, 1979) has been made through electrophysiological mapping of inferior olive receptive fields and have been proposed as the actual functional unit of the cerebellar cortex (Apps and Garwicz, 2005).

### 1.1.1.3 Zebrin II as another indicator of longitudinal band organization

Another important discovery regarding the longitudinal arrangement of the cerebellar cortex came from the finding of different molecular expression banding patterns (Scott, 1963), particularly the aldolase C or Zebrin II bands (Brochu et al, 1990), which during embryonic development may correlate with the birth of Purkinje cells subpopulations (Hashimoto and Mikoshiba, 2003). Purkinje cells stripes expressing Zebrin II alternate with stripes of non-expressing cells producing a highly stereotyped pattern that has been found to be tightly related to topographic olivocerebellar projection patterns and thus has been widely used as a reference map to identify the modules in rodents (Sugihara and Shinoda, 2004; Sugihara and Nguyen Quy, 2007) (**Figure 2E**). Moreover, the Zebrin II stripes could relate to a functional compartmentalization of the cerebellar cortex given that specific olivary sub-nuclei receive inputs from different sources in the brain and spinal cord further transmitting these signals to specific populations of Purkinje cells and associated output nuclei within a single compartment.

In summary, despite a lack of consensus in the field regarding the cerebellar anatomical and functional organization, a two-dimensional coordinate system of transversal and longitudinal zones of olivo-cortico-nuclear microcircuits seems to be preserved across evolution and may reflect the identity of such microcircuit as cerebellar functional units. However, in order to understand how the information is integrated and processed in these microcircuits, we need to zoom in and look at its cellular composition and connectivity.

### 1.1.2 FUNDAMENTAL CEREBELLAR CIRCUIT ARCHITECTURE:

The cerebellar cortex has been largely considered a homogeneous structure that runs all along the cerebellar convolutions and is composed of highly repetitive blocks or microcircuits containing similar cell types and fibres. While this is partially true, local differences in terms of specific cell type densities, cell type morphologies, molecular expression patterns and, ultimately, physiological properties, can be found along the cerebellar cortex (for a review, see Cerminara et al., 2015). For instance, one of the clearer examples are the observed differences in electrophysiological properties between Purkinje cells expressing or not the previously mentioned Zebrin II molecule across a variety of modules and lobules (Xiao et al., 2014; Zhou et al, 2014), which may further reflect the subjacent differences in function accounted by them. These regional differences are not going to be treated in detail here, however, they need to be taken into account when trying to understand or predict functional heterogeneity on the cerebellar circuits.

#### 1.1.2.1 General organization

The sole output of the cerebellar cortex towards the deep cerebellar nuclei, and in consequence the central core of cerebellar cortical information processing, is provided by Purkinje cells. They are GABAergic neurons organized in an ordered monolayer; all their cell bodies constitute the Purkinje cell layer and divide the

cerebellar cortex in two other layers. At this level we can also find the cell bodies of the candelabrum cells, local interneurons recently identified, and most likely inhibitory, whose properties and functions in the circuit remain unclear (for a general review on cerebellar cortex interneurons see Schilling et al., 2008). Purkinje cells extend their dendritic arbour in to the outer layer, the molecular layer, where they receive inputs from two main excitatory fibres, the parallel fibres and the climbing fibres. In this layer we can also find the molecular layer interneurons, the basket and stellate cells, which provide local inhibition and have important and complementary roles in shaping Purkinje cell activity and general circuit function (Brown et al., 2019). The parallel fibres are the axons sent by the granule cells, small, densely packed and highly numbered neurons that give name to the innermost layer, the granular layer. It receives one of the two main afferent inputs to the cerebellum, the mossy fibres. It also contains different interneurons both inhibitory, Golgi cells and Lugaro cells; and excitatory, the unipolar brush cells. In particular, Golgi cells form synaptic complexes with the mossy fibres terminals and the granule cell dendrites named cerebellar glomeruli which are fundamental for the granular layer circuit organization and activity (see D'Angelo et al., 2013 for a review on Golgi cell physiology) (**Figure 3**).

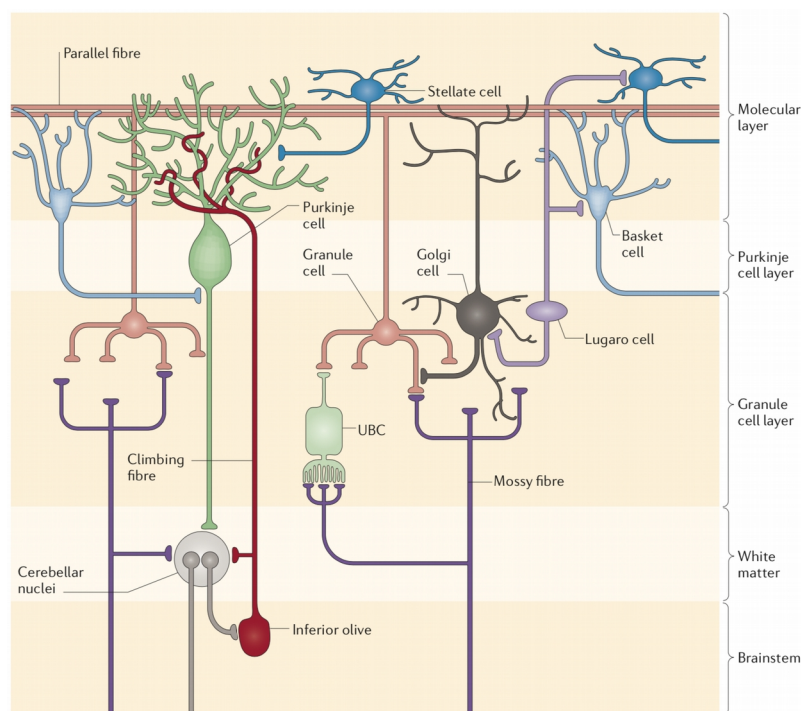


**Figure 3. Fundamental architecture of the cerebellar circuit.** The cerebellar cortex comprises the molecular layer, the Purkinje cell layer and the Granule cell layer. The deep cerebellar nuclei are embedded in the white matter of the cerebellum. The Purkinje cells are the only output from the cerebellar cortex. They receive two main excitatory inputs, the climbing fibres, generated in the inferior olive and directly synapsing onto them, and the mossy fibres, arriving from many different sources and indirectly influencing the Purkinje cells after relay in the granule cells. The granule cells send their ascending axons in to the molecular layer where they bifurcate and form the parallel fibres. Multiple local interneurons are found in the different layers: stellate and basket cells in the molecular layer, and Golgi cells, Lugaro cells and unipolar brush cells (UBCs) in the granule cell layer. Both the climbing and mossy fibres also contact directly the deep cerebellar nuclei and different local interneurons. (From Cerminara et al., 2015).

### 1.1.2.2 Purkinje cells: the core of the circuit

Purkinje cells are highly unusual in the central nervous system, both because of their morphology and physiology. Regarding morphology, they are among the biggest neurons in the brain and they present a profuse and intricate spiny dendritic arbour, which is oriented perpendicularly to the transverse bundle of parallel fibres in the rostro-caudal axis as an almost two-dimensional fan-like planar structure (**Figure 4A**). Regarding its physiology, they generate two different types of action potentials: the simple spikes, fired at a high frequency rate (around 40 Hz in average but exceeding 100 Hz in some cases) and driven by mossy fibre-granule cell-parallel fibre inputs (Eccles et al., 1967, Llinás and Sugimori, 1980) and/or by their spontaneous firing (Häusser and Clark, 1997); and the complex spikes, driven by the climbing fibre input and characterized by a high-frequency burst occurring at a short frequency rate (1-12 Hz; Eccles et al., 1967).

The specific firing pattern of a single Purkinje cell is the result of the integration of thousands of inputs. Up to 175.000 *en passant* synapses from more than 100.000 parallel fibres are distributed in the distal dendrites of a single Purkinje cell of the adult rat cerebellum (Napper and Harvey, 1988) (**Figure 4B**). However, electrophysiological studies *in vitro* and *in vivo* have suggested that approximately 80 % of these synapses are very weak and do not generate detectable electrical responses (Ekerot and Jörntell, 2001; Isope and Barbour, 2002). They also receive the input of a single climbing fibre from the inferior olive which, in turn, establishes around 1000 synapses in the proximal dendrites constituting an exceptionally strong synaptic connexion characterized by a highly reliable transmission of both single action potentials and high frequency bursts (Simpson et al., 1996; Maruta et al., 2007).

The activity driven by these two inputs, together with its intrinsic properties, is further modulated by the action of the molecular layer interneurons, which outnumber the Purkinje cells by 10:1 and establish nearly 1500 synapses in to each of them (Korbo et al., 1993). This ratio has been further supported by *in vitro* experiments in which each Purkinje cell received inputs from 9 interneurons on average (Häusser et al., 2004). The upper and middle dendritic arbour is contacted by relatively short axons from the stellate cells (Palay and Chan-Palay, 1974) oriented parallel to the Purkinje cells main axis in the parasagittal axis. The proximal dendrites, soma and axon initial segment are wrapped by long-range terminals from about 50 basket cells from the same parasagittal plane (Szentágothai, 1965) in a structure named the pinceau (Ramón y Cajal, 1911) (**Figure 4B-D**). This structure is able to mediate near-instantaneous feed-forward and lateral inhibition by directly controlling the extracellular voltage at the spike initiation site in a mechanism known as ephaptic inhibition (Korn and Axelrad, 1980; Blot and Barbour, 2014).

Finally, Purkinje cells send their axonal projections to the output nuclei of the cerebellum, that is, the deep cerebellar and certain vestibular nuclei. As mentioned previously, Purkinje cells from a particular longitudinal zone project specifically to a restricted subregion of these nuclei where they contact both

excitatory and inhibitory populations (Teune et al., 1998). The former constitutes the output to multiple ascending and descending tracks while the later seems to project back to the inferior olive (Teune et al., 2000). Purkinje cells axons also emit recurrent collaterals which extent mainly parasagittally, up to 200  $\mu\text{m}$  (Braitenberg and Atwood, 1958), but also through shorter (around 100  $\mu\text{m}$ ) mediolateral projections (Hawkes and Leclerc, 1989; Sugihara et al., 2009). Such collaterals modulate the activity of other Purkinje cells through direct synapses or through indirect local interneurons inhibition (Orduz and Llano, 2007; Witter et al., 2016).

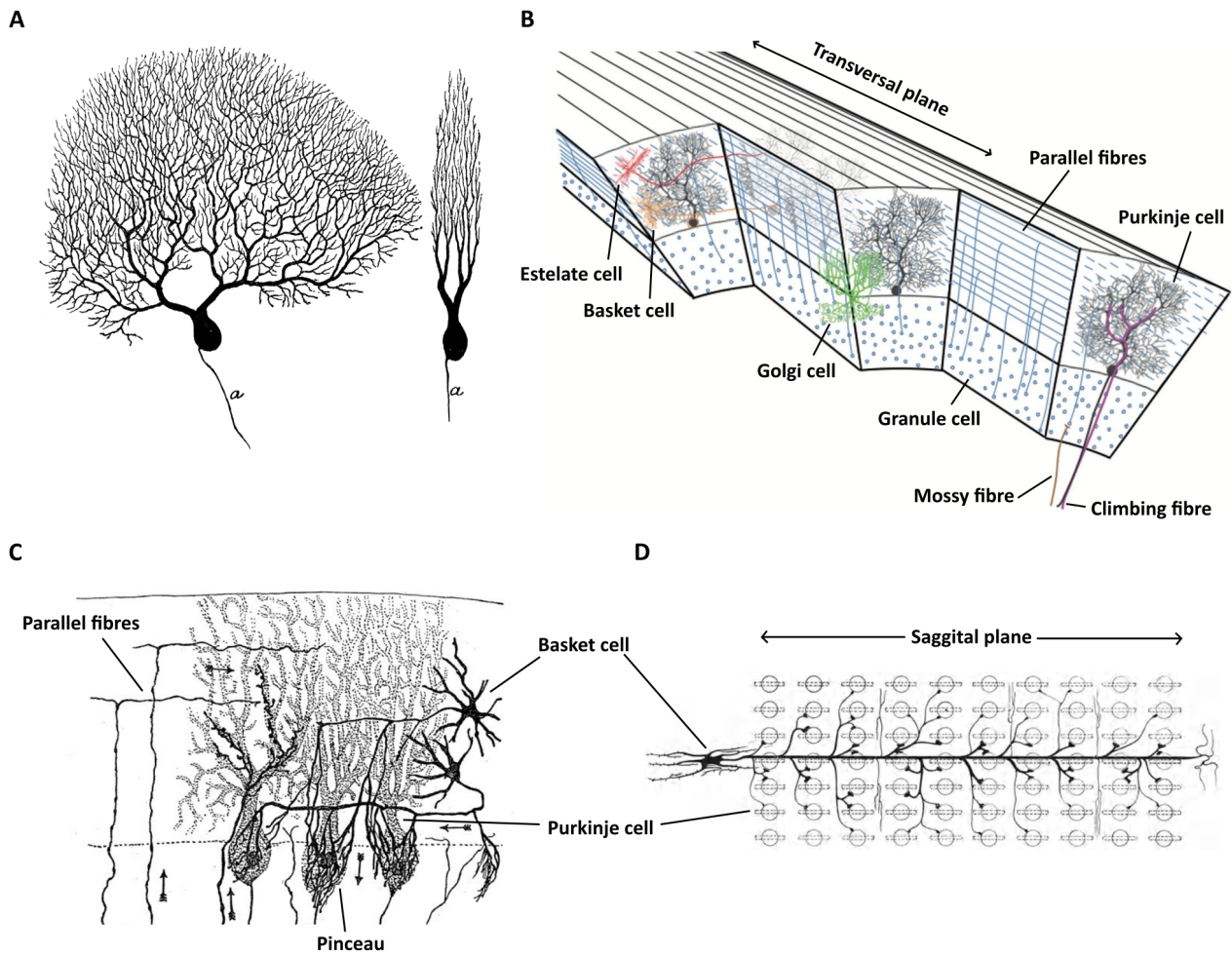


**Figure 4. Purkinje cell morphology and connectivity.** **A)** Drawing of a Purkinje cell in a sagittal plane (left) and a transversal plane (right) showing the characteristic fan-like planar structure (From Piersol, 1908). **B)** A parasagittal cut of the cerebellar cortex revealing the topographical arrangement and connectivity of the different cell types. The parallel fibres run perpendicular to the main axis of the Purkinje cells which receive inputs from thousands of them. A single climbing fibre is wrapped around the proximal dendrites of a Purkinje cell. The molecular layer interneurons also distribute their inputs to the Purkinje cells following the parasagittal plane (adapted from Rokni et al., 2008). **C)** Drawing showing the contacts established by many basket cells around the cell body and the axon initial segment of each Purkinje cell forming the structure known as the pinceau (adapted from Ramón y Cajal, 1894). **D)** Schematic showing the field of action of a single basket cell. They send collaterals in the parasagittal plane and contact up to several dozens of Purkinje cells in a parasagittal beam (adapted from Szentágothai, 1965).

### 1.1.2.3 Granule cell layer: The input stage

Despite of the central role of the Purkinje cells in cerebellar cortical circuitry, the principal cells of the granule cell layer, the granule cells, as well as their main inhibitory input, the Golgi cells, deserve similar attention. As mentioned above, granule cells are the most numerous neurons in the central nervous system accounting for more than the 50 % of the total (Herculano-Houzel, 2010) and outnumbering the Purkinje cells by more than 400:1 in rats (Korbo et al., 1993). They integrate and transfer the information of one of the main input systems of the cerebellum, the mossy fibres, and thus are considered as the input stage (**Figure 5A**). Granule cells are glutamatergic, small, extremely densely packed and with a characteristic dendritic arbour composed of only 2-7 short dendrites, each of them finishing in a claw-shape (Palay and Chan-Palay, 1974) integrated in a cerebellar glomerulus (so named because of its similarity in structure to the glomeruli of the olfactory bulb; Held, 1867) (**Figure 5B**). The cerebellar glomeruli are complex synaptic arrangements where two pre-synaptic elements, one excitatory, a single mossy fibre, and one inhibitory, the axon terminals from Golgi cells, contact dendritic terminals from many granule cells (up to 53 in rats; Jakab and Hámori, 1998) and Golgi cells (**Figure 5C**). Moreover, the glomerular compartment, which is wrapped in a glial sheet, may acts as a diffusion barrier that helps to create a microenvironment in which neurotransmitter spillover helps to tightly control tonic inhibition from Golgi cells and cross-talk between them and mossy fibres what, in turns, orchestrates a complex control of input/output relationship in the granule cells (DiGregorio et al., 2002; D'Angelo et al, 2013). Thus, the glomerulus can be seen as the minimal computational unit in the granule cell layer as all the granule cell dendrites integrated on it will be modulated by the same elements in a highly controlled microenvironment.

Regarding granule cell axons, they ascend vertically through the granule cell and Purkinje cell layers and then bifurcate in the molecular layer in a characteristic T-shape forming the parallel fibres. Parallel fibres run in the transversal plane and typically extend over long distances establishing synapses with hundreds of Purkinje cells (**Figure 5A**). For instance, numerical calculations in rat estimated that a single parallel fibre establishes up to 675 synapses onto half of the Purkinje cells they pass through (Napper and Harvey, 1988; Harvey and Napper, 1991), along a mean distance of 4.4 mm (Pichitpornchai et al, 1994). Normally, only one or two synapses per Purkinje cell are observed and about half of these contacts are done in Purkinje cells nearby the bifurcation point. The other half is spread in a decreasing gradient towards the distal ends of the parallel fibre (Pichitpornchai et al, 1994). Moreover, in their ascending branch prior to bifurcating, granule cell axons form around 30 en passant synapses onto the dendritic arbours of the few Purkinje cells that they traverse (Gundappa-Sulur et al., 1999). Finally, granule cells also contact molecular layer interneurons and Golgi cells both by the ascending branches of the axon (Hámori, 1981; Sultan and Bower, 1998; Cesana et al., 2013) and via the parallel fibres (Palay and Chan-Palay, 1974).

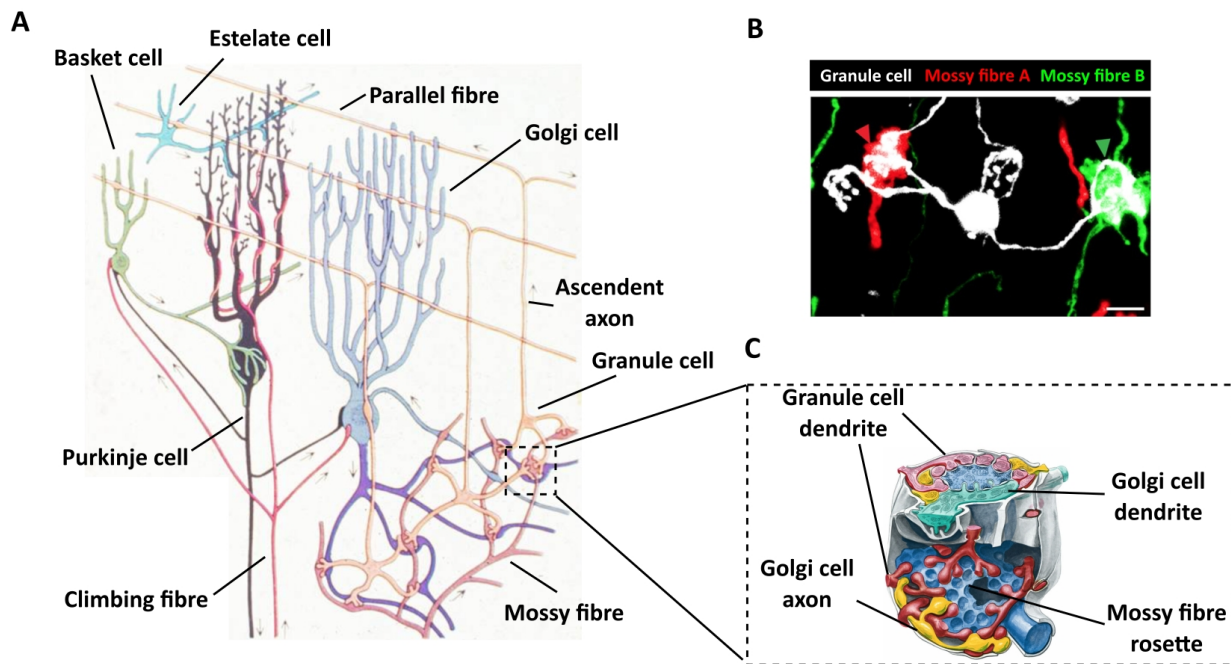


**Figure 5. Granule cell morphology and connectivity.** **A)** Schematic representation of the cerebellar cortex showing the dense distribution of granule cells, their morphology and their close interaction with the Golgi cells and the mossy fibres in the glomeruli (region in the dashed square). Notice the characteristic axonal projections of the granule cells with an ascending branch which bifurcates in the molecular layer and forms the parallel fibres. The ascending axon form synapses with the Purkinje cells (not shown in the schema) and the Golci cells. The parallel fibres synapse onto Golgi cells, Purkinje cells and molecular layer interneurons. The Golgi cell morphology is also depicted with a dendritic arbour (in light blue) divided in a basolateral plexus spreading in the granule cell layer and a dense apical tree located in the molecular layer and a ramified axon (in purple) which contacts hundreds of granule cells and mossy fibres in the glomeruli. (Adapted from Kandel et al., 2000) **B)** Detailed morphology of a granule cell revealed by immunofluorescence. It is easily appreciated the four short dendrites finishing in a claw shape which contacts a mossy fibre rosette in the glomerulus. Mossy fibres from two different origins were stained in different colours (red and green)(adapted from Huang et al., 2013). **C)** Schematic representation of a cerebellar glomerulus. A single mossy fibre rosette is contacted by dendrites of many granule cells (in red) and Golgi cells (in green) and by the inhibitory projection of a Golgi cell (in yellow). All the structure is surrounded by a glial capsule (in grey) forming an enclosed microenvironment (adapted from Eccles et al., 1967).

As mentioned above, Golgi cells are the main inhibitory input at this layer and form a tight relationship with granule cells. They normally reside just below the Purkinje cell layer and extend their apical dendrites in to the molecular layer, where they receive thousands of excitatory inputs from the granule cells parallel fibres; while their basolateral dendrites stay in the granule cell layer receiving hundreds of synapses from the ascending branches of the granule cells axons (Cesana et al., 2013) and getting contacted directly by mossy fibres in around 40 cerebellar glomeruli (Kanichay and Silver, 2008). They are supposed to receive inhibitory inputs from molecular layer interneurons (Palay and Chan-Palay, 1974; Eccles et al, 1967), however, recent electrophysiological studies failed to record post-synaptic inhibitory currents after stimulating them and suggested that the inhibitory input may come from other Golgi cells (Hull and Regher, 2012). Lugaro cells,

the other inhibitory interneurons of the granule cell layer, also inhibit Golgi cells (Dumoulin, 2001). Moreover, it has been recently reported the presence of gap junctions between Golgi cells apical dendrites leading to strong electrical coupling (Dugué et al, 2009). Such a profuse combination of inputs is further transmitted through their particularly large and widely ramified axons allowing them to inhibit and control hundreds to thousands of granule cells (there are 430 granule cells per Golgi cell in rats, Korbo et al., 1993). Interestingly, Golgi cells, while less restricted, also display preferential parasagittal orientation in both their dendrites (Sillitoe et al., 2008) and their axons (Barmack and Yahnitsa, 2008), although their extension may be large enough to cover more than one microzone.

## **1.2 CEREBELLAR INFORMATION PROCESSING**

### **1.2.1 ORIGIN AND ORGANIZATION OF THE CEREBELLAR INPUTS**

The inferior olivary complex receives inputs from a broad range of sources: sensorimotor information from the cerebral cortex by relay in the mesodiencephalic nuclei; vestibular and visual signals from pre-tectal nuclei, superior colliculus and vestibular nuclei and proprioceptive information from the spinal cord and trigeminal nucleus (Brown et al., 1977; see also a review in Rondi-Reig et al., 2014). All these inputs arrive to specific subnuclei in the olivary complex following a strict topographical distribution which is then respected in the olivo-cerebellar projections thanks to the precise arrangement of the climbing fibres (Sugihara and Shinoda, 2004)(**Figure 6A**). Thus, a neuron from a specific subregion in a specific olivary nucleus emits multiple climbing fibres (in rat each olivary neuron emits around 7 climbing fibres; Sugihara et al., 1999) which spread exclusively in a constrained longitudinal zone. Each of these climbing fibre contacts a single Purkinje cell which, in consequence, receive olivary information from a specific source. However, these are not the only olivo-cerebellar projections since they also send collaterals that innervate the neurons in the deep cerebellar nuclei, which receive the axonal projections from the same Purkinje cells they control (Voogd and Bigaré, 1980) (**Figure 6Aiii**).

The second excitatory input to the cerebellum are the mossy fibres which, as described previously, establish synaptic complexes with the neurons of the granule cell layer in the cerebellar glomeruli (**Figure 5A and C**). Mossy fibres arise from a multitude of pre-cerebellar nuclei which, as for the climbing fibres, relay information from different sources: sensorimotor information from the cortex routes through nuclei in the pons (Voogd, 1969; Bower et al., 1981); complex and highly integrated motor information reaches the cerebellum from the lateral reticular nucleus (see Alstermark and Ekerot, 2013); vestibular information comes from the vestibular nuclei; and primary somatosensory information coming from the spinal cord arrive through the dorsal column nuclei and spino-cerebellar direct projections (Yaginuma and Matsushita, 1986) while that coming from the facial portion routes through the trigeminal nuclei (Van Ham and Yeo, 1992). Thus, the topographical distribution of such a wide input network in to the cerebellum is again a capital issue for understanding its integration in to the circuit.

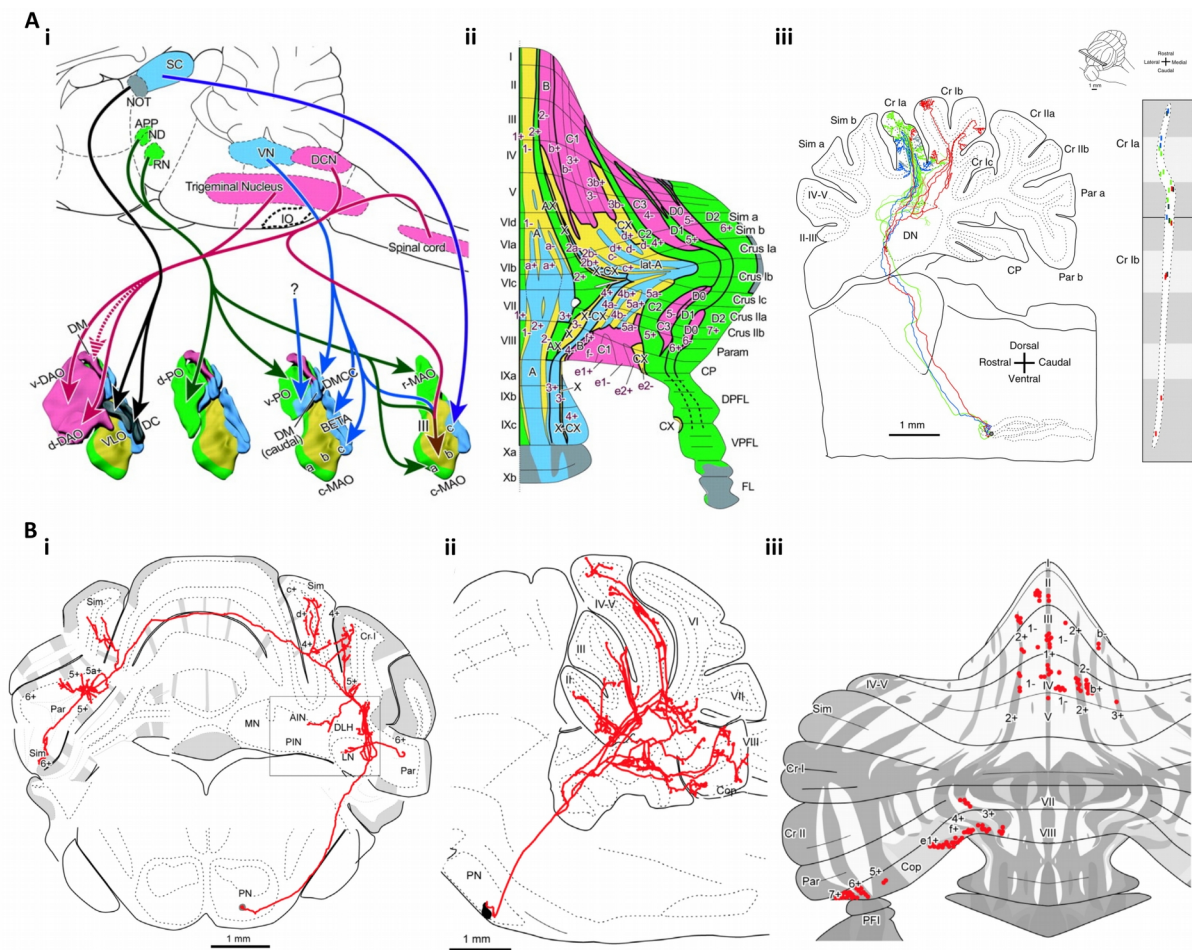


**Figure 6. Topographic organization of the climbing and mossy fibres.** **A**, Schematic representation of the different sources of information in the nervous system and their topographically restricted distribution in discrete sub-regions of the inferior olivary system (i). Each of these olivary sub-regions send climbing fibre projections to specific areas of the cerebellar cortex, establishing a map based on the kind of information that is being processed (ii). The Zebrin II bands are named in lower case letters or with numbers. The modules are indicated with capital letters (adapted from Sugihara and Shinoda, 2004). (iii) Reconstruction of three climbing fibre axons arising from neighbouring neurons in the inferior olive. Each climbing fibre enters the cerebellum, send collaterals to the deep cerebellar nuclei, and reach the cerebellar cortex where it spreads in the sagittal plane giving rise to a reduce number of collaterals which contact a Purkinje cell each (left panel). All these collaterals are restricted to a very narrow parasagittal band but spread across different lobules (right) (adapted from Sugihara et al., 2001). **B**, **i**) Reconstruction of a single mossy fibre projection to the cerebellum in a coronal plane. It enters the cerebellum, send collaterals to the deep cerebellar nuclei (region inside the square) and then spread bilaterally in the transversal plane sending collaterals to different zones. **ii**) Reconstruction of other mossy fibre in a sagittal plane. Each of these collaterals at a particular medio-lateral location spread parasagittally and contact multiple lobules. **iii**) Schematic representation of the cerebellar cortical areas receiving inputs from a single mossy fibre. Notice how the terminals are distributed in clusters of parasagittal bands with partial overlapping with the Zebrin II bands (adapted from Biswas et al., 2019). AIN, nucleus interpositus anterior; APP, area parafascicular prerubralis; BETA, subnucleus  $\beta$ ; c(r)-MAO, caudal (rostral) medial accessory olive; CP or cop, copula pyramidis; CrI-II, Crus I-II; DC, DC of Kooy; DCN, dorsal column nucleus; d(v)-DAO, dorsal (ventral) dorsal accessory olive; DLH, dorsolateral hump; DM, dorsomedial subnucleus of the principal olive; DMCC, dorsomedial cell column; DN, dentate nucleus (same as LN, lateral nucleus); DPFL, dorsal paraflocculus; d(v)-PO, dorsal (ventral) lamella of the principal olive; FL, flocculus; IO, inferior olive; MN, medial nucleus; ND, nucleus of Darkschewitsch; NOT, nucleus of the optic track; Par or param, paramedian lobule; PN, pontine nucleus; RN, red nucleus; SC, superior colliculus; Sim, lobule Simplex; VPLF, ventral paraflocculus.

In sharp contrast to the single zone specificity observed for climbing fibres, mossy fibres seem to be much more spread in the mediolateral axis and in most case a single pre-cerebellar neuron extends its axonal projection bilaterally reaching multiple zones in multiple lobules (**Figure 6Bi**). However, more detailed analysis reveals that while the main axon does extend widely mediolaterally, each secondary branch gives rise to the mossy fibres that enters the cerebellar cortex and form their characteristic terminals is mostly restricted to specific clusters within a longitudinal stripe (Wu et al., 1999; Serapide et al., 2001; Shinoda et al., 2010) (**Figure 6Bii**), which may overlap with the Zebrin II bands (Ji and Hawkes, 1994) (**Figure 6Biii**). Interestingly, later anatomical studies show a certain degree of alignment between the mossy fibre and the climbing fibres systems with information coming from the same original source overlapping in the cerebellar cortex (Voogd et al, 2003; Pijpers et al., 2006) (**Figure 7**). As in the case of the climbing fibres, the mossy fibre system also sends collaterals that reach the deep cerebellar and vestibular nuclei (Chan-Palay, 1973; Shinoda et al., 1992). These collaterals seem to present a rough correspondence between the cortical and nuclear projections (Wu et al., 1999).

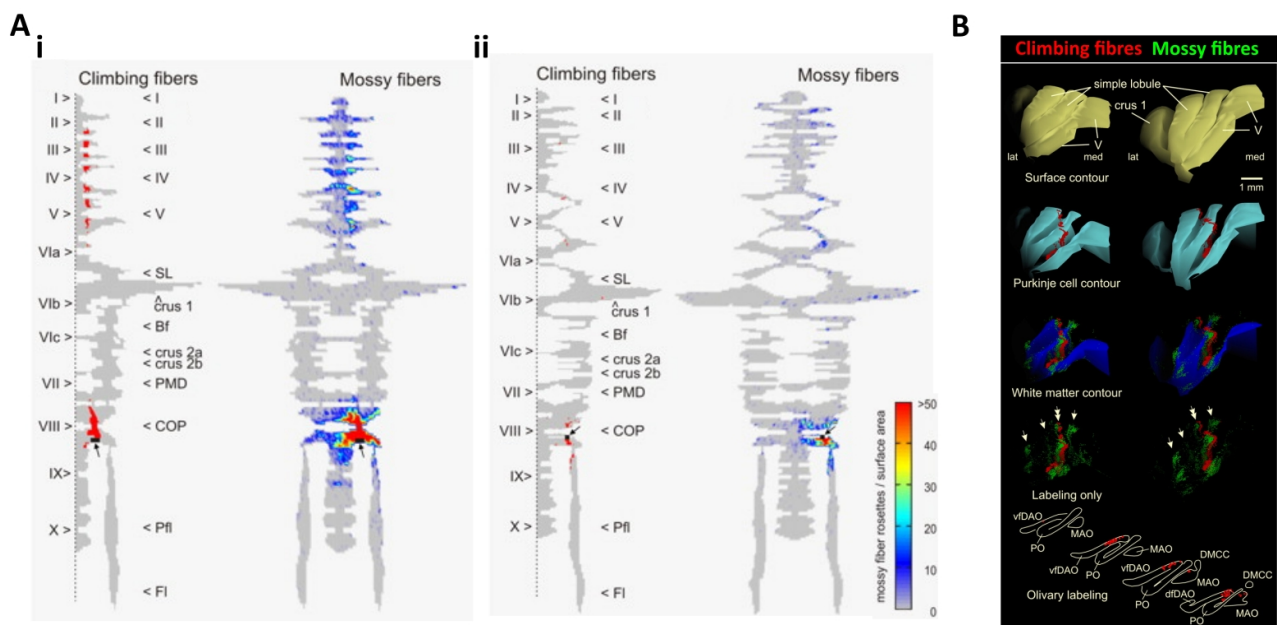


**Figure 7. Partial overlap between mossy fibres and climbing fibres in the cerebellar cortex. A, i-ii)** Two examples of the topographical relationship of mossy and climbing fibre afferents obtained after injection of the cholera toxin b subunit, an anterograde and retrograde tracer, into specific climbing fibre-defined cerebellar zones. The distribution of labelled collaterals are reconstructed on the unfolded cerebellar cortex. The injection sites are indicated by the black arrow, the climbing fibre collaterals are labeled in red (left side of the panels) and the density of mossy fibre collaterals in colour coded (right side of panels). Note the partial overlap in the distributions of both types of fibres. **B)** Three dimensional reconstruction showing the correspondence of mossy and climbing fibre collateral labelling in a particular region. Note the strip of mossy fibre terminals overlapping with the climbing fibre labelling (double white arrows) and the additional stripes with no correspondence (single white arrow). The origin of the climbing fibres in the inferior olive is also display (adapted from Pijpers et al., 2006). Bf, buried folium; COP, copula pyramidis; d(v)fDAO, dorsal (ventral) fold of dorsal accessory olive; DMCC, dorsomedial cell column; FI, flocculus; MAO, medial accessory olive; PMD, paramedian lobule; PO, principal olive; Pfl, paraflocculus; SL, lobule Simplex; VLO, ventrolateral outgrowth.

The cerebellum also receive an important modulatory input. Serotonergic fibres mainly from the medullary- and pontine reticular formation form a dense network in the granule cell layer but also in the molecular layer (see Oostland and van Hooft, 2016). Cholinergic afferents from many nuclei in the lower brain stem, but mostly from the medial vestibular nucleus, are also distributed in the cerebellar cortex (see Zhang et al., 2016 for a review). Moreover, a putative dopaminergic projection from the ventral tegmental area to the cerebellum has also been proposed (Ikai et al., 1992). In support of the existence of these projections, dopamine receptors are expressed in the cerebellum (Barili et al., 2000) and recently they have been associated to a role in multiple cognitive functions in mice (Locke et al., 2018).

### 1.2.2 PHYSIOLOGICAL RELEVANCE OF THE ANATOMICAL MAPS

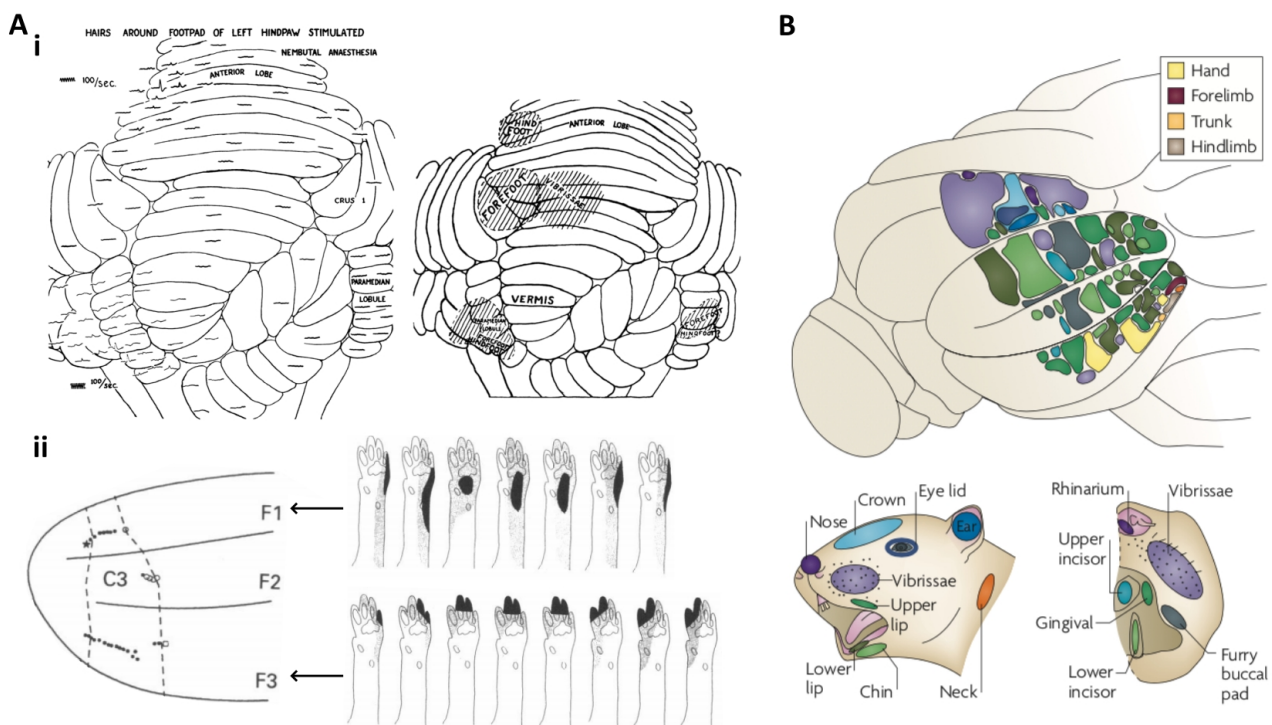


**Figure 8. Receptive fields in the cerebellum.** **A, i)** Early electrophysiological mapping studies of the somatosensory receptive fields in the cerebellar cortex of the anaesthetized cat. In the left panel are represented the evoked responses after stimulating the left hindpaw and in the right panel are summarized the receptive fields of different regions (from Snider and Stowell, 1944). **ii)** Detailed study of the cutaneous nociceptive climbing fibre inputs restricted to the C3 module in the anterior cerebellum. Each dot represent a recorded cell and the shaded areas in the forelimb schemas represent the region where the strongest response was elicited. The organization of the receptive fields follows the parasagittal distribution of the climbing fibres (adapted from Ekerot et al., 1990). **B)** Spatial distribution on the cerebellar cortex of the rat of the receptive fields obtained in the granule cell layer after stimulation of different body parts. Unlike the climbing fibre receptive fields, the mossy fibre receptive fields present a fractured somatotopical mosaic pattern of patches (from Apps and Hawkes, 2009).

Functional mapping of the receptive fields of peripheral or cortical stimulations on both the climbing fibre and mossy fibre systems were carried out almost in parallel with the above described anatomical dissection. Indeed, early proprioceptive and exteroceptive receptive field mapping showed the presence of multiple homunculi representation in the anterior zone (Adrian, 1943) and posterior cerebellum (Snider and Stowell, 1944) in cats (**Figure 8Ai**). Later studies employing more advanced electrophysiological recording techniques allowed a more precise mapping, which turned out to have a well correspondence with the anatomical findings. Thus, climbing fibre receptive fields from peripheral stimulations were found to be restricted to specific cerebellar microzones receiving common inferior olive inputs (eg., Ekerot et al., 1991) (**Figure 8Aii**). In contrast with its spatial specificity, the nature of the information carried by climbing fibre inputs seems to be multimodal (Garwicz et al., 1992; Ohmae and Medina, 2015). Indeed, it has been proposed that climbing fibres signal sensory errors, that is, unexpected sensory consequences of an ongoing behaviour (Ohmae and Medina, 2015).

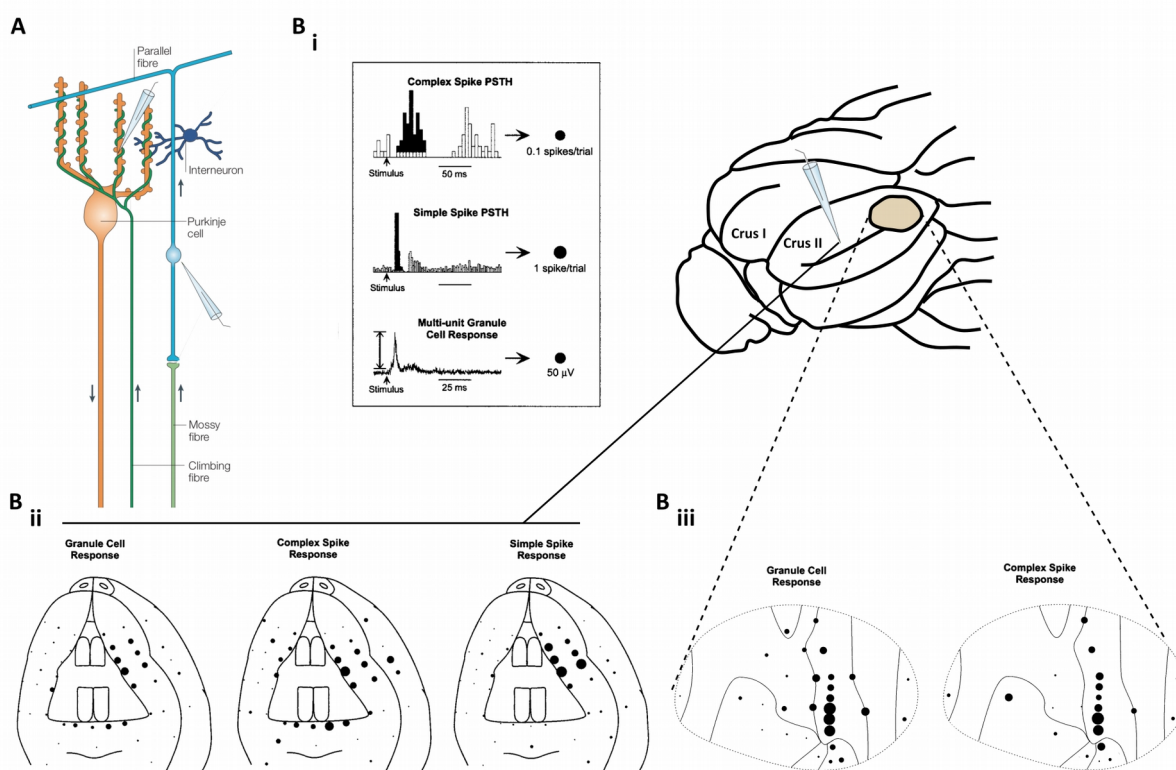


**Figure 9. Overlap of mossy and climbing fibres receptive fields.** **A)** Schematic representation of the experimental approach to test the overlapping in the mossy and climbing fibre systems. The climbing fibre receptive fields are obtained based on the presence of complex spikes in the recordings of the Purkinje cell layer. The granule cell layer multiunit activity is employed to measure the receptive fields of the mossy fibres. The simple spike activity represent the receptive field of the granule cell to Purkinje cell transmission (adapted from Apps and Garwicz, 2005). **B)** The size of the responses measured in the cerebellar cortex after the stimulation of different body parts in the rat were translated into increasing diameter dots (**i**). The mossy and climbing fibre receptive fields for a particular recording position in the Crus II were plotted in a schematic representation of the face of the rat showing a high degree of overlapping (**ii**). Applying a focal peripheral stimulus on the lower incisors, the receptive fields along the surface of a region in the Crus II were also measured. Again, the patterns shown great overlapping (adapted from Brown and Bower, 2001).

Regarding granule cell receptive fields, they were found to be organized mostly in more or less elongated patches (Shambes et al., 1978, Bower et al., 1981; Ekerot and Jörntell, 2001) (**Figure 8B**) which may correspond to the mediolateral parallel projection to multiple microzones found in anatomical studies (Wu et al., 1999; Shinoda et al., 2010). Similarly, in line with the anatomical finding of a certain degree of overlap between climbing fibres and mossy fibres from the same origin (Voogd et al, 2003; Pijpers et al., 2006), when receptive fields of both systems were recorded in parallel they presented a close correspondence (Brown and Bower, 2001) (**Figure 9**). Finally, when considering the nature of the information integrated by single granule cells there is a lot of controversy in the field. Based on the convergence of inputs and the divergence of outputs carried out by the granule cells, one of the early assumptions was that granule cell coding may be sparse and that different mossy fibre streams would contact each of the few dendrites thus acting as a pattern classification device (Marr, 1969; Albus, 1971). While some studies agreed with such assumptions showing multi-modal granule cells (Huang et al., 2013; Chabrol et al., 2015), other have shown both uni-modal granule cells (Bengtsson and Jorntell, 2009) and dense rather than sparse coding during natural behaviours (Giovannucci et al., 2017; Knogler et al., 2017; Wagner et al., 2017).

### 1.2.3 DEEP CEREBELLAR NUCLEI AND CEREBELLAR LOOPS

While Purkinje cells are the only output from the cerebellar cortex, the final gate towards the brain and the spinal cord are the deep cerebellar and vestibular nuclei. However, much less attention has been given to this stage of the cerebellar circuit in comparison to the cortex, which has been classically considered as the site of information processing and computation (Eccles et al., 1967). It is clear now though that the cerebellar nuclei are not mere relay centres and they must be considered as another fundamental computational stage of the cerebellar circuitry. Indeed, given the opposite nature of the excitatory inputs from climbing fibre and mossy fibre collaterals and the inhibition from the Purkinje cells excited by these same fibres, such a microcircuit enables fine temporal coding in which cerebellar nuclei activity will be shaped by tight control of excitation/inhibition balance.

It has been already briefly described in previous sections that the cortico-nuclear projections are topographically organized following the zonation pattern (Voogd et al., 2003). Similarly, the collaterals sent by the afferent projections, the climbing and mossy fibres, also follow such organization (Voogd and Bigaré, 1980, Wu et al., 1999) (**Figure 10A**). Thus, even in a certain nucleus we can define subdivisions based on the specific pattern of inputs received which turns out to be mostly organized in the rostrocaudal axis (Sugihara and Shinoda, 2007). Such compartmentalization may relate not only to the information processing carried out by the cerebellar microcircuit in which a certain sub-nuclei is embedded but to the topographical organization of efferent projections to specific targets.

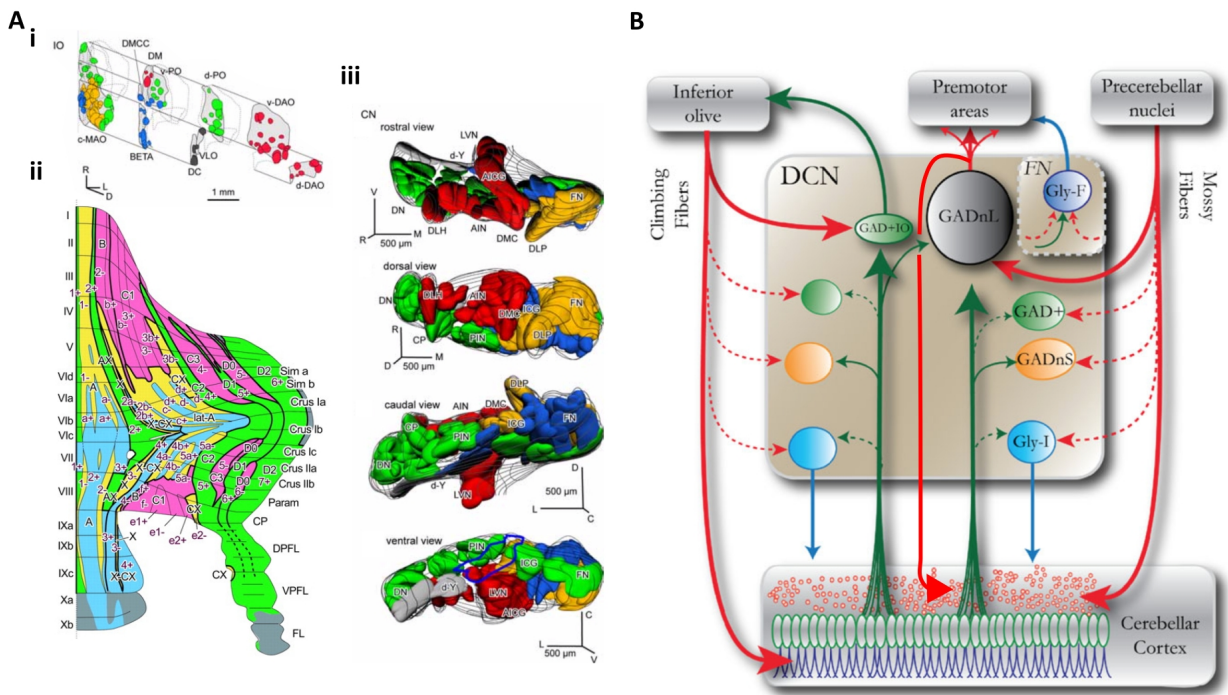


**Figure 10. Loops with the deep cerebellar nuclei.** **A)** The discrete olivo-cerebellar circuits revealed by localized injections of anterograde tracers in specific sub-nuclei of the inferior olive (**i**) where not restricted to the cerebellar cortex (**ii**) and the topographical distribution of collaterals in to the deep cerebellar nuclei also showed multiple subdivisions on them (**iii**). This subdivisions also receive the cerebellar cortical inputs from areas innervated by collateral of the same climbing fibres which contact them (same colour code in all panels, the magenta and cyan in panel ii correspond to red and blue in panels I and iii) (adapted from Sugihara and Shinoda, 2007). **B)** Schematic drawing showing the main neuronal populations in the deep cerebellar nuclei and the intrinsic and extrinsic connectivity patterns. The red arrows represent glutamatergic projections, in green are the GABAergic axons and the blue ones are glycinergic or mixed glycinergic/GABAergic projections. The solid lines denote confirmed connections while dashed lines represent uncertain ones. Note the presence of at olivo-cortico-nucleo-olivary and cortico-nuclear closed loops (adapted from Uusisaari and Knöpfel, 2011). AICG, anterior interstitial cell group; AIN, nucleus interpositus anterior; BETA, subnucleus  $\beta$ ; c(r)-MAO, caudal (rostral) medial accessory olive; CP, copula pyramidis; DC, dorsal cap of Kooy; DCN, deep cerebellar nucleus; d(v)-DAO, dorsal (ventral) dorsal accessory olive; DLH, dorsolateral hump; DM, dorsomedial subnucleus of the principal olive; DMC, dorsomedial crest; DN, dentate nucleus; DPFL, dorsal paraflocculus; d(v)-PO, dorsal (ventral) lamella of the principal olive; d-Y, dorsal group of Y nucleus; FN, fastigial nucleus; FL, flocculus; GAD, glutamic acid decarboxylase; GADnL, large GAD-negative cells; GADnS, small GAD-negative cells; Gly-I, non spontaneous glycinergic/GABAergic cells; Gly-F, projecting glycinergic neurons from the fastigial nucleus; ICG, interstitial cell group; IO, inferior olive; LVN, lateral vestibular nucleus; Param, paramedian lobule; PIN, nucleus interpositus posterior; Sim, lobule Simplex; VPLF, ventral paraflocculus.

Regarding the cerebellar nuclei internal composition and organization, early seminal works performed by Chan Palay (1973, 1977) described heterogeneous cell populations based on morphological discrimination which she already associated with local interneurons and different types of projecting neurons. Latter studies have further characterized the physiological properties of these different populations as well as their connectivity (Uusisaari and Knöpfel, 2011, 2012) (**Figure 10B**). The large glutamatergic projecting neurons are the main target of the previously described olivo-cortico-nuclear and mossy cell circuits. These inputs

seem to also contact a non-GABAergic (putatively glutamatergic) and a GABAergic populations of local interneurons. Additionally, a population of glycinergic projection neurons has been described exclusively in the fastigial nucleus (Bagnall et al., 2009). Another glycinergic sub-population has been found to receive mossy fibre collaterals and project to the granule cell layer constituting a nucleo-cortical inhibitory pathway (Uusisaari and Knöpfel, 2010). Finally, a GABAergic population receive inputs from climbing fibre collaterals and then project back to the same inferior olive compartment (De Zeeuw et al, 1997). These cells also receive the input of the Purkinje cells contacted by the same climbing fibres which sent the collaterals keeping the same topographical organization and, thus, establishing closed olivo-cortico-nuclear loops (Teune et al, 2000) (**Figure 10B**).

These are not the only loops found in the cerebellar circuit, the early finding of nucleo-cortical projections (Gould and Graybiel, 1976; Tolbert et al., 1976) led to the study of their topographical organization, which revealed partially preserved reciprocity with the cortico-nuclear pathways, thus constituting cortico-nuclear loops (Gould, 1979; Trott et al., 1998a, b). Nucleo-cortical projections are mainly composed by axonal collaterals from the main glutamatergic extra-cerebellar projecting neurons, which establish mossy fibre-like contacts with granule cells and Golgi cells in the granule cell layer (Houck and Person, 2015; Gao et al., 2016). However, as mentioned before, glycinergic nuclear cells, which turned out to co-release GABA, also project to the granule cell layer and specifically contact Golgi cells (Ankri et al., 2015) (**Figure 10B**).

#### 1.2.4 THE TARGETS OF THE CEREBELLUM

The deep cerebellar nuclei and the vestibular nuclei are the only output of the cerebellum. It has been already mentioned the specificity of the inhibitory projection to the inferior olive through the nucleo-olivary pathways (De Zeeuw et al, 1997). However, the main glutamatergic population project to a wide range of structures across the brain and the spinal cord. As occurs with the cerebellar inputs, topographically restricted populations in the cerebellar output nuclei project to specific extra-cerebellar regions, many of which also send inputs to the cerebellum (Teune et al., 2000). These include different nuclei in the pontine and medullary reticular formations (Angaut et al., 1985), the midline, the zona incerta of the hypothalamus (Voogdt, 2004) and the thalamus (Teune et al., 2000). For instance, in the midline there are important cerebellar projections to the red nucleus (Angaut et al., 1987), the superior colliculus or the periaqueductal gray. In the thalamus, the cerebellar inputs reach primary thalamic relay nuclei such as the ventrolateral nucleus, thalamic motor-associated nuclei like the ventromedial nucleus and intralaminar nuclei including centromedian, centrolateral or parafascicular nuclei (Teune et al., 2000). Importantly, the cerebello-thalamic projections constitute the main pathway between the cerebellum and cerebral cortex. More detailed description of cerebello-cerebral projections and their functional roles will be address later in the introduction.

### 1.3 INTEGRATION OF THE ELEMENTS IN TO THE CIRCUIT

As evidenced by the previous sections, in order to fully understand the cerebellar circuits' physiology and function we need to bring together the exquisite topographical distribution and the electrophysiological particularities of their different elements. Indeed, some of the earliest hypotheses on cerebellar computation and function were established after these anatomical considerations and under the general assumption of the cerebellar role in the control of voluntary movements (Braitenberg and Atwood, 1958; Braitenberg, 1961; Eccles et al, 1967).

#### 1.3.1 THE BEAM HYPOTHESIS

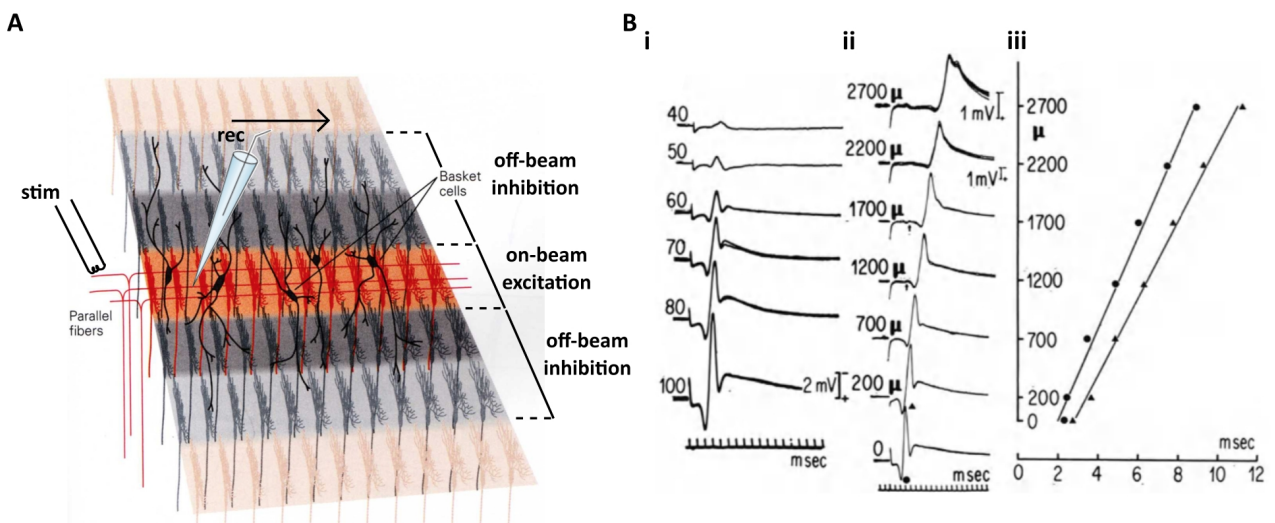


**Figure 11. First experiments leading to the beam hypothesis.** **A)** Experimental design in which a stimulating electrode was positioned on the surface of the cerebellum to drive pulses of different strengths while the activity of Purkinje cells and molecular layer interneurons were recorded. The stimulation produce excitation of the parallel fibres situated below the stimulating electrode which then excite all the cells which are contacted by them, i.e., Purkinje cells, molecular layer interneurons and Golgi cells. Given the parasagittal projections of the basket cells, a potential on-beam excitation / off-beam inhibition pattern may be generated (adapted from Eccles et al., 1967 and Ghez, 2000). **B, i)** For stimulations at a given distance from the recording electrode, increase in the strength of the stimulus increased the amplitude of the response. **ii)** Moving apart the stimulating and the recording electrodes inside the area of parallel fibres excited by the stimulation drove responses of almost similar amplitudes but with increasing latencies. **iii)** Plot showing the linear increase in the latency of the peaks of initial positivity (triangles) and negativity (circles) of the response relative to the distance from the focal activation (from Eccles et al., 1967).

Considering the anatomical data it is quite obvious that the general organization of the cerebellar cortical circuit is composed of small units (microzones) mainly oriented in the parasagittal axis. Purkinje cell, climbing fibres, molecular layer interneurons and Golgi cells all follow that plane. On the other hand, parallel fibres run perpendicularly to all these elements in a mediolateral plane and could therefore modulate activity preferentially all along their extension. Indeed, early electrophysiological studies

employing focal superficial stimulation of the cerebellar cortex, and in consequence activating a bundle of parallel fibres, drove responses which propagated with linearly increasing delays in the mediolateral axis (Eccles et al., 1966) (**Figure 11**). Such on-beam activation would subsequently cause a net off-beam inhibition through the molecular layer interneurons which, as introduced previously in this chapter, extend their axons in the parasagittal direction (Braitenberg and Atwood, 1958). These observations led to the so-called “beam hypothesis” (Eccles et al., 1967) which postulated that the wave of excitation propagated along the parallel fibres beams will sequentially activate Purkinje cells with a temporally precise dynamic while molecular layer interneurons and Golgi cells will sharpen and sculpt this on-beam effect by off-beam inhibition (Cohen and Yarom, 2000; Gao et al., 2006). This would allow the cerebellar circuit to transform spatial distribution of inputs into a temporal code, which would be particularly suited for the organization of sequences of movements necessary for motor coordination.

### 1.3.2 REVISITING THE MODELS FROM A PHYSIOLOGICAL PERSPECTIVE: PATCHES VERSUS BEAM

There are nonetheless critical mismatches between the expected responses based on these theories and the actual receptive fields found under physiological conditions. The patch-like distribution of receptive fields in the granule cells has been already introduced in this chapter, however, if beam theory were correct, such receptive field should be translated in to a beam of excitation at the Purkinje cell and molecular layer interneurons level. Instead, soon after his beam theory postulation, Eccles failed in finding evidence of such on-beam excitatory waves after peripheral stimulation. The patterns of Purkinje cells responsive to the stimulation were not organize in the transversal axis following the parallel fibre track as he predicted but they appeared in patches resembling the receptive fields of the granule cells (see Eccles, 1973) (**Figure 8B**). These results were replicated and extended later showing similar patches in both Purkinje cells and molecular layer interneurons (Ekerot and Jörntell, 2001). Notably, some studies did find on-beam patterns of activity in Purkinje cells (Heck et al., 2007; Bosman et al., 2010), however, the fact that granule cell receptive fields exhibit a variety of shapes which are particularly enlarged in certain regions could generate a confounding beam-like pattern also in the Purkinje cells potentially explaining this discrepancy (Apps and Garwicz, 2005).

How to reconcile the mismatch between the anatomical predictions from the parallel fibre organization and the physiological receptive fields of granule cell activity? An early hypothesis postulated by Llinás (1982) proposed a dual role of granule cells: a powerful focal activation exerted through the ascending branch of the axonal projection and a more subtle and widespread modulatory effect through the parallel fibres. This hypothesis was initially supported by the observation of preferential activation of Purkinje cells immediately overlying the granule cells activated by a certain receptive field (Bower and Woolston, 1983; Isope and Barbour, 2002) while other possibilities were also explored. For instance, the anisotropic distribution of synapses along the length of the parallel fibres (Pichitpornchai, 1994), the silent nature of the majority of

the parallel fibre-Purkinje cell synapses (Ekerot and Jörntell, 2002; Isope and Barbour, 2002) or a major role of the molecular layer interneurons in shaping the mediolateral transmission of the excitatory wave through feedforward inhibition (Santamaria et al., 2007, Walter et al., 2009) apart from their role in lateral inhibition in the sagittal axis (Dizon and Khodakhah, 2011).

### 1.3.3 THE MARR-ALBUS-ITO THEORY

Following the detailed anatomico-electrophysiological description and its functional interpretation presented by Eccles (1967), David Marr published two years later a seminal theoretical paper (1969) in which he proposed that the cerebellar cortex acts as a supervised learning machine following an algorithm known in machine learning as a perceptron (Rosenblatt, 1958)(**Figure 12A**). Basically, the granule cells would generate a distributed pattern of activity from the received mossy fibre input, which would be spread through the parallel fibres and stored in the synapses between them and the Purkinje cells by a long lasting potentiation mechanism only when there is simultaneous activation of the climbing fibres. Thus, the climbing fibre system would acquire the properties of a teaching signal controlling the learning of a particular pattern of activity in the cerebellar cortex. This model was later revised by Albus (1971) who proposed that a depression rather than a potentiation in the parallel fibre-Purkinje cell synapsis may be the fundamental learning mechanism (**Figure 12B**). More than 10 years later, Ito confirmed experimentally the purely theoretical predictions of Albus when he described the existence of *in vivo* long-term depression mechanisms after co-activation of parallel fibres and climbing fibres (Ito et al., 1982; Ito and Kano, 1982) (**Figure 12C**). This led to the establishment of the Marr-Albus-Ito model for cerebellar computational principles.

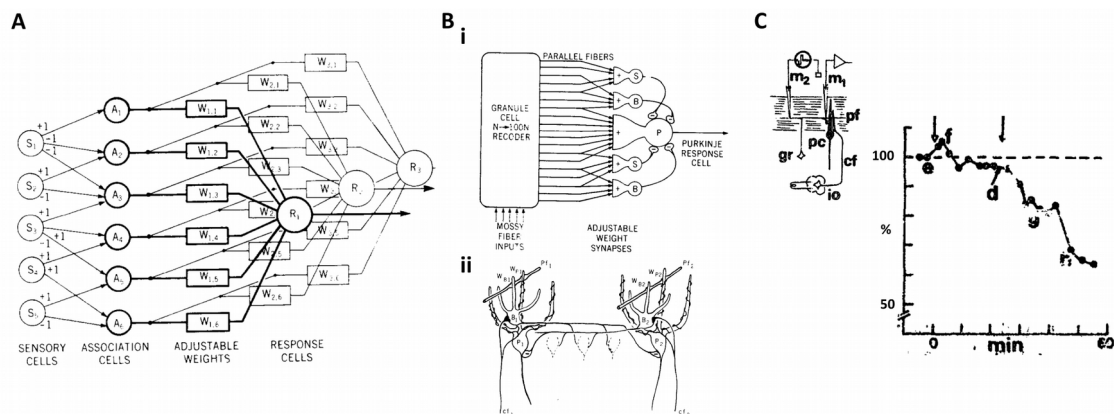


**Figure 12. Marr-Albus-Ito model.** **A**) Schematic representation of a Perceptron in which a sensory stage transmit the signals to an associative stage which recode the inputs assigning adjusted weights to them prior arriving to a response stage which sums all the weighted inputs to produce or not an output. By adjusting the weights various classifications can be made on a set of input patterns (from Albus, 1971). **B, i**) Interpretation of the cerebellar cortex as a Perceptron in which the granule cells act as associative network for the pre-cerebellar inputs and the Purkinje cell acts as response cells. The molecular layer interneurons sum the inhibition and then transmit it to the Purkinje cells. **ii**) The climbing fibre was proposed as the responsible of adjusting weights by applying long-term synaptic depression (from Albus, 1971). **C**) Demonstration of the long-term depression in the parallel-fibre to Purkinje cell synapses after co-activation of the climbing fibre and the parallel fibre (second arrow) (Ito and Kano, 1982).

### 1.3.4 CONNECTING THE PATCHES

How would the patches of mossy fibres receptive fields fit then with the previous hypothesis on cerebellar computation? Indeed, the spread of similar inputs in multiple parallel microzones at different mediolateral and antero-posterior locations (i.e., multiple modules and lobules) could fit particularly well with the Marr-Albus-Ito model as it may multiplex in an efficient way the information allowing for efficient parallel processing and positional coding of sensorimotor commands (Apps and Garwicz, 2005; Heck et al, 2007). Nevertheless, such efficient parallel processing would still require the lateral communication between microzones performed by the parallel fibres. Recent findings employing local photostimulation of granule cell patches revealed stereotyped distal connectivity patterns onto Purkinje cells and molecular layer interneurons which did not matched with specific Zebrin II bands (Valera et al., 2016) (**Figure 13**). Interestingly, clusters of Purkinje cells and molecular layer interneurons did not perfectly matched suggesting that granule cells could control specific distal Purkinje cell populations through feedforward inhibition. Such connectivity patterns are in line with the majority of silent synapses across the parallel fibres (Isope and Barbour, 2002). However, given that this study was carried out while blocking inhibition, the integration of these distal connectivity patterns under physiological conditions remains uncertain and understanding how such mediolateral connectivity works is still a main issue for cerebellar physiology.

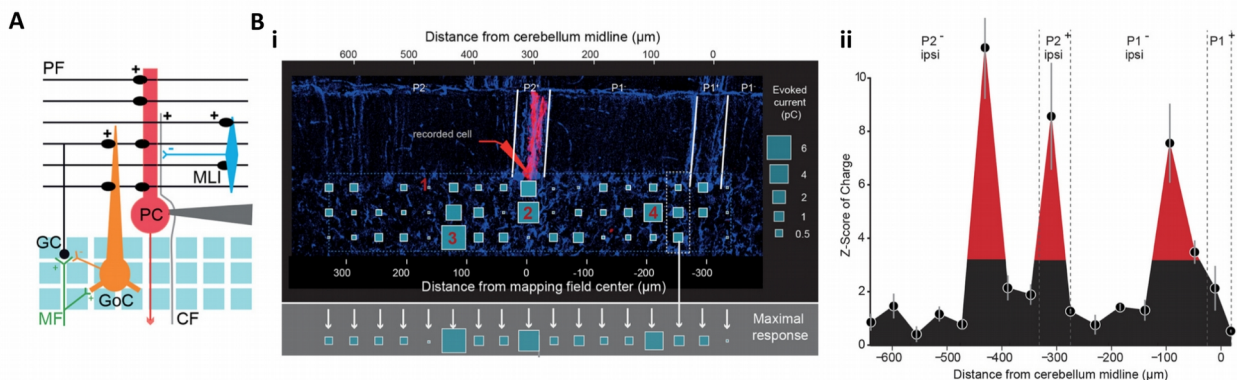


**Figure 13. Hotspots of distal granule cell connectivity.** **A)** Schematic representation of the experimental design. A Purkinje cell (PC) was recorded and glutamate was photorelease at multiple locations in the granule cell layer (blue squares) mimicking the excitatory input by the mossy fibres (MF). The inhibition was blocked and the climbing fibres (CF) were not excited. Other cells implicated in the circuit are also depicted (Golgi cells (GoC), molecular layer interneurons (MLI)). **B, i)** Example of the granule cell (GC) input pattern in to a single Purkinje cell (labeled in red). Each blue square represents a glutamate photorelease site and the size of it is proportional to the evoked response. The maximal response obtained at each mediolateral position is indicated at the bottom and establish the connectivity pattern. **ii)** Mean connectivity pattern for Purkinje cells in a particular location revealed hotspots of distal strong connections (red area) surrounded by silent patches (black area) (From Valera et al., 2016).

## 1.4 INTEGRATION OF ACTIVITY PATTERNS AND SYNAPTIC PLASTICITIES IN TO THE CEREBELLAR MODELS

One of the main complications when one tries to understand cerebellar computation is the inhibitory nature of the Purkinje cells. Given that these are the only output towards the deep cerebellar nuclei, the final cerebellar output may represent to certain extent a mirror image of their activity. As mentioned at the beginning of this chapter, Purkinje cells exhibit a characteristic dual activity pattern, a high frequency firing of simple spikes and a low frequency firing of complex spikes (Eccles et al., 1967). However, in order to understand cerebellar physiology, we need first to understand 1) how is Purkinje cell activity modulated by the cerebellar inputs during behaviour, 2) how these activity patterns are transferred and integrated by the deep cerebellar nuclei and 3) how different plasticity mechanisms act on them.

### 1.4.1 SPATIOTEMPORAL FIRING PATTERNS

While classic views of cerebellar integration and receptive fields of Purkinje cells were constructed based exclusively on changes in the firing rate of simple and complex spikes, it is now clear that the spatio-temporal organization of the activity is similarly important (see De Zeeuw et al., 2011 for a review) (**Figure 14A**). Indeed, alteration in firing frequency regularity has been associated to different motor deficits such as ataxias (Walter et al., 2006).

In the absence of synaptic inputs, Purkinje cells exhibit an intrinsic self-paced simple spike firing rate, which is highly regular and fast (30-150Hz, Häusser and Clark, 1997). Moreover, in the absence of external excitatory drive, the self-paced intrinsic activity of molecular layer interneurons establish a tonic inhibitory drive which mostly increase the irregularity of Purkinje cells firing rather than the overall firing rate both in vitro (Häusser and Clark, 1997) and in vivo (Wulff et al., 2009). Under physiological conditions, the basal tone of excitatory granule cell inputs also increases the irregularity of simple spikes (De Zeeuw et al., 2011). It has been proposed that such irregular pattern is indeed formed by short regular motifs which, on average, last only few milliseconds (Shin et al., 2007) (**Figure 14B**). Furthermore, the existence of Purkinje cell up and down-states or bistability, both intrinsically and externally modulated, may also influence the particular structure of these activity patterns (Loewenstein et al., 2005). As discussed previously, peripheral stimulation generates patches of Purkinje cell activation, which synchronizes their simple spike firing in a coherent manner (Bower and Wooston, 1983). Such pattern of synchronization can indeed affect wider zones in both the mediolateral (Bosman et al., 2010) and sagittal planes (Heck et al, 2007). However, parallel fibre excitation not only modulates transiently the firing rate but also modifies the temporal structure of the firing, inducing regular firing motifs for longer periods in ensembles of Purkinje cells (Shin et al., 2007, Loewenstein et al., 2005).

Regarding complex spikes, they are driven exclusively by the inferior olive input. Olivary neurons exhibit intrinsic oscillatory activity at frequencies of 2-4 Hz or 6-9 Hz related to membrane potential dynamics

(Khosrovani et al., 2007) (**Figure 14C**). Neighbouring olivary neurons are connected through gap junctions (Llinás et al., 1974), which facilitate local synchronicity and coherent oscillations that is then transmitted to the cerebellar cortex innervated by common climbing fibres input, that is, mainly following the zonal organization (Blenkinsop and Lang, 2006). This oscillatory profile raised the possibility that external input to the olivocerebellar system not only produce a phasic activation but also modify the frequency and phase of these oscillations (Khosrovani et al., 2007; Llinás, 2009). Organized complex spike firing has been found also across different microzones, mostly during ongoing behaviours (Welsh et al., 1995; Ozden et al., 2009). This may reflect common pre-olivary inputs (De Zeeuw et al., 1998) or the dynamic modulation of olivary neurons ensembles by, for instance, the cerebellar nucleo-olivary loops (Lang et al., 1996; Chaumont et al., 2013).

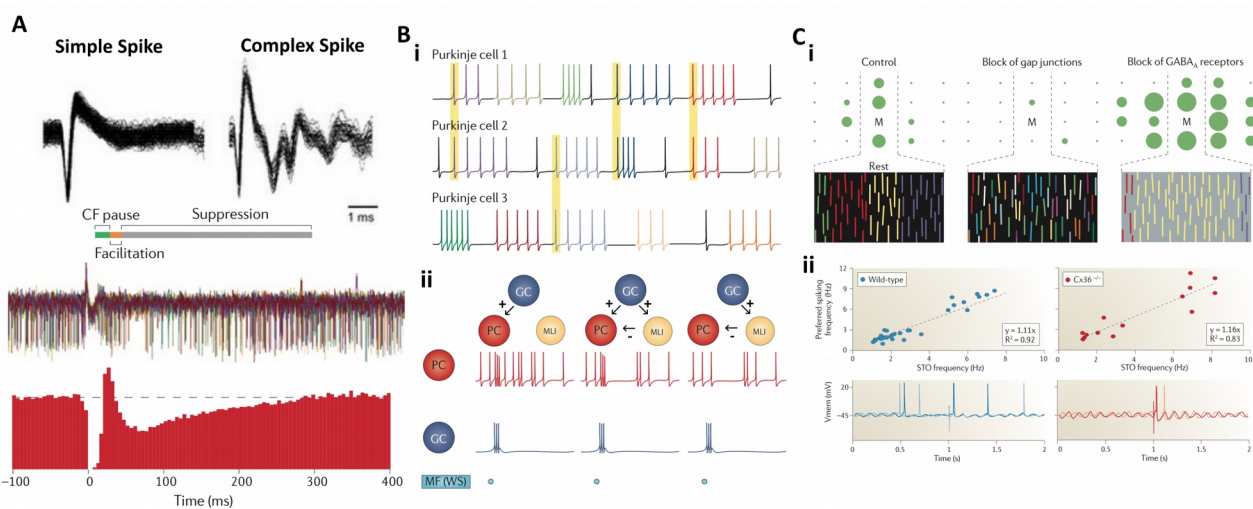


**Figure 14. Simple and complex spikes patterns.** **A**) Simple and complex spikes waveforms (top panel). Simple spikes fire at high frequency range while complex spikes occur at a low frequency. The firing of a complex spike transiently modifies the firing of simple spikes (middle and bottom panels). The stereotypical pattern induced starts with a brief pause of  $\sim 10$  msec, followed by a short facilitation and a longer depression. **B, i)** The patterns of simple spikes are characterized by a big inter-spike interval variability, however, short motifs of regular spiking can be distinguished (colour coded) and the onset of a new motif can be spatially coordinated across Purkinje cell populations. **ii)** The spatio-temporal profile of simple spike activity triggered by a peripheral stimulus (blue dot at the bottom) is shaped by the interplay of granule cells (GC), Purkinje cells (PC) and molecular layer interneurons (ML). **C, i)** The complex spikes synchrony across different Purkinje cells (each dot) in respect to a “master” cell (M) is indicated by the diameter of the dot. In normal conditions, synchrony is mostly restricted to cerebellar microzones (colour coded inside the dashed lines which delimit a cerebellar zone) and this pattern depends on the presence of gap junctions in the inferior olive and the local inhibitory networks in the cerebellar cortex. **ii)** The neurons of the inferior olive present sub-threshold oscillations which affect the specific spike timing. This modulation is less reliable in animals lacking the gap junctions (Cx36<sup>-/-</sup>). Moreover, the phase of the sub-threshold oscillations is reset upon the arrival of a peripheral stimulus producing a reliable spiking pattern. This resetting is also less pronounced in the absence of gap-junctions. (all panels in the figure adapted from De Zeeuw et al., 2011 except the examples of simple and complex spike waveform, reproduced from Katoh et al., 2015).

Simple spikes and complex spikes activity patterns do not work in isolation but they influence each other. Stereotyped patterns of simple spikes are observed in relationship to a complex spike, thus immediately after its arrival there is a characteristic pause in simple spike firing that last approximately 10 milliseconds usually followed by a transient facilitation and then by a longer suppression (Simpson et al., 1996) (**Figure 14A**). This post-complex spike pattern may depend on the local activity of molecular layer interneurons which are indeed affected by climbing fibres through glutamate spillover (Szaphiro and Barbour, 2007). The simple spikes also modulate the complex spikes through the above mentioned nucleo-olivary loops (Lang et al., 1996; Chaumont et al., 2013).

#### 1.4.2 READ-OUT OF THE CORTICAL ACTIVITY PATTERNS BY THE DEEP CEREBELLAR NUCLEI

As already explained, an afferent copy of the inputs to the cerebellar cortex also reach the deep cerebellar nuclei through axon collaterals. It is therefore important to understand how direct excitation and indirect inhibition through Purkinje cell firing patterns are integrated to produce the physiologically relevant cerebellar output patterns particularly considering that dozens to several hundreds of Purkinje cells from single microzones converge on to an individual cerebellar nuclei cell (De Zeeuw and Berrebi, 1995) (**Figure 15**).

Given that simple spikes occur at much higher rates than complex spikes, we can infer that cerebellar nuclei cells are under a tonic GABAergic tone in which individual Purkinje cell spikes have poor or none direct impact. Thus, population rather than individual coding may be controlling the firing of cerebellar nuclei neurons and the synchronization of Purkinje cells patterns during ongoing behaviours may signal the timing for such activity (Gauck and Jaeger, 2000; Shin et al., 2007). Regarding the effect of climbing fibres inputs, complex spikes drive a strong inhibition, which can be followed by a rebound excitation when occurring synchronously, mostly in the GABAergic population projecting back to the inferior olive (Hoebeek et al, 2010) (**Figure 15Bi, ii**).

The excitatory drive exerted by mossy fibre and climbing fibre collaterals, which are much less convergent than the Purkinje cell inputs, is in overall shut down by the net inhibitory tone. However, the coordinated spatiotemporal patterns of cerebellar cortical activity may provoke network excitability oscillation in the deep cerebellar nuclei which would boost the efficacy of the direct excitatory drive (De Zeeuw et al., 2008). Moreover, excitatory and inhibitory nucleocortical circuits are known to participate in the coordination of the deep nuclei and cortex and to have important physiological roles during behaviour and learning (Gao et al., 2016) (**Figure 15Biii**).

Thus, oscillations across all elements of the cerebellar circuit may play a crucial role in shaping the cerebellar output and coordinating activity across long-range cerebello-cerebral networks. This is a fundamental aspect of my PhD research and thus, a brief description of the cerebellar oscillations will be now presented.

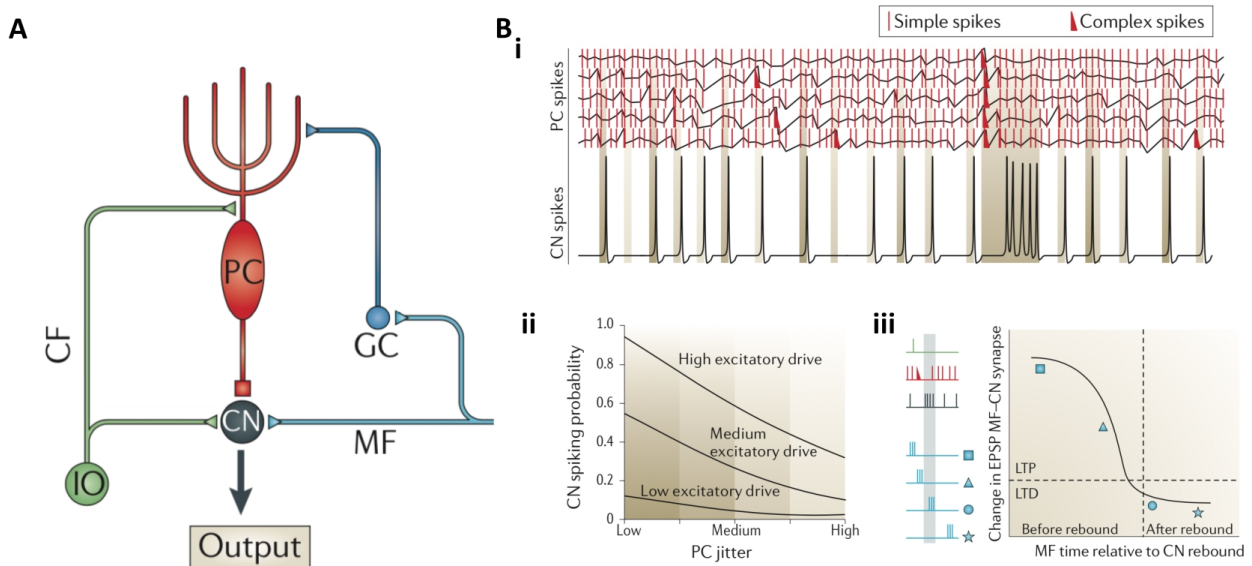


**Figure 15. Read-out of patterns in cerebellar nuclei.** **A)** Schematic representation of the fundamental circuit between the cerebellar inputs, the inferior olive (IO) and the mossy fibres (MF), the cerebellar cortical neurons, the granule cells (GC) and the Purkinje cells (PC), and the deep cerebellar nucleus (CN). The output of the cerebellum will be determined by the spatio-temporal integration of all these inputs onto the deep cerebellar nucleus **B, i)** Example of the temporal pattern of activity of five Purkinje cells innervating a single cerebellar nuclei neuron and the firing of that cell. When the level of synchrony between the different Purkinje cells increases (shaded areas) the probability of rebound firing in the deep cerebellar nucleus also increases. When the complex spikes are temporally aligned the deep cerebellar cell presents a strong rebound firing. **ii)** Plot representing the increase in cerebellar nucleus firing probability with the reduction of the jitter in the inputs from the different Purkinje cells. **iii)** The temporal relationship between the activity of all the elements in the cerebellar circuit determines the plasticity rule obtained in the synapses between the parallel fibres and the Purkinje cells. For a given pattern of activity from the inferior olive (in green), the Purkinje cell (in red) and the cerebellar nuclei cell (in black), different timings of a similar input from the mossy fibres (in blue) drive a completely different level and sign of plasticity (all panels in the figure adapted from De Zeeuw et al., 2011).

### 1.4.3 OSCILLATIONS IN THE OLIVOCEREBELLAR SYSTEM

The main body of electrophysiological studies performed in the cerebellum is composed exclusively of single unit and intracellular recordings. While the relevance of these techniques is out of question, they neglect an important component of the organization of activity in the network, that is the synchronicity of the cell populations and their relationship to the local field potential oscillations (Isope et al., 2002). Whereas the oscillatory activity in other regions of the nervous system has been extensively study (Buzsaki, 2006), not much is known about the oscillations in the cerebellum. Recently, the main oscillatory

phenomena observed in the olivocerebellar system were reviewed by Courtemanche and colleagues (Courtemanche et al., 2013) (**Figure 16**).

As previously mentioned, clusters of electrically coupled neurons in the inferior olive show coherent intrinsic membrane oscillations (Llinás et al., 1974). In vitro, these oscillations were found in the range of 1-7 Hz while in vivo they were found at 6-12 Hz (Chorev et al., 2007). Importantly, they underwent phase reset upon external stimulation (Leznik et al., 2002), a mechanism which has been hypothesized to be determinant for transmitting the error signal to the cerebellar cortex (Llinás, 2009). Moreover, these coherent subthreshold oscillations in the inferior olive are under control of the cerebellar nuclear inhibitory input (Lefler et al., 2014), further supporting the functional relevance of this synchronous activity.

In the granule cells layer, the main oscillatory component in rats, both awake and anaesthetized, was found in the 5-12 Hz range. The power of this activity was maximal during periods of immobility and they correlated with the multiunit activity of the granule cells and weakly with Purkinje cell simple spikes. Similar patterns were obtained in primates but the 14-20 Hz range (Courtemanche et al., 2013). The mechanisms underlying these oscillations rely on the organization of the synaptic inputs, the intrinsic connectivity between mossy fibres, granule cells and Golgi cells (Solinas et al., 2007; Dugué et al., 2009) and the intrinsic properties of the granule cells membrane (D'Angelo et al., 2001). The functional relevance of these slow oscillations in the granule cell layer has been mainly addressed through the analysis of their synchronization across different cerebellar regions or between the cerebellum and other brain regions. Regarding the former, coordinated activity was tested in the paramedian lobule in primates between two electrodes placed in the sagittal and the coronal planes. While under rest conditions coordination was restricted to the sagittal plane, suggesting a zonal organization, when animals performed a task of active expectancy, both sagittal and coronal synchronization was observed (Courtemanche et al., 2009). This suggested that the level of granule cells inter-modular coordination is dynamically modulated depending on the behavioural demands. Synchronicity in the granule cell layer oscillatory range was also tested between paramedian lobule and primary somatosensory cortex or primary motor cortex in primates performing active versus passive expectancy tasks (Courtemanche and Lamarre, 2005). High levels of coordination were preferentially found during active expectancy with the former suggesting functional engagement of both regions during the task. Interestingly, in rats, coherence in the granule cell layer oscillatory range (5-12 Hz) between Crus II and primary somatosensory cortex was also observed during free whisking (O'Connor et al., 2002) further suggesting functional communication during sensorimotor integration. Furthermore, synchronization in the same frequency range has been observed between the fastigial nucleus and the prefrontal cortex suggesting that deep cerebellar nuclei also exhibit oscillatory activity supportive of long-range interactions (Watson et al., 2014).

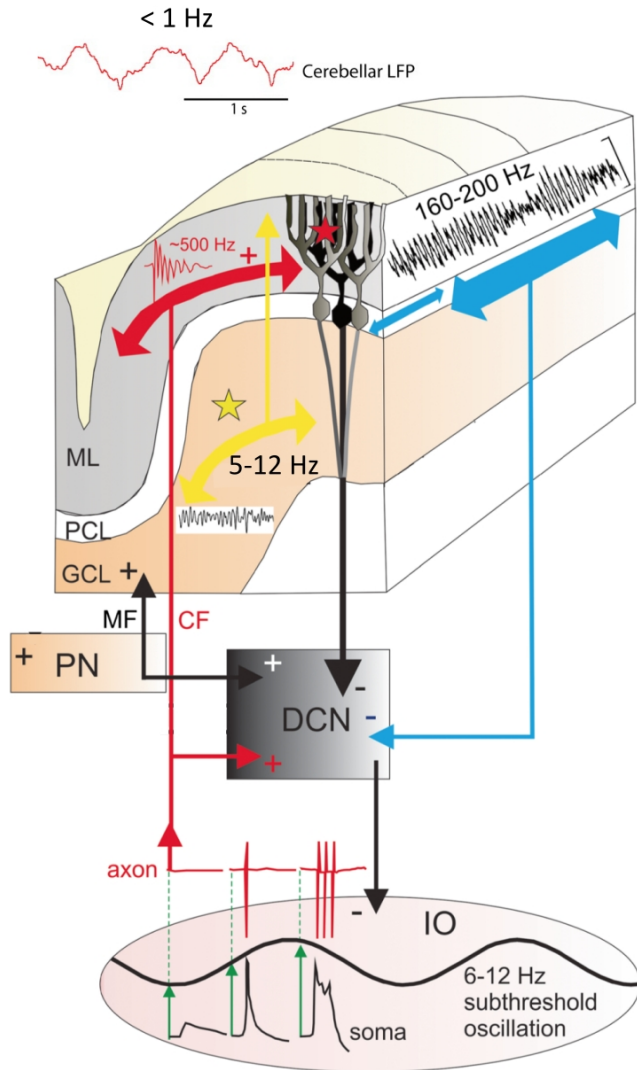


**Figure 16. Oscillations in the cerebellar circuits.**

Oscillatory activity in the cerebellar circuits have been identified at multiple locations. First, the inferior olive present sub-threshold oscillations in the range of 6-12 Hz in vivo which entrain the firing of the nuclear neurons and the climbing fibre input to the cerebellum. This activity generates a complex spike, a short burst of ~500 Hz, which plays an important role in the induction of plasticity (red star). In the granule cell layer the main oscillatory activity in rodents is also in the 5-12 Hz range. These oscillations are mainly coordinated in the parasagittal plane during rest (yellow arrow) but they can spread also transversally during specific behaviours. They also play a role in the plasticity in the granule cell layer (yellow star). In the Purkinje cell layer, the oscillations are dominated by a high frequency component (between 160 – 200 Hz). A higher peak up to 250 Hz have been also reported in awake rats. Finally, infra-slow oscillations (<1 Hz) in the local field potential recorded ifrom the cerebellar cortex have been observed in mice under anaesthesia and awake. They seem to be entrained by neocortical slow oscillations. (Adapted from Cheron et al., 2015 and Ros et al., 2009)

The activity in the Purkinje cell and molecular layers is dominated by a high frequency component (higher than 150 Hz) in different species such as cat (Isope et al., 2002), mouse (Cheron et al., 2005) and rats (de Solages et al., 2008; Middleton et al., 2008). They are locally generated, most likely through a mechanism implicating the recurrent Purkinje cell collaterals. Moreover, intra-cerebellar synchronization at this frequency range, both at sagittal and coronal planes, seems to be equally restricted to a small area (around 250  $\mu\text{m}$ ) (de Solages et al., 2008).

Finally, the presence of infra-slow oscillations (below 1 Hz) both in the Crus II of both anaesthetized and awake mice suggest an entrainment of the cerebellar cortex by the neocortex (Ros et al., 2009). The highly correlated cerebellar multiunit activity further support a local generator of these oscillations rather than a volume conducted signal from a distant region. Entrainment of hippocampal activity by the neocortical slow-oscillations is observed during non-REM sleep and participates in the process of memory consolidation (Latchoumane et al., 2017).

#### 1.4.4 MULTIPLE PLASTICITY SITES IN THE CEREBELLAR CIRCUIT

Since the demonstration by Ito (Ito and Kano, 1982) of the predicted role of a long-term depression mechanism between the parallel fibres and the Purkinje cells controlled by the co-occurrence of climbing fibre and parallel fibre excitation proposed by Albus (1971), most of the attention regarding plasticity rules in the cerebellar circuitry has been focussed on this particular area. While some work has challenged the central role of long-term depression and even proposed long-term potentiation at the same synapses as the main mechanism for cerebellar learning, at least in certain cerebellar regions and certain learning paradigms such as those involving in visuo-vestibular processing (Schonewille et al., 2011), recent findings emphasize the general principle proposed by Ito (Yamaguchi et al., 2016; Kakegawa et al., 2018; see also Yamazaki and Lennon, 2019). However, whereas such a mechanism is undeniably important, other plasticities operate at many other locations in the circuit. Indeed, to the date at least 9 sites have been identified including granule cells layer, molecular layer and deep cerebellar nuclei (see D'Angelo, 2014 for a review) (**Figure 17**). Affecting different plasticities at different sites has specific impacts on the cerebellar function (for instance, see Rochefort et al., 2011 and Lefort et al., 2019). In order to fully understand the governing principles of learning in the cerebellum, all these plasticities sites and rules need to be considered as part of an integrated closed loop in which they work in a synergistic manner (Gao et al., 2012; Mapelli et al., 2015).

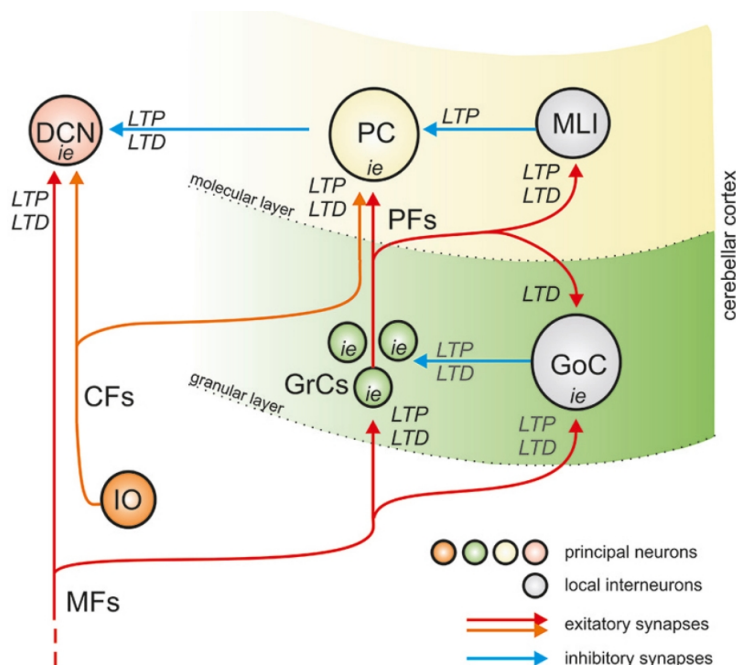


**Figure 17. Synergistic plasticity in the cerebellar circuit.** Schematic representation of the cerebellar circuit and all the sites where plasticity has been described. In the granule cell layer, plasticity may serve to improve spatio-temporal recoding of mossy fibre inputs into new granule cell spike patterns. This patterns may be stored in a distributed network in the Purkinje cells and molecular layer interneurons through multiple plasticity mechanisms entrained by the climbing fibre activity. All these mechanisms shape the cerebellar cortical output which interact in the deep cerebellar nuclei with their own plasticity-dependent stored information. (From Mappelli et al., 2015).

**CHAPTER 2:**

**Cerebro-cerebellar loops: Beyond motor control**



As introduced before, the cerebral cortex and the cerebellum are bidirectionally connected through multiple pathways. While multiple brain cortical regions send inputs to the cerebellum through two routes, one through the pontine nuclei which end as mossy fibres and the other relaying in the inferior olivary complex which send then climbing fibres, cerebellum sends information to the cerebrum mainly through cerebello-thalamo-cortical connections.

The classical theories about the functional role of the cerebellum has always been influenced by the main phenotypical spectrum observed after lesions or deficits of the cerebellar structure, that is, different motor disorders characterized by the preserved ability of generating movements but a clear inability in coordinate, adapt and temporally structure them (Holmes, 1917). Based on these observations, the interpretation about the profuse cortico-cerebellar projections was that it may primarily come from motor or sensorimotor related cortices (Evarts and Thach, 1969) in order to provide the cerebellum with the information needed to coordinate, correct and adapt the ongoing movements during behaviour (Allen and Tsukahara, 1974). Following a similar logic, the cerebello-thalamocortical projections were supposed to be concentrated in the thalamic regions involved in motor functions that would then relay the cerebellar information back to motor related cortices (Evarts and Thach, 1969; Allen and Tsukahara, 1974). Under this perspective, although the nature of the inputs was found to be clearly motor and non-motor (Wiesendanger and Wiesendanger, 1982a,b), the cerebellar output would remain exclusively under the motor domain.

The development of advanced anterograde and retrograde trans-synaptic tracing techniques provided an absolute breakthrough for the understanding of long-range neuronal networks, which impacted particularly the study of those regions that connect mainly through poly-synaptic pathways, including the cerebellum. Thus, it was proved early that profuse connectivity exists between the primary motor or the premotor cortices and the cerebellum (Brodal, 1978), as well as between the deep cerebellar nuclei and the ventrolateral thalamic nucleus, part of the so-called motor-thalamus (Angaut et al., 1985). However, it was similarly found that the cerebellum not only receives cortical information from virtually all cortical regions (Wiesendanger and Wiesendanger, 1982a, b), but it also projects to associative divisions of the thalamus that relay cerebellar information to a broad range of cortical areas implicated in different non-motor or cognitive processes (Jones, 1985). Moreover, the corticocerebellar and the cerebello-cortical pathways were found to be organized in parallel closed loops emphasizing the integration of the cerebellum in different neural networks potentially involved in motor and non-motor functions (Kelly and Strick, 2003).

The existence of such connectivity was difficult to conceal with the early cerebellar models, which needed a profound reinterpretation. Soon, the purely motor centred interpretation of the cerebellar function was extended to a broader sensorimotor domain. But, how could this explain connectivity with high order associative areas such as prefrontal cortex (Kelly and Strick, 2003)? Other hypotheses postulated that the

cerebellum carries out a reference frame transformation centred in the ongoing motor state, what could explain why all cerebral regions interact somehow with the cerebellum (Kawato, 1999). However, a growing body of evidence clearly suggest that the cerebellar roles extend beyond the motor domain and that it is engaged in many cognitive functions (see Koziol et al., 2014). For instance, a variety of cognitive deficits were added to the well-established motor deficits associated to cerebellar pathologies (see Schmahmann, 2019) and recently, cerebellar structural alterations have been associated as a robust risk factor for general psychiatric disorders (Romer et al., 2018), convincing even to prior detractors of the potential role of the cerebellum in cognitive processes (Hariri, 2019). Moreover, recent findings demonstrated cerebellar involvement in the maintenance and stabilization of the hippocampal cognitive maps (Rocheffort et al., 2011; Lefort et al., 2019) or in social behaviour through a direct projection to the ventral tegmental area, a dopaminergic region implicated in the reward circuitry in the brain (Carta et al., 2019).

The organization of cerebro-cerebellar connectivity and the involvement of the cerebellum in non-motor functions are central concepts for the conceptual development of my thesis. Thus, in this chapter I will focus precisely on the cerebello-cerebellar pathways, their anatomo-functional organization and how they may support cerebellar engagement in non-motor functions.

## **2.1 ANATOMICAL SUBSTRATES FOR CEREBRO-CEREBELLAR LOOPS**

### **2.1.1 PROJECTIONS FROM THE CEREBRUM TO THE CEREBELLUM**

As mentioned in the introduction of this section, the cerebral cortex reaches the cerebellum via two pathways. The first one derives from collaterals of the corticospinal tract generated in the motor cortex that contact the red nucleus which in turn projects to the inferior olive (Humphrey et al., 1976, 1984). The second one is the corticopontine pathway which, unlike the previous one, is composed by descending axons originated in an enormous variety of cortical areas, ranging from motor, premotor, supplementary motor or primary somatosensory cortices (Brodal, 1978) to the prefrontal, parietal, parahippocampal or cingulate cortices (Leergaard and Bjaalie, 2007), that is, virtually from all the cortex (**Figure 18A**). Interestingly, the different cortical afferents route through discrete and different pontine nuclei or subpopulations establishing parallel tracks (Leergaard and Bjaalie, 2007) (**Figure 18B**). These discrete populations give rise to the mossy fibres that reach specific cerebellar regions: the anterior lobe receives mainly motor and premotor information while the posterior lobe receives both premotor and prefrontal information (in the hemispherical Crus I), motor information (in Crus II) and somatosensory and parietal association areas information (in the paramedian lobe) (Brodal, 1979). All this anatomical mapping was performed in primates and cannot be assumed to be similar in other species, particularly in evolutionary distant mammals as the rodents. In particular, the cerebellar hemispheres, which are precisely the main recipient of the cortico-ponto-cerebellar projections (Brodal, 1979), have undergone a great expansion during anthropoid ape evolution (Whiting and Barton, 2003). However, a recent comparative study between

rodent and primate cerebellar organization has identified homology between the Crus I in rodents and the Crus I and Crus II in primates (Sugihara, 2017).

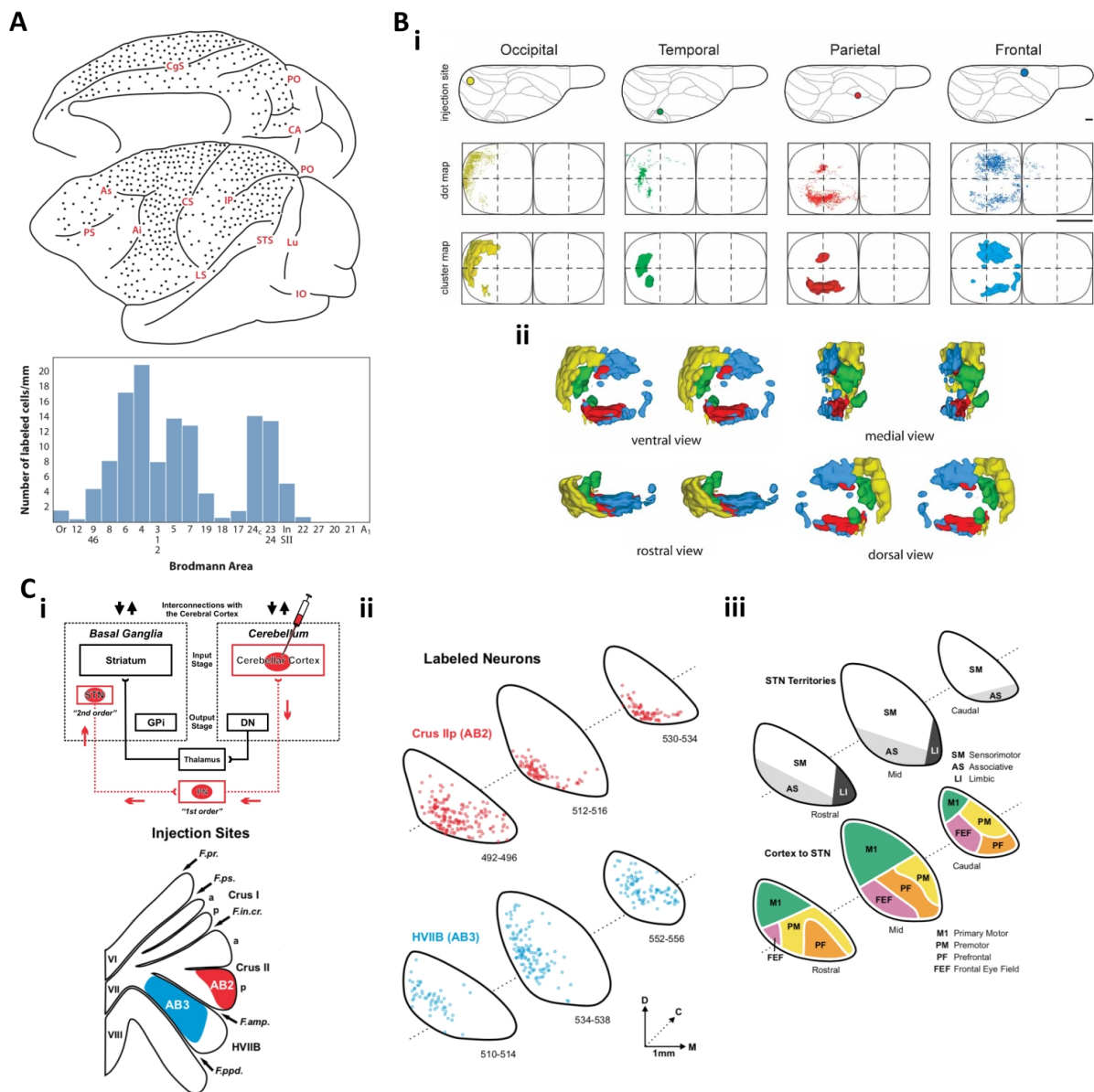


**Figure 18. Cerebral inputs to the cerebellum.** **A)** Schematic representation of the relative density of corticopontine projecting neurons (indicated by the dots) in the brain of the macaque (top). The actual density values for different cortical areas are plotted in the bottom. Note the spread of the cortico-pontine projections to almost all the cerebral cortex (From Strick et al., 2009). **B, i)** Discrete injections of anterograde tracers in different cortical areas in the rat revealed topographically restricted projections to the pontine nuclei which establish three-dimensional domains (iii) (from Leergaard and Bjaalie, 2007). **C, i)** Experimental design in which injections of rabies virus, retrograde trans-synaptic tracer, into discrete cerebellar cortical areas were used to identify the projecting di-synaptic pathways between the basal ganglia and the cerebellum in primates (top). The injection sites were located in the lateral Crus II and the hemispherical part of lobule VII (HVII) (bottom). **ii)** Rabies positive cells were found in the subthalamic nuclei (STN) after injections in both locations, however, they occupied different topographic distributions. **iii)** The labeled cells after Crus II injections were located in the associative territory of the STN where while HVII injections labeled cells were in the sensorimotor domain (from Bostan et al., 2010).

Apart from the cerebral cortex, the basal ganglia, a subcortical region implicated in a plethora of motor and non-motor functions (see Middleton and Strick, 1994), was found to project also to the cerebellar cortex through pontine nuclei relay in primates (Bostan et al., 2010) (**Figure 18C**). The projections arise from multiple domains of the subthalamic nuclei and keep separate pathways which terminate in discrete locations in the cerebellar hemispheres: Crus II receives inputs originated in associative territories of the subthalamic nucleus (see Parent et al. 1995 for a functional subdivision) while the hemispherical part of the lobule VII was contacted by projections coming from the sensorimotor territory. This was the first demonstration of a direct influence of the basal ganglia onto the cerebellum, two structures that until then were thought to work in parallel networks which subserve to different aspects of motor control (Doya, 2000).

If as it seems to be the case, the only route for non-motor information towards the cerebellum is through the pontine nuclei-mossy fibres projections and no olivocerebellar inputs carries such information, the potential mechanisms underlying cerebellar learning, which highly depends on the climbing fibre activity, would be difficult to infer. However, in an electrophysiological mapping study carried out in rats a novel prefrontal cortex-olivo-cerebellar pathway was proposed (Watson et al., 2009). While no anatomical supporting data was presented, these results open the door to the existence of cortico-olivo-cerebellar pathways from non-motor cortical areas.

### 2.1.2 PROJECTIONS FROM THE CEREBELLUM TO THE CEREBRUM

All the cerebellar nuclei send projections to the cerebral cortex through cerebello-thalamo-cortical pathways (**Figure 19A**). However, the dentate and interposed nuclei seem to be more profusely interconnected. That is in line with the preferential involvement of the cerebellar hemispheres in such pathways. Once again, a fine topographical organization is maintained all along the connections. Early studies from Strick and colleagues using transneuronal tracers in primates demonstrated the division of the dentate nuclei in motor and non-motor domains (see Dum and Strick, 2003) (**Figure 19Aiii**). The rostro-dorsal motor domain maintains the somatotopic organization found in the anterior zone of the cerebellum, which is its main input, and projects through different portions of the ventrolateral thalamic nucleus to primary motor, supplementary motor and premotor areas (Schell and Strick, 1984; Middleton and Strick, 1997). On the other hand, Crus II in the cerebellar cortex projects to different output channels in the ventro-caudal non-motor domain which then connect with multiple areas in prefrontal and posterior parietal cortices through thalamic relay in a different subset of ventrolateral thalamus territories (**Figure 19Aiv**).

Apart from the projection through the ventrolateral thalamic nuclei, the cerebellar nuclei also send efferent projections to ventromedial and intra-laminar thalamic nuclei (centromedian, centrolateral and parafascicular), which are considered associative thalamus (**Figure 19Aii**). Except for the dentate nuclei, to date we lack a systematic anatomo-functional dissection of the preferential thalamic target for individual

cerebellar nuclei and their further projections to the cerebellar cortex. Few early studies performing electrophysiological mapping suggested a cerebellar projection from the cerebellar vermis and the fastigial nucleus to limbic structures such as the cingulate cortex, the amygdala or even the hippocampus (Annad et al., 1959; Snider and Maiti, 1976). However, the anatomical substrate for such projection continued elusive. In general, in contrast to the massive cerebro-ponto-cerebellar projection, the cerebello-thalamic pathways are much less dense. However, electrophysiological studies have shown that they are rather powerful. For instance, a recent study tracking the projections from interpositus nucleus in mice found a dense and powerful innervation of the ventrolateral nucleus and minor innervation of the ventromedial and centrolateral nuclei (Gornati et al., 2018).

The thalamic nuclei are composed of heterogeneous cell populations which have been classically divided as “core” or “matrix” neurons (Jones, 1998), although more recent categorisations expand this concepts in order to capture the diversity existent in higher associative thalamic nuclei (Clascá et al., 2012). The former projects in a topographically restricted manner to middle layers of the cortex and may thus transmit its driver input in a receptive field like manner. The latter, on the other hand, sends more diffuse projections to many cortical regions mainly in superficial layers and may have a large network effect (Jones, 1998). The ventrolateral thalamic nucleus is composed of a majority of core neurons (Kuramoto et al., 2009) while the other cerebellar-recipient thalamic nuclei contain more matrix neurons (Deschènes et al., 1996; Kuramoto et al., 2015). This could explain why the main cerebello-thalamic pathway target the ventrolateral nuclei which, in order to transfer topographically restricted information to the cortex, may require more dense projections.

Apart from the main cerebello-thalamo-cortical projections, another pathway may relay cerebellar information to the cortex. For instance, recent finding demonstrated the existence of direct monosynaptic pathway from the deep cerebellar nuclei to the ventral tegmental area (Carta et al., 2019). The ventral tegmental area sends profuse dopaminergic inputs to a wide range of cortical areas, such as prefrontal cortex or the hippocampus; and sub-cortical areas, like the striatum (Beier et al., 2015). Thus, the cerebellar-ventral tegmental area projections may reach and modulate activity in the cerebral cortex through direct (without a subcortical relay) or indirect (relaying in some of the subcortical targets) pathways. Other modulatory pathways may involve other brainstem nuclei in the hypothalamus or the raphe, for instance, which are known to receive direct cerebellar inputs and to project direct and indirectly to cerebral cortex (see for instance Steinbusch et al., 1978 and Teune et al., 2000).

Finally, both motor and non-motor domains of the dentate nucleus, as well as a less prominent population in fastigial and interpose nuclei, in the primate cerebellum were found to also project to the striatum through thalamic relay in the intra-laminar and ventrolateral nuclei (Hoshi et al., 2005) (**Figure 19B**).

Interestingly, di-synaptic pathways from the cerebellum to the striatum have been demonstrated in rats (Ichinohe et al., 2000) as well as in mice (Chen et al., 2014).

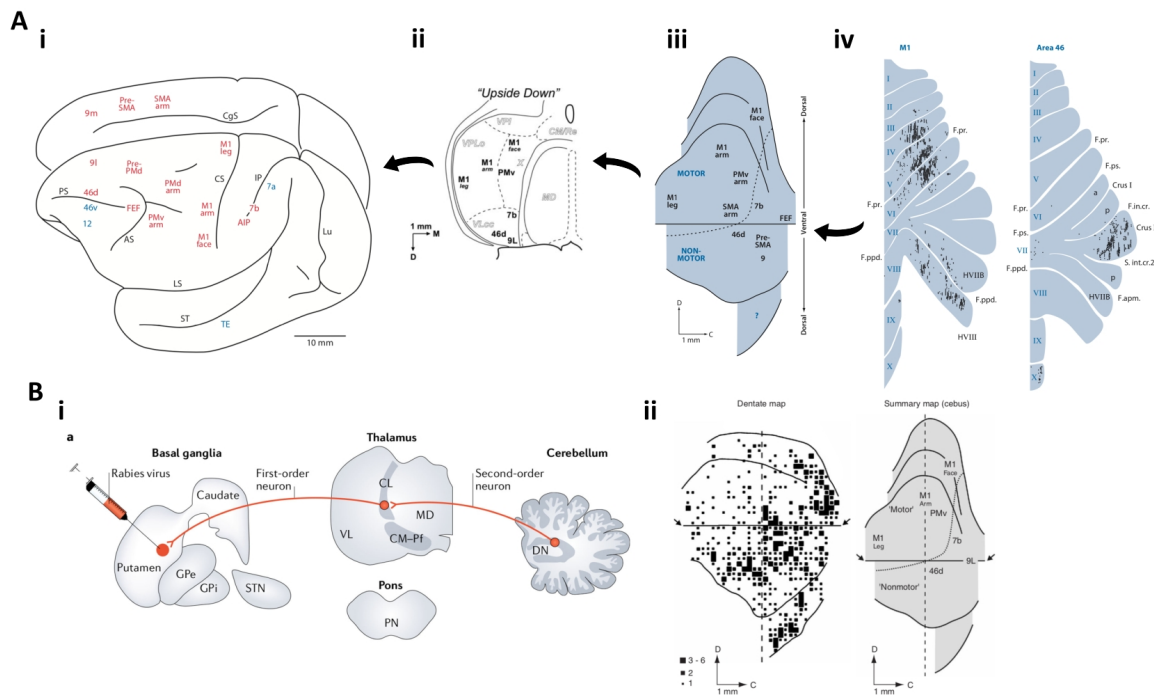


**Figure 19. Cerebellar projections to the cerebrum.** **A, i**) Schematic representation of the macaque brain with the regions receiving cerebellar projections coloured in red and those that don't receive any coloured in blue. In black are indicated the main brain sulcus. **ii**) The projections to specific cortical regions route through different subregions of specific thalamic nuclei. **iii**) Based on the distribution of the output channels in the dentate nuclei, a rostro-dorsal motor domain and a ventro-caudal non-motor domain can be distinguished in primates. Moreover, a somatotopic map of the body is maintained in the motor domain. **iv**) Finally, topographically restricted areas of the cerebellar cortex project to specific cortical areas. Projections to higher association areas as the prefrontal cortex arise preferentially from the hemispherical Crus II while projections to the motor cortex are distributed in the anterior and posterior zones (all panels from Strick et al., 2009 except panel ii, from Dum and Strick, 2003). **B, i**) Injections of rabies virus in the putamen in the basal ganglia revealed a di-synaptic projection from the dentate nucleus relayed in the central lateral thalamic nucleus (CL) (From Bostan and Strick, 2018). **ii**) The density of these projections is represented by increasing size black squares and is plotted on an unfolded schema of the dentate nucleus of primate. Projections to the basal ganglia are sent from the motor and non-motor domain, however, higher density is seen in the non-motor ventro-caudal portion (From Hoshi et al., 2005).

### 2.1.3 CLOSED-LOOPS IN THE CEREBRO-CEREBELLAR PATHWAYS

As it may be noticed, most of the cortical regions which project to the cerebellum through pontine relay receive also a cerebellar projection after a relay in the thalamus. Indeed, the few cortical regions that do not project to the cerebellum are consistently devoid of cerebellar inputs. If we also consider that all these pathways run as parallel discrete routes then it may be asked whether this organization reflects the establishment of cerebro-cerebellar loops.

Again here, the group of Peter Strick gave an exceptional use to the technical approach of the trans-synaptic tracing and, in particular, the combination of anterograde and retrograde tracers. In a seminal work (Kelly and Strick, 2003) they injected rabies virus, an efficient trans-synaptic tracer, in one of two different cortical regions, the primary motor cortex in the arm area or the dorsolateral prefrontal cortex, of primates. Once identified the exact distribution of Purkinje cells projecting to those cortical regions, they injected a herpes virus strain, which is trans-synaptically transmitted anterogradely, into the same cortical location to explore this time the distribution of granule cells. They observed a striking overlap between the Purkinje cells projecting to and the granule cells receiving from a particular cortical region demonstrating the organization of the cerebello-cerebral circuits in closed-loops (**Figure 20A**). This finding further supported the idea of specific cerebellar regions engaged in independent long-range networks involved in both motor and non-motor functions.

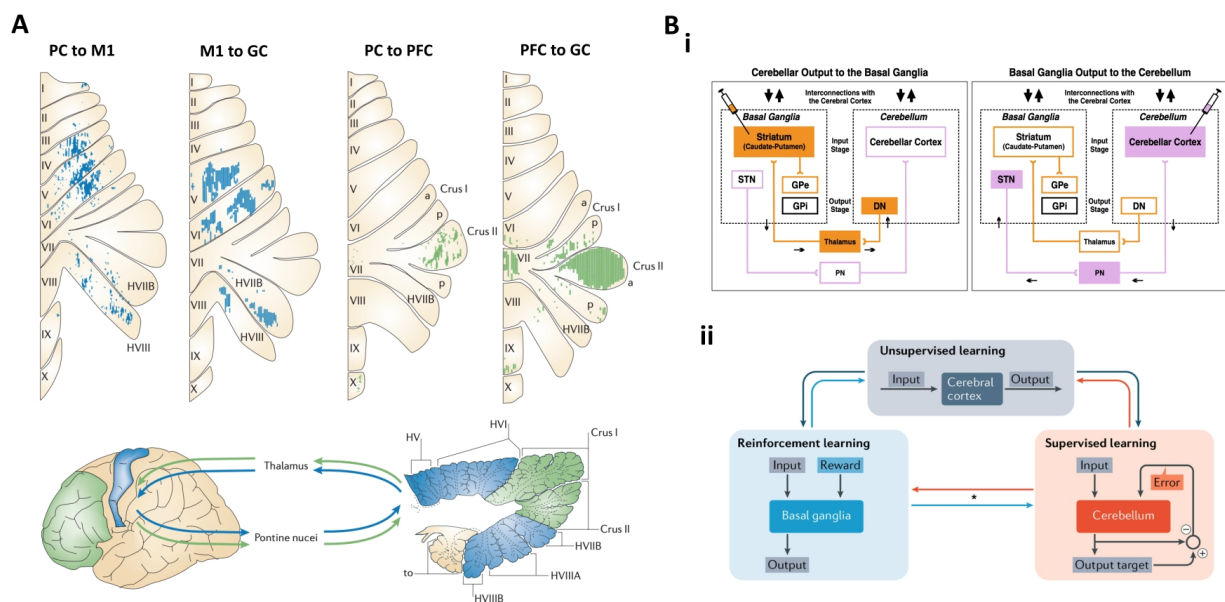


**Figure 20. Cerebro-cerebellar loops.** **A**) Reconstruction of the cerebellar areas projecting to and receiving information from the motor cortex (M1, in blue) and the prefrontal cortex (PFC, in green) obtained employing dual retrograde trans-synaptic tracing strategies (top). Note the overlap between areas containing Purkinje cells projecting to the cortex and granule cells receiving projection from the same cortical area. This results evidenced the organization of the cerebro-cerebellar circuits in closed loops of cortico-ponto-cerebello-thalamo-cortical connectivity (bottom) (From Ramnani, 2006). **B, i**) Schema representing the circuits interconnecting the cerebellum and the basal ganglia and the experimental paradigm employed to reveal such connectivity. Injections of rabies virus in the striatum allowed the identification of di-synaptic projections from the dentate nucleus (DN) through thalamic relay as well as a tri-synaptic projection to the external globus pallidus (Gpe). When the injections were located in the cerebellar cortex, a di-synaptic projection from the subthalamic nucleus (STN) with relay in the pontine nuclei (PN) were also revealed. Thus, a cerebello-basal ganglia open loop is established (from Bostan and Strick, 2010). **ii**) Different computational operations, a reinforcement learning in the basal ganglia and a supervised learning in the cerebellum, can be performed in parallel but in a concerted manner thanks to the interconnectivity between them and the cerebral cortex, which itself is specialized in performing unsupervised learning (from Bostan and Strick, 2018).

While the anatomical connectivity linking the cerebellum and the cerebrum seems to follow the general rule of being organized in separate closed-loops, the existence of open loops or convergent rather than separated pathways has been also observed. For instance, the previously described connectivity between basal ganglia and cerebellum may not strictly acquire the form of a closed-loop but a reciprocal connectivity with the neocortex that allow both systems to interact in a functional network contributing with parallel computational programs during behaviour (Bostan and Strick, 2010) (**Figure 20 Bi**). In particular, it has been proposed that the cerebellum may apply supervised learning strategies while the basal ganglia uses reinforcement learning. Both strategies may complement each other and contribute to the unsupervised learning performed in the cerebral cortex (Doya, 2000; Bostan and Strick, 2018) (**Figure 20Bii**). Examples of convergence can be identified at different stages of the circuit, for example, inputs from the vibrissa related primary sensory and primary motor cortices route through separate pontine pathways but converge in the Crus I lateral region of the cerebellar cortex in mice providing a demonstration of anatomical substrates for sensorimotor integration (Proville et al., 2014). Another example of potential convergence in the cerebello-cerebral system is the reduction of functional interaction through gamma band oscillatory synchronization between primary sensory and primary motor cortices during whisking when the deep cerebellar nuclei are silenced (Popa et al., 2013) suggesting a role of the cerebellum in coordinating both cortical regions during sensorimotor control.

## **2.2 PHYSIOLOGICAL EVIDENCE FOR CEREBELLAR ENGAGEMENT IN NON-MOTOR FUNCTIONS**

### **2.2.1 FUNCTIONAL RELEVANCE OF THE ANATOMICAL PATHWAYS**

While the insights obtained from the anatomical studies were fundamental in shaping the concept of the cerebellum as a node in a plethora of long-range neural networks involved in many motor and non-motor functions, a further analysis of their functional relevance is fundamental and still in its infancy. As occurred with the development of tracing techniques for the anatomy, main advances in functional and physiological cerebellar research have been achieved thanks to the development and employment of powerful technical approaches in animal models. In particular, the development of highly dense recording techniques, both imaging and electrophysiological; and tools that allow to control specific populations with high temporal resolution, like optogenetics, have increased our potential to unravel the functional role of cerebellum in non-motor functions.

For instance, in a recent study employing local optogenetic silencing of Purkinje cells combined with electrophysiological and functional magnetic resonance imaging in mice the functional relevance of many of the anatomically confirmed pathways was further demonstrated (Choe et al., 2018) (**Figure 21A**). They specifically target a region between lobules V and VI near the lobule simplex which is known to drive motor responses in the forelimb. They were able to track responses, through changes in blood-oxygen-level-dependent signals and single cell firing, in a broad range of cerebral regions including motor, retrosplenial

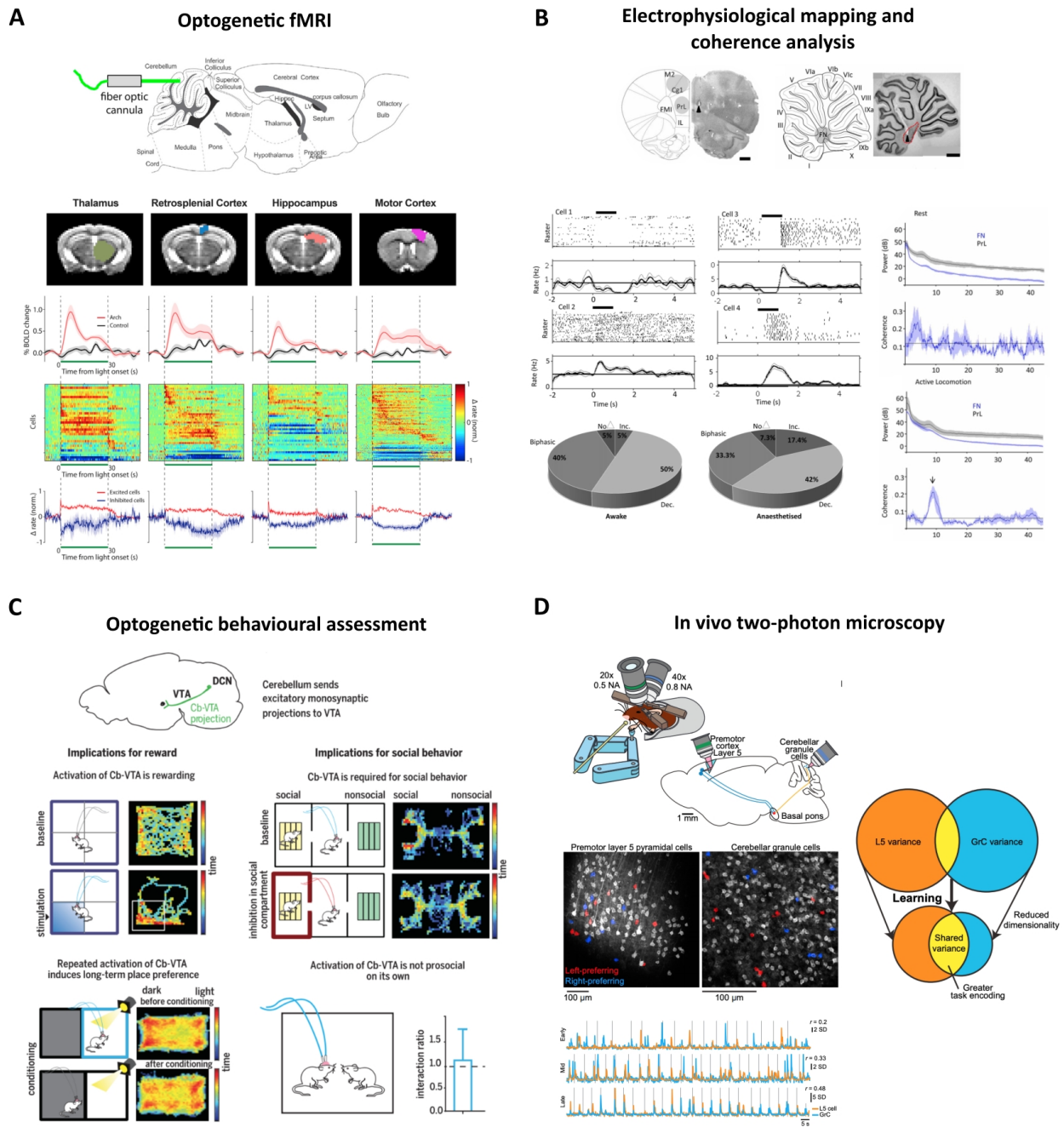


**Figure 21. Recent methodological approaches for demonstrating the functional relevance of the anatomical cerebello-cerebral pathways.** **A**) By combining optogenetic manipulation of the cerebellar circuits with functional magnetic resonance imaging (fMRI) and electrophysiological recordings in mice, a whole brain mapping of the functional connectivity of a cerebellar region was achieved. Responses at the level of blood-oxygen-level dependent (BOLD) signals and single cells activity were observed in broad cerebral regions (from Choe et al., 2018). **B**) Simultaneous electrophysiological recordings of single cell and local field potentials activity in the cerebellar fastigial nucleus and the prefrontal cortex of rats allowed to perform electrophysiological mapping of the responses in the latter after stimulation of the former as well as measurement of synchrony of the oscillatory activity between the two structures. Both evoked activity and oscillatory coupling was observed and showed dynamic modulation depending on the behavioural state (from Watson et al., 2014). **C**) By selectively optogenetically activating the deep cerebellar nuclei (DCN) projections to the ventral tegmental area (VTA) in mice in vivo allowed to demonstrate the functional relevance of these connections as well as to dissect the specific contribution of the cerebellum in modulating reward-dependent behaviours such as

place-preference or social behaviours (from Carta et al., 2019). **D)** Recording the activity of hundreds of cells simultaneously in the premotor cortex and the granule cell layer of the cerebellar area which is anatomically connected with the former thanks to the employment of dual two-photon calcium imaging in mice performing a goal-directed movement task allowed to investigate the levels of spatio-temporal correlations between both structures. There was an increase in this correlation during the learning of the task which indicate a faithful transmission of the information only when the animals are actively engaged in the behaviour (from Wagner et al., 2019).

and limbic cortices, thalamus and, notably, hippocampus. Other studies demonstrated the physiological relevance of cerebellar fastigial nucleus projections to the prefrontal cortex in rats not only by recording evoked responses in cell populations but showing the behavioural-dependent synchronization of the oscillatory activity in both regions (Watson et al., 2014) (**Figure 21B**). Indeed, the analysis of the coordinated activity of interconnected regions has been proven to be a powerful tool when studying their dynamic functional engagement and it has been one of the key approaches employed during my PhD.

Moreover, by selectively modulating the cerebellar neuronal populations that project to a particular region in the brain, the specific contribution of the cerebellum to the different networks can be tested. In this regard, the cerebello-striatal circuit was functionally dissected in mice using optogenetic activation specifically of the terminals of dentate neurons in the intra-laminar thalamic nuclei which further reach the dorsal striatum (Chen et al., 2014). They were able to demonstrate the excitatory drive of the cerebellum in this circuit and, furthermore, they shown through it cerebellum can modulate cortico-striatal plasticity as well as impose aberrant activity leading to dystonia. In another study, the same research group identified the monosynaptic connection between the cerebellum and the ventral tegmental area and further demonstrated that this projection is more active during social behaviours and is sufficient to drive rewarding signals, which ultimately modulate them (Carta et al., 2019) (**Figure 21C**).

The employment of *in vivo* two-photon calcium imaging, a technique that allow the visualization of the activity of hundreds of cells simultaneously, has been recently applied in the cerebellar cortex revealing that the granule cells in multiple lobules encode the expectation of reward during a goal-directed forelimb movement task (Wagner et al., 2017). In other study by the same group (Wagner et al., 2019) (**Figure 21D**), they have simultaneously recorded the activity of granule cells in the cerebellum and pyramidal cells in the premotor cortex from areas that are known to be interconnected through a cortico-ponto-cerebellar pathway during a similar task. They have demonstrated that the activity in both areas acquire high levels of spatio-temporal correlation during the execution of the task emerging upon learning. This further suggests that the cortical information is faithfully recapitulated in the granule cell layer once the animals have learned the task.

## 2.2.2 THE CEREBELLAR COGNITIVE AFFECTIVE SYNDROME IN HUMANS

For decades the cerebellum has been neglected from functional imaging studies in humans both under pathological conditions and when testing a plethora of cognitive tests. One of the reasons has been purely technical as the location and structure of the cerebellum makes it difficult to track, especially when we considering relatively old studies. However, with the fast improvement of these techniques during the last decades such limitations have been extremely reduced but yet only a small proportion of the functional imaging studies include the cerebellum in to their analysis. The second, but maybe principal, reason is purely theoretical and implies that most of the researchers in cognitive neuroscience assume that the cerebellum will not be implicated in whatever cognitive function they are testing. Of course, as it has been emphasized multiple times across this introduction, this idea is mainly anchored in the general belief that the cerebellum is a purely motor structure and in the main phenotypical characteristics of the cerebellar deficits, that is, ataxia, dysmetria of the limbs and/or problems with the speech or the oculomotor control.

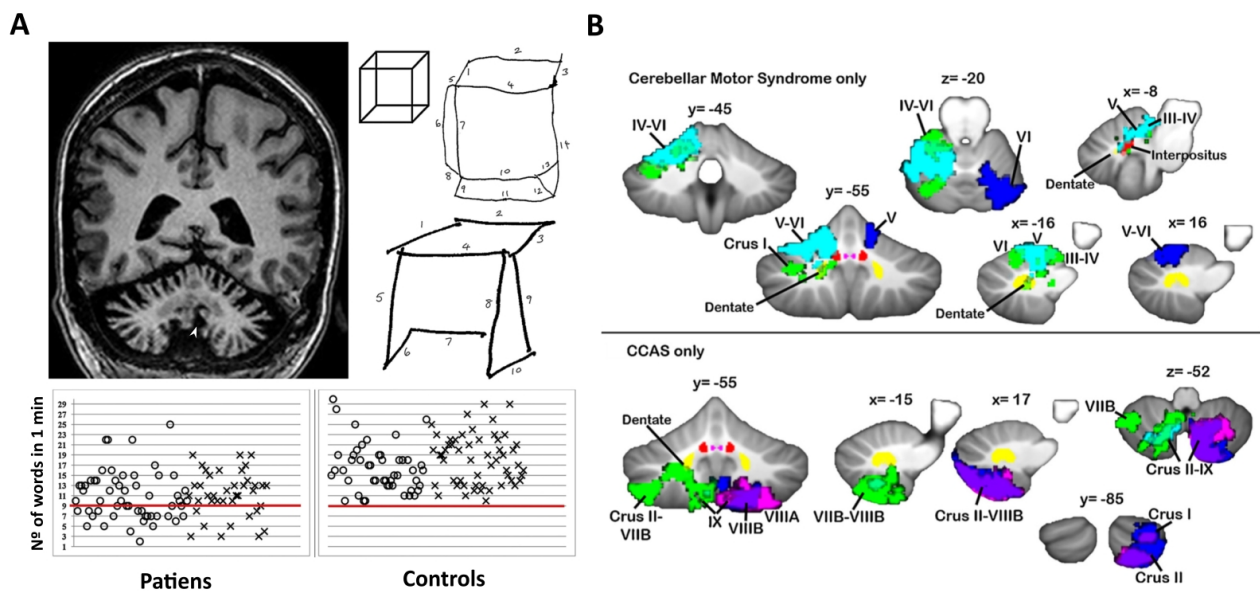
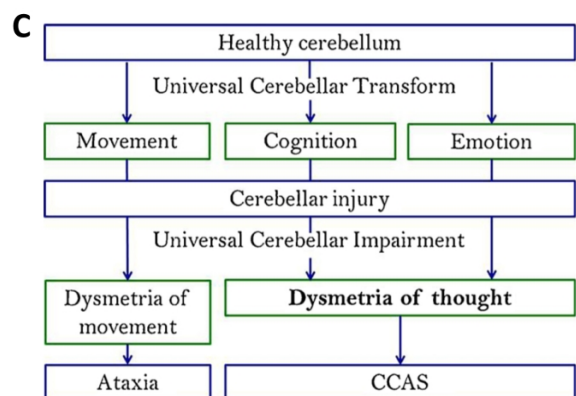


**Figure 22. The Cerebellar Cognitive Affective Syndrome (CCAS).** **A)** Examples of a patient with diffuse cerebellar atrophy (white arrow) and results of a visuo-spatial task where they had to reproduce a cube after verbal description or copy it from a model. At the bottom are plotted the results of a verbal fluency task in cerebellar patients and controls showing worst performance of the formers (the red line indicate cut-off for the task). **B)** Topographical distribution of cerebellar lesions with exclusive motor or CCAS syndrome. Motor deficits were associated with the anterior lobe and CCAS with the posterior lobe. **C)** Schematic of the dysmetria of thought and universal cerebellar transform theories (from Schmahmann, 2019).



With the advent of some of the previously introduced observations from anatomical and functional studies in animal models demonstrating the broad connectivity of the cerebellum with cerebral cortical and subcortical structures implicated in different cognitive functions some clinicians and cognitive neuroscientist started to focus their attention in the cerebellum. In particular, the extensive work from Schmahmann and colleagues during the last thirty years has completely changed the understanding of the clinic and cognitive approach to this structure (see Schmahmann, 2019 for a review). They extended the pathophysiology associated to the cerebellar deficits to a whole range of cognitive and affective impairments, differentiating a motor cerebellar syndrome from a cognitive affective cerebellar syndrome (Schmahmann and Sherman, 1997, 1998) (**Figure 22**). They proposed that the spectrum of symptoms would entirely depend on the cerebellar region affected (**Figure 22B**) and associated the presence of lesions in the posterior cerebellar vermis (mainly lobule VI and VII) and hemispheres (mainly Crus I and Crus II) with a range of impairments in executive function, attention, visuo-spatial memory, inappropriate behaviour, problems in the language production and a net lowering of intellectual function. In an analogy to the motor dysmetria associated to cerebellar damage in the anterior lobe they proposed a dysmetria of thought when the damage is located in those regions. Thus, they assumed the theoretical concept of a universal cerebellar transform, that is, a constant cerebellar computation which is applied invariantly across the whole cerebellum and whose specific output will entirely depend on the kind of information being processed, that is sensorimotor in the anterior lobe of the cerebellum and cognitive in the posterior lobe (Schmahmann and Sherman, 1997; see also Schmahmann, 2019 for a review) (**Figure 22C**).

### 2.2.3 THE CEREBELLUM AS A GENERAL PREDICTOR FOR PSYCHIATRIC DISEASES

From the concept of dysmetria of thought and the broad interconnectivity of the cerebellum with multiple large cerebral networks a new dimension in the understanding of the psychiatric disorders has been recently explored. Indeed, while previous studies have proposed the potential involvement of the cerebellum in, for instance, schizophrenia (Andreasen et al., 1998) or autism disorders (Peter et al., 2016; Stoodley et al., 2017); recent studies found that structural alterations of the cerebellar circuit are a general predictor for common mental disorders (Moberget et al., 2019; Romer et al., 2019).

One of the hypotheses for such broad impact on normal cognitive development is that the cerebellum may play a role during development in the correct wiring in other brain areas (Reeber et al., 2013; Limperopoulos et al., 2014). In a recent study using chemogenetic perturbation of the cerebellar activity at specific locations during a critical period in juvenile mice they found important disturbances of cognitive and social capacities in adulthood (Badura et al., 2018). Interestingly, the impairments were region specific and the acute disruption of the very same regions in the adult shown in general less or no impact, thus pointing to a role of the different cerebello-cerebral pathways in the behavioural maturation in juvenile life.

#### 2.2.4 THE ROLE OF THE CEREBELLUM IN SLEEP REGULATION AND SLEEP DISORDERS

After a series of experiments in cats undergoing partial or total lesions of the cerebellum, its implication in regulating the sleep-wake cycle was clearly established (see De Andrés et al., 2011). The cerebellum is involved in the control of motor activities during sleep such as the postural adjustment and the control of muscle atonia and eyes' muscles activation during REM sleep (Cunchillos and De Andrés, 1982). However, it seems to be involved as well in the intrinsic regulation of sleep cycle as changes in the ratios of wakefulness, drowsiness, non-REM and REM sleep were observed after lesion of the fastigial nuclei, localized cortical regions or the fibre tracks leaving the cerebellum towards the brain (De Andrés et al., 2011). Indeed, antagonistic effects were observed between lesions in the cerebellar cortex or the deep cerebellar nuclei, so that the former induced increased sleep, both non-REM and REM, while the later induced an increase in wakefulness and drowsiness. In parallel to the behavioural observations, some electrophysiological studies showed changes in the cortical electroencephalogram following cerebellar lesions which suggested the implication of cerebello-thalamic projections (Reinoso-Suárez, 1992). Moreover, cerebellar structure and connectivity alterations have been observed in humans in a range of sleep disorders such as chronic and fatal familial insomnia or obstructive sleep apnea. Furthermore, patients of different cerebellar diseases including multiple types of ataxia often manifest in sleep complaints (see DelRosso and Hoque, 2014).

In summary, it seems clear that the cerebellum is part of the large sleep regulating network which involves many subcortical and cortical regions and that its role may be beyond the motor control during different behavioural states in the sleep-awake cycle. However, although there are few studies showing modulation of the cerebellar electroencephalogram and neuronal activity during sleep (see Canto et al., 2017 for a review), our understanding of the cerebellar physiology across different behavioural states is still extremely limited. As part of my PhD research I have also tried to address this issue which is treated in the paper under preparation included in the results.



**CHAPTER 3:**

**Evidence of cerebello-hippocampal interaction**



The previous section emphasized the existence and importance of multiple cerebello-cerebral loops supporting a wide range of cognitive functions such as working memory, attention or emotion. Indeed, several lines of evidences indicate that the cerebellum is also involved in spatial cognition. Despite the intense employment of different animal models with cerebellar specific mutations a doubt remained in the separation of motor versus non-motor deficits (for reviews see Petrosini et al., 1998; Rondi-Reig and Burguière, 2005). Conditional knockout with a specific alteration of plasticities in cerebellum revealed navigation deficits independent of motor deficits (Burguière et al., 2005). In humans, among the non-motor deficits described in the cerebellar cognitive affective syndrome (Schmahmann and Sherman, 1997), they identify visuo-spatial disorganization and impaired visuo-spatial memory. Later functional imaging studies described the existence of a functional cerebellar topography (Stoodley and Schmahmann, 2008) and identified activity in a specific cerebellar region, namely Crus I, during different spatial task and, more recently, during spatial and sequence-based navigation in virtual environments (Igloi et al., 2009, 2015).

While it is clear that the neural network underlying spatial cognition includes multiple brain regions such as the striatum, the thalamus and multiple cortical areas (see Grieves and Jeffery, 2017), regions that are proven to be connected with the cerebellum, the central role of the hippocampal formation in such a network is undeniable (see Moser et al., 2017). It is then obvious to ask whether the cerebellum and the hippocampus are directly influencing each other to constitute a cerebello-hippocampal loop and what role it plays in behavior.

The potential cerebello-hippocampal interaction and its anatomical and physiological substrates have been the focus of my PhD. Thus, in this last chapter of the introduction I will describe the accumulated evidence supporting the existence of such interaction and its physiological relevance.

### **3.1 THE HIPPOCAMPUS AND SPATIAL COGNITION**

The hippocampus is one of the most extensively studied structures in modern neuroscience. There are multiple reasons underlying that fact. First, its exquisite anatomical organization with a highly structured topographical arrangement of the different inputs in specific layers drew the attention of many anatomists, Ramón y Cajal or Lorente de Nó having been among the first. As in the case with the cerebellum, their detailed anatomical descriptions were fundamental for subsequent research and still up to date (see Larriva-Sahd, 2014 for a review in the contributions of Lorente de Nó) (**Figure 23Ai**). Second, precisely because of its organization, the hippocampus is a particularly good structure to exploit extracellular electrophysiological techniques such as the local field potential recordings. Indeed, the study of oscillatory activity in the hippocampus and its relationship to the activity of local cell populations has been particularly fruitful (see Buzsaki, 2002). Finally, the hippocampus was soon identified as an important centre for declarative memory formation (Scoville and Milner (1957). Thus, intensive subsequent efforts have been put in order to better understand the underlying mechanisms for such a fundamental function (see

Eichenbaum, 2000, 2004; Marshall and Born, 2007 for reviews). During the last few decades, its role in spatial memory and spatial cognition in particular has focussed the attention of many researchers (see Hartley et al., 2013; Moser et al., 2017).

It is beyond the scope of this dissertation to present an exhaustive description of the hippocampus and the massive related literature, however, I am going to briefly introduce the basis of its anatomy and connectivity, as well as the fundamental concepts about its role in spatial cognition and memory. Moreover, for the matter of simplicity, I will focus my description in the hippocampus of rodents.

### 3.1.1 FUNDAMENTAL ANATOMY OF THE HIPPOCAMPAL FORMATION

In this work, the term hippocampal formation refers to the group of adjoining regions including the dentate gyrus, the hippocampus proper (further subdivided in CA3, CA2 and CA1), the subiculum, the presubiculum, the parasubiculum and the entorhinal cortex. They are considered as a whole because they establish an extensive loop of information processing following a highly unidirectional flow (**Figure 23Aii**).

#### 3.1.1.1 Fundamental hippocampal circuit

The entorhinal cortex can be seen as the input stage for cortical information into the hippocampal formation loop as well as one of the output stages of the processed information back to the cortex, along with the subiculum. This dual role has been classically identified at the anatomical level with a dichotomy between the superficial layers (II and III), acting as the input channels, and the deeper layers (V and VI), acting as the outputs (Andersen et al., 2007). However, such sharp separation may be inaccurate as we now know that there is certain degree of bidirectionality and re-afferences along the circuit, which may have important functional and physiological consequences (Witter et al., 2013). Thus, the neurons in layer II project to the granule cells in the dentate gyrus and to the principal cells in CA3 and CA2 subfields giving rise to the classically considered indirect pathway on contraposition to the direct projections from layer III to the CA1 subfield and the subiculum. The dentate gyrus projects through the mossy fibres to the CA3 which subsequently project through the Schaffer collaterals to the CA1, conforming the classical tri-synaptic pathway. To this circuit we need to add the CA2 region which also receives projections from CA3 and projects to CA1. However, it also projects back to the CA3 as well as to layer II in the entorhinal cortex (Rowland et al., 2013). Both the CA1 and the subiculum project back to the entorhinal cortex, however, they reach the deep layers V and VI which in turn projects to the cortex. The subiculum is also one of the main outputs from the hippocampal formation to the cortex and mainly to subcortical regions while CA1 sends efferent projections specifically to prefrontal cortex (Andersen et al., 2007). The subiculum also projects to the pre- and parasubiculum. These regions are bilaterally interconnected and form modest associative networks with many other regions of the hippocampal formation. Thus, they are known to project to the subiculum, dentate gyrus and hippocampus (Kohler, 1985). However, their main output is to the entorhinal cortex with the presubiculum reaching the layer III and the parasubiculum the layer II. A characteristic

feature of the different relays of the indirect pathway is their heavy associative and commissural connectivity (Andersen et al., 2007). On the other hand, the connectivity pattern in the direct pathway is organized in topographically restricted loops meaning that for a given source in the entorhinal cortex, the recipient area in CA1 will project back to the same entorhinal region as well as to the recipient area in the subiculum (Naber et al., 2001). Moreover, to completely close the loop, interconnections between the deep and superficial layers of the entorhinal cortex have been also described (Kloosterman et al., 2003) (**Figure 23B**).

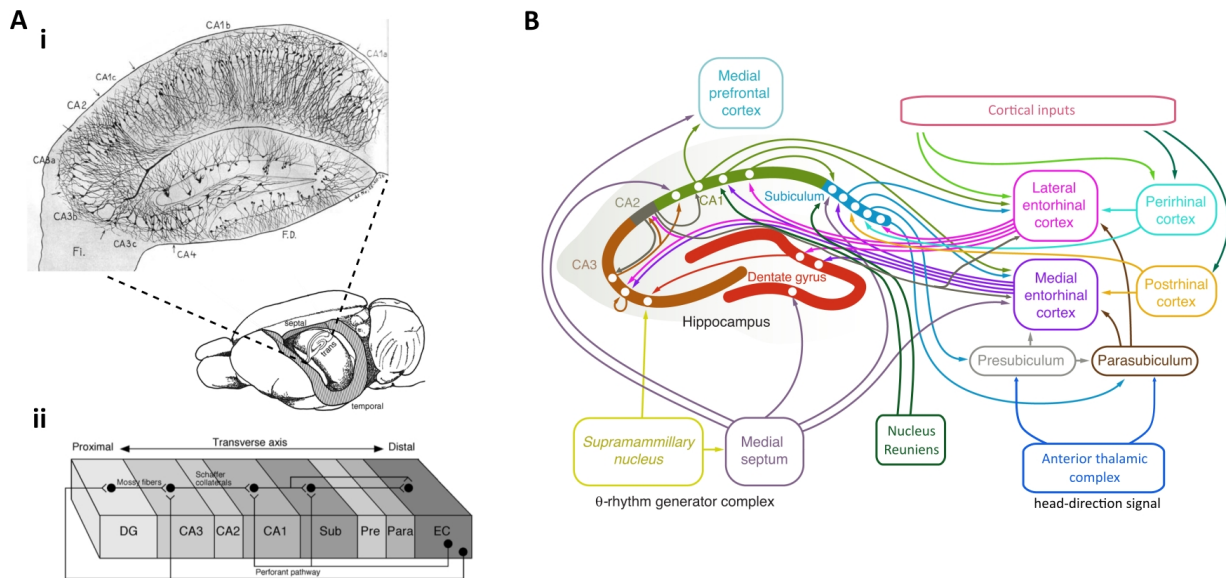


**Figure 23. Fundamental anatomy and connectivity of the hippocampal formation. A, i)** Drawing of the hippocampus by Lorente de N3. The different cell types morphology and projections are well represented. The sub-divisions of the CA field were done based on the regional anatomical differences (from Lorente de N3, 1934). **ii)** The hippocampal formation establishes a fundamentally unidirectional loop of information. It contains the classical tri-synaptic circuit entorhinal cortex (EC)-dentate gyrus (DG) via perforant path, DG-CA3 via mossy fibres, CA3-CA via Schaffer collaterals; and the direct pathway EC-CA1 via the perforant pathway (from Andersen et al., 2007). **B)** Summary diagram of the actual and much more complex connectivity patterns in the hippocampal formation. Note that the associative and commissural projections are not included nor the neuromodulatory inputs from noradrenergic, serotonergic and dopaminergic systems (adapted from Kleinfeld et al., 2016).

Apart from the reciprocal connectivity with the cortex, the hippocampal formation receives and sends projections to multiple subcortical areas. The amygdaloid complex, mainly the lateral and basal nuclei, projects to the entorhinal cortex and also to the CA3, CA1 and subiculum. All these regions but CA3 project back to it. The medial septum and the nuclei of the diagonal band of Broca send profuse cholinergic and GABAergic inputs to all the hippocampal formation (Swanson and Cowan, 1979). The hypothalamic supramammillary area also gives rise to projections that arrives exclusively in the dentate gyrus and the CA2 and co-release glutamate and GABA (Hashimoto et al., 2018). There are also several inputs from brain

stem nuclei carrying noradrenergic (the locus coeruleus), serotonergic (raphe nuclei) and dopaminergic (ventral tegmental area) neuromodulatory signals (Andersen et al., 2007). Finally, the midline thalamic nuclei, mainly the nucleus reuniens, project to the CA1 and the subiculum while the anterior thalamic complex projects exclusively to the pre- and parasubiculum (Andersen et al., 2007).

#### 3.1.1.2 Topographical organization of the hippocampal formation

In rodents, the hippocampal formation forms an elongated, banana shaped structure with its long axis (named septo-temporal axis) curving from the midline near the septal nuclei over into the temporal lobe. The intrinsic composition, the different inputs/outputs and even the genetic expression patterns change along the septo-temporal axis (Strange et al., 2014). Furthermore, multiple studies performing localized lesions at different locations also suggested involvement in different functions (Nadel, 1968; Stevens and Cowey, 1973; Moser et al., 1993). Thus, a subdivision of the hippocampal formation in a dorsal (septal) and a ventral (temporal) domain was soon acquired by the field, linking the former to a role in spatial memory encoding and the latter to stress and emotional behaviour (Moser and Moser, 1998). While such segregation remains generally accepted (Fanselow and Dong, 2010), it is also clear that there is an anatomo-functional gradient rather than a dichotomy (Strange et al., 2014) (**Figure 24Ai**).

The topographical arrangement of the cortical inputs along the hippocampal formation is fundamentally determined by their distribution into the entorhinal cortex. In this regard, the entorhinal cortex is classically subdivided in a lateral and a medial region. Such division not only relies on the coordinates of their anatomical location or their histological particularities but it mainly reflects different channels of communication relaying and computing different kinds of information. Indeed, while certain cortical regions project more or less in a similar degree to both divisions (piriform, temporal and frontal cortices) there is a difference on the weight of the insular inputs, which arrive preferentially to the lateral entorhinal cortex, and the cingulate, parietal and occipital inputs, which preferentially innervate the medial entorhinal cortex (Burwell and Amaral, 1998). Moreover, the medial entorhinal cortex is preferentially reciprocally connected with the postrhinal cortex, which is involved in multimodal visuospatial processing whereas the lateral entorhinal cortex is preferentially connected with the perirhinal cortex, mostly involved in object processing (**Figure 24Aii**). The projections from both are distributed in two different layers at the dentate gyrus, CA3 and CA2 subdivisions, thus, cells in a given location of these structures integrate medial and lateral inputs. However, in the CA1 and subiculum, the entorhinal projections differentially distribute along the transversal axis. The lateral entorhinal cortex projects to the region around the border between CA1 and subiculum (distal CA1 and proximal subiculum) while the medial entorhinal cortex projects to the proximal CA1 and the distal subiculum (Amaral, 1993). Moreover, both medial and lateral entorhinal cortex projections also follow a septo-temporal topography (Dolorfo and Amaral, 1998) (**Figure 24B**). Thus, dorsolateral entorhinal inputs arrive to septal regions of the hippocampal formation while those coming from ventromedial

locations arrive to temporal ones. Interestingly, this is in line with the dorsal versus ventral gradient previously mentioned as areas involved in emotional regulation, such as the infralimbic or prelimbic cortices, arrive preferentially to ventromedial locations in the entorhinal cortex while those involved in spatial processing, like retrosplenial cortex, arrive to the dorsolateral ones (Strange et al., 2014). Similarly, the inputs from the amygdaloid complex, also carrying information with emotional content, are mainly located in the ventromedial entorhinal cortex.

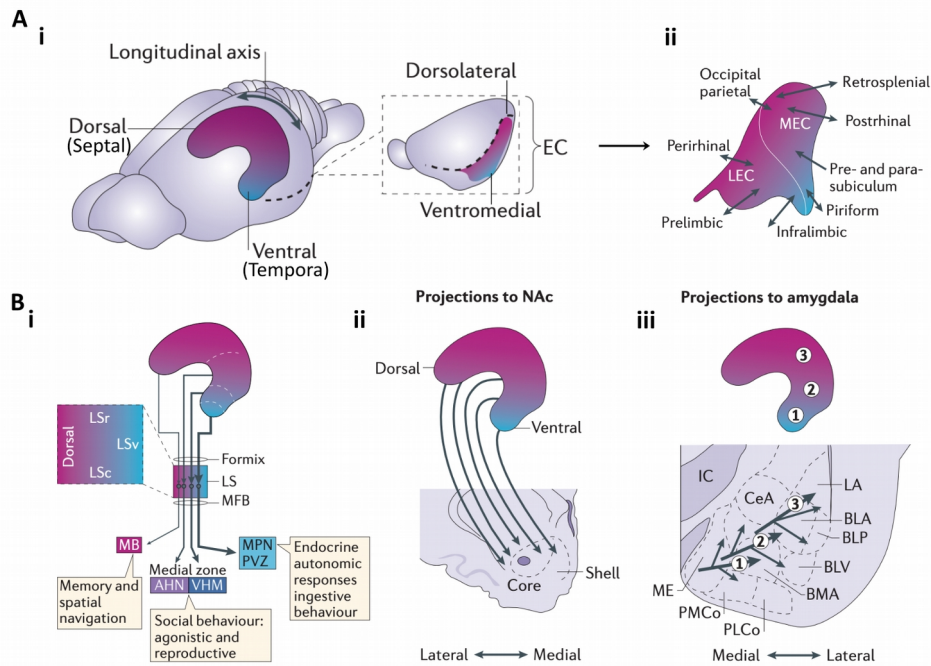


**Figure 24. Septo-temporal anatomical-functional topography.** **A, i)** The information processed by the hippocampal formation circuit is topographically distributed along the septo-temporal (dorso-ventral) axis (colour coded) and is in line with a dorsolateral-ventromedial axis in the projections from the entorhinal cortex to the rest of the circuit. **ii)** The cortical inputs to the medial and lateral entorhinal cortices are topographically distributed along the dorsolateral-ventromedial axis establishing a gradient rather than completely discrete patches. The dorsolateral region receives information from cortical areas involved in spatial processing while the ventromedial part process information from the limbic system and is involved in emotional regulation. **B)** The functional segregation is also maintained in the outputs from the hippocampal formation. **i)** Projections to specific fields of the lateral septum (LS) which then project to different targets. **ii)** Latero-medial transformation of the hippocampal dorso-ventral axis in the projections to the nucleus accumbens of the basal ganglia and the amygdala (**iii**) (All panels from Strange et al., 2014).

The outputs from the hippocampal formation are topographically organized as well. As a general principle, the regions in the entorhinal cortex which receive inputs from a particular cortical area also send projections back to them. Furthermore, the projections to subcortical areas from the CA1 and the subiculum follow the septo-temporal axis. Thus, multiple gradients following this axis can be found in the distribution of inputs to the lateral septum (dorso-ventral gradient), the amygdaloid complex (medio-lateral gradient) and the nucleus accumbens (latero-medial gradient) (Strange et al., 2014).

### 3.1.2 SPATIAL ENCODING CELLS IN THE HIPPOCAMPAL FORMATION

Since the observations of the famous HM case, an epileptic patient that underwent a bilateral temporal lobe dissection and lost the capacity to construct new memories, an enormous number of studies confirmed the critical role of the hippocampal formation in the acquisition of long-term declarative memory (Eichenbaum, 2000). The finding of multiple cells along the different regions of the hippocampal formation exhibiting spatial-modulated activity independently of the animal's ongoing behaviour led to the concept of a spatial representation encoded in this structure, which could anchor specific memories in the spatial context (Moser et al., 2017).

The first spatial coding cell population to be described were the hippocampal place cells (O'Keefe and Dostrovsky, 1971). These are principal cells located in dentate gyrus, CA3 and CA1 which characteristically fire at a low rate across most of a given environment except within a circumscribed region (its place field) where they highly increase their firing rate (**Figure 25Ai**). Different place cells recorded simultaneously possess different place fields which, at the population level, map the whole environment. Thus, the hippocampal place code may act as a neural substrate for a cognitive spatial map (O'Keefe and Nadel, 1978). Place cells appear upon the first entry into a novel environment and can be highly stable, that is, preserve the same spatial representation, for months (Thompson and Best, 1990). However, different sets of place cells are active in different environments and those cells which are active in more than one does not encode "similar" places. Indeed, sufficiently salient changes in a given environment can also induce a reconfiguration of the hippocampal place code, process known as remapping (Muller and Kubie, 1987) (**Figure 25Aii**).

Latter, Ranck, Muller and Taube discovered the head-direction cells in the dorsal presubiculum (Taube et al., 1990). This cells fire specifically when the animal faces a certain direction independently of its location, behaviour or trunk position (**Figure 25C**). Like it happens with the place cells code, different head-direction cells have specific preferred directions and at the network level the whole angular space is represented what may constitutes a cognitive compass. The head direction system anchors on allothetic cues, thus, when those are maintained constant, the preferred direction of the head-direction cells is stable as well as the angular distance between a given pair of them. On the other hand, changes in the polarizing cues provoke a coherent rotation in all the system (Goodridge et al., 1998) (**Figure 25C**). Head-direction selectivity was subsequently found in cell populations in several other brain areas including the anterodorsal (Taube, 1995) and lateral dorsal thalamic nuclei (Mizumori and Williams, 1993), the lateral mammillary nuclei (Stackman and Taube, 1998), the retrosplenial cortex (Chen et al., 1994) and the entorhinal cortex (Sargolini et al., 2006). They conform a large interconnected network with presumably hierarchical organization (Taube, 2007).

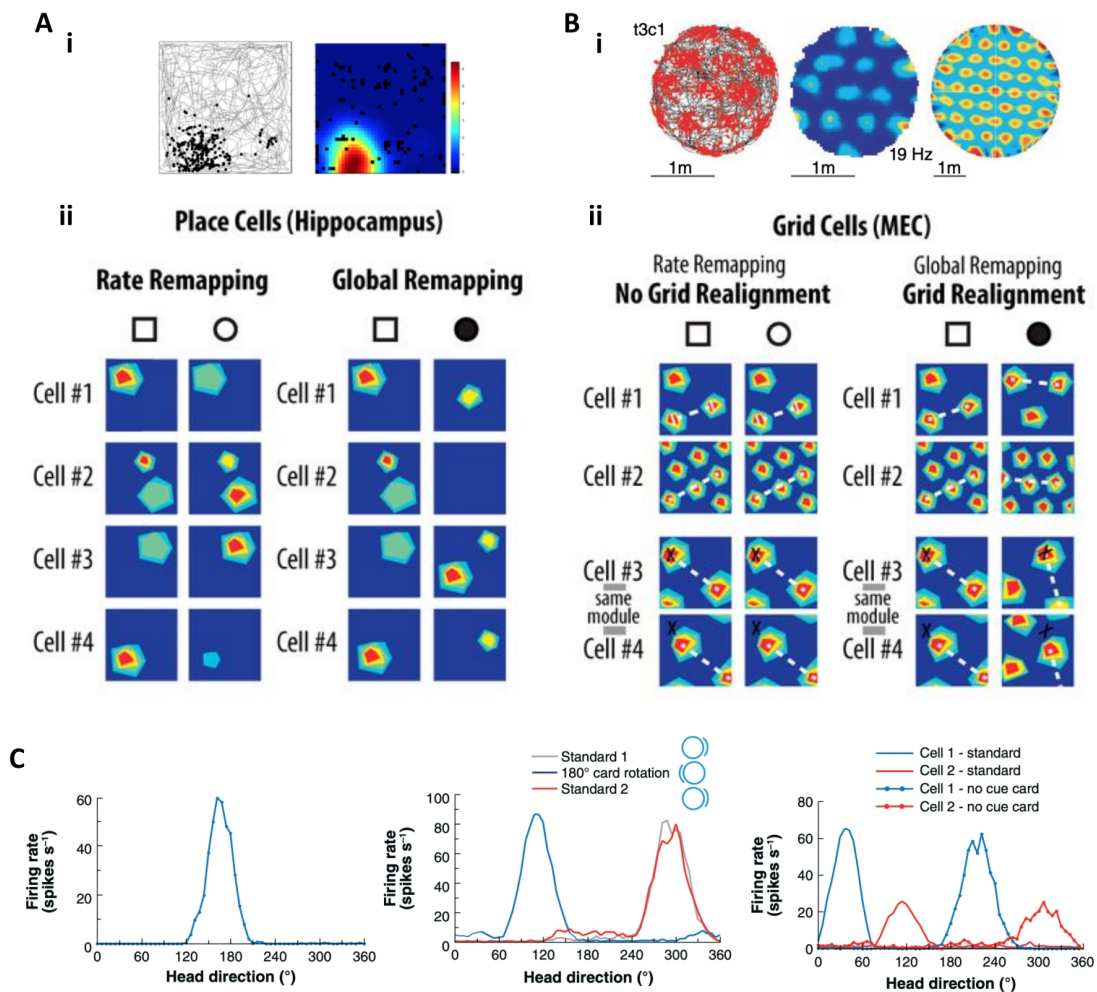


**Figure 25. Main spatial coding cell populations in the hippocampal formation.** **A, i)** Example of a place cell in the CA1 of the hippocampus. When the animal traversed (trajectory indicated in grey in the left plot) a particular location of the environment, this particular cell was active (spikes represent by black dots). When the rate map is computed it reveals the place field of the cell. **ii)** The place cells exhibit robust and stable spatial selectivity when re-entering in a familiar environment, however, salient changes in the environment induce changes in the spatial map known as remapping. When the change is subtle the spatial selectivity remains but there is a change in the firing rate inside the place field. When the changes are salient enough a global remapping occurs (from Rennó-Costa and Tort, 2017). **B, i)** Example of a grid cell in the medial entorhinal cortex (MEC). When the animal explores the environment this cell fires at multiple locations (left, trajectory in grey and spikes as red dots) and multiple place fields appear (centre) in a periodic hexagonal grid pattern (right) characterized by the distance between the fields and the orientation of the grid (from Moser et al., 2017). **ii)** Same as the place cells, grid cells can suffer remapping which does not affect the distance between the fields but provokes a grid realignment (from Rennó-Costa and Tort, 2017). **C)** Example of a head-direction cell recorded in the anterodorsal nucleus of the thalamus (left). The firing rate of this cell is nearly zero at most of the head directions but increase drastically when the heading is oriented to a specific direction. The preferred firing direction is controlled by an external cue as it rotates in agreement with the displacement of the cue (centre). The removal of the external cue produces a coherent rotation in all the head-direction cell population (right) (from Taube, 2007).

After the discovery of place cells and head-direction cells, the grid cells were first identified in the layers II and III of the medial entorhinal cortex (Fyhn et al., 2004; Hafting et al., 2005) and subsequently in the pre- and parasubiculum (Boccaro et al., 2010). These cells, as place cells, fire at specific locations in the environment. However, they display multiple firing fields which create a grid-like periodic hexagonal pattern (**Figure 25Bi**). For a given grid cell, a specific phase (the two-dimensional offset of the grid relative to an external reference point), spacing (distance between vertices) and orientation (the angle between the axes through the vertices and an external reference) can be defined. Unlike place cells, neighbouring cells present similar grid characteristics but their specific phases are distributed potentially covering for the whole “offset” map. Different grid scales are organized in modules along the dorso-ventral axis of the medial entorhinal cortex (Stensola et al., 2012) with tendency for bigger scales towards the ventral direction. Interestingly, the offset relationship between two given grid cells is preserved across different environments in spite of the modification of their individual phase and orientation (Fyhn et al., 2007) (**Figure 25Bii**). This phenomenon was called grid realignment and is indicative of an intrinsic spatial phase structure. Overall, the grid cell system is considered to play a major role in path-integration acting as a metric system for spatial navigation (McNaughton et al., 2006).

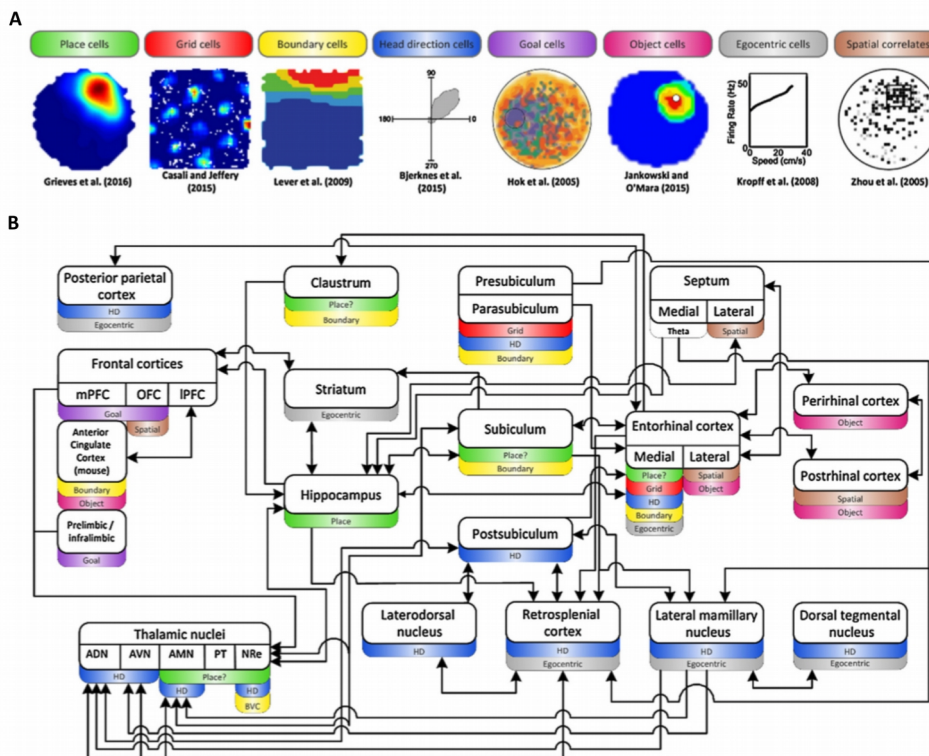


**Figure 26. Distributed spatial coding network in the brain.** **A)** Apart from the place, grid and head-direction cells, many other populations exhibit activity which encodes for particular aspects related with the spatial processing. There are boundary cells which encode specific distance from the boundaries of the environment, goal and object cells which also present a place field but it is anchored to a goal or an object location, egocentric cells which encode for parameters such as speed or movement which are centred in a self-reference frame. **B)** These different cell populations are distributed along a large neural network highly interconnected and centred around the hippocampal formation (from Grievens and Jeffery, 2017).

Along with place, grid and head-direction cells, many other neuronal populations have been found to encode for some spatially modulated information inside and outside the hippocampal formation (see Grieves and Jeffery, 2017 for a review and more references) (**Figure 26**). For instance, some of these populations include cells firing at the boundaries of an environment or at fixed distance from them (boundary/border cells), modified place cells encoding for goals (goal cells) or objects (object cells) locations or cells encoding linear and angular velocity (speed and angular velocity cells, respectively) (**Figure 26A**). It is then clear that spatial cognition heavily relies on processing carried out in the hippocampal formation but it is actually distributed across a large brain network (**Figure 26B**).

### 3.1.3 INFORMATION NEEDED TO CONSTRUCT SPATIAL COGNITIVE MAPS

Since the discovery of all the above mentioned spatial encoding cells strong efforts have been made in order to unravel the underlying mechanisms responsible for their activity. One of the main strategies to address this issue has employed manipulation of the different sensory information modules to investigate the effects that those exert on spatial coding (see Poucet et al., 2013 and Poucet et al., 2015 for reviews).

It is clear now that we can differentiate between the role of two different information modalities: external stimuli available from the environment (allothetic cues such as visual, olfactory and tactile information) and internal information related to one's self-motion (idiothetic cues such as vestibular or proprioceptive information). As previously explained, the phenomena of place cell remapping, grid cells realignment or head-direction cell reorientation can be induced by placing the animal in a new environment or modifying the most salient allothetic cues in a familiar one, particularly, visual cues (Muller and Kubie, 1987; Taube et al., 1990; Fyhn et al., 2007) (**Figure 25**). However, experiments performed in total darkness or even in blind animals show persistent place cell (Save et al., 1998; Zhang and Manahan-Vaughan, 2014) and head-direction cell (Stackman et al., 2003) coding, thus demonstrating that self-motion information alone is sufficient to maintain the spatial representation in the absence of allothetic cues. Notably, the quality of this representation is indeed remarkably reduced and even disrupted after long periods of navigation with no external cue available (Goodridge et al., 1998; Save et al., 2000; Zhang and Manahan-Vaughan, 2014; Pérez-Escobar et al., 2016). Moreover, grid cells activity, which is believed to be the one providing the self-motion based position track in the absence of sensory information (Poucet et al., 2013), seems to be compromised in the absence of visual information (Chen et al., 2016; Pérez-Escobar et al., 2016). In a recent work, however, it has been shown that grid cells in a one-dimensional circular track, in which the visual cue is out of the field of view most of the time, acquired a new firing pattern which code integrated distance rather than traveled distance or time (Jacob et al., 2019). This suggests that path-integration mechanisms are sufficient for shaping grid cell activity under such circumstances. However, this mechanism was consistently introducing a mismatch between the travel and the integrated distance. These observations led to the hypothesis that self-motion information alone permits tracking of oneself position through path integration

mechanisms, however, this process inherently produces errors which tend to accumulate (Etienne and Jeffery, 2004). Thus, allothetic information may be used to recalibrate an idiothetic based system and, consequently, both are essential to efficiently navigate through the environment and maintain an accurate and stable cognitive map (Poucet et al., 2015). Allothetic and idiothetic cues may provide parallel and complementary sources of information to the navigational systems which, depending on the behavioural demands, may rely more on one or the other.

### 3.2 EVIDENCE OF CEREBELLO-HIPPOCAMPAL INTERACTION

#### 3.2.1 ANATOMICAL AND PHYSIOLOGICAL STUDIES SUPPORTING CEREBELLAR PROJECTIONS TO THE HIPPOCAMPUS

The first mention of putative connectivity from the cerebellum to the hippocampus comes from extensive electrophysiological mapping of different brain structures responses to cerebellar cortical stimulation in cats (Whiteside and Snider, 1953) or dogs (Anand et al., 1959). They described variable short-latency (1-3 msec) responses in the hippocampus after stimulation of the posterior vermis and hemispheres. These results were extended later by combined studies of axonal degeneration and/or electrophysiological mapping in cats (Harper and Heath, 1973) and monkeys (Heath and Harper, 1974). They targeted the fastigial nucleus and described diffused evoked responses bilaterally in the hippocampus with temporal delays typical of monosynaptic projections. Similarly, they noticed the presence of degenerating terminals in multiple locations of the hippocampal formation, including CA1, dentate gyrus and subicular regions. Interestingly, the patterns were quite similar in both cats and monkeys suggesting preserved connectivity. In a later study, single unit responses to fastigial stimulation were also recorded in the cat hippocampus (Newman and Reza, 1979). However, they observed two different latencies, a short one in the range of 7-17 msec and a longer one peaking at 20 msec. None of them were suggestive of monosynaptic connections and rather indicated multiple poly-synaptic pathways.

Another clue pointing to the existence of functional pathways from the cerebellum to the hippocampus comes from a study showing that in a mouse genetic model lacking cerebellar plasticity, the hippocampal place code was totally disrupted when the animals performed self-motion based navigation (Rocheffort et al., 2011). Following this discovery, another group demonstrated that manipulating the cerebellar circuit at the onset of seizures in a mouse model of temporal lobe epilepsy was sufficient to stop them (Krook-Magnuson et al., 2014). In this study they used on-line seizure detection to trigger optogenetic activation or inhibition of Purkinje cells in the vermis or the hemisphere. Both regions successfully stopped the ongoing seizures (**Figure 27B**) and, for vermal stimulations, there were also long-lasting effects as the time between spontaneous seizures was increased in more than a 150% (**Figure 27C**). These results not only provide another form of evidence for cerebello-hippocampal connections but also suggest that these connections can influence intrinsic circuits in the hippocampus most likely through modulation of plasticity mechanisms.

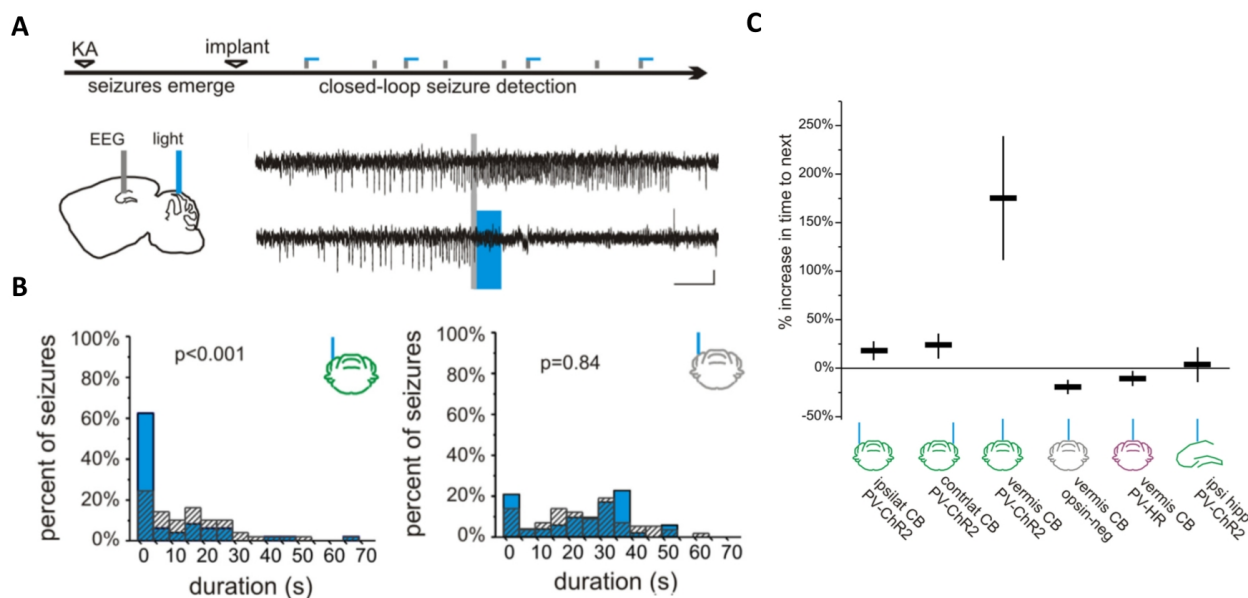


**Figure 27. Closed-loop optogenetic cerebellar stimulation inhibits spontaneous hippocampal seizures.** **A)** Experimental design in which temporal lobe epilepsy was induced in mice by injecting kainic acid (KA) into the dorsal hippocampus. Channelrhodopsin 2 (ChR2) was also expressed in the cerebellum under the promoter of parvalbumin gene, so that all Purkinje cells express it. An optic fibre was implanted on the surface of the hemisphere or the vermis. The electroencephalogram from the hippocampus was recorded and used to detect the onset of hippocampal seizures what triggered a close-loop optogenetic stimulation. **B)** The optogenetic stimulation in both the hemisphere and the vermis (not shown) succeeded in diminishing the duration of the seizures (left) while stimulation in mice non-expressing the ChR2 did not produced any effect (right). **C)** The closed-loop optogenetic stimulation in the vermis not only stopped the seizures but also prevented them to spontaneously occur as shown by the increase in time to the next epileptic event (from Krook-Magnuson et al., 2014).

### 3.2.2 EARLY ANATOMICAL AND PHYSIOLOGICAL STUDIES SUPPORTING HIPPOCAMPAL PROJECTIONS TO THE CEREBELLUM

Simultaneously, other studies focussed in the other direction, addressing the potential projections from the hippocampal formation towards the cerebellum employing similar electrophysiological mapping approaches. Stimulation of the fornix, the main output from the hippocampal formation, was found to drive electrical responses in the cerebellar cortex in guinea pigs with delays of 2-3 msec (Green and Morin, 1952). In a later study in cats, stimulations directly applied to the dorsal and ventral hippocampus also produced evoked potentials in the cerebellar granule cell layer of the vermis in the posterior lobe, however, they observed two different components in these responses with delays of 10-15 msec and 30 msec suggesting again multiple poly-synaptic pathways. In agreement with this hypothesis, single cell recordings in the lobule VI of the cerebellar cortex in cats also shown responses to bilateral hippocampal stimuli with similar delay distributions (Newman and Reza, 1979). Moreover, they suggested that the early response may be associated to a pathway involving mossy fibre inputs while the later response may be attributed to a relay in the inferior olive. Indeed, based on the Purkinje cells firing pattern modulation they presented in their work

that is most likely the case since they observed the typical profile of complex spike-simple spikes pause-rebound simple spikes firing described years later as a signature of climbing fibre excitation (Simpson et al., 1996). In this study, they also mapped the preferential hippocampal region eliciting the cerebellar responses which resulted to be confined mostly to the CA region of the dorsal hippocampus with little or no response from dentate gyrus or parahippocampal sites. Finally, in another study in rat, fornix stimulation drive responses in cells recorded in a broader area of the cerebellar cortex including vermal lobules IV-VII, paravermal lobule VI and lobule simplex in the hemisphere (Saint-Cyr and Woodward, 1980). They also referred to mossy and climbing fibres contribution to the hippocampal-cerebellar connectivity.

While these intensive and detailed electrophysiological mapping studies offered compelling evidence for functional pathways connecting cerebellum and hippocampus in a reciprocal manner, the absence of consistent anatomical studies accompanying those hampered further interpretations and hypothesis on the functional role of such circuits.

### 3.2.3 EVIDENCE FOR A CEREBELLAR ROLE IN SPATIAL NAVIGATION

Apart from the early electrophysiological mapping studies, much indirect evidence clearly pointed to the existence of functionally relevant cerebello-hippocampal loops implicated in spatial cognition. Most of them were obtained after investigations carried out in rodents presenting cerebellar lesions or mutations affecting cerebellar development or physiology. Early studies demonstrated that these different models suffered from spatial orientation impairments (Lalonde et al., 1988; Goodlett et al., 1992; Rondi-Reig et al., 2002), however, they also presented motor coordination deficits. Thus, the dissociation of the motor and cognitive component was difficult.

The employment of cerebellar transgenic mice models which maintain intact motor capabilities helped overcome this problem. For instance, the L7-PKCI mice are characterised by a specific inactivation of parallel fibre-Purkinje cell long-term depression without motor coordination problems or basal electrophysiological modification (De Zeeuw et al., 1998). These mice presented deficits in the procedural aspects of spatial memory based goal-directed navigation in a hippocampal dependent task, the Morris Water Maze task which consists in locating a hidden platform during forced swimming (Morris, 1984), while no deficit was observed in visually-guide goal-directed navigation, when the platform was visible (Burguière et al., 2005) (**Figure 28Ai**). They were able to access the memory of a goal location but they failed to adjustment their trajectories in order to efficiently reach it. This clearly suggested that the cerebellum receives and uses hippocampal information.

In a following study using the same mouse model (Rochefort et al., 2011) the activity of the hippocampal place cells was recorded in mice exploring an open field under two conditions: with external cues available, allowing an allocentric-based representation of the space; and in absence of external cues, forcing self-motion based navigation. While no deficit was observed in the allocentric condition, when the animals had

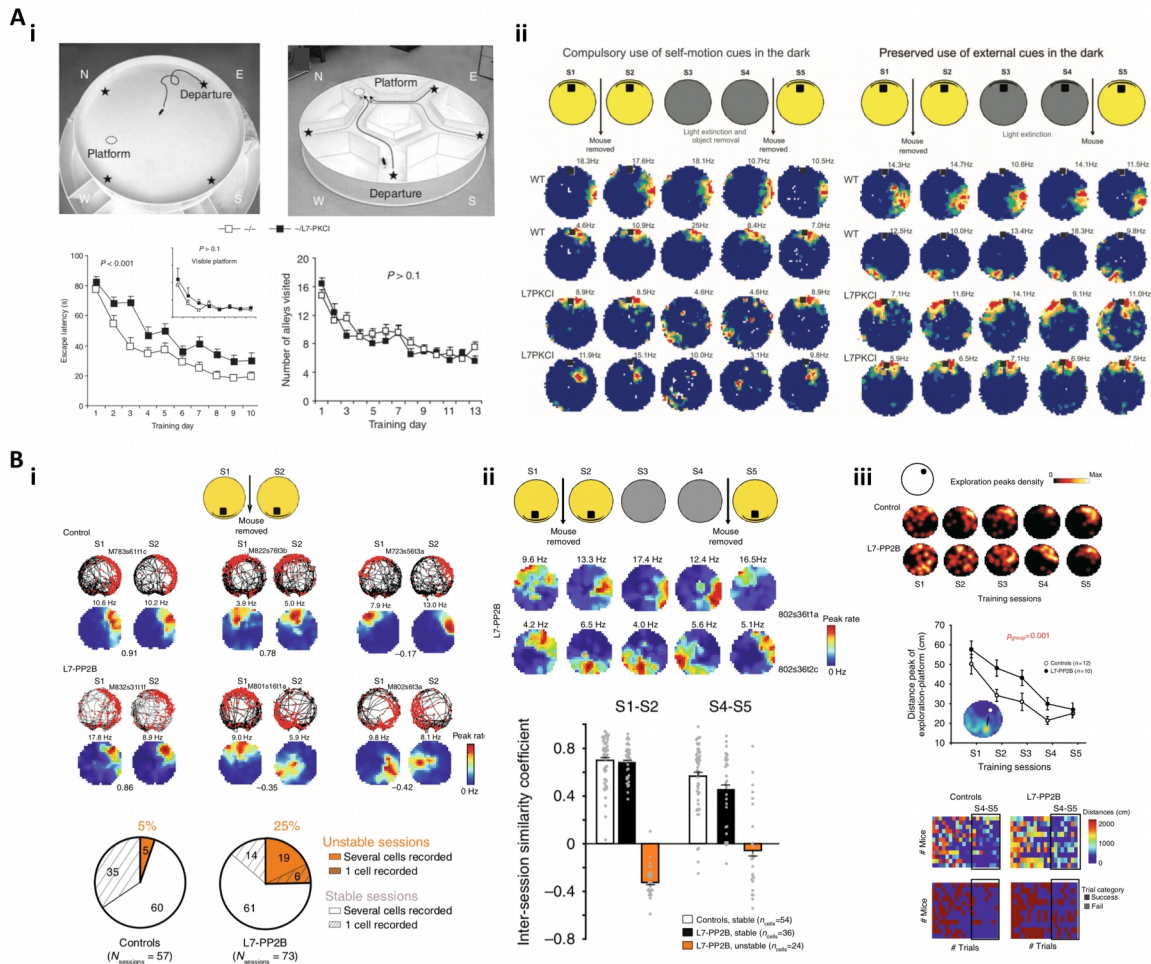


**Figure 28. Hippocampal-dependent navigation impairments in two cerebellar mutant mice with plasticity deficits.** **A, i)** L7-PKCI mice, a cerebellar mutant lacking long-term depression in the parallel fibre-Purkinje cell synapses, were tested in the Morris Water Maze (MWM), a hippocampal dependent spatial memory task where animals have to locate a hidden platform to escape from a swimming pool, and the Sarmaze, a modified version where the trajectories are delimited by alleys. The mutant mice were significantly worse than controls in the MWM with the hidden platform but not when a visual cue indicate its location nor in the Sarmaze. This results indicated that the mutant mice present a deficit in the procedural aspects of the spatial navigation most likely due to a failure in the adjustment of the trajectories during goal-directed behaviour (from Burguière et al., 2005). **ii)** Hippocampal place cells in the mutant and controls were recorded while exploring a familiar arena with a salient visual cue and an object as allothetic cues. No differences were observed when an allothetic cue was present. However, a total disruption of the hippocampal place code was observed when only idiothetic cues were available. This result suggests that the mutants have a deficit in path-integration (from Rochefort et al., 2011). **B, i)** Recordings of hippocampal place cells were obtained in L7-PP2B mice, a cerebellar mutant lacking long-term potentiation in the parallel fibre-Purkinje cell synapses. Among the mutant mice, a larger proportion of the individuals presented spontaneous rotation of the whole place code when exploring a familiar arena with an object and a visual cue in a constant position, suggesting a deficit in the anchoring of the spatial representation to a constant reference frame. **ii)** They did not present any disruption of the place code during self-motion based navigation. However, they had a significant reduction on the inter-session similarity when re-entering in the familiar environment. **iii)** Finally, they were tested in the MWM and they presented deficits in the allocentric and the egocentric (not shown) navigation as they explored more in further locations from the platform than controls (top and middle panels). Moreover, they again showed higher levels of variability than control as represented by the higher proportion of failed trials even in a late phase of learning. All together, this mice seems to present a deficit in the anchoring of the reference frame to both external and internal cues (from Lefort et al., 2019).

to rely on self-motion information the hippocampal place code was totally disrupted (**Figure 28Aii**). This disruption was associated with deficits in self-motion based goal-directed navigation as evidenced by the Morris Water Maze task, pointing to an impairment in the path integration process. Interestingly, a recent study carried out in a different mutant line, the L7-PP2B, which lack synaptic and intrinsic forms of long term potentiation in the Purkinje cells (Schonewille et al., 2010), also presented hippocampal place code impairments (Lefort et al., 2019). However, unlike the L7-PKCI, a certain population of place cells was highly unstable in the allocentric condition showing consistent place map rotation upon re-exposition to a familiar environment (**Figure 28Bi**). Surprisingly, during the self-motion based condition the hippocampal place code was unaffected (**Figure 28Bii**), in clear contrast to the L7-PKCI mice suggesting a sophisticated control of the hippocampal place code by the cerebellum and multiple mechanisms and pathways. When spatial navigation was tested in the Morris Water Maze task, deficits during both the allocentric and self-motion based conditions were observed suggesting that intact cerebellar long-term plasticity is required for navigating independently of the sensory context (**Figure 28Biii**).

In another study, the analysis of the functional networks underlying exploration and goal-directed sequence-based navigation in mice using graph theory analysis of whole brain c-Fos staining quantification revealed widespread networks for both behaviours (Babayan et al., 2017). However, while during the former the network was more widespread and centred around the cerebral cortex and the basal ganglia, during the latter it was much more specific and dominated by hippocampal and cerebellar activity, mainly a cluster including lobules IV/V, VI, simplex and Crus I, which displayed highly correlated activity. Thus, these results further support the idea of cerebello-hippocampal network interaction during goal-directed sequence-based navigation.

## SCIENTIFIC QUESTION AND INTRODUCTION TO THE RESULTS

Summarizing what it has been introduced in the last chapter of the introduction, accumulating evidences clearly suggest that the cerebellum is an important node in functional networks involving the hippocampus and plays a role in both the use and the stabilization of the hippocampal place code during different strategies of navigation. However, while these evidences are solid and compelling, we are still at the beginning of understanding how cerebellum and hippocampus functionally interacts.

Few assumptions can be made based on the current knowledge about the cerebellar complex organization and its integration in functional networks with other cerebral regions. First, given the topographical organization of the cerebellum in discrete parallel processing pathways, we expect that a putative projection from the cerebellum to the hippocampus may be restricted to specific domains rather than sparsely distributed along the cerebellar cortex. Second, since it seems that the fundamental cerebello-cerebral connectivity involves thalamic or brainstem nuclei relays, we expect to find poly-synaptic pathways rather than a monosynaptic projection as it has been proposed by certain early studies. Third, the cerebellum is able to engage with other brain areas upon behavioural demands and context. Since hippocampal activity too is profoundly modulated by the ongoing behaviour we expect to observe a dynamic pattern of interaction which may depend on the specific task in which the individuals are engaged.

So, the main questions regarding the putative cerebello-hippocampal connectivity are: 1) are they short (di- or tri-synaptic) pathways connecting the cerebellum with the hippocampus?, 2) if so, which specific areas in the cerebellum are involved in such projections?, and 3) what are the physiological mechanisms that support functional interaction between both regions?

During my PhD I have tried to answer these questions and now I am going to introduce the results that I have obtained during these years. They will be presented as two separate papers. The first one has been already published so it is going to be directly inserted in its final form. In this paper we have demonstrated the existence of di- and tri-synaptic pathways projecting from topographically restricted cerebellar regions to the dorsal hippocampus by employing a retrograde trans-synaptic rabies virus-based strategy. Then, oriented by these anatomical findings, we have used simultaneous multi-site local field potential recordings to show that these cerebellar regions and the hippocampus dynamically synchronize their oscillatory activity in the theta range during behaviour. Particularly, we have observed a significant increase in such coordinated activity specifically during goal-directed behaviour. Therefore, our findings have contributed to the understanding of both the anatomical and the electrophysiological substrates for cerebello-hippocampal interaction.

The anatomical tracing study was mainly the work of Pauline Obiang, a very talented post doc who was about to leave the lab when I first arrived, and Aurelie Watilliaux, an engineer in the lab who collaborated in

the quantification of the labelling. My contribution to the anatomical study was mainly the analysis and interpretation of the results. For the electrophysiology, I performed the experiments in collaboration with Thomas Watson, another postdoc in the lab who taught me all the methodological aspects of the electrophysiological recordings, and I was also responsible of the analysis of these data.

The second paper is presented as a preliminary draft. On it we focus our attention in the modulation of the cerebellar activity and its interaction with the hippocampus across sleep states. There is no much information available regarding the changes undergone by the cerebellar activity during sleep. Therefore, we have taken advantage of our long recordings in the homecage during which the animals went through the whole sleep-wakefulness cycle to perform a description of the electrophysiological features of the sleeping cerebellum. Moreover, since we recorded simultaneously in the hippocampus, we have also studied the potential mechanisms of interaction during the different sleep-states. Our results showed clear changes in the cerebellar activity during sleep and a novel mechanisms for potential functional interaction with the hippocampus.

# **RESULTS**



**CHAPTER 1:**

Anatomical and electrophysiological foundations of  
cerebello-hippocampal interaction.



# Anatomical and physiological foundations of cerebello-hippocampal interaction

Thomas Charles Watson<sup>1†‡§#</sup>, Pauline Obiang<sup>1†</sup>, Arturo Torres-Herraez<sup>1†</sup>, Aurélie Watilliaux<sup>1</sup>, Patrice Coulon<sup>2</sup>, Christelle Rochefort<sup>1</sup>, Laure Rondi-Reig<sup>1\*</sup>

<sup>1</sup>Neuroscience Paris Seine, Cerebellum, Navigation and Memory Team, CNRS UMR 8246, INSERM, UMR-S 1130, Sorbonne Universités, University Pierre and Marie Curie, Paris, France; <sup>2</sup>Institut de Neurosciences de la Timone, CNRS and Aix Marseille Université, Marseille, France

**Abstract** Multiple lines of evidence suggest that functionally intact cerebello-hippocampal interactions are required for appropriate spatial processing. However, how the cerebellum anatomically and physiologically engages with the hippocampus to sustain such communication remains unknown. Using rabies virus as a retrograde transneuronal tracer in mice, we reveal that the dorsal hippocampus receives input from topographically restricted and disparate regions of the cerebellum. By simultaneously recording local field potential from both the dorsal hippocampus and anatomically connected cerebellar regions, we additionally suggest that the two structures interact, in a behaviorally dynamic manner, through subregion-specific synchronization of neuronal oscillations in the 6–12 Hz frequency range. Together, these results reveal a novel neural network macro-architecture through which we can understand how a brain region classically associated with motor control, the cerebellum, may influence hippocampal neuronal activity and related functions, such as spatial navigation.

DOI: <https://doi.org/10.7554/eLife.41896.001>

## Introduction

The cerebellum is classically associated with motor control. However, accumulating evidence suggests its functions may extend to cognitive processes including navigation (*Petrosini et al., 1998; Burguière et al., 2005; Rondi-Reig and Burguière, 2005; Buckner, 2013; Koziol et al., 2014; Stoodley et al., 2017*). Indeed, anatomical and functional connectivity has been described between cerebellum and cortical areas that are engaged in cognitive tasks (*Kim et al., 1994; Kelly and Strick, 2003; Ramnani, 2006; Watson et al., 2009; Watson et al., 2014; Stoodley and Schmahmann, 2010*). Furthermore, the cerebellum has recently been found to form functional networks with subcortical structures associated with higher order functions, such as the basal ganglia (*Kelly and Strick, 2004; Hoshi et al., 2005; Bostan et al., 2010; Chen et al., 2014*; see *Bostan and Strick, 2018* for review), ventral tegmental area (*Rogers et al., 2011; Carta et al., 2019*) and hippocampus (*Rochefort et al., 2013; Iglói et al., 2015; Yu and Krook-Magnuson, 2015; Babayan et al., 2017*).

In the hippocampus, spontaneous local field potential (LFP) activity (*Iwata and Snider, 1959; Babb et al., 1974; Snider and Maiti, 1975; Krook-Magnuson et al., 2014*) and place cell properties (*Rochefort et al., 2011; Lefort et al., 2019*) are profoundly modulated following cerebellar manipulation (*Rondi-Reig et al., 2014* for review). A recent study has also described, at the single cell and blood-oxygen-level-dependent signal level, sustained activation in the dorsal hippocampus during optogenetic enhancement of cerebellar nuclei output in head-fixed mice (*Choe et al., 2018*). These data point toward the existence of an anatomical projection from the cerebellum to the hippocampus. However, the direct or indirect nature of the connection between the two structures remains unclear. The suggestion of a direct connection between these two structures has been claimed by a

**\*For correspondence:**

laure.rondi-reig@upmc.fr

<sup>†</sup>These authors contributed equally to this work

**Present address:** <sup>‡</sup>Centre for Discovery Brain Sciences, University of Edinburgh, Edinburgh, United Kingdom; <sup>§</sup>Simons Initiative for the Developing Brain, University of Edinburgh, Edinburgh, United Kingdom; <sup>#</sup>Patrick Wild Centre for Autism Research, University of Edinburgh, Edinburgh, United Kingdom

**Competing interests:** The authors declare that no competing interests exist.

**Funding:** See page 23

**Received:** 10 September 2018

**Accepted:** 30 May 2019

**Published:** 17 June 2019

**Reviewing editor:** Richard B Ivry, University of California, Berkeley, United States

© Copyright Watson et al. This article is distributed under the terms of the [Creative Commons Attribution License](https://creativecommons.org/licenses/by/4.0/), which permits unrestricted use and redistribution provided that the original author and source are credited.

recent tractography study in humans (Arrigo *et al.*, 2014) and the presence of short-latency evoked field potentials (2–4 ms) in cat and rat hippocampi after electrical stimulation of the cerebellar vermal and paravermal regions (Whiteside and Snider, 1953; Harper and Heath, 1973; Snider and Maiti, 1976; Heath *et al.*, 1978; Newman and Reza, 1979). However, secondary hippocampal field responses have also been described, at a latency of 12–15 ms following cerebellar stimulation, suggesting the existence of an indirect pathway (Whiteside and Snider, 1953).

Taken together, even if these studies provide compelling physiological evidence of cerebellar influences on the hippocampus, they do not provide direct evidence of neuroanatomical connectivity between the two regions. Given the known complex, modular functional and anatomical organization of the cerebellum (Apps and Hawkes, 2009) this represents a major gap in our understanding of the network architecture linking the two structures. In addition, these studies provide no measure of dynamic physiological communication or associated synchronization between the two structures, which is thought to be essential for maintaining distributed network functions (e.g. Fries, 2005).

Therefore, this study addresses two fundamental, unanswered questions: which regions of the cerebellum are anatomically connected to the hippocampus and what are the spatio-temporal dynamics of synchronized cerebello-hippocampal activity during behavior? To address these unresolved questions, we used rabies virus as a retrograde transneuronal tracer to determine the extent and topographic organization of cerebellar input to the hippocampus. Based upon the anatomical tracing results, we then studied the levels of synchronization between LFPs recorded simultaneously from the cerebellum and dorsal hippocampus in freely moving mice as a proxy for potential cross-structure interactions. We reveal that specific cerebellar modules are anatomically connected to the hippocampus and that these inter-connected regions dynamically synchronized their activity during behavior.

## Results

To study the topographical organization of ascending, cerebello-hippocampal projections, we unilaterally injected rabies virus (RABV), together with fluorescent cholera toxin  $\beta$ -subunit (CTb), into the left hippocampus. The extent of the injection site, identified by the presence of fluorescent CTb, included both CA1 (stratum lacunosum-moleculare) and DG (molecular layer, granule cell layer and hilus, *Figure 1—figure supplement 1*).

### Cerebellar projections to the hippocampus are precisely topographically organized

We characterized the presence of retrograde transneuronally RABV-infected neurons after survival times of 30, 48, 58 and 66 hr (Suzuki *et al.*, 2012; Aoki *et al.*, 2017; Coulon *et al.*, 2011). At 30 hr post-infection, staining was found predominantly in the medial septum diagonal band of Broca (MSDB), the lateral and medial entorhinal cortices, the perirhinal cortex and the supramammillary nucleus of the hypothalamus (SUM). Sparse staining was also found in a subset of mice, in the raphe nucleus and in other hypothalamic and thalamic regions (*Figure 1—figure supplement 2*). All these structures correspond to first-order relays as CTb staining was also systematically associated with each of the sites containing rabies infected neurons (*Figure 1—figure supplement 3*). Importantly, no RABV or CTb labeling was found in the cerebellum at this time-course ruling out the existence of a direct cerebello-hippocampal DG pathway in mice. Interestingly, among these putative first relays, the septum, the hypothalamus and the raphe nucleus receive direct projections from the deep cerebellar nuclei in cat (Paul *et al.*, 1973), rat (Teune *et al.*, 2000) and Macaca (Haines *et al.*, 1990). In accordance with this, some RABV-infected neurons were observed in the deep cerebellar and vestibular nuclei 48 hr post-hippocampal infection and some labeled cells were found in the cerebellar cortex at 58 hr p.i. (*Figure 1A*, inset, *Figure 1—figure supplement 4*) suggesting the existence of single-relay pathways (i.e. di-synaptic connections) between the cerebellum and hippocampus.

At 48 hr post-infection, RABV labeling was also found in mammillary bodies, amygdala and several midbrain and pontine regions such as the periaqueductal gray (PAG), the nucleus incertus and the laterodorsal tegmental nucleus (LtDG). These regions, which are known to receive direct projections from the DCN (Teune *et al.*, 2000) were neither stained with CTb nor RABV-positive at 30 hr post-infection and therefore represent a putative additional pathway involving two relays between the cerebellum and the hippocampus (*Figure 1—figure supplement 4*).



Figure 1 continued

line), and cerebellar cortex (66 hr, orange line). Upper right, schematic view of the posterior cerebellar cortex indicating regions of highest labeling following rabies virus injection (red, vermis lobule VI; green, Crus I; gray, paraflocculus). (B-E) Representative photomicrographs showing labeling in the cerebellar and vestibular nuclei 58 hr post-infection. Left panels show low-magnification view, right panels show magnified view of area indicated by dashed box. Solid arrow heads indicate the presence of the very few labeled cells in the IntP. (F) Pooled, normalized counts of rabies labeled cells in the ipsi- and contralateral cerebellar and vestibular nuclei 58 hr post-infection (n = 5 mice). No significant differences were found between ipsi- and contralateral nuclei (nuclei x hemisphere two-way ANOVA, hemisphere effect  $F_{(1, 4)}=1.31 \times 10^{-5}$ ,  $p=0.99$ , interaction effect  $F_{(3, 12)}=2.79$ ,  $p=0.09$ , nuclei effect  $F_{(3, 12)}=9.38$ ,  $p=0.002$ ). (G) Normalized cell counts in the fastigial nucleus (left) and dentate nucleus (right), according to their rostro-caudal position relative to bregma. Open circles, contralateral count; filled circles, ipsilateral count (n = 5 mice). (H-K) Representative photomicrographs of the resultant labeling in lobule VI, Crus I, paraflocculus and lobule II at 66 hr post-infection. (L) Normalized count of rabies labeled cells in anterior (black bar; lobule II to lobule IV/V); central (dark gray bar; lobule VI to Crus II); posterior (clear bar; lobule VIII and lobule IX) and flocculonodular (Floc. Nod., light gray bar; lobule X, flocculus and paraflocculus) cerebellum 66 hr post-infection (n = 5 mice; one-way ANOVA with FDR correction,  $F_{(3, 16)}=19.11$ ,  $p<0.0001$ ). (M) Normalized cell count of rabies labeled cells in all assessed lobules 66 hr post-infection. Color coding of bars indicate assignment of lobules to either anterior, central, posterior or vestibular cerebellum as indicated in L. Abbreviations: Dent., Dentate nucleus; Fast., fastigial nucleus; Fast. DL, dorsolateral fastigial nucleus; Floc. Nod., flocculonodular lobe; Interp., nucleus interpositus; IntA, nucleus interpositus anterior; IntDL, dorsolateral nucleus interpositus; IntP, nucleus interpositus posterior; i-Sim, ipsilateral simplex lobule; c-Sim, contralateral simplex lobule; i-Crus I, ipsilateral Crus I; c-Crus I, contralateral Crus I; i-Crus II, ipsilateral Crus II; c-Crus II, contralateral Crus II; i-Par, ipsilateral paramedian lobule; c-Par, contralateral paramedian lobule; i-CP, ipsilateral copula; c-CP, contralateral copula; i-Floc, ipsilateral flocculus; c-Floc, contralateral flocculus; i-PF, ipsilateral paraflocculus; c-PF, contralateral paraflocculus; Vestib., vestibular nuclei. \*\*  $q < 0.01$ , \*\*\*  $q < 0.001$ .

DOI: <https://doi.org/10.7554/eLife.41896.002>

The following source data and figure supplements are available for figure 1:

**Source data 1.** Summary table of RABV labeling in the cerebellum 58 hr post hippocampal infection.

DOI: <https://doi.org/10.7554/eLife.41896.008>

**Figure supplement 1.** Location of rabies virus injections for the four experimental groups.

DOI: <https://doi.org/10.7554/eLife.41896.003>

**Figure supplement 2.** Structures labeled 30 hr after hippocampal rabies injection.

DOI: <https://doi.org/10.7554/eLife.41896.004>

**Figure supplement 3.** Analysis of CTB retrograde labeling indicates that rabies labeled structures at 30 hr post-infection are potential first relay regions.

DOI: <https://doi.org/10.7554/eLife.41896.005>

**Figure supplement 4.** Summary table of RABV labeling across brain structures 48 hr after hippocampal rabies injection Overview of RABV labeling in different brain regions 48 hr post rabies injection in the hippocampus.

DOI: <https://doi.org/10.7554/eLife.41896.006>

**Figure supplement 5.** The topographical distribution of DCN labeling at 66 hr.

DOI: <https://doi.org/10.7554/eLife.41896.007>

58 hr post-infection, abundant and strong staining was found in the fastigial and dentate nuclei, with almost no staining in the interpositus (Figure 1B–F). Within the fastigial and dentate, RABV-labeled cells were found to be topographically restricted to caudal and central regions, respectively (Figure 1G).

Following 66 hr of incubation, the number of strongly labeled cells increased in the DCN and vestibular nuclei (Figure 1A); however, the topographical distribution remained unchanged (Figure 1—figure supplement 5). At the level of the cerebellar cortex, longitudinal clusters of RABV+ Purkinje cells (PCs) were found bilaterally across highly restricted central and flocculo-nodular regions (Figure 1L). In the central cerebellum (i.e. lobules VI, VII and associated hemispheres), clusters were particularly concentrated in lobule VI and Crus I (Figure 1H,I,M). In the flocculo-nodular cerebellum, RABV-labeled cells were found in the dorsal and ventral paraflocculus (Figure 1J and M and Figure 2B). Within the vermis we identified a single cluster of RABV+ Purkinje cells that extended across both lobule VIa and lobule VIb-c (Figure 2). In contrast, within Crus I, RABV-labeled Purkinje cells were arranged in two spatially isolated clusters, one located rostro-laterally and the other caudo-medially (Figure 2).

The topographical arrangement of RABV-labeled PCs in longitudinal clusters is in keeping with the well-described modular organization of the cerebellum (e.g. Apps and Hawkes, 2009). Mapping of molecular marker expression patterns, such as zebrin II banding, provides a reliable basis from which modules can be defined and recognized in the cerebellar cortex of rodents. Thus, to further assign the observed PC clusters to previously described cerebellar zones, we used a double

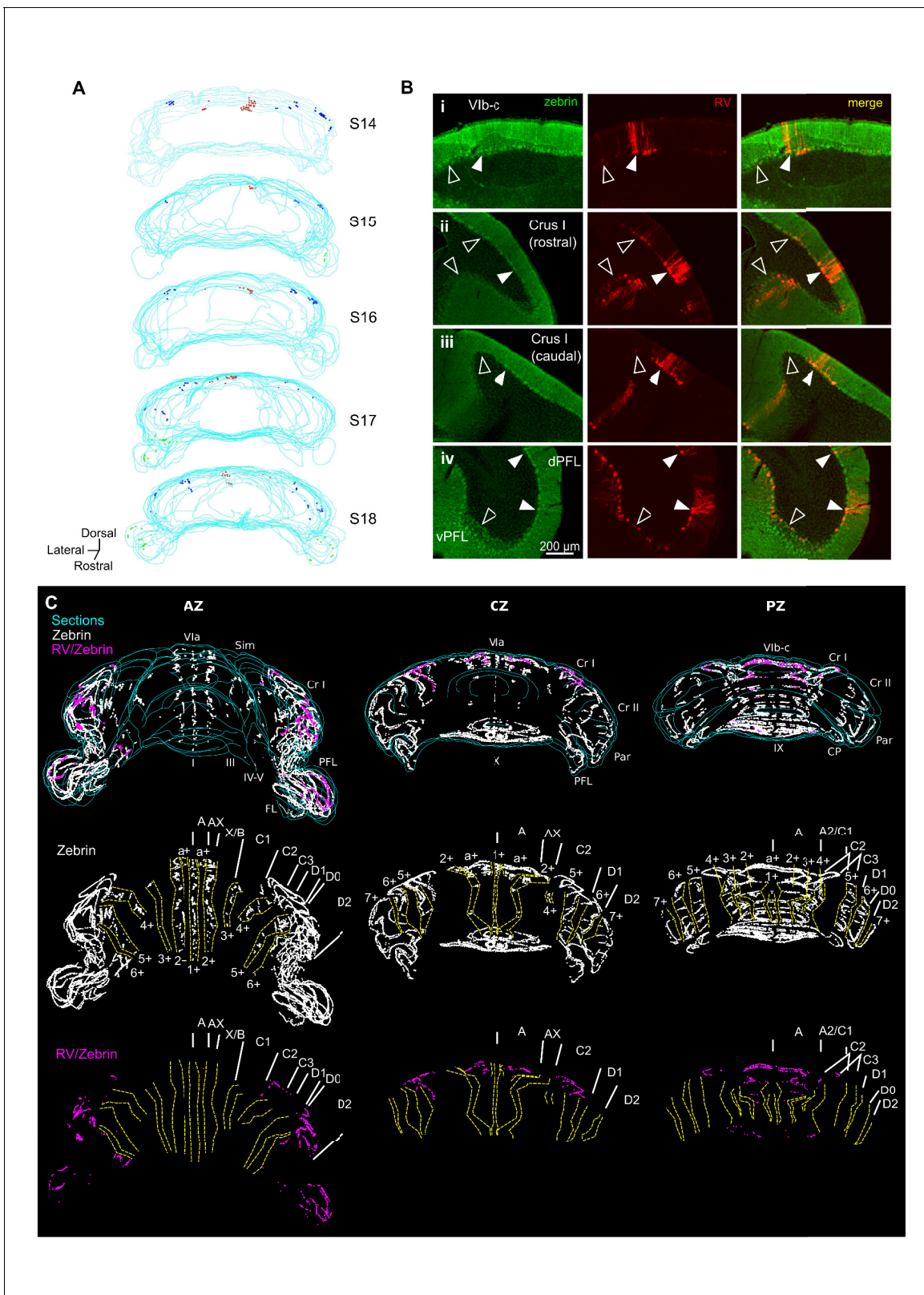


**Figure 2.** Different cerebellar modules project to the hippocampus. **(A)** 3-D reconstruction showing the location of RABV+ Purkinje cells in the most labeled cerebellar lobules at 66 hr post-infection. Red, blue and green dots represent RABV+ Purkinje cells in lobule VI, Crus I and paraflocculus, respectively. **(B)** Photomicrographs from case S18 showing double staining against zebrin II (green, left column), RABV (red, central column) and merge (right column) in lobule VI (i), Crus I (ii and iii) and paraflocculus (iv). RABV+ Purkinje cells were also zebrin positive and were organized in clusters of *Figure 2 continued on next page*

Figure 2 continued

strongly labeled RABV+ cells (filled arrow-heads) surrounded by weakly labeled RABV+ Purkinje cells (unfilled arrow-heads). (C) Assignment of the RABV+ clusters to specific cerebellar modules for case S18 in the anterior (AZ; left), central (CZ; central column) and posterior (PZ; right column) zones. First row shows stacked sections with zebrin-positive Purkinje cells (white dots) and RABV+ Purkinje cells, which were also zebrin positive (purple dots, strong and weakly labeled cells included); central row shows reconstructed principal zebrin bands (delineated by yellow dashed lines and named from 1+ to 7+; nomenclature from *Sugihara and Quay, 2007*) and cerebellar modules (capital letters; defined as in *Sugihara and Quay, 2007*); and bottom row shows the location of the RABV+/zebrin Purkinje cells (purple dots) in relation to reconstructed zebrin bands and modules. Abbreviations, I, lobule I; III, lobule III; IV/V, lobule IV/V; VIa and VI b-c, lobule VIa and VI b-c, respectively; IX, lobule IX; X, lobule X; Sim, lobule simplex; Cr I, Crus I; Cr II, Crus II; Par, paramedian lobule; CP, copula, PFL, paraflocculus, FL, flocculus.; dPFC and vPFC, dorsal and ventral paraflocculus, respectively.

DOI: <https://doi.org/10.7554/eLife.41896.009>

immunohistochemical approach to stain for both RABV and aldolase C (zebrin II) in one animal (case S18) after 66 hr of infection (**Figure 2B**) (*Brochu et al., 1990; Sugihara and Shinoda, 2004*). Lobule VI, Crus I and paraflocculus are mostly zebrin-positive regions (*Sugihara and Quay, 2007*), and we found that RABV-labeled Purkinje cells co-localized with zebrin II in all the observed clusters (**Figure 2B**). In the vermis, lobule VIa RABV-labeled PCs were mostly located in the a+ band. The few RABV-labeled cells found in lobule VII were confined to the 2+ band. Thus, together, these labeled cells belong to the a+//2+ pair that constitutes part of the cerebellar A module (**Figure 2C**) (*Sugihara, 2011*). In Crus I, the rostromedial cluster of RABV-labeled PCs was aligned with the anterior 6+ zebrin band corresponding to module D2. The caudomedial cluster was in continuation with the posterior 5+ zebrin band suggesting that it is part of the paravermal module C2 (**Figure 2C**). In the paraflocculus, the assignment of the RABV-labeled cells to specific modules was not addressed given the complex morphology of this region. However, the presence of RABV-labeled cells both in the dorsal and ventral paraflocculus suggests the involvement of more than one module (**Figure 2B–C**) (*Voogd and Barmack, 2006*).

Cerebellar modules are also defined by their outputs through the deep cerebellar and vestibular nuclei (*Apps and Hawkes, 2009; Ruigrok, 2011*). The presence of RABV-labeled cells in the fastigial nucleus is consistent with the involvement of module A. Similarly, the D2 module is routed through the dentate nuclei in which we found robust RABV labeling. We also found RABV+ cells in the nucleus interpositus posterior, which provides the output of module C2. Finally, RABV labeling was observed in the vestibular nuclei, which may represent the output of RABV+ Purkinje cell clusters observed in the ventral paraflocculus.

Together, our neuroanatomical tracing data indicate that cerebellar projections to the hippocampus emanate from three distinct cerebellar modules. It also suggests the existence of multiple, convergent pathways from the DCN to the hippocampus.

### Cerebello-hippocampal physiological interactions in a familiar home-cage environment

In order to question the potential functional relevance of cerebello-hippocampal anatomical connectivity, we implanted mice ( $n = 21$ ) with arrays of bipolar LFP recording electrodes in bilateral dorsal hippocampus (HPC) and unilaterally in two highly RABV-labeled regions of the central cerebellum, lobule VI (midline) and Crus I (left hemisphere). For comparison, we also simultaneously recorded LFP from cerebellar regions with minimal RABV labeling (lobule II or lobule III; **Figure 1M; Figure 3A and B**). Data were excluded from further analysis in cases where postmortem histological inspection revealed that electrode positions were off-target (**Figure 3—figure supplement 1**).

The spectral profile of cerebellar and hippocampal LFP activity was first assessed during active movement in a familiar home-cage environment (epochs with speed  $>3$  cm/s; see Materials and methods). Within the HPC, a dominant 6–12 Hz theta oscillation was similarly observed in both hemispheres (**Figure 3—figure supplement 2B**; left HPC: mean 6–12 Hz z-score power =  $4.17 \pm 0.20$ ,  $n = 17$ ; right HPC: mean 6–12 Hz z-score power =  $4.52 \pm 0.16$ ,  $n = 19$ ; unpaired t test,  $t_{34} = 0.007$ ,  $p = 0.1731$ ), thus, when LFPs from both hippocampi were available we averaged the spectral power from left and right hemispheres (**Figure 3C**, mean 6–12 Hz z-score power =  $4.35 \pm 0.14$ ). In the cerebellar recordings, low-frequency oscillations in the delta (2–4 Hz) and high-frequency activity in the mid-high gamma (50–140 Hz) range were prevalent. A clear peak in the 6–12 Hz band was not detected in the power spectrum of any of these recordings, which had

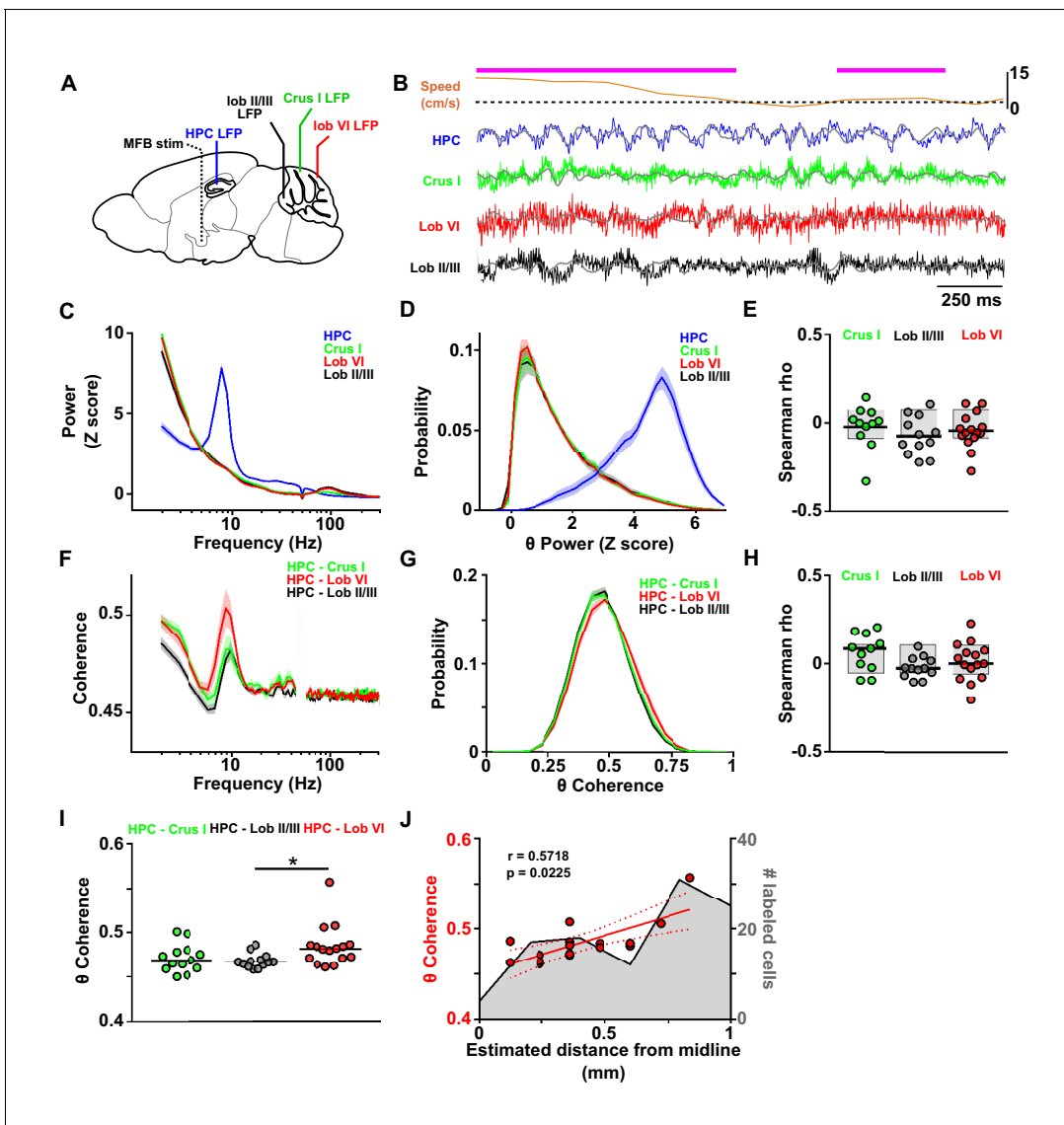


**Figure 3.** Assessment of cerebello-hippocampal interactions during active movement in the homecage. (A) Schematic representation of recording and stimulation electrode implant positions. (B) Representative simultaneous raw LFP recordings (colored lines) and LFP filtered in the theta frequency range (0, 6–12 Hz, overlaid gray lines) recorded during active movement in the homecage condition as defined by instantaneous speed. Solid magenta line indicates data epochs in which speed was above the required threshold for inclusion in further analysis (3 cm/s, dashed line (20 mice). In one mouse in which speed data was not available we used neck electromyograph (EMG) data to define periods of active movement). (C) Averaged z-score of the power spectra from hippocampal LFP ( $n = 21$ , mean between left and right hemisphere LFPs when both recording electrodes were on target) and cerebellar cortical regions Crus I ( $n = 12$ ), lobule II/III ( $n = 13$ ) and lobule VI ( $n = 16$ ) during homecage exploration (speed above 3 cm/s). (D) Probability distribution of the instantaneous z-scored theta power for each of the recorded regions. Hippocampal theta power followed a negatively skewed distribution while cerebellar theta power followed a positively skewed distribution. (E) Correlation between the instantaneous z-scored theta power for each of the cerebellar recorded regions and instantaneous speed. Horizontal line indicates mean. Gray-shaded bars represent the confidence levels obtained from bootstrapped data with  $\alpha = 0.05$ . Theta power was not significantly correlated with speed in any of the cerebellar recordings (Crus I,  $n = 11$ ; lobule II/III,  $n = 12$ ; lobule VI,  $n = 15$ ). (F) Averaged coherence between cerebellar cortical recordings (color coded) and hippocampus (when both hippocampal recording electrodes were on target we averaged the coherence obtained with left and right hemispheres; Crus I,  $n = 12$ ; lobule II/III,  $n = 13$ ; lobule VI,  $n = 16$ ) during homecage exploration (speed above 3 cm/s). (G) Probability distribution of the instantaneous hippocampal-cerebellar theta coherence (color coded). All the recording combinations followed normal distributions. (H) Correlation between the instantaneous hippocampal-cerebellar theta coherence (color coded) and the instantaneous speed. Horizontal line indicates mean. Gray-shaded bars represent the confidence levels obtained from bootstrapped data with  $\alpha = 0.05$ . HPC-cerebellar theta coherence was not significantly correlated with speed in any of the recording combinations. (I) Theta coherence between cerebellar recordings and hippocampus (average between coherence with left and right hemisphere LFPs when both recordings were on target; Crus I - HPC,  $n = 12$ ; lobule II/III - HPC,  $n = 13$ ; lobule VI - HPC,  $n = 16$ ). Lobule VI-HPC coherence was significantly higher than that observed with lobule II/III (horizontal line indicates median coherence for each combination; \*, Kruskal-  
*Figure 3 continued on next page*

Figure 3 continued

Wallis with FDR correction, Kruskal-Wallis statistic = 6.75,  $p = 0.0342$ ; lobule VI-HPC vs lobule II/III-HPC,  $p = 0.0246$ ). J, Mean lobule VI-HPC theta coherence plotted against the estimated medio-lateral position of the recording electrode in lobule VI (red dots;  $n = 16$ , when both hippocampal recording electrodes were on target we averaged the coherence obtained with left and right hemispheres; Spearman  $\rho = 0.5718$ ,  $p = 0.0225$ ). In gray, number of RABV+ cells counted across lobule VI 66 hr after injection in the left HPC as a function of medio-lateral position (0.2 mm bins;  $n = 5$  mice). Shading indicates S.E.M. Abbreviations, LFP, local field potential; HPC, dorsal hippocampus; lob II/III, lobule II/III, lob VI, lobule VI, MFB stim, medial forebrain bundle stimulation.

DOI: <https://doi.org/10.7554/eLife.41896.010>

The following source data and figure supplements are available for figure 3:

**Source data 1.** Assessment of cerebello-hippocampal interactions during active movement in the homecage.

DOI: <https://doi.org/10.7554/eLife.41896.015>

**Figure supplement 1.** Reconstructed location of the implanted electrodes.

DOI: <https://doi.org/10.7554/eLife.41896.011>

**Figure supplement 2.** Cerebello-hippocampal coherence patterns are similar across hemispheres during active movement in homecage.

DOI: <https://doi.org/10.7554/eLife.41896.012>

**Figure supplement 3.** Experimental setup for simultaneous recording of photo-identified Purkinje cells and hippocampal local field potential.

DOI: <https://doi.org/10.7554/eLife.41896.013>

**Figure supplement 4.** Polar plots and associated histograms of cerebellar units significantly phase locked to hippocampal 6–12 Hz oscillations.

DOI: <https://doi.org/10.7554/eLife.41896.014>

similar levels of 6–12 Hz z-score power (**Figure 3C**; Crus I:  $1.57 \pm 0.10$ ,  $n = 12$  mice; lobule II/III:  $1.57 \pm 0.13$ ,  $n = 13$  mice; lobule VI:  $1.47 \pm 0.07$ ,  $n = 16$  mice; one-way ANOVA,  $F_{(2, 38)}=0.34$ ,  $p=0.7131$ ).

In order to explore any potential state-dependent organization of theta oscillations in our recordings, we computed the distributions of instantaneous power in this frequency range (**Figure 3D**). If the power of theta oscillations was organized in differential states, we would expect to observe a multimodal distribution; however, we found unimodal power distributions in both the hippocampal and cerebellar recordings. The former was negatively skewed suggesting that the peak observed in the hippocampal power spectra is representative of sustained theta activity in the analyzed epochs. In contrast, the cerebellar theta distribution profile was positively skewed suggesting that activity in this frequency range, although of lower power than in the hippocampus, is also sustained within the cerebellar cortical regions we recorded from.

Previous studies have described correlations between locomotion speed and purkinje cell discharge in cerebellar vermal lobules V and VI (*Sauerbrei et al., 2015*; *Muzzu et al., 2018*). Furthermore, cerebellar nuclei - prefrontal cortex theta coherence has also been found to increase during active locomotion compared to rest (*Watson et al., 2014*). Therefore, we next asked if running speed could be modulating theta power in the cerebellar cortex. To do so, we computed the correlation between instantaneous speed and instantaneous theta power in each cerebellar region; however, none were significantly correlated (**Figure 3E**; Crus I,  $n = 11$ , mean Spearman  $\rho = -0.02 \pm 0.04$ , bootstrap confidence level =  $[-0.09 \ 0.08]$ ; lobule II/III, mean Spearman  $\rho = -0.07 \pm 0.03$ , bootstrap confidence level =  $[-0.08 \ 0.08]$ ; lobule VI, mean Spearman  $\rho = -0.04 \pm 0.03$ , bootstrap confidence level =  $[-0.08 \ 0.08]$ ).

As an indicator of cross-structure interaction (*Fries, 2005*), we next calculated coherence between LFP recorded from the different cerebellar subregions and left or right HPC. We found no statistically significant influence of hippocampal laterality on the measured cerebello-hippocampal coherence (**Figure 3—figure supplement 2**; Crus I-HPC left,  $n = 11$ , Crus I-HPC right,  $n = 11$ , Mann-Whitney test,  $U = 59$ ,  $p=0.9487$ ; lobule II/III-HPC left,  $n = 11$ , lobule II/III-HPC right,  $n = 12$ , Mann-Whitney test,  $U = 63$ ,  $p=0.8801$ ; lobule VI-HPC left,  $n = 15$ , lobule VI – HPC right,  $n = 14$ , Mann-Whitney test,  $U = 105$ ,  $p>0.99$ ). Therefore, for further analysis, when both hippocampal recording electrodes were on target we first calculated coherence with the cerebellar LFP for each hemisphere then averaged the two. Thus, for each mouse we obtained one coherence value per cerebello-hippocampal recording combination. In cases in which only one of the hippocampal recording electrodes was on target, we excluded the off target recording in our calculations of cerebello-hippocampal coherence.

A clear peak in coherence was observed for all cerebello-hippocampal combinations in the theta frequency range (6–12 Hz, **Figure 3F**; Crus I-HPC,  $n = 12$ ; lobule II/III-HPC,  $n = 13$ , lobule VI-HPC,  $n = 16$ ; frequencies between 48 and 52 Hz have been excluded due to notch filtering to remove electrical contamination of the LFP signals; see Materials and methods). We found that significant variations in coherence level were restricted to those within the theta frequency (frequency band (theta, 6–12 Hz; beta, 13–29 Hz; low gamma, 30–48 Hz) x cerebello-hippocampal combination two way repeated measures ANOVA, frequency band effect  $F_{2,76} = 22.42$ ,  $p < 0.0001$ ; combination effect  $F_{2,38} = 2.843$ ,  $p = 0.0707$ ; interaction effect,  $F_{4,76} = 3.825$ ,  $p = 0.0069$ ; post-hoc multiple comparisons with FDR correction revealed significant differences between combinations only in the theta band). In addition, as theta coherence has already been reported as a potential mechanism for long-range network interactions between the hippocampus and the cerebellum (**Hoffmann and Berry, 2009**; **Wikgren et al., 2010**) and theta oscillations are known to play an important role in intra-hippocampal network organization, in particular for spatial navigation (see **Buzsáki and Moser, 2013** for overview), we focused our analysis on activity within this frequency range. As for the instantaneous LFP power, we next asked if theta coherence between the different cerebello-hippocampal LFP combinations was organized in a state-dependent manner. To address this question, we computed the distribution of instantaneous coherence within this bandwidth. In line with the analysis of LFP power distributions, we did not observe any multi-modality and all combinations followed gaussian distributions (**Figure 3G**). Correlation analysis between instantaneous speed and instantaneous theta coherence failed to show significant relationships for any cerebello-hippocampal combination (**Figure 3H**; Crus I-HPC, mean Spearman rho =  $0.06 \pm 0.03$ , bootstrap confidence level =  $[-0.08 \ 0.08]$ ; lobule II/III-HPC, mean Spearman rho =  $-0.02 \pm 0.02$ , bootstrap confidence level =  $[-0.08 \ 0.08]$ ; lobule VI-HPC, mean Spearman rho =  $0.01 \pm 0.03$ , bootstrap confidence level =  $[-0.09 \ 0.08]$ ). Significant differences across recording combinations were observed within the theta bandwidth (**Figure 3I**; Crus I-HPC, median [25–75 interquartile range (IQR)] coherence =  $0.471 [0.461–0.480]$ ; lobule II/III-HPC, median [IQR] coherence =  $0.467 [0.462–0.471]$ ; lobule VI-HPC, median [IQR] coherence =  $0.481 [0.471–0.486]$ ; Kruskal-Wallis with FDR correction, Kruskal-Wallis statistic =  $6.75$ ,  $p = 0.0342$ ) and post-hoc analysis revealed that LFP oscillations were significantly more synchronized between hippocampus and lobule VI than with lobule II/III (corrected  $p = 0.0246$ ). Within lobule VI, theta coherence was significantly correlated to the mediolateral position of the recording electrode, which was consistent with the mediolateral location of greatest RABV-labeled PCs (**Figure 3J**; Spearman rho =  $0.572$ ,  $p = 0.0225$ ).

Next, to ascertain if local cerebellar spiking activity is coordinated or modulated by hippocampal theta oscillations we recorded single, photo-identified Purkinje cells from lobule VI of head-fixed L7-ChR2 mice (selectively expressing channelrhodopsin in Purkinje cells;  $n = 6$ ) simultaneously with hippocampal LFP during periods of active movement. This allowed us to calculate the degree of phase-locking between the cerebellar spikes and hippocampal LFP, which circumvents volume conduction issues associated with LFP-LFP correlations (e.g. **Vinck et al., 2011**; **Nolte et al., 2004**; **Sirota et al., 2008**; **Stam et al., 2007**). We recorded a total of 22 units, of which 16 (from four mice) were classified as Purkinje cells based upon their responsivity to blue light illumination (see **Figure 3—figure supplement 3**). Of these 16 Purkinje cells, 31% (5 units) were significantly phase locked to the hippocampal 6–12 Hz oscillation (**Figure 3—figure supplement 4**) during periods of active movement (see Materials and methods). Of the six non-photo responsive units, 1 (16.7%) was significantly phase locked (**Figure 3—figure supplement 4D,E**). The mean vector angle of the significantly phase-locked units was  $231 \pm 18^\circ$ .

## Cerebello-hippocampal interactions during the learning of a goal-directed behavior

To further characterize the dynamics of cerebello-hippocampal interactions, we quantified cerebello-hippocampal theta coherence during a goal-directed task. A subset of mice ( $n = 8$ ) were trained to traverse a linear track to get a reward (medial forebrain bundle stimulation, see Materials and methods) at a fixed position (**Figure 4A**).

Across training, mice improved their performance as shown by the optimization of their path (**Figure 4A**), significant increase in the mean number of rewards obtained per day of training (**Figure 4B**; mean number of rewards obtained on 1<sup>st</sup> day =  $17 \pm 4$ , mean number of rewards obtained on 7th day =  $68 \pm 11$ ; repeated measures Friedman test, Friedman statistic =  $37.91$ ,

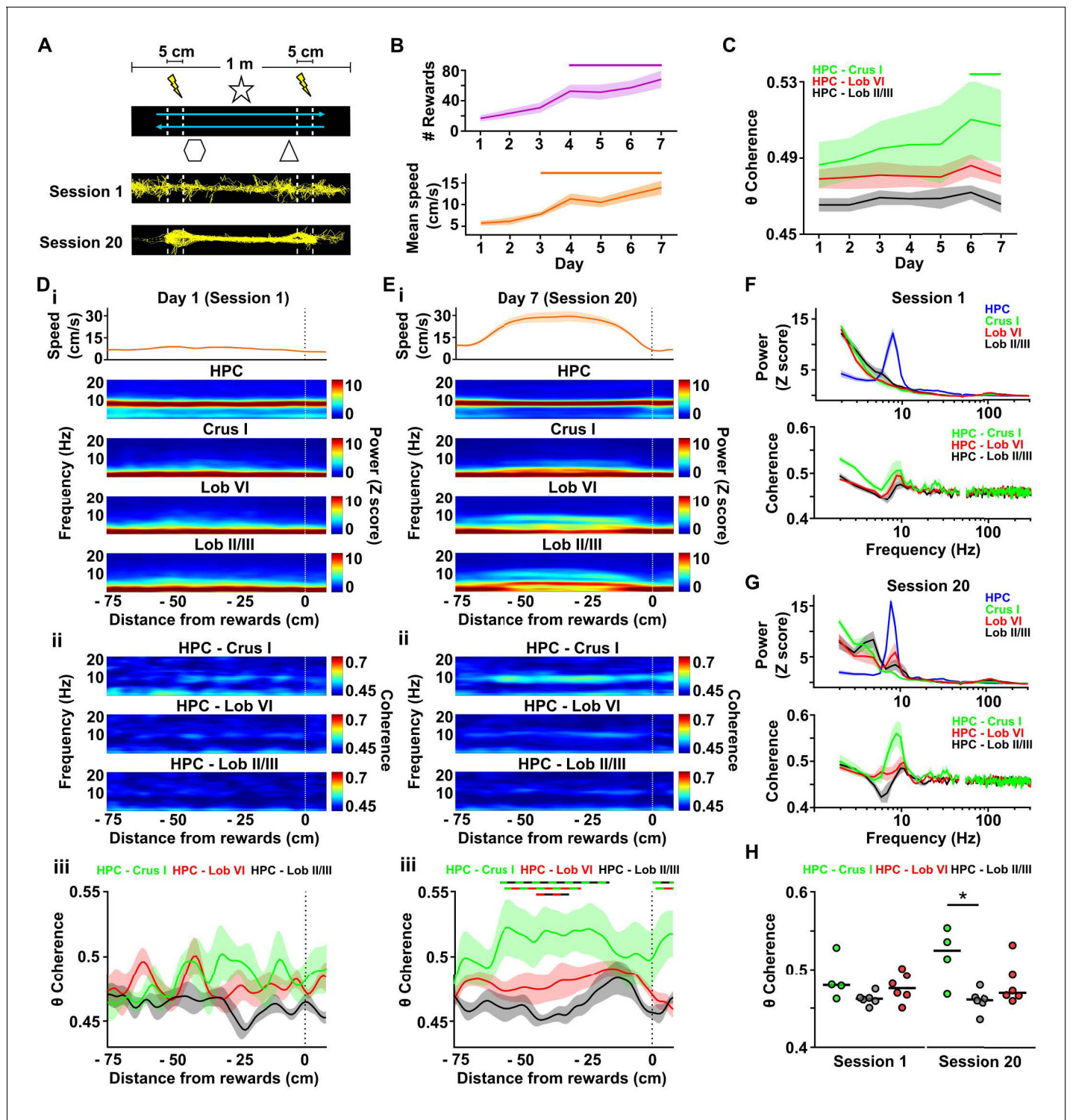


**Figure 4.** Cerebello-hippocampal interactions during goal-directed behavior. (A) Mice learned to traverse a 1 m linear track to receive a medial forebrain bundle stimulation (lightening symbols) upon reaching invisible goal zones ( $n = 8$  mice). Representative trajectories from early (session 1) and late (session 20) training show the transition from exploratory to goal-directed behavior. (B) Mice improved their performance in the task across days as shown by increases in the mean number of rewards obtained (average of the three sessions per day, repeated measures Friedman test with FDR correction, Friedman statistic = 37.91,  $p < 0.0001$ ; solid line, day 1 vs days 4–7,  $p < 0.01$ ) and mean speed (average of the three sessions per day, repeated measures Friedman test with FDR correction, Friedman statistic = 36.32,  $p < 0.0001$ ; solid line, day 1 vs days 4–7,  $p < 0.05$ ). (C) Overall cerebello-hippocampal theta coherence per day (average of the three sessions per day) during learning of the linear track task (when both hippocampal recording electrodes were on target we averaged the coherence obtained with left and right hemispheres; Crus I,  $n = 4$ ; lobule II/III,  $n = 6$ ; lobule VI,  $n = 8$ ). (D) Speed (cm/s) and power (Z score) heatmaps for HPC, Crus I, Lob VI, and Lob II/III on Day 1 (Session 1). (E) Speed (cm/s) and power (Z score) heatmaps for HPC, Crus I, Lob VI, and Lob II/III on Day 7 (Session 20). (F) Power (Z score) and coherence heatmaps for HPC-Crus I, HPC-Lob VI, and HPC-Lob II/III on Session 1. (G) Power (Z score) and coherence heatmaps for HPC-Crus I, HPC-Lob VI, and HPC-Lob II/III on Session 20. (H) Theta coherence for Session 1 and Session 20. \* indicates a significant difference between sessions for HPC-Crus I and HPC-Lob VI.

Figure 4 continued

$n = 6$ ). Hippocampus-Crus I coherence increased significantly compared with first day (day of training  $\times$  cerebello-hippocampal combination two-way ANOVA with FDR correction, day effect  $F_{6,84} = 3.873$ ,  $p = 0.0018$ ; solid line, day 1 vs days 6–7,  $p < 0.01$ ). (D) i, Top: Mean speed aligned by distance from the reward location (position 0) averaged across runs during session 1. Bottom: Mean power spectrogram aligned by distance from reward and averaged across runs during session one for hippocampus LFP ( $n = 8$ , mean between left and right hemisphere LFPs when both hippocampal recordings were on target) and cerebellar cortical regions (Crus I,  $n = 4$ ; lobule II/III,  $n = 6$ ; lobule VI,  $n = 6$ ). ii, Mean coherogram aligned by distance from reward location (position 0) averaged across runs during session one for each hippocampal-cerebellar combination (when both hippocampal recording electrodes were on target we averaged the coherence obtained with left and right; Crus I,  $n = 4$ ; lobule II/III,  $n = 6$ ; lobule VI,  $n = 6$ ). iii, Mean theta coherence aligned by distance from reward and averaged across runs during session one for each hippocampal-cerebellar combination (mean between coherence with left and right hemisphere LFPs when both recordings were on target; Crus I,  $n = 4$ ; lobule II/III,  $n = 6$ ; lobule VI,  $n = 6$ ). No significant differences between hippocampal-cerebellar combination or distances from reward were observed, but a significant interaction effect was obtained (distance  $\times$  combination two-ways repeated measures ANOVA with FDR correction; combination effect,  $F_{2,13} = 2.33$ ,  $p = 0.1365$ ; distance effect,  $F_{84,1092} = 1.043$ ,  $p = 0.3772$ ; interaction effect,  $F_{168,1092} = 1.332$ ,  $p = 0.0053$ ). (E) Same as D for session 20. Significant differences were observed between hippocampal-cerebellar combinations (distance  $\times$  combination two-ways repeated measures ANOVA with FDR correction; combination effect,  $F_{2,13} = 6.145$ ,  $p = 0.0132$ ; distance effect,  $F_{84,1092} = 1.682$ ,  $p = 0.0002$ ; interaction effect,  $F_{168,1092} = 1.271$ ,  $p = 0.0163$ ). Post-hoc analysis revealed sustained (at least for five consecutive cm) differences between Crus I-HPC and lobule II/III-HPC coherence at distances from  $-60$  to  $-20$  cm from reward (solid green/black line), between lobule VI-HPC and lobule II/III-HPC coherence between  $-44$  and  $-31$  cm from reward (solid red/black line) and also between Crus I-HPC and lobule VI-HPC coherence between  $-59$  and  $-36$  cm from reward (solid green/red line). (F) Top: Averaged LFP power between  $-60$  and  $-20$  cm from reward (session 1). Bottom: Averaged coherence between  $-60$  and  $-20$  cm from reward (session 1). The spurious peak in the 49–51 Hz band generated for the electrical noise has been removed. (G) Same as J for session 20. (H) Averaged theta coherence between  $-60$  and  $-20$  cm from reward between cerebellar recordings and hippocampus during session 1 (left) and session 20 (right, coherence averaged between left and right hemisphere LFPs when both hippocampal recording electrodes were on target; Crus I,  $n = 4$ ; lobule II/III,  $n = 6$ ; lobule VI,  $n = 6$ ). Crus I-HPC coherence was significantly higher than that observed with lobule II/III in the session 20 (\*, Kruskal-Wallis with FDR correction, Kruskal-Wallis statistic = 7.989,  $p = 0.0103$ ; Crus I-HPC vs lobule II/III-HPC,  $p = 0.0110$ ).

DOI: <https://doi.org/10.7554/eLife.41896.016>

The following source data and figure supplements are available for figure 4:

**Source data 1.** Cerebello-hippocampal interactions during goal-directed behavior.DOI: <https://doi.org/10.7554/eLife.41896.021>**Figure supplement 1.** Cerebello-hippocampal coherence patterns are conserved across hemispheres during goal-directed behavior.DOI: <https://doi.org/10.7554/eLife.41896.017>**Figure supplement 2.** Distributions and correlations during goal-directed behavior.DOI: <https://doi.org/10.7554/eLife.41896.018>**Figure supplement 3.** Calculation of the imaginary part of coherence during goal-directed behavior.DOI: <https://doi.org/10.7554/eLife.41896.019>**Figure supplement 4.** Cerebello-hippocampal coherence patterns during running or goal-directed movement in a virtual environment.DOI: <https://doi.org/10.7554/eLife.41896.020>

$p < 0.0001$ ) and the significant increase in their mean speed (**Figure 4B**; mean speed on 1st day =  $5.74 \pm 0.54$  cm/s, mean speed on 7th day =  $13.94 \pm 1.63$  cm/s; repeated measures Friedman test, Friedman statistic = 36.32,  $p < 0.0001$ ). Thus, we next explored the dynamics of cerebello-hippocampal theta coherence across this learning period. We confirmed the absence of a laterality effect on the power spectra calculated at the beginning (**Figure 4—figure supplement 1A**; Session 1; HPC left,  $n = 6$ , median [IQR] 6–12 Hz z-score power = 5.842 [5.683 6.384]; HPC right,  $n = 7$ , median [IQR] 6–12 Hz z-score power = 6.261 [4.919 6.587]; Mann-Whitney test,  $U = 18$ ,  $p = 0.7308$ ) or end (**Figure 4—figure supplement 1B**; Session 20; HPC left, median [IQR] 6–12 Hz z-score power = 5.850 [5.583 6.002]; HPC right: median [IQR] 6–12 Hz z-score power = 5.898 [5.511 6.110]; Mann-Whitney test,  $U = 20$ ,  $p = 0.9452$ ) of training. Consequently, we averaged the spectral power from left and right hemispheres when both were available. Similarly, no differences on coherence between left and right hippocampi and the different cerebellar recordings were observed at the beginning (**Figure 4—figure supplement 1C,E**; Session 1; Crus I-HPC left,  $n = 3$ , median [IQR] 6–12 Hz coherence = 0.4789 [0.4557 0.5326]; Crus I-HPC right,  $n = 3$ , median [IQR] 6–12 Hz coherence = 0.4802 [0.4687 0.5238]; Mann-Whitney test,  $U = 4$ ,  $p > 0.99$ ; lobule II/III-HPC left,  $n = 4$ , median [IQR] 6–12 Hz coherence = 0.4574 [0.4513 0.4709]; lobule II/III-HPC right,  $n = 5$ , median [IQR] 6–12 Hz coherence = 0.4633 [0.4549 0.4663]; Mann-Whitney test,  $U = 8$ ,  $p = 0.7302$ ; lobule VI-

HPC left,  $n = 6$ , median [IQR] 6–12 Hz coherence = 0.4764 [0.4653 0.4904]; lobule VI-HPC right,  $n = 5$ , median [IQR] 6–12 Hz coherence = 0.4684 [0.4558 0.4857]; Mann-Whitney test,  $U = 10$ ,  $p = 0.4286$ ) or end (**Figure 4—figure supplement 1D,F**; Session 20; Crus I-HPC left, median [IQR] 6–12 Hz coherence = 0.5357 [0.4747 0.5574]; Crus I-HPC right, median [IQR] 6–12 Hz coherence = 0.5137 [0.4616 0.5500]; Mann-Whitney test,  $U = 3$ ,  $p = 0.7$ ; lobule II/III-HPC left, median [IQR] 6–12 Hz coherence = 0.4596 [0.4466 0.4769]; lobule II/III-HPC right, median [IQR] 6–12 Hz coherence = 0.4595 [0.4422 0.4736]; Mann-Whitney test,  $U = 10$ ,  $p = 0.7302$ ; lobule VI-HPC left, median [IQR] 6–12 Hz coherence = 0.4702 [0.4662 0.5124]; lobule VI-HPC right, median [IQR] 6–12 Hz coherence = 0.4665 [0.4610 0.5066]; Mann-Whitney test,  $U = 12$ ,  $p = 0.6623$ ) of training so the averaged coherence between cerebellum and both hippocampal hemispheres was computed when possible.

We first examined overall, mean cerebello-hippocampal theta coherence as learning progressed. We observed significant changes over training (**Figure 4C**; Crus I-HPC,  $n = 4$ ; lobule II/III-HPC,  $n = 6$ ; lobule VI-HPC,  $n = 6$ ; day of training  $\times$  cerebello-hippocampal combination two-way repeated measures ANOVA with FDR correction, day effect  $F_{6,84} = 3.873$ ,  $p = 0.0018$ ) and post-hoc analysis revealed that only Crus I-HPC coherence significantly increased when comparing with values observed on the first day of training ( $p < 0.01$  for days 6 and 7). We next examined detailed power spectra and coherence dynamics at the level of individual sessions from first day of training (session 1), when animals exhibited an exploratory behavioral profile, and the last day of training (session 20), when animals performed efficient goal-directed behavior (**Figure 4**). This allowed us to investigate the spatial dynamics of both the cerebellar and hippocampal LFP profiles alongside coherence as mice traversed the linear track to reach the reward.

During session 1, mice approached the reward point with a sustained and low speed (**Figure 4Di**, top), which is in agreement with the exploratory behavioral profile illustrated by the distributed occupancy of their trajectories on the track (**Figure 4A** bottom). The hippocampal spectrogram was dominated by sustained activity in the theta band across the whole track. In contrast, clear activity in this frequency band was not apparent in the cerebellar recordings (**Figure 4Di**) and the LFP power profile was maintained at low levels across the track. This homogeneous pattern was consistent with the unimodal distributions of instantaneous hippocampal and cerebellar theta power (**Figure 4—figure supplement 2A**). Similarly, the coherograms did not reveal clear coherence in any of the cerebello-hippocampal combinations (**Figure 4Dii**). However, we found a significant interaction between the distance from reward and the theta coherence of different cerebello-hippocampal combinations (**Figure 4Diii**; distance from reward point  $\times$  combination two-way repeated measures ANOVA; combination effect,  $F_{2,13} = 2.33$ ,  $p = 0.1365$ ; distance effect,  $F_{84,1092} = 1.043$ ,  $p = 0.3772$ ; interaction effect,  $F_{168,1092} = 1.332$ ,  $p = 0.0053$ ). Post-hoc, FDR corrected, multiple comparisons revealed that significantly higher theta coherence was present between hippocampus and Crus I compared to lobule II/III at certain positions on the track prior to the reward point location (Crus I-HPC vs lobule II/III-HPC,  $p < 0.05$  from  $-29$  to  $-21$  cm from reward; lobule VI-HPC vs lobule II/III-HPC,  $p < 0.05$  from  $-25$  to  $-22$  cm from reward). As for the homecage recordings, instantaneous theta coherence for all cerebello-hippocampal combinations also followed gaussian, unimodal distributions during session one in the linear track (**Figure 4—figure supplement 2E**).

On the last day of training, during session 20, mice displayed goal-directed behavior on the track. This goal-directed profile was illustrated in the efficient running trajectories (**Figure 4A** bottom) and by the acceleration-plateau-deceleration speed profile observed along the track (**Figure 4Ei** top). As in session 1, the hippocampal spectrogram was dominated by sustained theta activity. On the other hand, cerebellar LFP power profiles were notably different from session one with the appearance of sustained activity in the theta and delta (2–4 Hz) frequency bands, particularly in lobule VI and lobule II/III (**Figure 4Ei** bottom). These differences were not related to transient bouts of theta activity as the instantaneous theta power probability distributions continued showing unimodal profiles (**Figure 4—figure supplement 2C**). Coherogram analysis also revealed changes in session 20, which were mainly reflected in sustained Crus I-HPC theta coherence spanning multiple positions on the track as animals actively approached the reward (**Figure 4Eii**). This pattern was not as apparent in the other cerebello-hippocampal combinations (**Figure 4Eiii**; distance from reward  $\times$  cerebello-hippocampal combination two-way repeated measures ANOVA, distance from reward effect  $F_{84,1092} = 1.682$ ,  $p = 0.0002$ ; combinations effect  $F_{2,13} = 6.145$ ,  $p = 0.0132$ ; interaction effect  $F_{168,1092} = 1.271$ ,  $p = 0.0163$ ) and post-hoc FDR corrected multiple comparisons revealed significantly higher

sustained theta coherence between hippocampus and Crus I than with lobule II/III from -60 to -20 cm or with lobule VI from -59 to -36 cm prior to the reward point. Lobule VI-HPC coherence was also higher than with lobule II/III at some positions on the track (-44 to -31 cm from reward) although it was not as sustained and prominent as Crus I-HPC coherence. Importantly, we also reproduced these findings when the imaginary part of coherency was computed, which is robust against contamination by volume conduction (**Figure 4—figure supplement 3**).

In order to better explore the differences between sessions 1 and 20 we then pooled power spectra (**Figure 4F and G** top panels) and coherence (**Figure 4F and G** bottom panels) between -60 and -20 cm from reward point (i.e. the range of distances where differences across recording combinations were most apparent in the coherograms). The appearance of a theta peak in the power spectra from all cerebellar recordings in session 20 compared with session one can be clearly seen (**Figure 4G**) as well as the increase in coherence limited to this frequency band (Session 20: frequency band (theta, beta, low gamma) x cerebello-hippocampal combination two way repeated measures ANOVA, frequency band effect  $F_{2,26} = 13.42$ ,  $p < 0.0001$ ; combination effect  $F_{2,13} = 6.545$ ,  $p = 0.0108$ ; interaction effect,  $F_{4,26} = 5.242$ ,  $p = 0.0031$ ; post-hoc multiple comparisons with FDR correction revealed significant differences between combination only in the theta band). We found that in session 20 theta coherence between hippocampus and Crus I was significantly higher than that obtained with lobule II/III (**Figure 4H** right; Crus I-HPC,  $n = 4$ , median [IQR] coherence = 0.525 [0.480–0.549]; lobule II/III-HPC,  $n = 6$ , median [IQR] coherence = 0.461 [0.452–0.468]; lobule VI-HPC,  $n = 6$ , median [IQR] coherence = 0.470 [0.465–0.503]; Kruskal-Wallis with FDR correction, Kruskal-Wallis statistic = 7.989,  $p = 0.0103$ ; Crus I-HPC vs lobule VI-HPC, corrected  $p = 0.0110$ ) while no significant difference was found in session 1 (**Figure 4H** left; Crus I-HPC,  $n = 4$ , median [IQR] coherence = 0.480 [0.466–0.516]; lobule II/III-HPC,  $n = 6$ , median [IQR] coherence = 0.462 [0.457–0.466]; lobule VI-HPC,  $n = 6$ , median [IQR] coherence = 0.476 [0.463–0.494]; Kruskal-Wallis with FDR correction, Kruskal-Wallis statistic = 4.779,  $p = 0.0887$ ).

Given that the speed profiles of mice changed significantly between sessions 1 and 20 on the linear track (**Figure 4B,D,G**) and seemed to mirror the observed modulation in theta power and coherence, we next correlated instantaneous cerebellar theta power (**Figure 4—figure supplement 2B,D**) and instantaneous theta coherence (**Figure 4—figure supplement 2F,H**) with instantaneous speed. In contrast to home-cage recordings, for all recorded cerebellar LFPs, theta power was significantly positively correlated with speed during both session 1 (**Figure 4—figure supplement 2B**; Crus I, median [IQR] Spearman rho = 0.213 [0.209 0.258], bootstrap confidence level = 0.081; lobule II/III, median [IQR] Spearman rho = 0.239 [0.065 0.343], bootstrap confidence level = 0.082; lobule VI, median [IQR] Spearman rho = 0.235 [0.090 0.284], bootstrap confidence level = 0.083) and session 20 (**Figure 4—figure supplement 2D**, Crus I, median [IQR] Spearman rho = 0.235 [0.056 0.465], bootstrap confidence level = 0.081; lobule II/III, median [IQR] Spearman rho = 0.310 [-0.010 0.490], bootstrap confidence level = 0.081; lobule VI, median [IQR] Spearman rho = 0.194 [0.105 0.550], bootstrap confidence level = 0.085). Cerebello-hippocampal theta coherence was not correlated with instantaneous speed during session 1 (**Figure 4—figure supplement 2F**; Crus I-HPC, median [IQR] Spearman rho = 0.024 [-0.033 0.237], bootstrap confidence level = 0.082; lobule II/III-hippocampus, median [IQR] Spearman rho = 0.0278 [-0.105 0.050], bootstrap confidence level = 0.075; lobule VI-HPC, median [IQR] Spearman rho = -0.001 [-0.052 0.045], bootstrap confidence level = -0.090). However, during session 20, lobule II/III-HPC theta coherence was anticorrelated with speed (**Figure 4—figure supplement 2H**; lobule II/III-HPC, median [IQR] Spearman rho = -0.086 [-0.182 0.012], bootstrap confidence level = -0.080) while lobule VI-HPC was weakly but significantly correlated with it (lobule VI-HPC, median [IQR] Spearman rho = 0.091 [-0.140 0.173], bootstrap confidence level = 0.090). Interestingly, the Crus I-HPC recording combination, which presented higher and sustained levels of theta coherence during this task, was not significantly correlated with instantaneous speed (Crus I-HPC, median [IQR] Spearman rho = 0.020 [-0.051 0.094], bootstrap confidence level = 0.083). Together, these findings suggest that the observed Crus I - HPC theta coherence dynamics during goal-directed behavior in the linear track cannot be explained by changes in running speed.

We also observed similar cerebello-hippocampal coherence dynamics in mice navigating for rewards in a virtual reality based linear track (**Figure 4—figure supplement 4A–C**,  $n = 6$ ). A marked spatial re-organization of cerebello-hippocampal theta coherence was apparent in those mice that showed behavioral modulation across training (as evidenced by increases in the number of rewards

across day of training and speed modulation on a run by run basis during approach to the reward location; **Figure 4—figure supplement 4G–I**). In contrast, mice that failed to show behavioral modulation across training, and displayed rather homogenous speed profiles, did not present such coherence dynamics (**Figure 4—figure supplement 4D–F**).

To examine whether the observed changes in coherence across learning of the linear track were specifically related to performance of the goal-directed task itself, we next conducted pairwise analysis of cerebello-hippocampal theta coherence levels across the following conditions: home-cage prior to any linear track training (HC pre, considered as baseline), the 1st and 20th linear track trials, and home-cage following the end of training in the linear track task (HC post) (see **Figure 5**).

From the three cerebello-hippocampal recording configurations, only Crus I-HPC theta coherence varied significantly across task conditions (**Figure 5**,  $n = 4$ , repeated measures Friedman test with FDR correction, Friedman statistic = 11.1,  $p = 0.0009$ ). At the outset of linear track learning (session 1), HPC-Crus I coherence values did not significantly differ from home-cage (HC pre, median [IQR] = 0.471 [0.461 0.495]; session 1, median [IQR] = 0.480 [0.466 0.516], corrected  $p = 0.1196$ ). However, during late stage linear track learning, the level of coherence was significantly higher than in home-cage recordings (HC pre, median [IQR] = 0.471 [0.461 0.495]; session 20, median [IQR] = 0.525 [0.480 0.550], corrected  $p = 0.0021$ ) and when mice were returned to the home-cage environment following completion of linear track training (HC post) the level of HPC-Crus I coherence dropped back to pre-training levels (HC pre, median [IQR] = 0.471 [0.461 0.495]; HC post, median [IQR] = 0.493 [0.471 0.505], corrected  $p = 0.0580$ ).

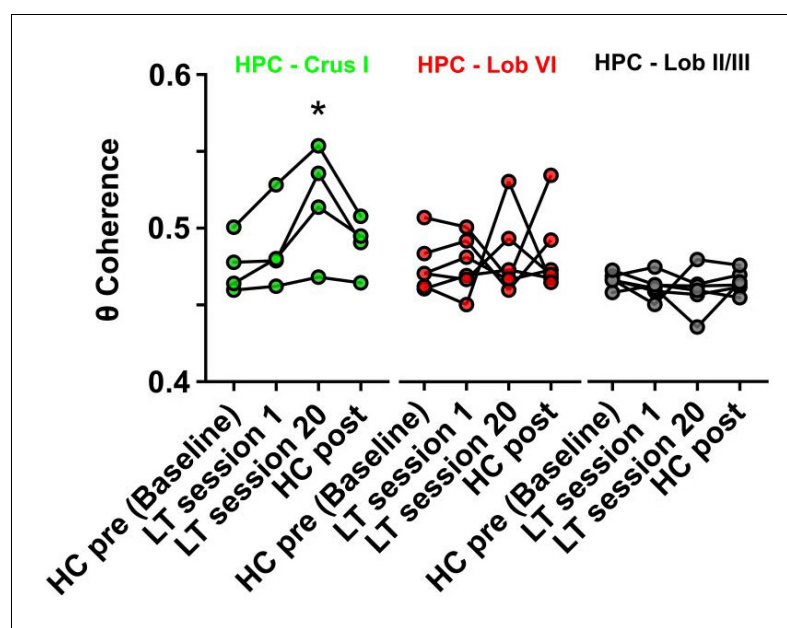


**Figure 5.** Hippocampal-Crus I theta coherence is dynamic. Comparisons of hippocampal-cerebellar theta coherence before and after acquisition of a goal-directed behavior in the linear track task. Levels of coherence during homecage active exploration before first session in the linear track were taken as a baseline. HPC-Crus I theta coherence became significantly different from baseline by session 20 in the linear track task and returned to baseline levels during a second homecage recording immediately following linear track session 20 ( $n = 4$ , repeated measures Friedman test with FDR correction, Friedman statistic = 11.1,  $p = 0.0009$ ; LT session 20 vs baseline,  $p = 0.0021$ ). No significant differences across conditions were observed for the other hippocampal-cerebellar combinations.

DOI: <https://doi.org/10.7554/eLife.41896.022>

The following source data is available for figure 5:

**Source data 1.** Hippocampal-Crus I theta coherence is dynamic.

DOI: <https://doi.org/10.7554/eLife.41896.023>

## Discussion

Taken together, our findings reveal previously undescribed cerebellar inputs to the hippocampus and offer novel physiological insights into a long-range neural network linking disparate brain regions initially assumed to support divergent behavioral functions, namely spatial navigation (hippocampus) and motor control (cerebellum). Projections from topographically restricted regions of cerebellar cortex discretely route through restricted parts of their associated nuclei en-route to the hippocampus through multiple, convergent pathways, involving one or two relays, from the DCN. Interestingly, the possible single-relay pathways we described points toward involvement of the medial septum and the supramammillary nucleus, two structures crucial for theta generation. Congruently, our physiological data suggest that these connected cerebellar regions may dynamically interact with the hippocampus during behavior, via theta (6–12 Hz) LFP coherence. Our findings thus offer an anatomical and physiological framework for cerebello-hippocampal interactions that could support cerebellar contributions to hippocampal processes (Burguière *et al.*, 2005), including spatial map maintenance (Rochefort *et al.*, 2011; Rondi-Reig *et al.*, 2014; Lefort *et al.*, 2019).

Whilst previous studies provide compelling physiological evidence of cerebellar influences on the hippocampus (Cooke and Snider, 1955; Iwata and Snider, 1959; Babb *et al.*, 1974; Snider and Maiti, 1975; Krook-Magnuson *et al.*, 2014; Choe *et al.*, 2018), they do not provide the spatial resolution afforded by neuroanatomical tracing. Indeed, to the best of our knowledge, anatomical tracing studies have failed to report a mono-synaptic ascending cerebello-hippocampal projection. This is consistent with our rabies virus tracing study, in which incubation periods of 48–58 hr were required before cell labeling was seen in the cerebellar nuclei. Such a timescale is indicative of a multi-synaptic pathway (Kelly and Strick, 2000; Ugolini, 2010; Suzuki *et al.*, 2012; Jwair *et al.*, 2017). Single relay pathways can be envisioned through the septum, the hypothalamus (potentially including the supramammillary nucleus (SUM)) and the raphe nucleus. Other pathways including two relays through either the lateral and medial entorhinal cortex and/or the perirhinal cortex are also possible. Interestingly, among the different regions labeled at 48 hr post-infection, several midbrain and pontine regions such as the PAG, the nucleus incertus and the LtDG are known to receive direct projections from the DCN and could therefore represent putative first-order relays between cerebellum and hippocampus.

Our anatomical results highlight three main inputs to the hippocampus emanating from the cerebellum. The first input we reveal originates from the vestibulo-cerebellum, specifically from the dorsal and ventral paraflocculus, which is likely routed via the vestibular and dentate nuclei (Voogd and Barmack, 2006). This anatomical connection between the vestibulo-cerebellum and the hippocampus reinforces the already well-described influence of the vestibular system on hippocampal-dependent functions (Stackman *et al.*, 2002; Goddard *et al.*, 2008; Zheng *et al.*, 2009).

In addition to the classically described vestibular pathway, our data reveal that the central cerebellum also provides inputs to the hippocampus from vermal lobule VI, routed through caudal fastigial nucleus, and from Crus I, routed through the dentate. Using a combination of RABV expression and zebrin II staining, we identified three specific cerebellar modules involved in these inputs: (1) the A module in lobule VI, (2) the hemispheric Crus I D2 module and (3) the Crus I paravermal C2 module. Of the latter two modules, C2 is likely less prominently anatomically connected with the hippocampus since the number of RABV+ cells in the nucleus interpositus posterior, its output nucleus (Apps and Hawkes, 2009), was minor compared with the other cerebellar nuclei. The convergence of inputs from disparate cerebellar zones (flocculo-nodular and central zones) and modules from vermal (A), paravermal (C2) and hemispheric (D2) regions in to the hippocampus suggest that its optimal function requires the integration of multiple aspects of sensory-motor processing carried out at these distinct cerebellar locations.

According to Voogd and Barmack (2006), based upon evidence from a wide range of species, the oculomotor cerebellum can be most broadly described to include lobule V, VI and VII. Given the highly conserved structure-function relationships of the vermal cerebellum (Sillitoe *et al.*, 2005), it seem likely that the mouse A module could also be considered part of the oculomotor cerebellum. In rat, it receives climbing fibers from the caudal medial accessory olive, and sends mainly ascending projections through the caudal portion of fastigial nucleus (Apps, 1990; Apps and Hawkes, 2009). The oculomotor vermis receives multiple sensory inputs which include visual, proprioceptive, vibrissae, vestibular and auditory inputs conveyed by both climbing and mossy fibers (Voogd and

**Barmack, 2006**). The D2 module receives its climbing fiber input from the dorsal cap of the principal olive and projects out of the cerebellum through the rostromedial dentate nucleus (**Herrero et al., 2006**). It receives mossy fiber inputs carrying somatosensory, motor (**Mihailoff et al., 1981**), and visual (**Edge et al., 2003**) information; along with inputs from the prefrontal cortex (**Kelly and Strick, 2003**). Climbing fiber inputs to this module relay information from the parvocellular red nucleus, which receives projections from premotor, motor, supplementary motor and posterior parietal areas. The majority of these cortical areas also receive projections from the D2 module after a thalamic relay in the ventro-lateral nucleus (**Kelly and Strick, 2003; Glickstein et al., 2011**).

Complementary to these anatomical results, our electrophysiological findings reveal coherent activity between the hippocampus and those cerebellar lobules that are anatomically connected with it (lobule VI and Crus I). This synchronization was restricted to the 6–12 Hz frequency range in the awake, behaving animal and showed dynamic profiles that were lobule dependent. Oscillations can align neuronal activity within and across brain regions, suggesting a facilitation of cross-structure interactions (e.g. **Singer, 1999; Fries, 2005**). Cerebellar circuits support oscillations across a range of frequencies (for review see **De Zeeuw et al., 2008; Cheron et al., 2016**). Of particular relevance to the current study are reports of oscillations within the theta frequency (~4–12 Hz), which have been described in the cerebellar input layers at the Golgi (**Dugué et al., 2009**) and granule cell (**Hartmann and Bower, 1998; D'Angelo et al., 2001**) level, and also in the cerebellar output nuclei (**Wang et al., 2014; Watson et al., 2014**).

Neuronal coherence has been described across the cerebro-cerebellar system at a variety of low frequencies (**O'Connor et al., 2002; Courtemanche and Lamarre, 2005; Soteropoulos and Baker, 2006; Rowland et al., 2010; Frederick et al., 2014; Watson et al., 2014; Chen et al., 2016**) and oscillations within the theta range are thought to support inter-region communication across a wide variety of brain regions (**Colgin, 2013**). Our finding that cerebello-hippocampal coherence is limited to the 6–12 Hz bandwidth is in keeping with previous studies on cerebro-cerebellar communication in which neuronal synchronization has been observed between the cerebellum and prefrontal cortex (**Watson et al., 2014; Chen et al., 2016**), primary motor cortex (**Soteropoulos and Baker, 2006; Rowland et al., 2010**), supplementary motor area (**Rowland et al., 2010**) and sensory cortex (**Rowland et al., 2010**). Furthermore, LFPs recorded in the hippocampus and cerebellar cortex are synchronized within the theta bandwidth during trace eye-blink conditioning in rabbits (**Hoffmann and Berry, 2009; Wikgren et al., 2010**). Human brain imaging studies have also described co-activation of blood oxygen level dependent signals in both cerebellar and hippocampal regions during navigation (**Iglói et al., 2015**) and spatio-temporal prediction tasks (**Onuki et al., 2015**), thus highlighting putative neuronal interactions between the two structures. Regarding studies in mice, a recent study has demonstrated the existence of statistically significant co-activation of the dorsal hippocampus and cerebellar lobules IV-V, lobule VI and Crus I after the acquisition of a sequence-based navigation task (**Babayán et al., 2017**).

Multiple lines of evidence suggest that the coherence described here is unlikely to have resulted from volume conduction: 1) Rather than using a common reference electrode, our recordings were bipolar, with each recording electrode being locally and independently referenced (**Kajikawa and Schroeder, 2011**). 2) If volume conduction of theta oscillations was emanating from a hippocampal source then it could be assumed that cerebellar regions in closer proximity to the hippocampus would show higher levels of coherence (**Figure 3—figure supplement 2**). However, we found that coherence values were not related to the relative distance between the hippocampus and cerebellar recording site. 3) By recording simultaneously from hippocampus and multiple cerebellar regions, we have been able to demonstrate that the observed coherence is non-homogenous among the different cerebellar lobules in contrast to what one would expect if theta was volume conducted from a common location. 4) We calculated the imaginary part of coherency, which is not influenced by volume conduction (**Nolte et al., 2004**), in the linear track paradigm and found results that were remarkably similar to those obtained using standard coherence analysis. 5) We showed that Purkinje cell spikes in lobule VI of the cerebellum can phase lock to hippocampal theta oscillations.

Importantly, we have shown for the first time that theta rhythms in the hippocampus preferentially synchronize with those in discrete regions of the cerebellum and that the degree of this coupling changes depending upon the behavioral context. Lobule VI-HPC coherence was dominant during active movement in the home-cage and remained stable during learning of the real world linear track task. On the other hand, Crus I - HPC coherence was highly dynamic, showing a significant

increase over learning of the real world linear track task and becoming dominant after the acquisition of a goal-directed behavior. Furthermore, we reveal that high Crus I-HPC coherence was sustained across the linear track when the animal performed goal-directed behavior but not during the early training, exploration phase. Such sustained coherence may be related to the ability of the cerebellum, and particular Crus I, to link internal and external sensory context with specific action toward the goal. In line with this hypothesis, a recent study has suggested that Purkinje cells in the Crus I region and neurons in its output, the dentate nucleus, exhibit firing rate modulation in anticipation of expected reward in a VR task (*Chabrol et al., 2018*). Interestingly, they show that the activity of Purkinje cells in lateral Crus I was modulated by running and/or visual flow speed. This is consistent with our examples showing that Crus I-HPC coherence remained present when animals performed goal-modulated behavior in VR, although multiple streams of sensory input, such as vestibular, whisker and olfactory, become irrelevant and even confounding in the head-restricted virtual environment task.

We next consider our results within the well characterized, modular understanding of cerebellar function. Within lobule VI, the A module receives multi-modal sensory information, mainly arising from collicular and vestibular centers (*Voogd and Barmack, 2006*). The superior colliculus plays a role in visual processing and generation of orienting behaviors (*Basso and May, 2017*), which might be relevant for the establishment and maintenance of the hippocampal spatial map, and thus may be required constantly during active movement, independent of the specific behavioral task. The persistent and similar levels of lobule VI-HPC coherence during active movement in the homecage and linear track task, in both real world and virtual reality environment tasks is in agreement with such a hypothesis.

In monkeys and humans, Crus I is anatomically and functionally associated with prefrontal cortex (*Kelly and Strick, 2003; Iglói et al., 2015*). In mouse Crus I, the D2 module receives convergent sensory and motor information (*Proville et al., 2014*). Furthermore, this module has been found to contain internal models, a neural representation of one's body and the external world based on memory of previous experiences, that are used for visuo-motor coordination (*Cerminara et al., 2009*). Similarly, the C2 module has been found to also participate in visuo-motor processing related to limb coordination during goal-directed reaching (*Cerminara and Apps, 2011*). Both modules might be particularly important during the acquisition of a goal-directed behavior such as our real-world linear track task in which animals needed to reach non-cued reward zones. Our finding that Crus I-HPC coherence increases during task learning fits with this hypothesis.

In summary, our results suggest the existence of anatomically discrete hippocampal-cerebellar network interactions with a prominent involvement of Crus I during goal-directed behavior. Both anatomical and electrophysiological data point toward involvement of the theta generating pathway in cerebellum-hippocampus interactions. The topographical dynamic weighting of these interactions may be tailored to the prevailing sensory context and behavioral demands.

## Materials and methods

Anatomical tracing studies were performed under protocol N°00895.01, in agreement with the Ministère de l'Enseignement Supérieur et de la Recherche. RABV injections were performed by vaccinated personnel in a biosafety containment level two laboratory.

All behavioral experiments were performed in accordance with the official European guidelines for the care and use of laboratory animals (86/609/EEC) and in accordance with the Policies of the French Committee of Ethics (Decrees n° 87–848 and n° 2001–464). The animal housing facility of the laboratory where experiments were made is fully accredited by the French Direction of Veterinary Services (B-75-05-24, 18 May 2010). Surgeries and experiments were authorized by the French Direction of Veterinary Services (authorization number: 75–752).

A total of 44 adult, male mice were used for this study. Seventeen adult male C57BL6-J mice were used for the anatomical tracing study, (Charles River, France) and 21 for the electrophysiology study (Janvier, France). Six adult male CD-L7ChR2 mice were used for the dual hippocampal LFP and cerebellar unit-recording study (in-house colony derived from Jackson labs stock, USA).

Mice received food and water *ad libitum*, were housed individually (08: 00–20: 00 light cycle) following surgery and given a minimum of 5 days post-surgery recovery before experiments commenced.

## Anatomy

### Rabies virus injections

All the RABV (the French subtype of Challenge Virus Standard; CVS-N2C) inoculations were performed in the Plasticity and Physio-Pathology of Rhythmic Motor Networks (P3M) laboratory, Timone Neuroscience Institute, Marseille, France. Mice ( $n = 17$ ) were injected intraperitoneally with an anesthetic mixture of ketamine (65 mg/kg; Imalgene, France) and xylazine (12 mg/kg; Rompun, Bayer) to achieve surgical levels of anesthesia, as evidenced by the absence of limb withdrawal and corneal reflexes and lack of whisking and were then placed in a stereotaxic frame (David Kopf Instruments, USA). The scalp was then incised, the skull exposed and a craniotomy drilled above the hippocampus.

Mice were injected with 200 nL of a mixture of one part 1% CTb Alexa Fluor 488 Conjugate (Invitrogen, distributed by Life Technologies, Saint Aubain, France) and four parts RABV in the left hippocampus (AP  $-2.0$ , ML  $+2.0$ , DV  $1.97$ ; **Figure 1—figure supplement 1 and**) using a Hamilton needle with internal diameter of  $\sim 200$   $\mu\text{m}$  (Hamilton, USA). Injections (200 nL/min) were performed using a pipette connected to a 10  $\mu\text{L}$  Hamilton syringe mounted on a microdrive pump. Following infusion, the pipette was left in place for 5 min. The incision was then sutured and the animals allowed to recover in their individual home cage for either 30 hr ( $n = 4$ ); 48 hr ( $n = 3$ ), 58 hr ( $n = 5$ ) or 66 hr ( $n = 5$ ). All animals were carefully monitored during the survival period and, in line with previous studies using these survival times, were found to be asymptomatic (**Ugolini, 2010**).

### Tissue preparation

At the end of the survival time, mice were deeply anesthetized with sodium pentobarbitone (100 mg/kg, intraperitoneal) then transcardially perfused with 0.9% saline solution (15 mL/min) followed by 75 mL of 0.1M phosphate buffer (PB) containing 4% paraformaldehyde (PFA; pH = 7.4). The brain was then removed, post fixed for 2–3 days in 4% PFA and then stored at 4°C in 0.1 M PB with 0.02% sodium azide. Extracted brains were then embedded in 3% agarose before being coronally sectioned (40  $\mu\text{m}$ ) on a vibratome. Serial sections were collected and divided in 4 vials containing 0.1 M PB so consecutive slices in each vial were spaced by 160  $\mu\text{m}$ .

### Injection site visualization

Sections from vial one were used to visualize the injection site by the presence of CTb. In most of the cases, the injected CTb was fluorescent and sections were directly mounted with Dapi Fluoromount G (SouthernBiotech, Alabama, USA). In the other cases (S4-5, S11-13 and S17-18), the sections were first rinsed with PB 0.1 M and then permeated with PB 0.1 M and 0.3% Triton X-100. They were then incubated overnight in a cholera toxin B subunit antibody raised in goat (goat anti-CTb, lot no. 703, List Biological Laboratories, USA) diluted 1: 2000 in a blocking solution (PB 0.1 M, 5% BSA). Subsequently, the sections were rinsed in PB 0.1 M and incubated for 4 hr at room temperature with donkey anti-goat secondary antibody (1: 1000 in the blocking solution; Alexa Fluor 555, Invitrogen, distributed by ThermoFisher Scientific, Massachusetts, USA). Finally, the sections were mounted with Dapi Fluoromount G.

The injection site was then visualized using a fluorescence microscope equipped with a fluorescein isothiocyanate filter (Axio Zoom V16, Carl Zeiss, France).

### Rabies virus labeled cell quantification

Sections from vial two were used for quantification and 3 D reconstruction of the RABV labeled cells. Sections mounted on gelatin-coated SuperFrost Plus slides (Menzel-Glaser, Braunschweig, Germany) were first rinsed with PB 0.1 M and pre-treated with 3%  $\text{H}_2\text{O}_2$  for 30 min in the blocking reaction against endogenous peroxidase. Following pretreatment, the sections were incubated overnight at room temperature with an anti-rabies phosphoprotein mouse monoclonal antibody (**Raux et al., 1997**) diluted at 1: 10000 in a blocking solution (PB 0.1 M, 0.1% BSA, goat serum 2% and 0.2% Triton X-100). The next sections were rinsed in PB 0.1 M and incubated 2 hr with a biotinylated affinity-purified goat anti-mouse IgG (1: 2000 in blocking solution; Santa-Cruz, Heidelberg, Germany). Then, they were also incubated using an avidin-biotin complex method (Vectastain Elite ABC-Peroxidase kit R.T.U. Universal, Vector Laboratories, Burlingame, CA, USA) to enhance sensitivity. For visualization, the sections were incubated in a 3,3'-diaminobenzidine-tetrahydrochloride (DAB) solution

(0.05% DAB and 0.015% H<sub>2</sub>O<sub>2</sub> in PB 0.1 M). Finally, they were counterstained with cresyl and cover-slipped.

Quantitative analyses of rabies-positive cells were performed using a computerized image processing system (Mercator, Exploranova, France) coupled to an optical microscope. The quantification of rabies-positive cells was carried out at 10x magnification. Structures were defined according to a standard atlas (*Franklin and Paxinos, 2007*). Immunoreactive neurons were counted bilaterally. Representative images were obtained using an Axio Zoom V16 microscope (Carl Zeiss, France).

### 3-D reconstruction

A Nikon Eclipse E800 microscope equipped with a digital color camera (Optronics, USA) was used to visualize mounted cerebellar sections under brightfield illumination. The contour of every fourth section was then manually drawn using Microfire software (NeuroLucida, MBF Bioscience, USA) and cell counts were performed. The sections were then aligned and stacked (160 μm spacing).

### Rabies virus-zebrin II double immuno-staining

For case S18, sections from vial three were mounted on gelatin-coated SuperFrost Plus slides (Menzel-Glaser, Braunschweig, Germany), rinsed with PB 0.1 M and then permeated and blocked in a solution of PB 0.1 M, 0.2% Triton X-100 and bovine serum 2.5% for 30 min. Then they were incubated for 48 hr at 4°C in a mix of rabbit polyclonal anti-Aldolase C primary antibody (a kind gift from Izumi Sugihara (*Sugihara and Shinoda, 2004*); No. 69075; 1:500000) and the mouse anti-rabies antibody used for the single RABV staining (1:5000) in a blocking solution (PB 0.1 M, 0.1% Triton X-100 and bovine serum 1%). Subsequently, the sections were first rinsed with PB 0.1% and then incubated in a mix of Rhodamine Red-XGoat anti-rabbit IgG (1: 5000; ref 111-295-144, Jackson Immuno Research) and donkey anti-mouse secondary antibody (1: 5000; Alexa Fluor 647, Invitrogen distributed by ThermoFisher Scientific, Massachusetts, USA) in blocking solution. Finally, the sections were mounted with Dapi Fluoromount G.

Images were obtained using an Axiozoom v16 microscope (Carl Zeiss, France) then cerebellar contours and labeled neurons were manually drawn for reconstruction of zebrin bands, cerebellar modules and location of the RABV+ cells.

## Electrophysiology procedures

### Preparation 1: Dual hippocampal – cerebellar LFP recording

#### Subjects and surgical protocols

Bipolar LFP recording electrodes (interpolar distance of ~0.5 mm; 140 μm diameter Teflon coated stainless-steel, A-M system, USA) were stereotaxically targeted to hippocampus (AP -2.2, ML +2.0, DV 1.0), lobule VI (AP -6.72, ML 0.0, DV 0.1), lobule II/III (AP -5.52, ML 0.0, DV 1.8) and Crus I (AP -6.24, ML 2.5, DV 0.1) of 21 C57BL6-J mice. Pairs of flexible stainless-steel wires were used to also record neck EMG (Cooner wire, USA).

In 15 C57BL6-J mice, bipolar stimulation electrodes (140-μm-diameter stainless steel; A-M system, USA) were also implanted at the left medial forebrain bundle [MFB; to serve as a reward signal; AP -1.4, ML +1.2, DV +4.8 (*Carlezon and Chartoff, 2007; de Lavilléon et al., 2015*). All electrode assemblies were fixed to the skull using a combination of UV activated cement (SpeedCem, Henry Shein, UK), SuperBond (SunMedical, Japan) and dental cement (Simplex Rapid, Kemdent, UK). Four miniature screws (Antrin, USA) were also attached to the skull for additional support and to serve as recording ground.

In six mice, a lightweight metal head fixation device (0.1 g) was also affixed to the implant. The total implant weight did not exceed 2.5 g (including head fixation post and cement).

#### Recording

Electrodes were attached to an electronic interface board (EIB 18, Neuralynx, USA) during surgery. Differential recordings were made via a unity-gain headstage preamplifier (HS-18; Neuralynx, USA) and Digital Lynx SX acquisition system (Neuralynx, USA). LFP and EMG Signals were bandpass-filtered between 0.1 and 600 Hz and sampled at 1 kHz. Mouse position was tracked at 30 Hz using video tracker software and infra-red LEDs attached to the headstage (Neuralynx, USA).

## Medial forebrain bundle (MFB) stimulation

Intracranial rewarding stimulation consisted of a 140 Hz stimulation train lasting 100 ms delivered through the headstage to the implanted electrodes (SD9k, Grass Technologies, USA). The optimal voltage for intracranial MFB was determined for each mouse with a nose-poke task prior to training (range, 1–6 V [de Lavilléon *et al.*, 2015]).

## Preparation 2: Simultaneous cerebellar single unit and hippocampal LFP recording

### Subjects and surgical protocols

General surgery procedures were similar to those used for preparation 1 (dual hippocampal – cerebellar LFP recording experiments). CD-L7Chr2 mice (selectively expressing Chr2 in Purkinje cells;  $n = 6$  mice) were implanted with bipolar LFP recording electrodes in the left hippocampus (AP  $-2.2$ , ML  $+2.0$ , DV  $1$ ) and a lightweight ( $<0.1$  g) recording chamber was constructed over the cerebellum. A silicon elastomer (QuickSil, World Precision Instruments, USA) was used to seal the chamber following surgery and between recording sessions. A stainless steel post ( $0.1$  g) was also affixed to the skull and used for head fixation. To measure movements, flexible stainless steel EMG electrodes were implanted in the front left forelimb.

### Recording

Animals were positioned in a custom-built head fixation device and placed on a floating Styrofoam ball (see virtual reality Materials and methods for further details). Hippocampal and EMG electrodes were connected to an electronic interface board (EIB 18, Neuralynx, USA). Filter and recording settings were the same as in preparation 1. For cerebellar single unit recordings, the silicon elastomer was removed from the recording chamber allowing the exposed cerebellar cortex to be viewed under a microscope (Leica, USA). Quartz based electrodes or tetrodes (impedance  $1$  mOhm at  $1$  Khz; Thomas Recording, Germany) were inserted in to the cerebellar cortex using a custom manipulator mounted on a stereotaxic frame (Kopf, USA). An optical fiber ( $600$   $\mu$ m diameter, Prizmatix, Israel) was mounted on a separate stereotaxic manipulator and positioned inside the chamber just above the cerebellar cortical surface within close proximity to the recording electrode. A low impedance silver ball reference electrode was also positioned within the chamber and a skull screw served as ground. A hydraulic micromanipulator was used to lower the optetrodes through the cerebellar cortical layers (Narishige, Japan).

Once units were identified, blue light pulses were used to photo-identify putative Purkinje cells ( $50$  mW/mm<sup>2</sup>,  $\sim 460$  nm,  $100$  ms delivered using a commercial LED driver, Prizmatix, Israel. Chaumont *et al.*, 2013). Cerebellar signals were recorded using an EIB 18 and headstage (HS-18, Neuralynx, USA) connected to the electrodes via a custom made adapter. Unit signals were band-pass filtered between  $0.3$  and  $9$  kHz while sampling was set at  $32$  kHz.

### Histology

After completion of all the experiments, mice were deeply anesthetized with ketamine/xylazine solution ( $150$  mg/kg) and electrolytic lesions created by passing a positive current through the electrodes ( $30$   $\mu$ A,  $10$  s). With the electrodes left in situ, the animals were perfused transcardially with saline followed by paraformaldehyde (4%).

Brains were extracted and post-fixed in paraformaldehyde (4%;  $24$  hr) then embedded in agarose ( $24$  hr). A freezing vibratome was used to cut  $50$   $\mu$ m thick sagittal cerebellar and coronal hippocampal sections. The sections were mounted on gelatinized slides and stained with cresyl violet. Recording locations were identified by localized lesions in the cerebellum and hippocampus and plotted on standard maps with reference to a stereotaxic atlas (Franklin and Paxinos, 2007).

## Behavioral procedures

### Familiar environment

All recordings were made in the animal's home-cage ( $30$  cm x  $10$  cm x  $10$  cm plastic box), with the lid removed and lasted a maximum of  $4$  hr. Recordings were made during the day between the hours of  $10$  am and  $6$  pm.

## Linear track – real world

The linear track was made in-house from 100 cm x 4 cm x 0.5 cm of black plastic positioned 20 cm above the surface of the experimental table. The behavioral assembly was located in a separate room from the experimenter and was surrounded on four sides by black curtains. Three salient visual cues were placed at fixed locations along the edge of the track (10 cm from the edge). Mice were trained to run in a sequential manner from one end of the track to the other in order to receive a reward, which consisted of an electrical stimulation of the MFB. The reward stimulation was delivered automatically when the mice reached a 5 cm wide goal-zone, which was located 10 cm from the end of the track. Timing of the reward signal was logged on the electrophysiological recordings via TTL signals. Sessions lasted 12 min and were repeated three times per day with an inter-session time of 5 min over 7 days. Between sessions, the track was cleaned with 20% ethanol.

## Linear track – virtual reality environment

A commercially available virtual-reality environment was used (Jet Ball, Phenosys, Germany), utilizing an air cushioned Styrofoam ball (200 mm), which served as a spherical treadmill for head restrained mice (Lasztóczy and Klausberger, 2016) (Figure 4—figure supplement 2). The floating ball assembly was positioned 20 cm from a series of six octagonally arranged TFT surround monitors (19 inch) such that the head restrained mice had an unobstructed view of the visual scene. Rotation of the Styrofoam ball was detected by an optical sensor (sampling frequency 5700 dots per inch at 1 kHz). The vertical axis signals were interpreted by the VR software as the forward and backward movement of the virtual position of the animal. Position within the VR was then translated to a voltage signal (zero to five volts, with five volts indicating the end of the track), and sent to the Digital Lynx SX (Neuralynx, USA) electrophysiology system via a DACQ interface (DACQ 6501, National Instruments, USA). The start of the VR display was logged on the electrophysiology recordings via a TTL signal. To provide a reward signal, when the mice reached a given location within the VR (10 cm from the end of the track) a TTL marker was sent to both the electrophysiological recording system (to provide a timestamp-marker of the event) and an electrical stimulus generator linked to the HS-18 headstage (in the same manner as for real world linear track experiments).

The virtual scene consisted of a 1 m long track with gray walls and included three salient visual cues. After 3 × 12 mins sessions of habituation to the head fixation on the floating-ball assembly, mice were trained to run on the linear track in 12 min sessions, three times per day with an inter-session interval of approximately 5 mins during 7 days. The number of rewards received by the animal was logged in the electrophysiology software (Cheetah 5.6.3, Neuralynx, USA).

## Behavioral and electrophysiological analysis

All data were processed in Matlab (Mathworks, USA), Spike 2 (Cambridge Electronic Design, UK) and Prism (Graphpad, USA).

### Behavior

In all conditions, behavioral data were analyzed using custom-made Matlab scripts. Instantaneous speed (or virtual speed) was derived from video tracking data (or virtual X and Y coordinates recorded as voltage signals in Neuralynx Cheetah software) and downsampled to 10 Hz for consistency with spectrogram and coherogram data (see below). Only epochs of active movement, defined by a sustained speed above 3 cm/s for a minimum of 4 s, were selected for further analysis.

In the home-cage environment, there was one case in which video tracking was not available and the epochs of active movement were thus defined by an amplitude threshold in EMG signal and the presence of a high theta/delta ratio in the hippocampal recordings.

For linear track and virtual reality-based experiments, active movement periods (instantaneous speed >3 cm/s) were analyzed from each 12 min session (three sessions per day) for overall calculations. Each session was then subdivided into trials (runs), that is, each time the animal traversed the track from one reward site to the other, and measurements of speed, power and coherence were averaged by distance from reward location in 1 cm bins normalized by the occupancy (time spent in each bin).

## Electrophysiology

LFP data was z-scored, notch filtered (filter centered to 50 Hz to remove electrical line noise) and detrended (using local-linear regression with a moving window of 1 s in 0.5 s steps to remove the DC component) prior to subsequent analysis. Multi-taper Fourier analyses (Chronux toolbox [Bokil et al., 2010]) were used to calculate power and coherence of the LFP data. We used a 1 s sliding window in 0.1 s step and four tapers for all analysis. Time points with large-amplitude, low frequency artifacts, identified by threshold crossings of the mean z-score power in 0.5–5 Hz band, were removed from further analysis. Similarly, peri-MFB electrical stimulation times ( $\pm 0.5$  s) in linear track and virtual environment conditions were also excluded from analysis.

For overall power spectra and coherence calculations, the means of the spectrograms and coherograms were respectively computed. Spectral power between 0.1 and 500 Hz was z-scored to homogenize values and reduce the impact of inter-animal and inter-region global variations. Frequency axes in both spectral power and coherence plots were presented in logarithmic scale to facilitate visualization across a large frequency band (1–300 Hz). Frequencies between 48–52 Hz were removed from coherence plots due to the presence of a spurious peak related to the notch filtering. Data duration of recordings made in the home-cage environment, varied across mice (range, 12 to 132 min). Therefore, to reduce the impact of data length on subsequent analyses and also to match with subsequent linear track experiments (duration of 12 min), for each mouse we concatenated the LFP in to 12 min blocks. When multiple 12 min blocks were available (number of data blocks ranged from 1 to 11), we calculated the average coherence across all blocks.

## Combined recordings of cerebellar units and hippocampal LFP

Cerebellar cell recordings were sorted using Spike2 software (CED, UK) where single units were verified with principal component analysis. We did not separate simple and complex spikes when calculating firing rate. For each cell, the firing rate was normalized against a 1 s pre photo-illumination period. Firing rate was then computed in 10 ms bins. A change of 1.96z was used to classify a significant change in firing rate during photo-illumination (Chaumont et al., 2013). For phase locking analysis, hippocampal LFP was bandpass filtered from 6 to 12 Hz. Circular statistics were used to quantify phase distribution (e.g. Jones and Wilson, 2005) of each cell and to determine significant phase-locking at  $p < 0.05$ .

## Statistical analysis

Statistical analyses were conducted using Matlab Statistical Toolbox and Prism (Graphpad, USA). Normality was assessed using a Shapiro-Wilk test. Parametric and non-parametric tests were then used accordingly.

For bootstrap calculations on the correlation of theta power and theta coherence with speed, we computed the Spearman's correlation between these variables and a randomly shuffled rearrangement of instantaneous speed values. We repeated this 1000 times in order to obtain the cumulative probability distribution of the random correlation values. The confident limits for  $\alpha = 0.05$  were obtained by finding the correlation values at probabilities of 0.025 and 0.975.

## Acknowledgements

This work was supported by the Fondation pour la Recherche Médicale DEQ20160334907-France, by the National Agency for Research ANR-17-CE16-0019-03 (LRR), by the CNRS and Aix-Marseille Université through UMR 7289 (PC). This work also received support under the program Investissements d'Avenir launched by the French Government and implemented by the ANR, with the references, PER-SU (LRR) and ANR-10-LABX-BioPsy (LRR). The group of LRR is member of the Labex BioPsy and ENP Foundation. Labex are supported by French State funds managed by the ANR within the Investissements d'Avenir programme under reference ANR-11-IDEX-0004-02. We thank Roxanna Ureta for help with histology, Lilith Sommer for help with behavioral experiments, Gregory Sedes and Nadine Francis for help developing analysis codes, and Richard Apps for his insightful comments. We are grateful to Richard Hawkes and Izumi Sugihara for generously providing the aldolase C antibody. Finally, we thank all members of the CEZAME team for helpful discussions of the experiments and manuscript.

## Additional information

### Funding

Funder	Grant reference number	Author
Fondation pour la Recherche Médicale	DEQ20160334907	Laure Rondi-Reig
Agence Nationale de la Recherche	ANR-17-CE16-0019-03	Laure Rondi-Reig
Centre National de la Recherche Scientifique		Patrice Coulon
Aix-Marseille Université		Patrice Coulon
Université Pierre et Marie Curie	ANR-10-LABX-BioPsy	Laure Rondi-Reig
Université Pierre et Marie Curie	ANR-11-IDEX-0004-02	Laure Rondi-Reig

The funders had no role in study design, data collection and interpretation, or the decision to submit the work for publication.

### Author contributions

Thomas Charles Watson, Formal analysis, Supervision, Validation, Investigation, Methodology, Writing—original draft; Pauline Obiang, Validation, Investigation, Methodology, Writing—review and editing; Arturo Torres-Herraez, Software, Formal analysis, Validation, Investigation, Visualization, Methodology, Writing—original draft; Aurélie Watilliaux, Formal analysis, Validation, Investigation, Methodology, Writing—review and editing; Patrice Coulon, Resources, Supervision, Investigation, Methodology, Writing—review and editing; Christelle Rochefort, Validation, Methodology, Writing—review and editing; Laure Rondi-Reig, Conceptualization, Resources, Supervision, Funding acquisition, Methodology, Writing—original draft, Project administration

### Author ORCIDs

Thomas Charles Watson  <https://orcid.org/0000-0002-5146-6981>

Arturo Torres-Herraez  <https://orcid.org/0000-0001-6333-5623>

Patrice Coulon  <https://orcid.org/0000-0003-2996-405X>

Laure Rondi-Reig  <https://orcid.org/0000-0003-1006-0501>

### Ethics

Animal experimentation: This study was performed in strict accordance with the recommendations in the Guide for the Care and Use of Laboratory Animals of the Ministère de l'Enseignement Supérieur et de la Recherche. All of the animals were handled according to approved institutional animal care agreement B75 0510. The protocol was approved by the Committee on the Ethics of Animal Experiments (expérimentation animale n°5) protocols #00895.02 and APAFIS#4315-2016042708195884v1. All surgery was performed under isoflurane gas anesthesia, and every effort was made to minimize suffering.

### Decision letter and Author response

Decision letter <https://doi.org/10.7554/eLife.41896.026>

Author response <https://doi.org/10.7554/eLife.41896.027>

## Additional files

### Supplementary files

- Transparent reporting form

DOI: <https://doi.org/10.7554/eLife.41896.024>

### Data availability

The individual values are plotted in all the graphs and the mean and SEM are also plotted or indicated at the legends. The Matlab codes used for the spectral analysis are part of a fully available, well documented toolbox (Chronux toolbox) and referenced in the text. The parameters used for these codes is indicated in the materials and methods section.

## References

- Aoki S**, Coulon P, Ruigrok TJH. 2017. Multizonal cerebellar influence over sensorimotor areas of the rat cerebral cortex. *Cerebral Cortex* **29**:598–614. DOI: <https://doi.org/10.1093/cercor/bhx343>
- Apps R**. 1990. Columnar organisation of the inferior olive projection to the posterior lobe of the rat cerebellum. *The Journal of Comparative Neurology* **302**:236–254. DOI: <https://doi.org/10.1002/cne.903020205>, PMID: 1705266
- Apps R**, Hawkes R. 2009. Cerebellar cortical organization: a one-map hypothesis. *Nature Reviews Neuroscience* **10**:670–681. DOI: <https://doi.org/10.1038/nrn2698>, PMID: 19693030
- Arrigo A**, Mormina E, Anastasi GP, Gaeta M, Calamuneri A, Quartarone A, De Salvo S, Bruschetta D, Rizzo G, Trimarchi F, Milardi D. 2014. Constrained spherical deconvolution analysis of the limbic network in human, with emphasis on a direct cerebello-limbic pathway. *Frontiers in Human Neuroscience* **8**:987. DOI: <https://doi.org/10.3389/fnhum.2014.00987>, PMID: 25538606
- Babayan BM**, Watilliaux A, Viejo G, Paradis AL, Girard B, Rondi-Reig L. 2017. A hippocampo-cerebellar centred network for the learning and execution of sequence-based navigation. *Scientific Reports* **7**:17812. DOI: <https://doi.org/10.1038/s41598-017-18004-7>, PMID: 29259243
- Babb TL**, Mitchell AG, Crandall PH. 1974. Fastigiobulbar and dentatohalamic influences on hippocampal cobalt epilepsy in the cat. *Electroencephalography and Clinical Neurophysiology* **36**:141–154. DOI: [https://doi.org/10.1016/0013-4694\(74\)90151-5](https://doi.org/10.1016/0013-4694(74)90151-5), PMID: 4129626
- Basso MA**, May PJ. 2017. Circuits for action and cognition: a view from the superior colliculus. *Annual Review of Vision Science* **3**:197–226. DOI: <https://doi.org/10.1146/annurev-vision-102016-061234>, PMID: 28617660
- Bokil H**, Andrews P, Kulkarni JE, Mehta S, Mitra PP. 2010. Chronux: a platform for analyzing neural signals. *Journal of Neuroscience Methods* **192**:146–151. DOI: <https://doi.org/10.1016/j.jneumeth.2010.06.020>, PMID: 20637804
- Bostan AC**, Dum RP, Strick PL. 2010. The basal ganglia communicate with the cerebellum. *PNAS* **107**:8452–8456. DOI: <https://doi.org/10.1073/pnas.1000496107>, PMID: 20404184
- Bostan AC**, Strick PL. 2018. The basal ganglia and the cerebellum: nodes in an integrated network. *Nature Reviews Neuroscience* **19**:338–350. DOI: <https://doi.org/10.1038/s41583-018-0002-7>, PMID: 29643480
- Brochu G**, Maler L, Hawkes R. 1990. Zebrin II: a polypeptide antigen expressed selectively by purkinje cells reveals compartments in rat and fish cerebellum. *The Journal of Comparative Neurology* **291**:538–552. DOI: <https://doi.org/10.1002/cne.902910405>, PMID: 2329190
- Buckner RL**. 2013. The cerebellum and cognitive function: 25 years of insight from anatomy and neuroimaging. *Neuron* **80**:807–815. DOI: <https://doi.org/10.1016/j.neuron.2013.10.044>, PMID: 24183029
- Burguière E**, Arleo A, Hojjati M, Elgersma Y, De Zeeuw CI, Berthoz A, Rondi-Reig L. 2005. Spatial navigation impairment in mice lacking cerebellar LTD: a motor adaptation deficit? *Nature Neuroscience* **8**:1292–1294. DOI: <https://doi.org/10.1038/nn1532>, PMID: 16136042
- Buzsáki G**, Moser EI. 2013. Memory, navigation and theta rhythm in the hippocampal-entorhinal system. *Nature Neuroscience* **16**:130–138. DOI: <https://doi.org/10.1038/nn.3304>, PMID: 23354386
- Carlezon WA**, Chartoff EH. 2007. Intracranial self-stimulation (ICSS) in rodents to study the neurobiology of motivation. *Nature Protocols* **2**:2987–2995. DOI: <https://doi.org/10.1038/nprot.2007.441>, PMID: 18007634
- Carta I**, Chen CH, Schott AL, Dorizan S, Khodakhah K. 2019. Cerebellar modulation of the reward circuitry and social behavior. *Science* **363**:eaav0581. DOI: <https://doi.org/10.1126/science.aav0581>, PMID: 30655412
- Cerminara NL**, Apps R, Marple-Horvat DE. 2009. An internal model of a moving visual target in the lateral cerebellum. *The Journal of Physiology* **587**:429–442. DOI: <https://doi.org/10.1113/jphysiol.2008.163337>, PMID: 19047203
- Cerminara NL**, Apps R. 2011. Behavioural significance of cerebellar modules. *The Cerebellum* **10**:484–494. DOI: <https://doi.org/10.1007/s12311-010-0209-2>, PMID: 20838949
- Chabrol F**, Blot A, Mrsic-Flogel TD. 2018. Cerebellar contribution to preparatory activity in motor neocortex. *bioRxiv*. DOI: <https://doi.org/10.1101/335703>
- Chaumont J**, Guyon N, Valera AM, Dugué GP, Popa D, Marcaggi P, Gautheron V, Reibel-Foisset S, Dieudonné S, Stephan A, Barrot M, Cassel JC, Dupont JL, Doussau F, Poulain B, Selimi F, Léna C, Isope P. 2013. Clusters of cerebellar purkinje cells control their afferent climbing fiber discharge. *PNAS* **110**:16223–16228. DOI: <https://doi.org/10.1073/pnas.1302310110>, PMID: 24046366
- Chen CH**, Fremont R, Arteaga-Bracho EE, Khodakhah K. 2014. Short latency cerebellar modulation of the basal ganglia. *Nature Neuroscience* **17**:1767–1775. DOI: <https://doi.org/10.1038/nn.3868>, PMID: 25402853
- Chen H**, Wang YJ, Yang L, Sui JF, Hu ZA, Hu B. 2016. Theta synchronization between medial prefrontal cortex and cerebellum is associated with adaptive performance of associative learning behavior. *Scientific Reports* **6**:20960. DOI: <https://doi.org/10.1038/srep20960>, PMID: 26879632

- Cheron G**, Márquez-Ruiz J, Dan B. 2016. Oscillations, timing, plasticity, and learning in the cerebellum. *The Cerebellum* **15**:122–138. DOI: <https://doi.org/10.1007/s12311-015-0665-9>, PMID: 25808751
- Choe KY**, Sanchez CF, Harris NG, Otis TS, Mathews PJ. 2018. Optogenetic fMRI and electrophysiological identification of region-specific connectivity between the cerebellar cortex and forebrain. *NeuroImage* **173**: 370–383. DOI: <https://doi.org/10.1016/j.neuroimage.2018.02.047>, PMID: 29496611
- Colgin LL**. 2013. Mechanisms and functions of theta rhythms. *Annual Review of Neuroscience* **36**:295–312. DOI: <https://doi.org/10.1146/annurev-neuro-062012-170330>, PMID: 23724998
- Cooke PM**, Snider RS. 1955. Some cerebellar influences on Electrically-Induced cerebral seizures. *Epilepsia* **C4**: 19–28. DOI: <https://doi.org/10.1111/j.1528-1157.1955.tb03170.x>
- Coulon P**, Bras H, Vinay L, . 2011. Characterization of last-order premotor interneurons by transneuronal tracing with Rabies virus in the neonatal mouse spinal cord. *The Journal of Comparative Neurology* **519**:3470–3487. DOI: <https://doi.org/10.1002/cne.22717>, PMID: 21800300
- Courtemanche R**, Lamarre Y. 2005. Local field potential oscillations in primate cerebellar cortex: synchronization with cerebral cortex during active and passive expectancy. *Journal of Neurophysiology* **93**:2039–2052. DOI: <https://doi.org/10.1152/jn.00080.2004>, PMID: 15590736
- D’Angelo E**, Nieuwenhuis T, Maffei A, Armano S, Rossi P, Taglietti V, Fontana A, Naldi G. 2001. Theta-frequency bursting and resonance in cerebellar granule cells: experimental evidence and modeling of a slow k<sup>+</sup>-dependent mechanism. *The Journal of Neuroscience* **21**:759–770. DOI: <https://doi.org/10.1523/JNEUROSCI.21-03-00759.2001>, PMID: 11157062
- de Lavilléon G**, Lacroix MM, Rondi-Reig L, Benchenane K. 2015. Explicit memory creation during sleep demonstrates a causal role of place cells in navigation. *Nature Neuroscience* **18**:493–495. DOI: <https://doi.org/10.1038/nn.3970>, PMID: 25751533
- De Zeeuw CI**, Hoebeek FE, Schonewille M. 2008. Causes and consequences of oscillations in the cerebellar cortex. *Neuron* **58**:655–658. DOI: <https://doi.org/10.1016/j.neuron.2008.05.019>, PMID: 18549777
- Dugué GP**, Brunel N, Hakim V, Schwartz E, Chat M, Lévesque M, Courtemanche R, Léna C, Dieudonné S. 2009. Electrical coupling mediates tunable low-frequency oscillations and resonance in the cerebellar golgi cell network. *Neuron* **61**:126–139. DOI: <https://doi.org/10.1016/j.neuron.2008.11.028>, PMID: 19146818
- Edge AL**, Marple-Horvat DE, Apps R. 2003. Lateral cerebellum: functional localization within crus I and correspondence to cortical zones. *European Journal of Neuroscience* **18**:1468–1485. DOI: <https://doi.org/10.1046/j.1460-9568.2003.02873.x>, PMID: 14511327
- Franklin K**, Paxinos G. 2007. *The Mouse Brain in Stereotaxic Coordinates*. Third Edition. Elsevier.
- Frederick A**, Bourget-Murray J, Chapman CA, Amir S, Courtemanche R. 2014. Diurnal influences on electrophysiological oscillations and coupling in the dorsal striatum and cerebellar cortex of the anesthetized rat. *Frontiers in Systems Neuroscience* **8**:145. DOI: <https://doi.org/10.3389/fnsys.2014.00145>, PMID: 25309348
- Fries P**. 2005. A mechanism for cognitive dynamics: neuronal communication through neuronal coherence. *Trends in Cognitive Sciences* **9**:474–480. DOI: <https://doi.org/10.1016/j.tics.2005.08.011>, PMID: 16150631
- Glickstein M**, Sultan F, Voogd J. 2011. Functional localization in the cerebellum. *Cortex* **47**:59–80. DOI: <https://doi.org/10.1016/j.cortex.2009.09.001>, PMID: 19833328
- Goddard M**, Zheng Y, Darlington CL, Smith PF. 2008. Locomotor and exploratory behavior in the rat following bilateral vestibular deafferentation. *Behavioral Neuroscience* **122**:448–459. DOI: <https://doi.org/10.1037/0735-7044.122.2.448>, PMID: 18410183
- Haines DE**, May PJ, Dietrichs E. 1990. Neuronal connections between the cerebellar nuclei and hypothalamus in macaca fascicularis: cerebello-visceral circuits. *The Journal of Comparative Neurology* **299**:106–122. DOI: <https://doi.org/10.1002/cne.902990108>, PMID: 1698835
- Harper JW**, Heath RG. 1973. Anatomic connections of the fastigial nucleus to the rostral forebrain in the cat. *Experimental Neurology* **39**:285–292. DOI: [https://doi.org/10.1016/0014-4886\(73\)90231-8](https://doi.org/10.1016/0014-4886(73)90231-8), PMID: 4573973
- Hartmann MJ**, Bower JM. 1998. Oscillatory activity in the cerebellar hemispheres of unrestrained rats. *Journal of Neurophysiology* **80**:1598–1604. DOI: <https://doi.org/10.1152/jn.1998.80.3.1598>, PMID: 9744967
- Heath RG**, Dempsey CW, Fontana CJ, Myers WA. 1978. Cerebellar stimulation: effects on septal region, Hippocampus, and amygdala of cats and rats. *Biological Psychiatry* **13**:501–529. PMID: 728506
- Herrero L**, Yu M, Walker F, Armstrong DM, Apps R. 2006. Olivo-cortico-nuclear localizations within crus I of the cerebellum. *The Journal of Comparative Neurology* **497**:287–308. DOI: <https://doi.org/10.1002/cne.20976>, PMID: 16705675
- Hoffmann LC**, Berry SD. 2009. Cerebellar theta oscillations are synchronized during hippocampal theta-contingent trace conditioning. *PNAS* **106**:21371–21376. DOI: <https://doi.org/10.1073/pnas.0908403106>, PMID: 19940240
- Hoshi E**, Tremblay L, Féger J, Carras PL, Strick PL. 2005. The cerebellum communicates with the basal ganglia. *Nature Neuroscience* **8**:1491–1493. DOI: <https://doi.org/10.1038/nn1544>, PMID: 16205719
- Iglói K**, Doeller CF, Paradis AL, Benchenane K, Berthoz A, Burgess N, Rondi-Reig L. 2015. Interaction between hippocampus and cerebellum crus I in Sequence-Based but not Place-Based navigation. *Cerebral Cortex* **25**: 4146–4154. DOI: <https://doi.org/10.1093/cercor/bhu132>, PMID: 24947462
- Iwata K**, Snider RS. 1959. Cerebello-hippocampal influences on the electroencephalogram. *Electroencephalography and Clinical Neurophysiology* **11**:439–446. DOI: [https://doi.org/10.1016/0013-4694\(59\)90043-4](https://doi.org/10.1016/0013-4694(59)90043-4), PMID: 13663818
- Jones MW**, Wilson MA. 2005. Theta rhythms coordinate hippocampal-prefrontal interactions in a spatial memory task. *PLOS Biology* **3**:e402. DOI: <https://doi.org/10.1371/journal.pbio.0030402>, PMID: 16279838

- Jwair S, Coulon P, Ruigrok TJ. 2017. Disynaptic subthalamic input to the posterior cerebellum in rat. *Frontiers in Neuroanatomy* **11**:13. DOI: <https://doi.org/10.3389/fnana.2017.00013>, PMID: 28293179
- Kajikawa Y, Schroeder CE. 2011. How local is the local field potential? *Neuron* **72**:847–858. DOI: <https://doi.org/10.1016/j.neuron.2011.09.029>, PMID: 22153379
- Kelly RM, Strick PL. 2000. Rabies as a transneuronal tracer of circuits in the central nervous system. *Journal of Neuroscience Methods* **103**:63–71. DOI: [https://doi.org/10.1016/S0165-0270\(00\)00296-X](https://doi.org/10.1016/S0165-0270(00)00296-X), PMID: 11074096
- Kelly RM, Strick PL. 2003. Cerebellar loops with motor cortex and prefrontal cortex of a nonhuman primate. *The Journal of Neuroscience* **23**:8432–8444. DOI: <https://doi.org/10.1523/JNEUROSCI.23-23-08432.2003>, PMID: 12968006
- Kelly RM, Strick PL. 2004. Macro-architecture of basal ganglia loops with the cerebral cortex: use of Rabies virus to reveal multisynaptic circuits. *Progress in Brain Research* **143**:449–459. DOI: [https://doi.org/10.1016/s0079-6123\(03\)43042-2](https://doi.org/10.1016/s0079-6123(03)43042-2), PMID: 14653187
- Kim SG, Uğurbil K, Strick PL. 1994. Activation of a cerebellar output nucleus during cognitive processing. *Science* **265**:949–951. DOI: <https://doi.org/10.1126/science.8052851>, PMID: 8052851
- Kozioł LF, Budding D, Andreasen N, D'Arrigo S, Bulgheroni S, Imamizu H, Ito M, Manto M, Marvel C, Parker K, Pezzulo G, Ramnani N, Riva D, Schmähmann J, Vandervert L, Yamazaki T. 2014. Consensus paper: the cerebellum's role in movement and cognition. *The Cerebellum* **13**:151–177. DOI: <https://doi.org/10.1007/s12311-013-0511-x>, PMID: 23996631
- Krook-Magnuson E, Szabo GG, Armstrong C, Oijala M, Soltesz I. 2014. Cerebellar directed optogenetic intervention inhibits spontaneous hippocampal seizures in a mouse model of temporal lobe epilepsy. *eNeuro* **1**. DOI: <https://doi.org/10.1523/ENEURO.0005-14.2014>, PMID: 25599088
- Lasztóczy B, Klausberger T. 2016. Hippocampal place cells couple to three different gamma oscillations during place field traversal. *Neuron* **91**:34–40. DOI: <https://doi.org/10.1016/j.neuron.2016.05.036>, PMID: 27387648
- Lefort JM, Vincent J, Tallot L, Jarlier F, De Zeeuw CI, Rondi-Reig L, Rochefort C. 2019. Impaired cerebellar purkinje cell potentiation generates unstable spatial map orientation and inaccurate navigation. *Nature Communications* **10**. DOI: <https://doi.org/10.1038/s41467-019-09958-5>, PMID: 31113954
- Mihailoff GA, Burne RA, Azizi SA, Norell G, Woodward DJ. 1981. The pontocerebellar system in the rat: an HRP study. II. hemispherical components. *The Journal of Comparative Neurology* **197**:559–577. DOI: <https://doi.org/10.1002/cne.901970403>, PMID: 7229128
- Muzzu T, Mitolo S, Gava GP, Schultz SR. 2018. Encoding of locomotion kinematics in the mouse cerebellum. *PLOS ONE* **13**:e0203900. DOI: <https://doi.org/10.1371/journal.pone.0203900>, PMID: 30212563
- Newman PP, Reza H. 1979. Functional relationships between the hippocampus and the cerebellum: an electrophysiological study of the cat. *The Journal of Physiology* **287**:405–426. DOI: <https://doi.org/10.1113/jphysiol.1979.sp012667>, PMID: 430426
- Nolte G, Bai O, Wheaton L, Mari Z, Vorbach S, Hallett M. 2004. Identifying true brain interaction from EEG data using the imaginary part of coherency. *Clinical Neurophysiology* **115**:2292–2307. DOI: <https://doi.org/10.1016/j.clinph.2004.04.029>, PMID: 15351371
- O'Connor SM, Berg RW, Kleinfeld D. 2002. Coherent electrical activity between vibrissa sensory areas of cerebellum and neocortex is enhanced during free whisking. *Journal of Neurophysiology* **87**:2137–2148. DOI: <https://doi.org/10.1152/jn.00229.2001>, PMID: 11929931
- Onuki Y, Van Someren EJ, De Zeeuw CI, Van der Werf YD. 2015. Hippocampal-cerebellar interaction during spatio-temporal prediction. *Cerebral Cortex* **25**:313–321. DOI: <https://doi.org/10.1093/cercor/bht221>, PMID: 23968839
- Paul SM, Heath RG, Ellison JP. 1973. Histochemical demonstration of a direct pathway from the fastigial nucleus to the septal region. *Experimental Neurology* **40**:798–805. DOI: [https://doi.org/10.1016/0014-4886\(73\)90113-1](https://doi.org/10.1016/0014-4886(73)90113-1), PMID: 4124980
- Petrosini L, Leggio MG, Molinari M. 1998. The cerebellum in the spatial problem solving: a co-star or a guest star? *Progress in Neurobiology* **56**:191–210. DOI: [https://doi.org/10.1016/S0301-0082\(98\)00036-7](https://doi.org/10.1016/S0301-0082(98)00036-7), PMID: 9760701
- Proville RD, Spolidoro M, Guyon N, Dugué GP, Selimi F, Isope P, Popa D, Léna C. 2014. Cerebellum involvement in cortical sensorimotor circuits for the control of voluntary movements. *Nature Neuroscience* **17**:1233–1239. DOI: <https://doi.org/10.1038/nn.3773>, PMID: 25064850
- Ramnani N. 2006. The primate cortico-cerebellar system: anatomy and function. *Nature Reviews Neuroscience* **7**:511–522. DOI: <https://doi.org/10.1038/nrn1953>, PMID: 16791141
- Raux H, Isefi F, Lafay F, Blondel D. 1997. Mapping of monoclonal antibody epitopes of the Rabies virus P protein. *The Journal of General Virology* **78** ( Pt 1):119–124. DOI: <https://doi.org/10.1099/0022-1317-78-1-119>, PMID: 9010294
- Rochefort C, Arabo A, André M, Poucet B, Save E, Rondi-Reig L. 2011. Cerebellum shapes hippocampal spatial code. *Science* **334**:385–389. DOI: <https://doi.org/10.1126/science.1207403>, PMID: 22021859
- Rochefort C, Lefort JM, Rondi-Reig L. 2013. The cerebellum: a new key structure in the navigation system. *Frontiers in Neural Circuits* **7**:35. DOI: <https://doi.org/10.3389/fncir.2013.00035>, PMID: 23493515
- Rogers TD, Dickson PE, Heck DH, Goldowitz D, Mittleman G, Blaha CD. 2011. Connecting the dots of the cerebro-cerebellar role in cognitive function: neuronal pathways for cerebellar modulation of dopamine release in the prefrontal cortex. *Synapse* **65**:1204–1212. DOI: <https://doi.org/10.1002/syn.20960>, PMID: 21638338
- Rondi-Reig L, Paradis AL, Lefort JM, Babayan BM, Tobin C. 2014. How the cerebellum may monitor sensory information for spatial representation. *Frontiers in Systems Neuroscience* **8**:205. DOI: <https://doi.org/10.3389/fnsys.2014.00205>, PMID: 25408638

- Rondi-Reig L**, Burguière E. 2005. Is the cerebellum ready for navigation? *Progress in Brain Research* **148**. DOI: [https://doi.org/10.1016/S0079-6123\(04\)48017-0](https://doi.org/10.1016/S0079-6123(04)48017-0), PMID: 15661192
- Rowland NC**, Goldberg JA, Jaeger D. 2010. Cortico-cerebellar coherence and causal connectivity during slow-wave activity. *Neuroscience* **166**:698–711. DOI: <https://doi.org/10.1016/j.neuroscience.2009.12.048>, PMID: 20036719
- Ruigrok TJ**. 2011. Ins and outs of cerebellar modules. *The Cerebellum* **10**:464–474. DOI: <https://doi.org/10.1007/s12311-010-0164-y>, PMID: 20232190
- Sauerbrei BA**, Lubenov EV, Siapas AG. 2015. Structured variability in purkinje cell activity during locomotion. *Neuron* **87**:840–852. DOI: <https://doi.org/10.1016/j.neuron.2015.08.003>, PMID: 26291165
- Sillitoe RV**, Marzban H, Larouche M, Zahedi S, Affanni J, Hawkes R. 2005. Conservation of the architecture of the anterior lobe vermis of the cerebellum across mammalian species. *Progress in Brain Research* **148**. DOI: [https://doi.org/10.1016/S0079-6123\(04\)48022-4](https://doi.org/10.1016/S0079-6123(04)48022-4), PMID: 15661197
- Singer W**. 1999. Neuronal synchrony: a versatile code for the definition of relations? *Neuron* **24**:49–65. DOI: [https://doi.org/10.1016/S0896-6273\(00\)80821-1](https://doi.org/10.1016/S0896-6273(00)80821-1), PMID: 10677026
- Sirota A**, Montgomery S, Fujisawa S, Isomura Y, Zugaro M, Buzsáki G. 2008. Entrainment of neocortical neurons and gamma oscillations by the hippocampal theta rhythm. *Neuron* **60**:683–697. DOI: <https://doi.org/10.1016/j.neuron.2008.09.014>, PMID: 19038224
- Snider RS**, Maiti A. 1975. Septal afterdischarges and their modification by the cerebellum. *Experimental Neurology* **49**:529–539. DOI: [https://doi.org/10.1016/0014-4886\(75\)90106-5](https://doi.org/10.1016/0014-4886(75)90106-5), PMID: 811491
- Snider RS**, Maiti A. 1976. Cerebellar contributions to the papez circuit. *Journal of Neuroscience Research* **2**:133–146. DOI: <https://doi.org/10.1002/jnr.490020204>, PMID: 950678
- Soteropoulos DS**, Baker SN. 2006. Cortico-cerebellar coherence during a precision grip task in the monkey. *Journal of Neurophysiology* **95**:1194–1206. DOI: <https://doi.org/10.1152/jn.00935.2005>, PMID: 16424458
- Stackman RW**, Clark AS, Taube JS. 2002. Hippocampal spatial representations require vestibular input. *Hippocampus* **12**:291–303. DOI: <https://doi.org/10.1002/hipo.1112>, PMID: 12099481
- Stam CJ**, Nolte G, Daffertshofer A. 2007. Phase lag index: assessment of functional connectivity from multi channel EEG and MEG with diminished bias from common sources. *Human Brain Mapping* **28**:1178–1193. DOI: <https://doi.org/10.1002/hbm.20346>, PMID: 17266107
- Stoodley CJ**, D’Mello AM, Ellegood J, Jakkamsetti V, Liu P, Nebel MB, Gibson JM, Kelly E, Meng F, Cano CA, Pascual JM, Mostofsky SH, Lerch JP, Tsai PT. 2017. Altered cerebellar connectivity in autism and cerebellar-mediated rescue of autism-related behaviors in mice. *Nature Neuroscience* **20**:1744–1751. DOI: <https://doi.org/10.1038/s41593-017-0004-1>, PMID: 29184200
- Stoodley CJ**, Schmahmann JD. 2010. Evidence for topographic organization in the cerebellum of motor control versus cognitive and affective processing. *Cortex* **46**:831–844. DOI: <https://doi.org/10.1016/j.cortex.2009.11.008>, PMID: 20152963
- Sugihara I**. 2011. Compartmentalization of the deep cerebellar nuclei based on afferent projections and aldolase C expression. *The Cerebellum* **10**:449–463. DOI: <https://doi.org/10.1007/s12311-010-0226-1>, PMID: 20981512
- Sugihara I**, Quy PN. 2007. Identification of aldolase C compartments in the mouse cerebellar cortex by olivocerebellar labeling. *The Journal of Comparative Neurology* **500**:1076–1092. DOI: <https://doi.org/10.1002/cne.21219>, PMID: 17183552
- Sugihara I**, Shinoda Y. 2004. Molecular, topographic, and functional organization of the cerebellar cortex: a study with combined aldolase C and olivocerebellar labeling. *Journal of Neuroscience* **24**:8771–8785. DOI: <https://doi.org/10.1523/JNEUROSCI.1961-04.2004>, PMID: 15470143
- Suzuki L**, Coulon P, Sabel-Goedknecht EH, Ruigrok TJ. 2012. Organization of cerebral projections to identified cerebellar zones in the posterior cerebellum of the rat. *Journal of Neuroscience* **32**:10854–10869. DOI: <https://doi.org/10.1523/JNEUROSCI.0857-12.2012>, PMID: 22875920
- Teune TM**, van der Burg J, van der Moer J, Voogd J, Ruigrok TJ. 2000. Topography of cerebellar nuclear projections to the brain stem in the rat. *Progress in Brain Research* **124**. DOI: [https://doi.org/10.1016/S0079-6123\(00\)24014-4](https://doi.org/10.1016/S0079-6123(00)24014-4), PMID: 10943123
- Ugolini G**. 2010. Advances in viral transneuronal tracing. *Journal of Neuroscience Methods* **194**:2–20. DOI: <https://doi.org/10.1016/j.jneumeth.2009.12.001>, PMID: 20004688
- Vinck M**, Oostenveld R, van Wingerden M, Battaglia F, Pennartz CM. 2011. An improved index of phase-synchronization for electrophysiological data in the presence of volume-conduction, noise and sample-size bias. *NeuroImage* **55**:1548–1565. DOI: <https://doi.org/10.1016/j.neuroimage.2011.01.055>, PMID: 21276857
- Voogd J**, Barmack NH. 2006. Oculomotor cerebellum. *Progress in Brain Research* **151**. DOI: [https://doi.org/10.1016/S0079-6123\(05\)51008-2](https://doi.org/10.1016/S0079-6123(05)51008-2), PMID: 16221591
- Wang YJ**, Chen H, Hu C, Ke XF, Yang L, Xiong Y, Hu B. 2014. Baseline theta activities in medial prefrontal cortex and deep cerebellar nuclei are associated with the extinction of trace conditioned eyeblink responses in guinea pigs. *Behavioural Brain Research* **275**:72–83. DOI: <https://doi.org/10.1016/j.bbr.2014.08.059>, PMID: 25200518
- Watson TC**, Jones MW, Apps R. 2009. Electrophysiological mapping of novel prefrontal - cerebellar pathways. *Frontiers in Integrative Neuroscience* **3**:18. DOI: <https://doi.org/10.3389/neuro.07.018.2009>, PMID: 19738932
- Watson TC**, Becker N, Apps R, Jones MW. 2014. Back to front: cerebellar connections and interactions with the prefrontal cortex. *Frontiers in Systems Neuroscience* **8**:4. DOI: <https://doi.org/10.3389/fnsys.2014.00004>, PMID: 24550789
- Whiteside JA**, Snider RS. 1953. Relation of cerebellum to upper brain stem. *Journal of Neurophysiology* **16**:397–413. DOI: <https://doi.org/10.1152/jn.1953.16.4.397>, PMID: 13070051

- Wikgren J**, Nokia MS, Penttonen M. 2010. Hippocampo-cerebellar theta band phase synchrony in rabbits. *Neuroscience* **165**:1538–1545. DOI: <https://doi.org/10.1016/j.neuroscience.2009.11.044>, PMID: 19945512
- Yu W**, Krook-Magnuson E. 2015. Cognitive collaborations: bidirectional functional connectivity between the cerebellum and the hippocampus. *Frontiers in Systems Neuroscience* **9**:177. DOI: <https://doi.org/10.3389/fnsys.2015.00177>, PMID: 26732845
- Zheng Y**, Goddard M, Darlington CL, Smith PF. 2009. Long-term deficits on a foraging task after bilateral vestibular deafferentation in rats. *Hippocampus* **19**:480–486. DOI: <https://doi.org/10.1002/hipo.20533>, PMID: 19072773



---

## Figures and figure supplements

Anatomical and physiological foundations of cerebello-hippocampal interaction

**Thomas Charles Watson et al**



## Figure 1 continued

dentate gyrus. Box shows a magnification of the labeling at 48 and 58 hr ( $n = 5$  mice for 58 hr and 66 hr, 30 hr,  $n = 4$  mice and 48 hr,  $n = 3$  mice). Middle, schematic representation of rabies injection site and survival times required to reach the cerebellar and vestibular nuclei (58 hr, dashed blue line), and cerebellar cortex (66 hr, orange line). Upper right, schematic view of the posterior cerebellar cortex indicating regions of highest labeling following rabies virus injection (red, vermis lobule VI; green, Crus I; gray, paraflocculus). (B-E) Representative photomicrographs showing labeling in the cerebellar and vestibular nuclei 58 hr post-infection. Left panels show low-magnification view, right panels show magnified view of area indicated by dashed box. Solid arrow heads indicate the presence of the very few labeled cells in the IntP. (F) Pooled, normalized counts of rabies labeled cells in the ipsi- and contralateral cerebellar and vestibular nuclei 58 hr post-infection ( $n = 5$  mice). No significant differences were found between ipsi- and contralateral nuclei (nuclei x hemisphere two-way ANOVA, hemisphere effect  $F_{(1, 4)}=1.31 \times 10^{-5}$ ,  $p=0.99$ , interaction effect  $F_{(3, 12)}=2.79$ ,  $p=0.09$ , nuclei effect  $F_{(3, 12)}=9.38$ ,  $p=0.002$ ). (G) Normalized cell counts in the fastigial nucleus (left) and dentate nucleus (right), according to their rostro-caudal position relative to bregma. Open circles, contralateral count; filled circles, ipsilateral count ( $n = 5$  mice). (H-K) Representative photomicrographs of the resultant labeling in lobule VI, Crus I, paraflocculus and lobule II at 66 hr post-infection. (L) Normalized count of rabies labeled cells in anterior (black bar; lobule II to lobule IV/V); central (dark gray bar; lobule VI to Crus II); posterior (clear bar; lobule VIII and lobule IX) and flocculonodular (Floc. Nod., light gray bar; lobule X, flocculus and paraflocculus) cerebellum 66 hr post-infection ( $n = 5$  mice; one-way ANOVA with FDR correction,  $F_{(3, 16)}=19.11$ ,  $p<0.0001$ ). (M) Normalized cell count of rabies labeled cells in all assessed lobules 66 hr post-infection. Color coding of bars indicate assignment of lobules to either anterior, central, posterior or vestibular cerebellum as indicated in L. Abbreviations: Dent., Dentate nucleus; Fast., fastigial nucleus; Fast. DL, dorsolateral fastigial nucleus; Floc. Nod., flocculonodular lobe; Interp., nucleus interpositus; IntA, nucleus interpositus anterior; IntDL, dorsolateral nucleus interpositus; IntP, nucleus interpositus posterior; i-Sim, ipsilateral simplex lobule; c-Sim, contralateral simplex lobule; i-Crus I, ipsilateral Crus I; c-Crus I, contralateral Crus I; i-Crus II, ipsilateral Crus II; c-Crus II, contralateral Crus II; i-Par, ipsilateral paramedian lobule; c-Par, contralateral paramedian lobule; i-CP, ipsilateral copula; c-CP, contralateral copula; i-Floc, ipsilateral flocculus; c-Floc, contralateral flocculus; i-PF, ipsilateral paraflocculus; c-PF, contralateral paraflocculus; Vestib., vestibular nuclei. \*\*  $q < 0.01$ , \*\*\*  $q < 0.001$ .

DOI: <https://doi.org/10.7554/eLife.41896.002>

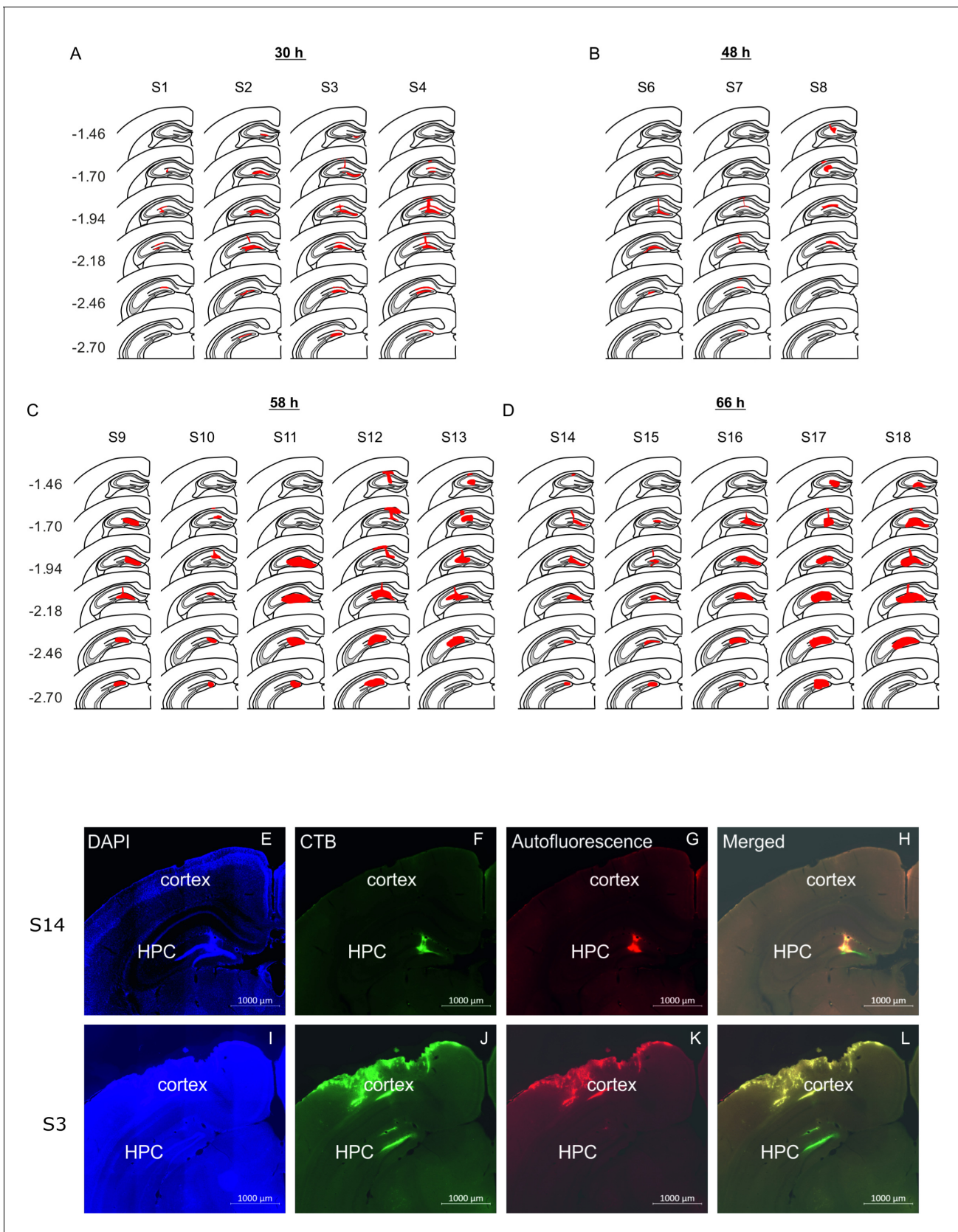


**Figure 1—figure supplement 1.** Location of rabies virus injections for the four experimental groups. RABV was co-injected with fluorescent CTB to visualize the injection spread. (A-D) The location of the injection is indicated by the red area on a standard coronal outline of the left hippocampus for Figure 1—figure supplement 1 continued on next page

Figure 1—figure supplement 1 continued

the 30 hr (A), the 48 hr (B), the 58 hr (C) and the 66 hr (D) survival time groups. Rostro-caudal position relative to bregma is indicated on the left (mm). Experimental ID for each case is shown above the sections. (E) Representative photomicrographs from two mice (S14 and S3) illustrating the spread of CTB used to define the site of rabies injection in the hippocampus.

DOI: <https://doi.org/10.7554/eLife.41896.003>

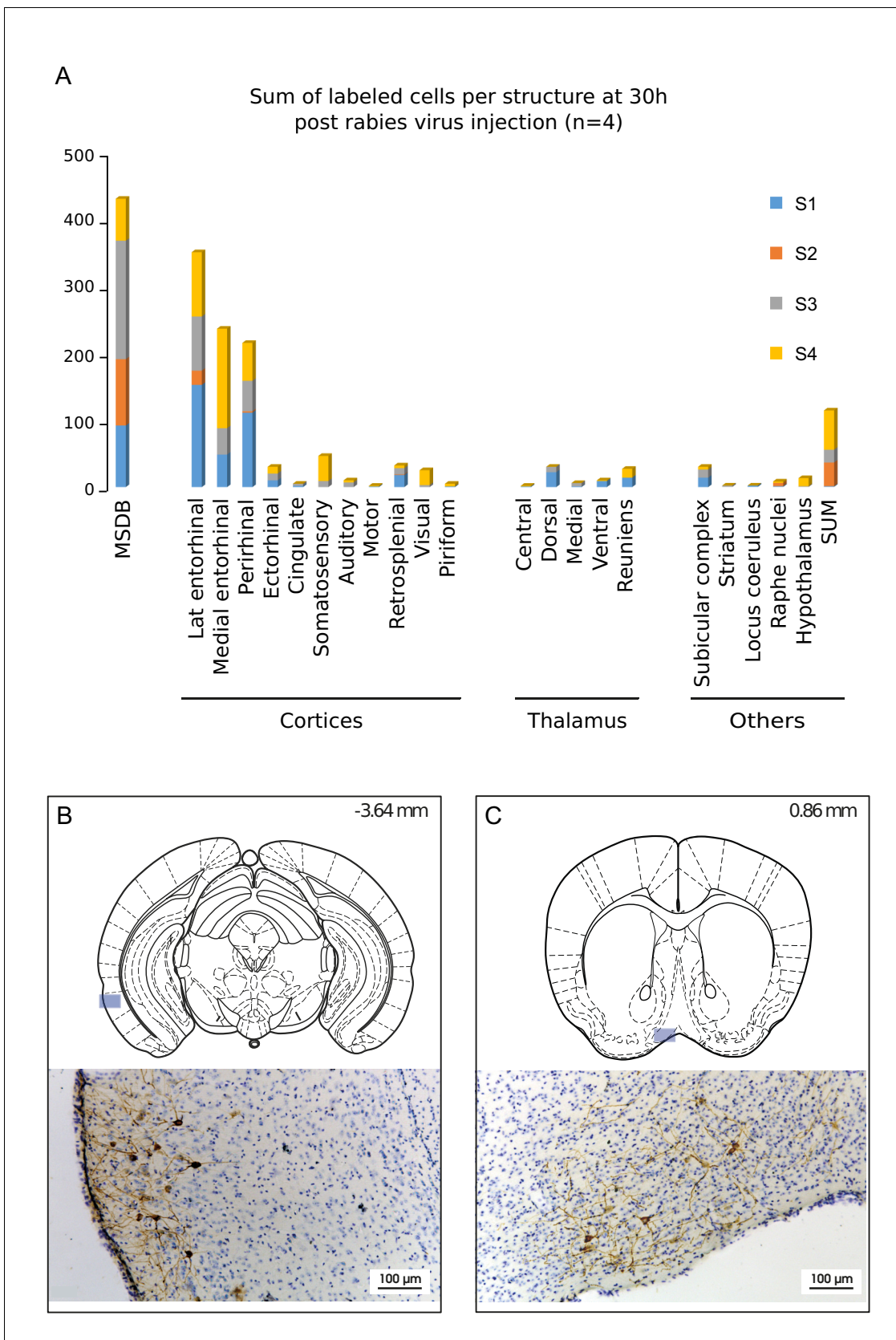


**Figure 1—figure supplement 2.** Structures labeled 30 hr after hippocampal rabies injection. (A) Cumulative sum of labeled cells per structure 30 hr post-hippocampal rabies injection (color coded for each case, n = 4 mice). B-C, Localization and representative photomicrographs of RABV in the two Figure 1—figure supplement 2 continued on next page

Figure 1—figure supplement 2 continued

main labeled regions at 30 hr, the lateral entorhinal cortex (B) and the MSDB (C). The position is indicated by a blue insert on a standard coronal outline of a brain section, and rostro-caudal position according to Bregma is indicated in the top-right corner. Abbreviations, Lat entorhinal cortex, lateral entorhinal cortex; MSDB, medial septum/diagonal band of Broca; SUM, supramammillary nucleus.

DOI: <https://doi.org/10.7554/eLife.41896.004>

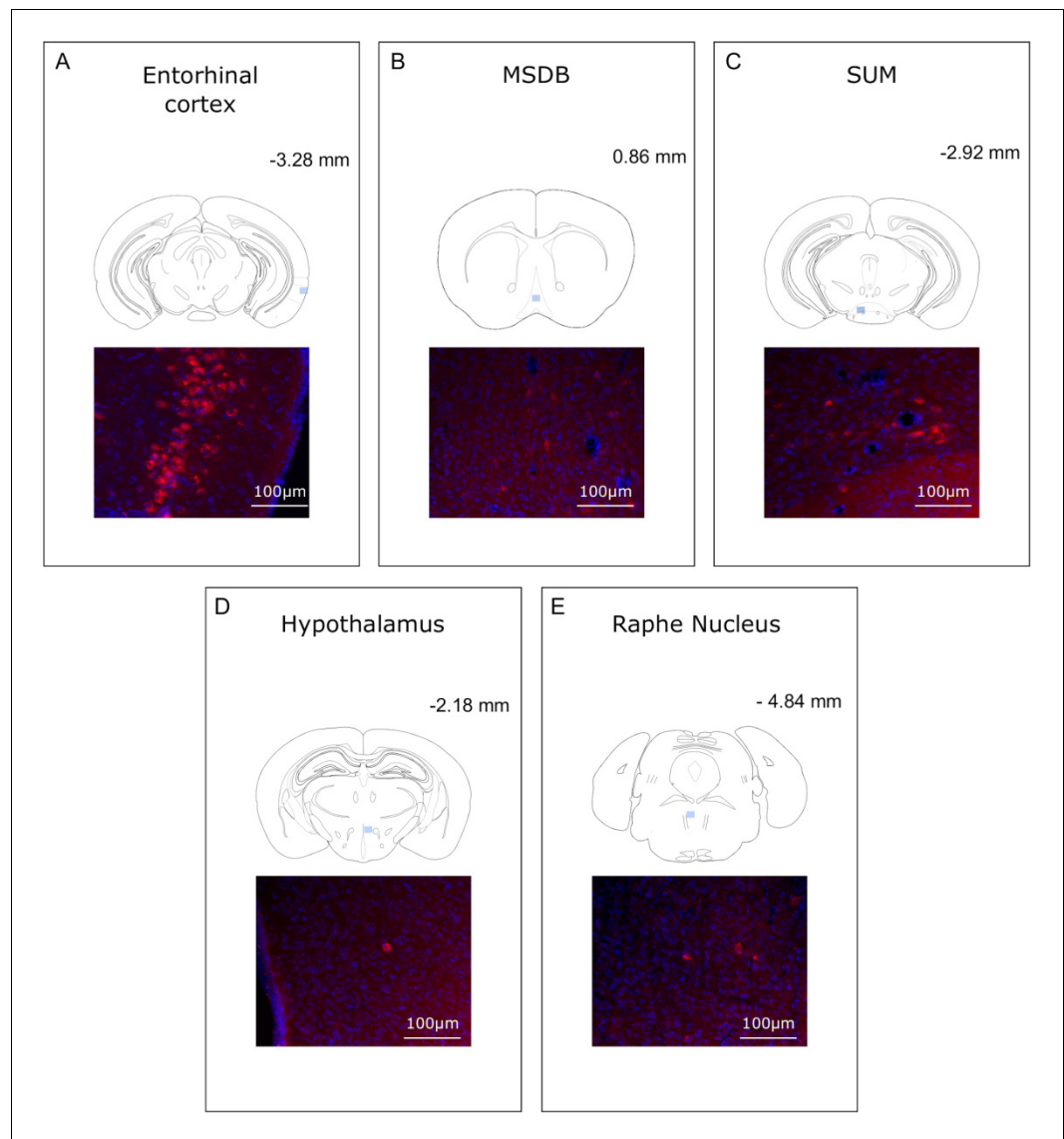


**Figure 1—figure supplement 3.** Analysis of CTB retrograde labeling indicates that rabies labeled structures at 30 hr post-infection are potential first relay regions. (A-E) Localization and representative photomicrographs of CTB-positive cells (red) in the entorhinal cortex, MSDB, SUM, hypothalamus and Raphe Nucleus, confirming that these regions are putative first relays to the hippocampus. Coronal sections are counterstained with DAPI (blue). The localization of the CTB staining is indicated by a blue insert on a standard coronal outline of a brain section, and rostro-caudal position according to Bregma is indicated in the top-right corner. Abbreviations; MSDB, medial septum/diagonal band of Broca; SUM, supramammillary nucleus.

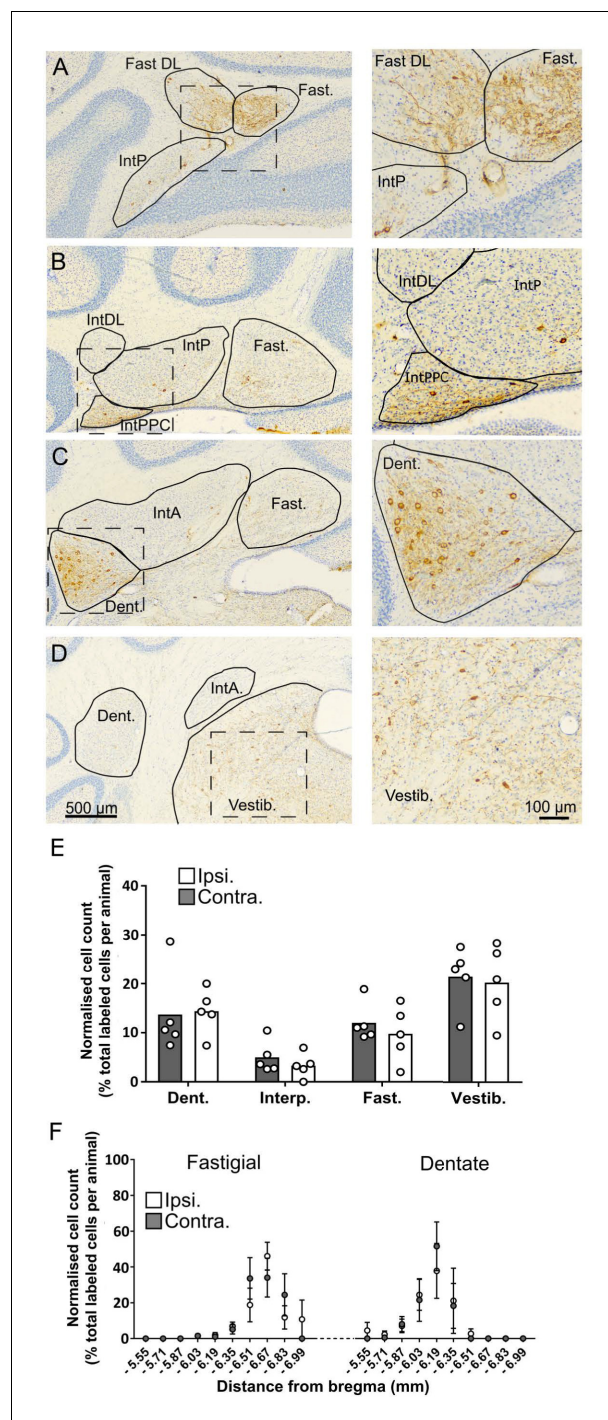
DOI: <https://doi.org/10.7554/eLife.41896.005>

RV+ cells at 48h post-infection	S6	S7	S8
MSDB	+++	++	+++
LEC	++	+++	++
MEC	-	+	++
Perirhinal cortex	+	++	++
Ectorhinal cortex	-	+++	++
Cingulate cortex	-	+++	++
Piriform cortex	-	++	++
Sensory cortices	++	++	++
Thalamus dorsal	-	++	+
Thalamus medial	-	++	-
Thalamus ventral	-	-	+
Reuniens	+	++	++
Raphe nuclei	++	++	++
Hypothalamus	++	++	++
Subicular complex	++	++	+++
Striatum	+	++	+
LC	-	-	+
SUM	+++	++	+++
Mammillary bodies	++	++	++
PAG	++	++	++
Amygdala	+	+	+
LtDg	+	++	++
Nucleus Incertus	++	++	++
Other pontine nuclei	++	++	++
Fastigial nu i.	0	0	0
c.	0	0	2
Interpositus nu i.	0	0	0
c.	0	1	1
Dentate nu i.	0	0	0
c.	0	0	1
Vestibular nu i.	0	0	0
c.	0	0	3
Cerebellar cortex	0	0	0

**Figure 1—figure supplement 4.** Summary table of RABV labeling across brain structures 48 hr after hippocampal rabies injection Overview of RABV labeling in different brain regions 48 hr post rabies injection in the hippocampus. The regions that were already stained at 30H post-infection are represented in gray. In two mice, few rabies-positive cells were detected in the deep cerebellar and vestibular nuclei. (-) denotes no labeling, (+/-) few cells, (+) minor labeling, (++) fair labeling, (+++) strong labeling. For the deep cerebellar and vestibular nuclei, ipsi (i.) and contralateral (c.) sides are distinguished. Sensory cortices include somatosensory, auditory and visual cortices. MSDB, medial septum/diagonal band of Broca; LEC, lateral entorhinal cortex; MEC, medial entorhinal cortex; LC, locus coeruleus; SUM, supramammillary nucleus; PAG, periaqueductal gray; LtDg, laterodorsal tegmental nucleus.

DOI: <https://doi.org/10.7554/eLife.41896.006>



**Figure 1—figure supplement 5.** The topographical distribution of DCN labeling at 66 hr. (A–D) representative photomicrographs showing labeling in the ipsilateral cerebellar and vestibular nuclei 66 hr after hippocampal rabies injection. Left panels show low magnification view, right panels show high-magnification view of area indicated by dashed box. E, Pooled, normalized counts of rabies labeled cells in the ipsi- and contralateral cerebellar and vestibular nuclei (n = 5 mice). No significant differences were found between ipsi- and contralateral nuclei (nuclei x hemisphere two-way ANOVA, hemisphere effect  $F_{(1, 4)}=1.14$ ,  $p=0.35$ , interaction effect  $F_{(3, 12)}=0.21$ ,  $p=0.89$ , nuclei effect  $F_{(3, 12)}=7.88$ ,  $p=0.004$ ). F, Normalized cell counts in the fastigial nucleus (left) and dentate nucleus (right) according to their rostro-caudal position relative to Bregma. Open circles, contralateral count; filled circles, ipsilateral count (n = 5 mice). Abbreviations: Dent., Dentate nucleus; Fast., fastigial nucleus; Figure 1—figure supplement 5 continued on next page

*Figure 1—figure supplement 5 continued*

Fast. DL, dorsolateral fastigial nucleus; Interp., nucleus interpositus; IntA, nucleus interpositus anterior; IntDL, dorsolateral nucleus interpositus; IntP, nucleus interpositus posterior; Vestib., vestibular nuclei.

DOI: <https://doi.org/10.7554/eLife.41896.007>

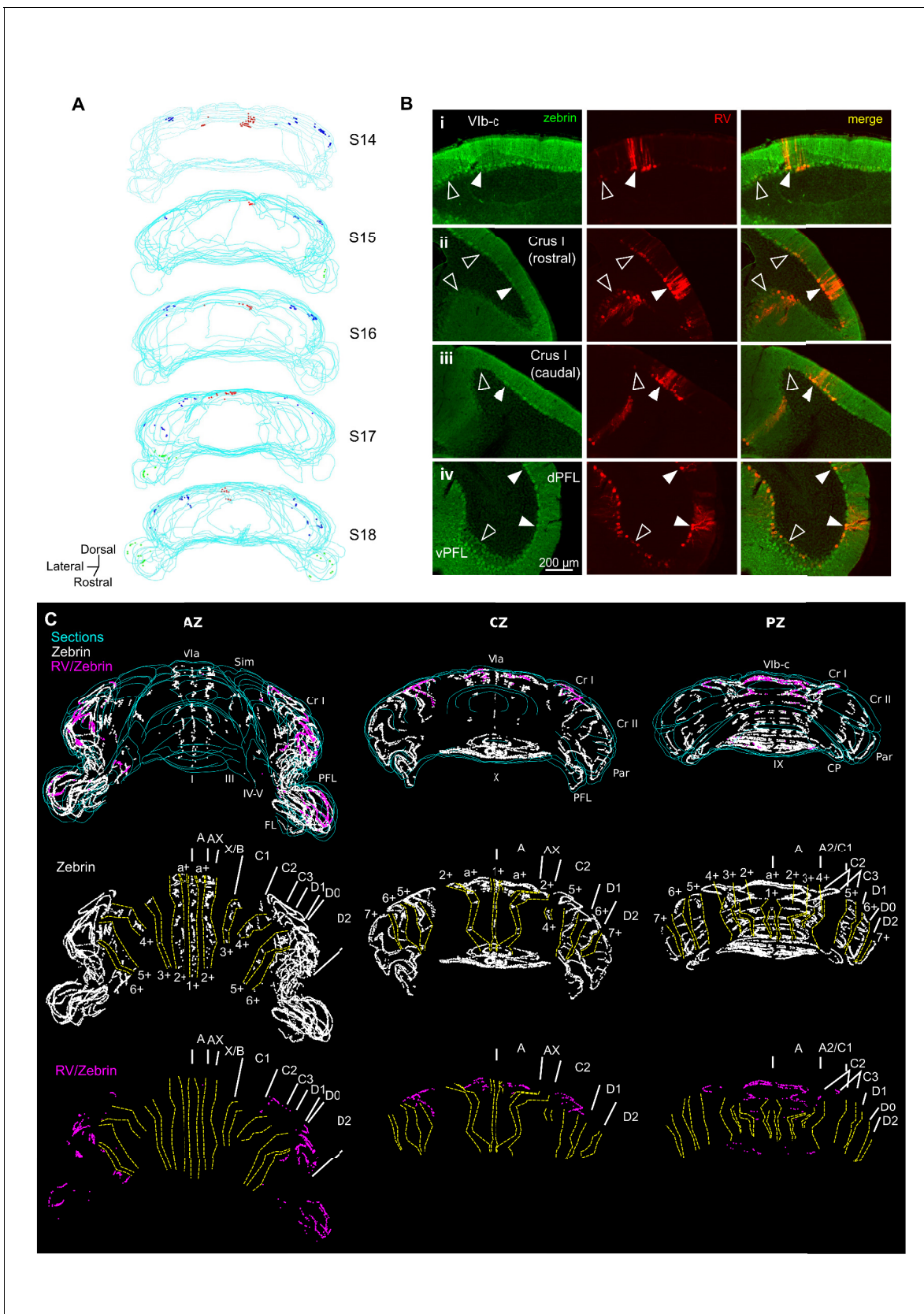
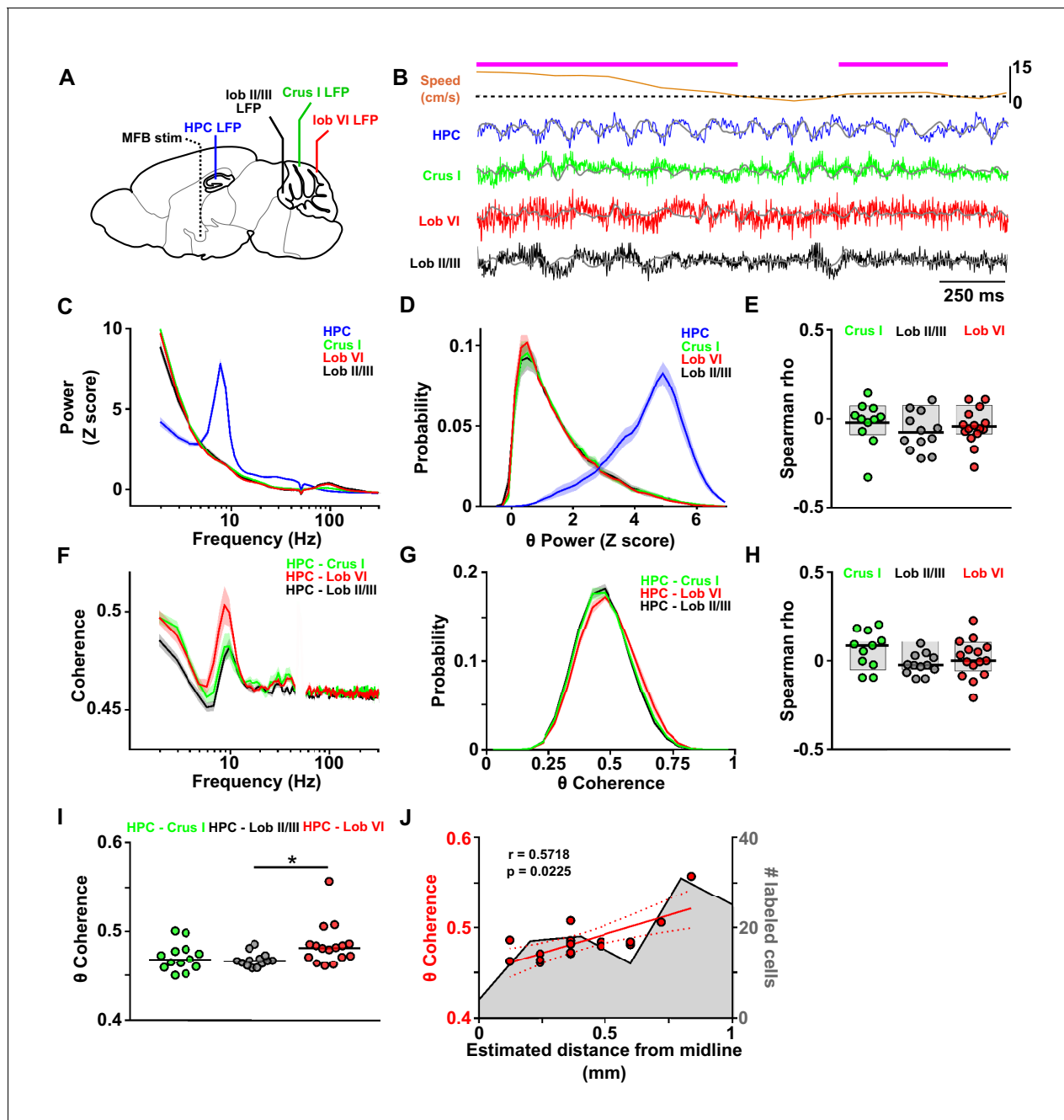


**Figure 2.** Different cerebellar modules project to the hippocampus. (A) 3-D reconstruction showing the location of RABV+ Purkinje cells in the most labeled cerebellar lobules at 66 hr post-infection. Red, blue and green dots represent RABV+ Purkinje cells in lobule VI, Crus I and paraflocculus, Figure 2 continued on next page

*Figure 2 continued*

respectively. (B) Photomicrographs from case S18 showing double staining against zebrin II (green, left column), RABV (red, central column) and merge (right column) in lobule VI (i), Crus I (ii and iii) and paraflocculus (iv). RABV+ Purkinje cells were also zebrin positive and were organized in clusters of strongly labeled RABV+ cells (filled arrow-heads) surrounded by weakly labeled RABV+ Purkinje cells (unfilled arrow-heads). (C) Assignment of the RABV+ clusters to specific cerebellar modules for case S18 in the anterior (AZ; left), central (CZ; central column) and posterior (PZ; right column) zones. First row shows stacked sections with zebrin-positive Purkinje cells (white dots) and RABV+ Purkinje cells, which were also zebrin positive (purple dots, strong and weakly labeled cells included); central row shows reconstructed principal zebrin bands (delineated by yellow dashed lines and named from 1+ to 7+; nomenclature from **Sugihara and Quy, 2007**) and cerebellar modules (capital letters; defined as in **Sugihara and Quy, 2007**); and bottom row shows the location of the RABV+/zebrin Purkinje cells (purple dots) in relation to reconstructed zebrin bands and modules. Abbreviations, I, lobule I; III, lobule III; IV/V, lobule IV/V; VIa and VI b-c, lobule VIa and VI b-c, respectively; IX, lobule IX; X, lobule X; Sim, lobule simplex; Cr I, Crus I; Cr II, Crus II; Par, paramedian lobule; CP, copula, PFL, paraflocculus, FL, flocculus.; dPFC and vPFC, dorsal and ventral paraflocculus, respectively.

DOI: <https://doi.org/10.7554/eLife.41896.009>



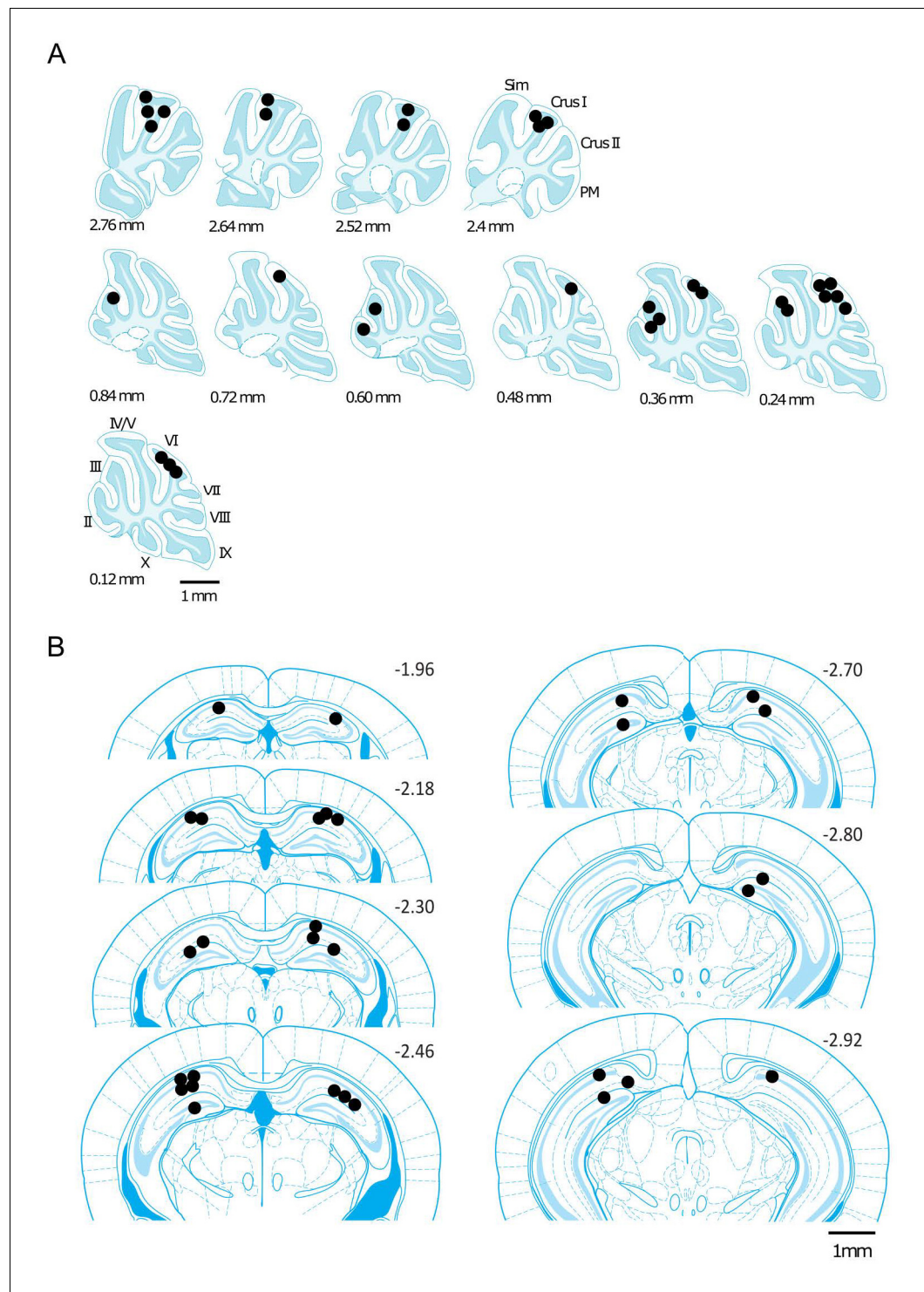
**Figure 3.** Assessment of cerebello-hippocampal interactions during active movement in the home cage. (A) Schematic representation of recording and stimulation electrode implant positions. (B) Representative simultaneous raw LFP recordings (colored lines) and LFP filtered in the theta frequency range ( $\theta$ , 6–12 Hz, overlaid gray lines) recorded during active movement in the home cage condition as defined by instantaneous speed. Solid magenta line indicates data epochs in which speed was above the required threshold for inclusion in further analysis (3 cm/s, dashed line (20 mice). In one mouse in which speed data was not available we used neck electromyograph (EMG) data to define periods of active movement). (C) Averaged z-score of the power spectra from hippocampal LFP ( $n = 21$ , mean between left and right hemisphere LFPs when both recording electrodes were on target) and cerebellar cortical regions Crus I ( $n = 12$ ), lobule II/III ( $n = 13$ ) and lobule VI ( $n = 16$ ) during home cage exploration (speed above 3 cm/s). (D) Probability distribution of the instantaneous z-scored theta power for each of the recorded regions. Hippocampal theta power followed a negatively skewed distribution while cerebellar theta power followed a positively skewed distribution. (E) Correlation between the instantaneous z-scored theta power for each of the cerebellar recorded regions and instantaneous speed. Horizontal line indicates mean. Gray-shaded bars represent the confidence levels obtained from bootstrapped data with  $\alpha = 0.05$ . Theta power was not significantly correlated with speed in any of the cerebellar recordings (Crus I,  $n = 11$ ; lobule II/III,  $n = 12$ ; lobule VI,  $n = 15$ ). (F) Averaged coherence between cerebellar cortical recordings (color coded) and hippocampus (when both hippocampal recording electrodes were on target we averaged the coherence obtained with left and right hemispheres; Crus I,  $n = 12$ ; lobule II/III,  $n = 13$ ; lobule VI,  $n = 16$ ). (G) Probability distribution of the instantaneous z-scored theta coherence for each of the recorded regions. Hippocampal theta coherence followed a negatively skewed distribution while cerebellar theta coherence followed a positively skewed distribution. (H) Correlation between the instantaneous z-scored theta coherence for each of the cerebellar recorded regions and instantaneous speed. Horizontal line indicates mean. Gray-shaded bars represent the confidence levels obtained from bootstrapped data with  $\alpha = 0.05$ . Theta coherence was not significantly correlated with speed in any of the cerebellar recordings (Crus I,  $n = 11$ ; lobule II/III,  $n = 12$ ; lobule VI,  $n = 15$ ). (I) Theta coherence for HPC-Crus I, HPC-lob II/III, and HPC-lob VI. Horizontal line indicates mean. Gray-shaded bars represent the confidence levels obtained from bootstrapped data with  $\alpha = 0.05$ . Theta coherence was not significantly correlated with speed in any of the cerebellar recordings (Crus I,  $n = 11$ ; lobule II/III,  $n = 12$ ; lobule VI,  $n = 15$ ). (J) Theta coherence and the number of labeled cells as a function of estimated distance from the midline. Horizontal line indicates mean. Gray-shaded bars represent the confidence levels obtained from bootstrapped data with  $\alpha = 0.05$ .  $r = 0.5718$ ,  $p = 0.0225$ .

Figure 3 continued on next page

*Figure 3 continued*

III,  $n = 13$ ; lobule VI,  $n = 16$ ) during homecage exploration (speed above 3 cm/s). (G) Probability distribution of the instantaneous hippocampal-cerebellar theta coherence (color coded). All the recording combinations followed normal distributions. (H) Correlation between the instantaneous hippocampal-cerebellar theta coherence (color coded) and the instantaneous speed. Horizontal line indicates mean. Gray-shaded bars represent the confidence levels obtained from bootstrapped data with  $\alpha = 0.05$ . HPC-cerebellar theta coherence was not significantly correlated with speed in any of the recording combinations. (I) Theta coherence between cerebellar recordings and hippocampus (average between coherence with left and right hemisphere LFPs when both recordings were on target; Crus I - HPC,  $n = 12$ ; lobule II/III - HPC,  $n = 13$ ; lobule VI - HPC,  $n = 16$ ). Lobule VI-HPC coherence was significantly higher than that observed with lobule II/III (horizontal line indicates median coherence for each combination; \*, Kruskal-Wallis with FDR correction, Kruskal-Wallis statistic = 6.75,  $p = 0.0342$ ; lobule VI-HPC vs lobule II/III-HPC,  $p = 0.0246$ ). J, Mean lobule VI-HPC theta coherence plotted against the estimated medio-lateral position of the recording electrode in lobule VI (red dots;  $n = 16$ , when both hippocampal recording electrodes were on target we averaged the coherence obtained with left and right hemispheres; Spearman rho = 0.5718,  $p = 0.0225$ ). In gray, number of RABV+ cells counted across lobule VI 66 hr after injection in the left HPC as a function of medio-lateral position (0.2 mm bins;  $n = 5$  mice). Shading indicates S.E.M. Abbreviations, LFP, local field potential; HPC, dorsal hippocampus; lob II/III, lobule II/III, lob VI, lobule VI, MFB stim, medial forebrain bundle stimulation.

DOI: <https://doi.org/10.7554/eLife.41896.010>



**Figure 3—figure supplement 1.** Reconstructed location of the implanted electrodes. The position of the implanted electrodes are represented by black dots on a standard sagittal outline of the cerebellum (A) or coronal outline of the hippocampus (B). The medio-lateral (in A) or rostro-caudal (in B) positions relative to midline or bregma, respectively, are indicated next to the outlines. Abbreviations, II, lobule II; III, lobule III; IV/V, lobule IV/V; VI, lobule VI; VII, lobule VII; VIII, lobule VIII; IX, lobule IX; X, lobule X; Sim, lobule simplex; PM, paramedian lobule.

DOI: <https://doi.org/10.7554/eLife.41896.011>

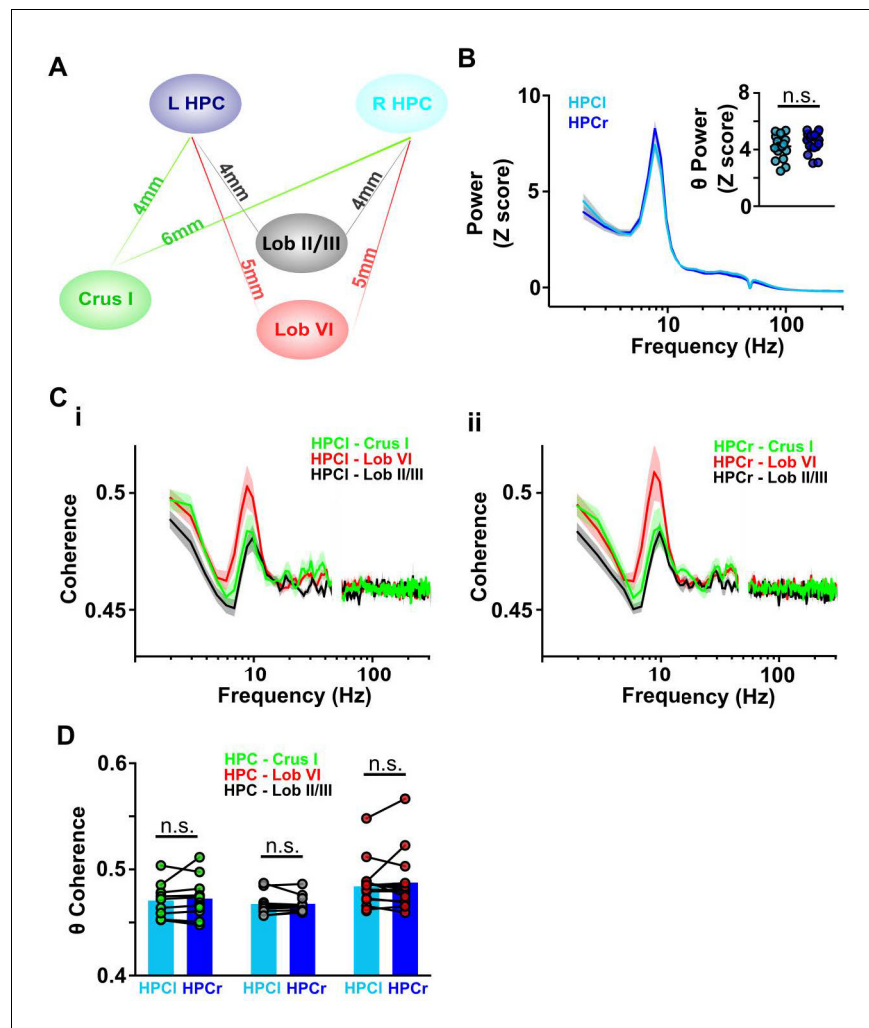


**Figure 3—figure supplement 2.** Cerebello-hippocampal coherence patterns are similar across hemispheres during active movement in homecage. (A) Schematic indicating approximate distances between recording sites in the cerebellum and left/right dorsal hippocampus (HPC). (B) Averaged LFP power from HPC left (light blue,  $n = 17$ ) and HPC right (dark blue,  $n = 19$ ) from **Figure 3C**. Inset: No significant difference was observed in the mean theta power between hemispheres (Unpaired t test,  $t = 1.392$ ,  $p = 0.1731$ ). (C) Averaged coherence between HPC left and cerebellar regions (i, Crus I,  $n = 11$ ; lobule II/III = 11; lobule VI,  $n = 15$ ) and HPC right and cerebellar regions (ii, Crus I,  $n = 11$ ; lobule II/III = 12; lobule VI,  $n = 14$ ). (D) Comparisons between cerebello-HPC left (light blue) and cerebello-HPC right (dark blue) theta coherence from panel C. No significant differences were observed for any cerebello-hippocampal combination (Crus I, Mann-Whitney test,  $U = 59$ ,  $p = 0.9487$ ; lobule II/III, Mann-Whitney test,  $U = 63$ ,  $p = 0.8801$ ; lobule VI, Mann-Whitney test,  $U = 105$ ,  $p > 0.99$ ).

DOI: <https://doi.org/10.7554/eLife.41896.012>

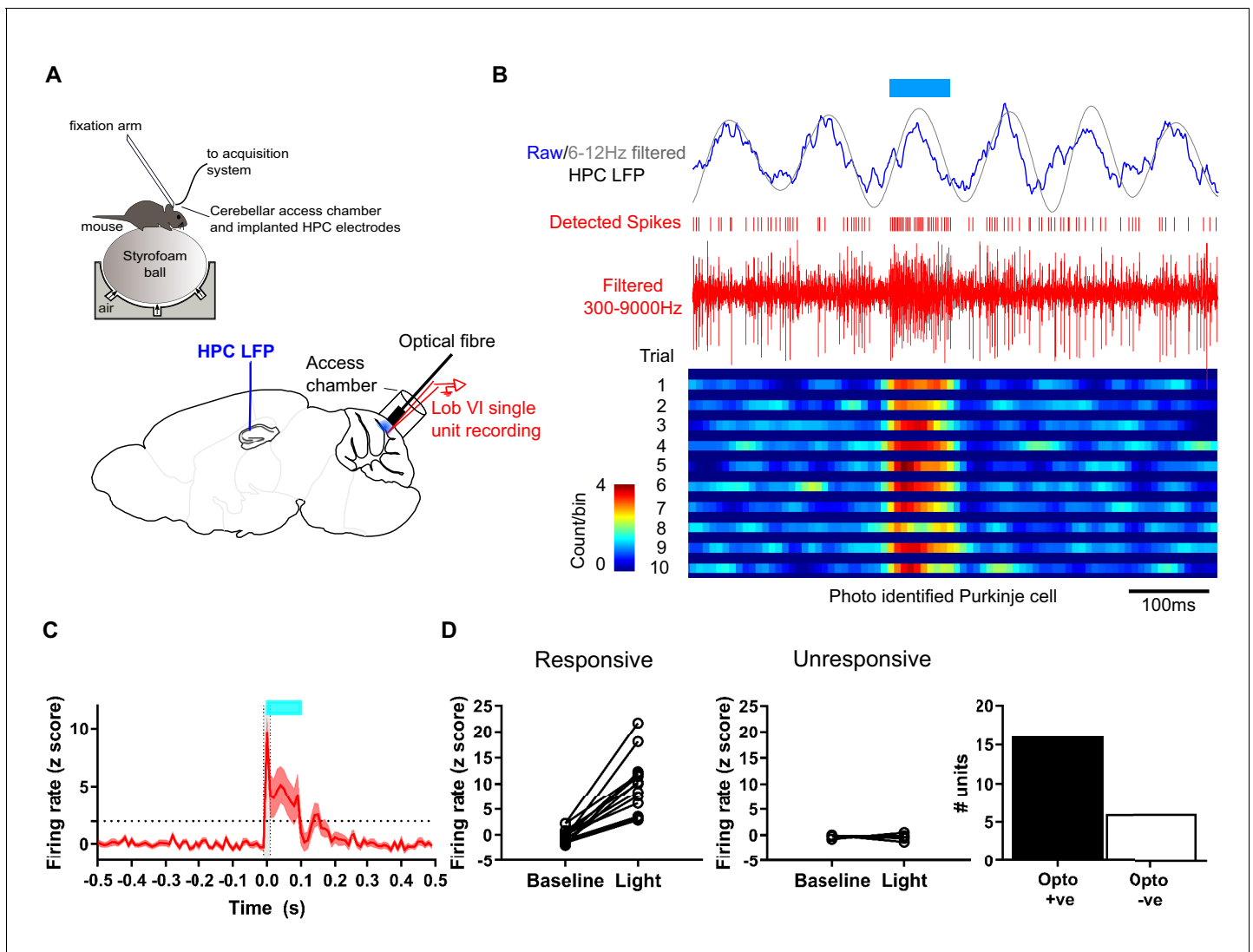


**Figure 3—figure supplement 3.** Experimental setup for simultaneous recording of photo-identified Purkinje cells and hippocampal local field potential. (A) Head-fixed L7-ChR2 mice were allowed to run freely on an air cushioned Styrofoam ball. LFP was recorded from left hippocampus through chronically implanted bipolar electrodes. An access chamber was constructed over the cerebellar vermis, allowing recording access to lobule VI. In addition, an optical fiber was placed on the cerebellar surface near the recording site to allow photo-activation of ChR2 +ve Purkinje cells. (B) Example recording, showing raw and 6–12 Hz filtered hippocampal LFP. Blue horizontal line indicates time of blue light (~460 nm) illumination through the optical fiber. Extracellular unit recording shown in red with detected spikes marked above. Below, color-coded raster plot showing a recorded unit and its activation profile during the blue light illumination period. Bins 10 ms. (C) Mean rate plot of all significantly photo-responsive units recorded in the cerebellum (shaded area indicated s.e.m.). Blue horizontal line indicates timing of blue light illumination. A total of 22 units were recorded from six mice. (D) Of those, 16 units, recorded from four mice, showed a significant increase in firing during the first 10 ms of blue light illumination ( $Z > 1.96$  increase from 10 ms pre-stimulation baseline level; dashed horizontal line) and six units, from four mice, were unresponsive ( $Z < 1.96$  increase from 10 ms pre-stimulation baseline level).

DOI: <https://doi.org/10.7554/eLife.41896.013>

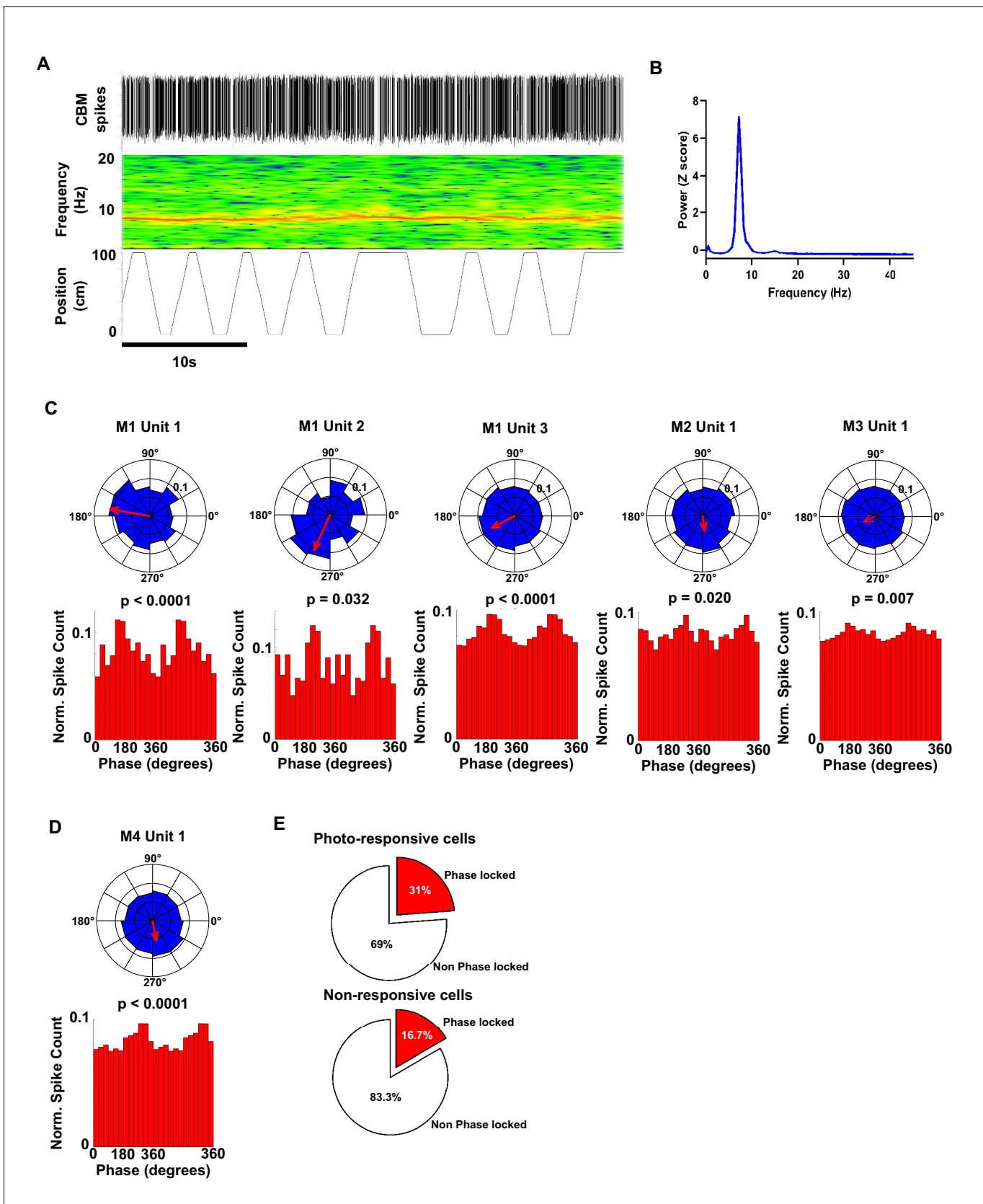


**Figure 3—figure supplement 4.** Polar plots and associated histograms of cerebellar units significantly phase locked to hippocampal 6–12 Hz oscillations. (A) Example 40 s epoch used for analysis of phase locking. Top, detected cerebellar spikes. Middle, hippocampal spectrogram. Bottom, Figure 3—figure supplement 4 continued on next page

*Figure 3—figure supplement 4 continued*

position tracking in virtual reality corridor. **(B)** Hippocampal power spectra calculated from the epoch shown in A. Note the prominent theta peak (~8 Hz). **(C)** Individual polar plots and phase distribution histograms for each photo responsive unit (five cells from three mice) that were significantly phase locked to the hippocampal 6–12 Hz oscillation. **(D)** Polar and phase distribution plots for the single non-responsive unit recorded that was significantly phase locked to hippocampal 6–12 Hz oscillation. P Rayleigh value for each cell plotted above histogram. **(E)** Pie charts showing the % of photo-responsive (upper) and photo non-responsive units (lower) that were phase locked to the hippocampal 6–12 Hz oscillation. From our sample, 31% (5 from 16 units) of photo-responsive units and 16% of non-responsive units were phase locked to the hippocampal 6–12 Hz oscillation, respectively.

DOI: <https://doi.org/10.7554/eLife.41896.014>

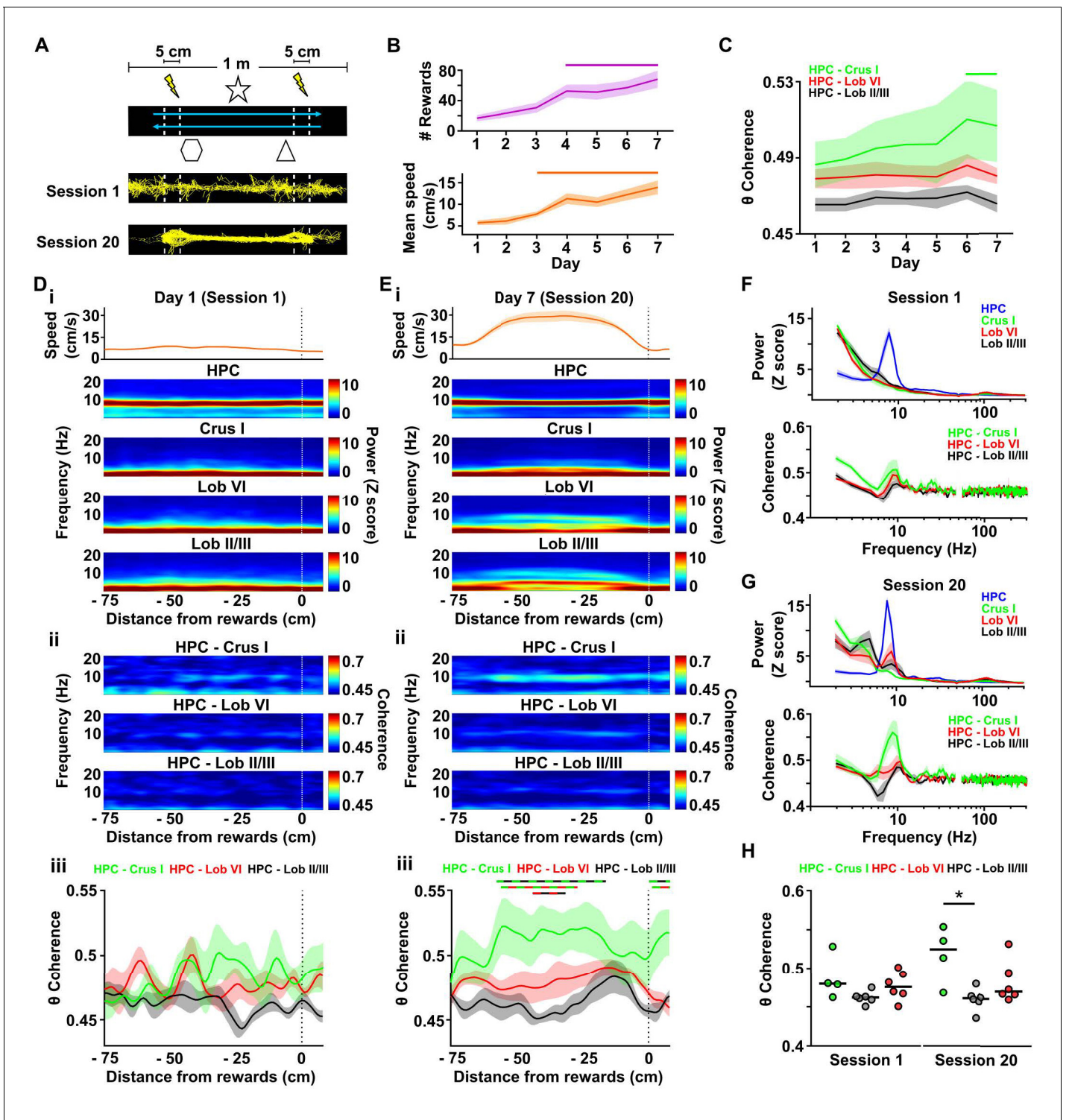


**Figure 4.** Cerebello-hippocampal interactions during goal-directed behavior. (A) Mice learned to traverse a 1 m linear track to receive a medial forebrain bundle stimulation (lightening symbols) upon reaching invisible goal zones ( $n = 8$  mice). Representative trajectories from early (session 1) and late (session 20) training show the transition from exploratory to goal-directed behavior. (B) Mice improved their performance in the task across days as shown by increases in the mean number of rewards obtained (average of the three sessions per day, repeated measures Friedman test with FDR correction, Friedman statistic = 37.91,  $p < 0.0001$ ; solid line, day 1 vs days 4–7,  $p < 0.01$ ) and mean speed (average of the three sessions per day, repeated measures Friedman test with FDR correction, Friedman statistic = 36.32,  $p < 0.0001$ ; solid line, day 1 vs days 4–7,  $p < 0.05$ ). (C) Overall cerebello-hippocampal theta coherence per day (average of the three sessions per day) during learning of the linear track task (when both hippocampal  
 Figure 4 continued on next page

## Figure 4 continued

recording electrodes were on target we averaged the coherence obtained with left and right hemispheres; Crus I,  $n = 4$ ; lobule II/III,  $n = 6$ ; lobule VI,  $n = 6$ ). Hippocampus-Crus I coherence increased significantly compared with first day (day of training  $\times$  cerebello-hippocampal combination two-way ANOVA with FDR correction, day effect  $F_{6,84} = 3.873$ ,  $p = 0.0018$ ; solid line, day 1 vs days 6–7,  $p < 0.01$ ). (D) i, Top: Mean speed aligned by distance from the reward location (position 0) averaged across runs during session 1. Bottom: Mean power spectrogram aligned by distance from reward and averaged across runs during session one for hippocampus LFP ( $n = 8$ , mean between left and right hemisphere LFPs when both hippocampal recordings were on target) and cerebellar cortical regions (Crus I,  $n = 4$ ; lobule II/III,  $n = 6$ ; lobule VI,  $n = 6$ ). ii, Mean coherogram aligned by distance from reward location (position 0) averaged across runs during session one for each hippocampal-cerebellar combination (when both hippocampal recording electrodes were on target we averaged the coherence obtained with left and right; Crus I,  $n = 4$ ; lobule II/III,  $n = 6$ ; lobule VI,  $n = 6$ ). iii, Mean theta coherence aligned by distance from reward and averaged across runs during session one for each hippocampal-cerebellar combination (mean between coherence with left and right hemisphere LFPs when both recordings were on target; Crus I,  $n = 4$ ; lobule II/III,  $n = 6$ ; lobule VI,  $n = 6$ ). No significant differences between hippocampal-cerebellar combination or distances from reward were observed, but a significant interaction effect was obtained (distance  $\times$  combination two-ways repeated measures ANOVA with FDR correction; combination effect,  $F_{2,13} = 2.33$ ,  $p = 0.1365$ ; distance effect,  $F_{84,1092} = 1.043$ ,  $p = 0.3772$ ; interaction effect,  $F_{168,1092} = 1.332$ ,  $p = 0.0053$ ). (E) Same as D for session 20. Significant differences were observed between hippocampal-cerebellar combinations (distance  $\times$  combination two-ways repeated measures ANOVA with FDR correction; combination effect,  $F_{2,13} = 6.145$ ,  $p = 0.0132$ ; distance effect,  $F_{84,1092} = 1.682$ ,  $p = 0.0002$ ; interaction effect,  $F_{168,1092} = 1.271$ ,  $p = 0.0163$ ). Post-hoc analysis revealed sustained (at least for five consecutive cm) differences between Crus I-HPC and lobule II/III-HPC coherence at distances from  $-60$  to  $-20$  cm from reward (solid green/black line), between lobule VI-HPC and lobule II/III-HPC coherence between  $-44$  and  $-31$  cm from reward (solid red/black line) and also between Crus I-HPC and lobule VI-HPC coherence between  $-59$  and  $-36$  cm from reward (solid green/red line). (F) Top: Averaged LFP power between  $-60$  and  $-20$  cm from reward (session 1). Bottom: Averaged coherence between  $-60$  and  $-20$  cm from reward (session 1). The spurious peak in the 49–51 Hz band generated for the electrical noise has been removed. (G) Same as J for session 20. (H) Averaged theta coherence between  $-60$  and  $-20$  cm from reward between cerebellar recordings and hippocampus during session 1 (left) and session 20 (right, coherence averaged between left and right hemisphere LFPs when both hippocampal recording electrodes were on target; Crus I,  $n = 4$ ; lobule II/III,  $n = 6$ ; lobule VI,  $n = 6$ ). Crus I-HPC coherence was significantly higher than that observed with lobule II/III in the session 20 (\*, Kruskal-Wallis with FDR correction, Kruskal-Wallis statistic = 7.989,  $p = 0.0103$ ; Crus I-HPC vs lobule II/III-HPC,  $p = 0.0110$ ).

DOI: <https://doi.org/10.7554/eLife.41896.016>

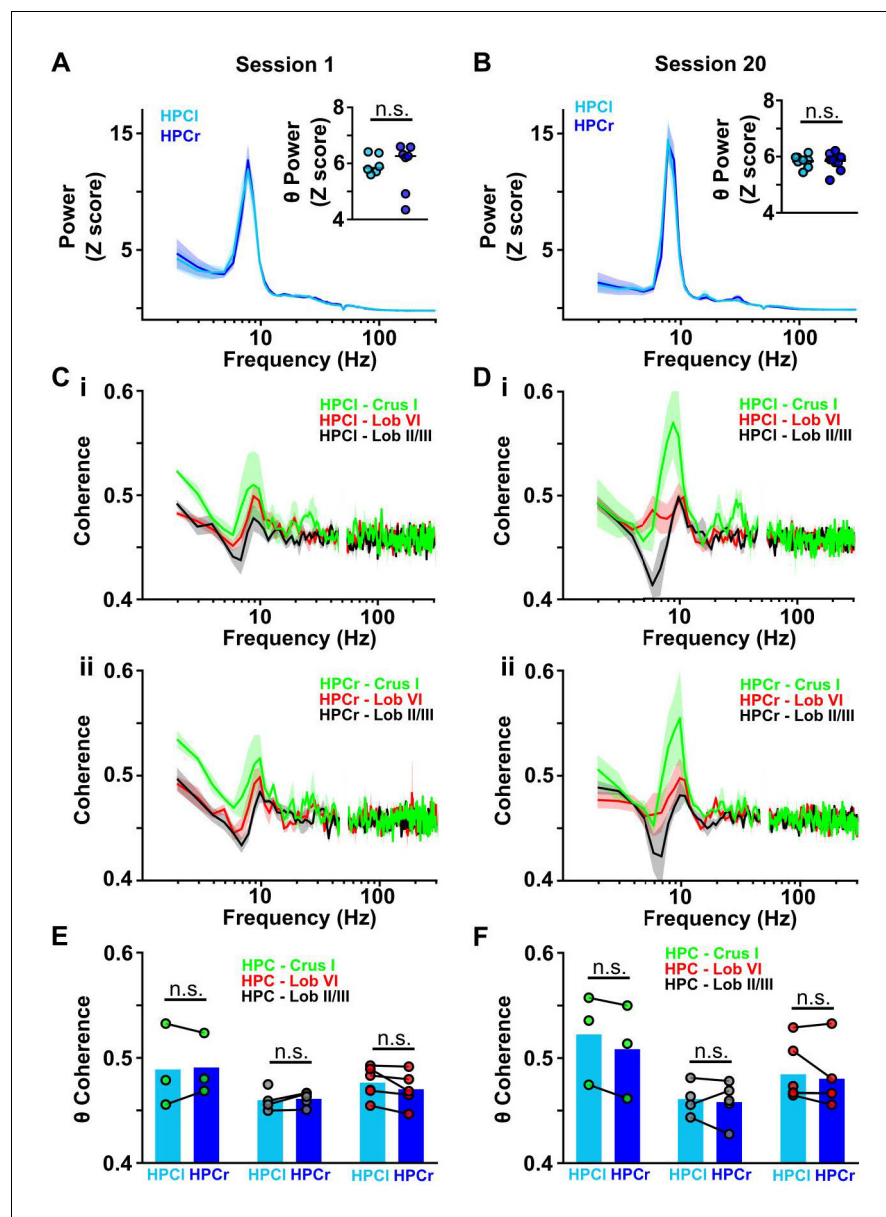


**Figure 4—figure supplement 1.** Cerebello-hippocampal coherence patterns are conserved across hemispheres during goal-directed behavior. (A) Averaged z-score LFP power from HPC left (light blue,  $n = 6$ ) and HPC right (dark blue,  $n = 7$ ) from **Figure 4J** (session 1). Inset: No significant difference in the mean  $\theta$  power was observed between both hemispheres (Mann-Whitney test,  $U = 18$ ,  $p = 0.7308$ ). (B) Same as A but for session 20 (related to **Figure 4K**). Inset: No significant difference in mean LFP theta power was observed between hemispheres (Mann-Whitney test,  $U = 20$ ,  $p = 0.9452$ ). (C) i: Averaged coherence between HPC left and cerebellar regions (color coded) from **Figure 4J** (Crus I,  $n = 3$ ; lobule II/III = 4; lobule VI,  $n = 6$ ). ii: Same for coherence with HPC right (Crus I,  $n = 3$ ; lobule II/III = 5; lobule VI,  $n = 5$ ). (D) Same as C for session 20 (related to **Figure 4K**). (E) Comparisons between cerebello-HPC left (light blue) and cerebello-HPC right (dark blue) theta coherence from panel C (Session 1). No significant differences were observed for any cerebello-hippocampal combination (Crus I, Mann-Whitney test,  $U = 4$ ,  $p > 0.99$ ; lobule II/III, Mann-Whitney test,  $U = 10$ ,  $p = 0.7302$ ; lobule VI, Mann-Whitney test,  $U = 10$ ,  $p = 0.4286$ ). (F) Same as E for session 20 (panel D). No significant differences were observed for any cerebello-hippocampal combination (Crus I, Mann-Whitney test,  $U = 3$ ,  $p = 0.7$ ; lobule II/III, Mann-Whitney test,  $U = 4$ ,  $p > 0.99$ ; lobule VI, Mann-Whitney test,  $U = 12$ ,  $p = 0.6623$ ).

DOI: <https://doi.org/10.7554/eLife.41896.017>

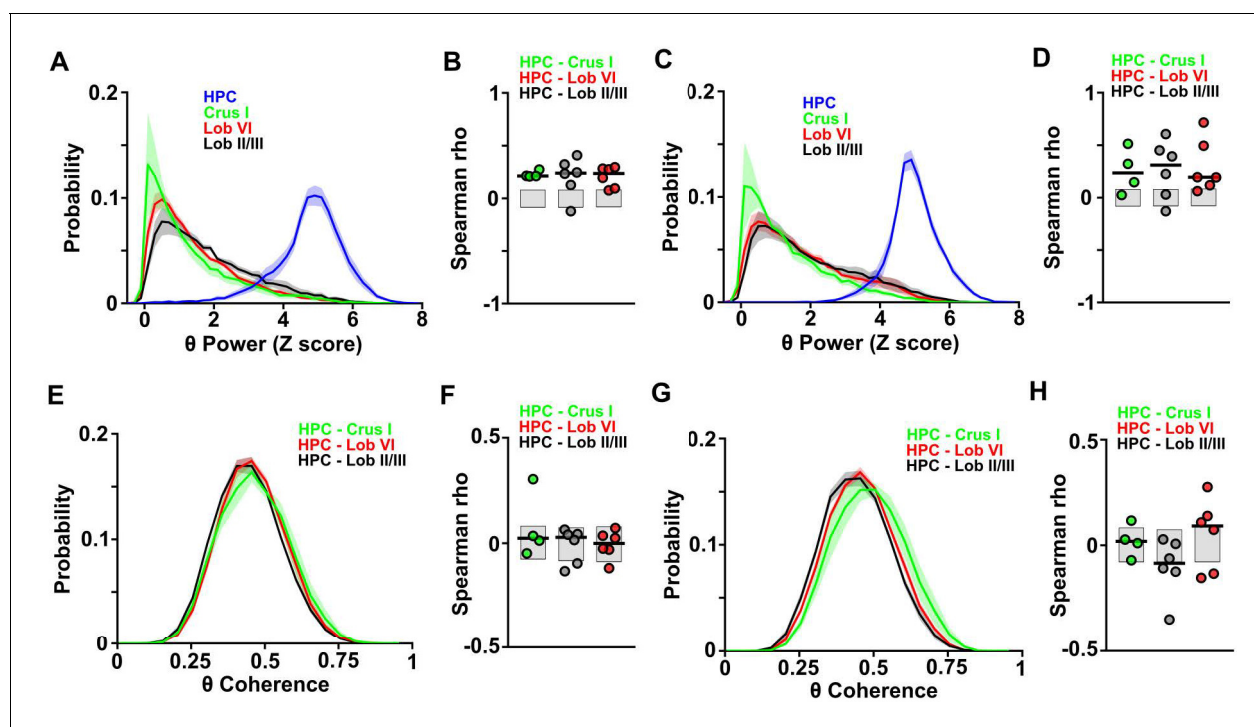


**Figure 4—figure supplement 2.** Distributions and correlations during goal-directed behavior. (A) Probability distribution of the instantaneous LFP theta power for each of the recorded regions during session one in the linear track. Hippocampal theta power followed a negatively skewed distribution while all cerebellar LFP theta power followed a positively skewed distribution. (B) Correlation between the instantaneous LFP theta power for each of the cerebellar regions and instantaneous speed during session one in the linear track. Gray-shaded bars represent the confidence levels obtained from bootstrapped data with  $\alpha = 0.05$ . Cerebellar theta power was significantly positively correlated with speed across all recorded regions (Crus I,  $n = 4$ , median rho Spearman = 0.2125; lobule II/III,  $n = 6$ , median rho Spearman = 0.2391; lobule VI,  $n = 6$ , median rho Spearman = 0.2353). (C) Same as A for session 20. (D) Same as B for session 20. Cerebellar theta power was significantly positively correlated with speed across all recorded regions (Crus I,  $n = 4$ , median rho Spearman = 0.2349; lobule II/III,  $n = 6$ , median rho Spearman = 0.3097; lobule VI,  $n = 6$ , median rho Spearman = 0.1941). (E) Probability distribution of instantaneous hippocampal-cerebellar theta coherence (color coded) and instantaneous speed during session one in the linear track. All combinations followed gaussian distributions. (F) Correlation between the instantaneous hippocampal-cerebellar theta coherence (color coded) and instantaneous speed during session one in the linear track. Gray-shaded bars represent the confidence levels obtained from bootstrapped data with  $\alpha = 0.05$ . Hippocampal-cerebellar theta coherence was not significantly correlated with speed across any of the recorded combinations. (G) Same as E for session 20. (H) Same as F for session 20. Lobule II/III-HPC theta coherence was significantly negatively correlated with speed ( $n = 6$ , median rho Spearman =  $-0.0859$ ) and lobule VI-HPC theta coherence was significantly positively correlated with speed ( $n = 6$ , median rho Spearman = 0.0911). Crus I-HPC theta coherence was not correlated with speed (Spearman rho = 0.024).

DOI: <https://doi.org/10.7554/eLife.41896.018>

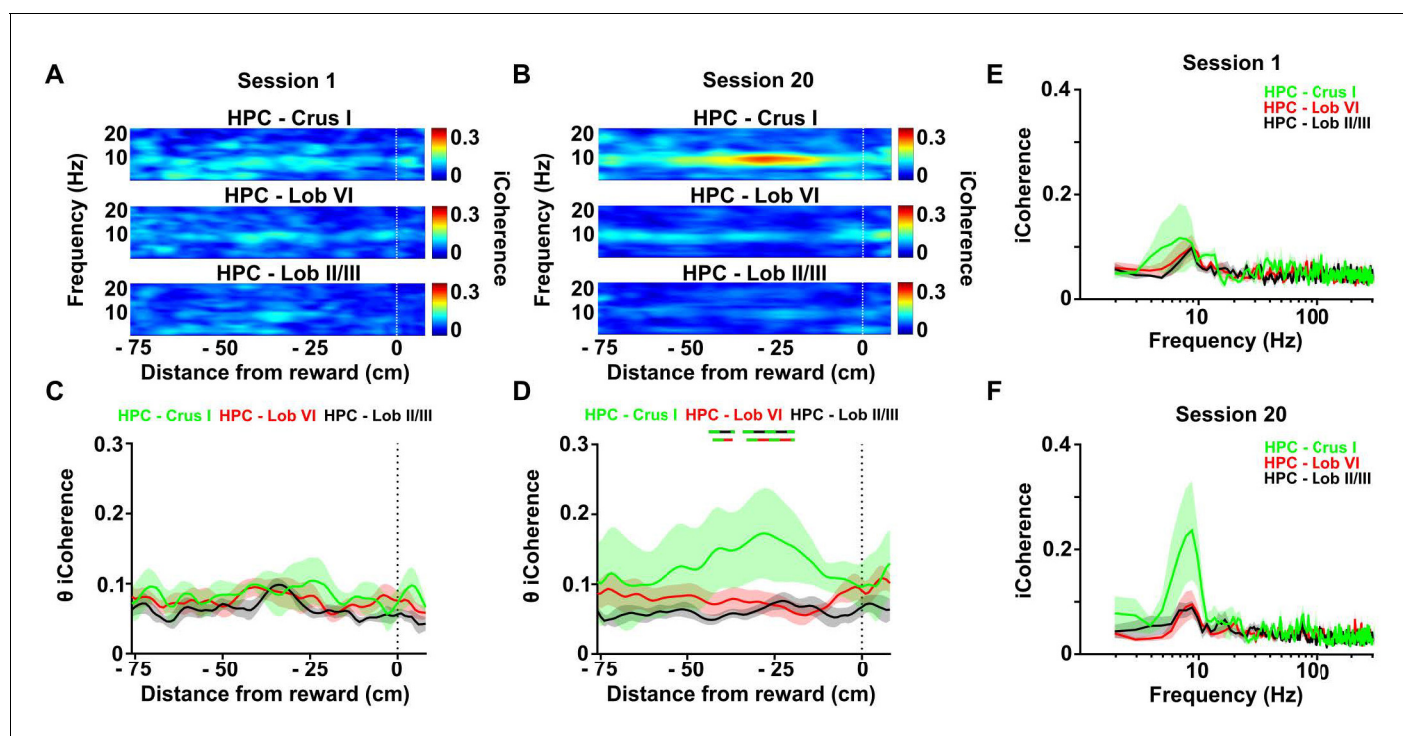


**Figure 4—figure supplement 3.** Calculation of the imaginary part of coherence during goal-directed behavior. (A) Mean coherogram plotted using the imaginary part of coherence, aligned by distance from reward and averaged across runs during session one for each hippocampal-cerebellar combination (mean coherence between left and right hemisphere LFPs when both hippocampal recording electrodes were on target; Crus I,  $n = 4$ ; lobule II/III,  $n = 6$ ; lobule VI,  $n = 6$ ; related to **Figure 4E**). (B) Same as A but for session 20 (related to **Figure 4H**). (C) Mean imaginary theta coherence aligned by distance from reward averaged across runs during session one for each hippocampal-cerebellar combination (mean coherence between left and right hemisphere LFPs when both recording electrodes were on target; Crus I-HPC,  $n = 4$ ; lobule II/III-HPC,  $n = 6$ ; lobule VI-HPC,  $n = 6$ ). No significant differences between hippocampal-cerebellar combinations was observed (distance  $\times$  combination two-way repeated measures ANOVA with FDR correction; combination effect,  $F_{2,13} = 1.065$ ,  $p = 0.3730$ ; interaction effect,  $F_{168,1092} = 0.6713$ ,  $p = 0.9993$ ). (D) Same as C for session 20. A significant interaction between hippocampal-cerebellar combination and distance from reward was observed (distance  $\times$  combination two-way repeated measures ANOVA with FDR correction; interaction effect,  $F_{168,1092} = 1.588$ ,  $p < 0.0001$ ). Post-hoc analysis revealed sustained differences between Crus I-HPC and lobule II/III-HPC coherence at distances from  $-42$  to  $-40$  and from  $-34$  to  $-23$  cm from reward (solid green/black line) and between Crus I-HPC and lobule VI-HPC coherence from  $-33$  to  $-23$  cm (solid green/red line). (E) Imaginary coherence from C (session 1) averaged between  $-42$  and  $-23$  cm from reward. (F) Imaginary coherence from D (session 20) averaged between  $-42$  and  $-23$  cm from reward.

DOI: <https://doi.org/10.7554/eLife.41896.019>

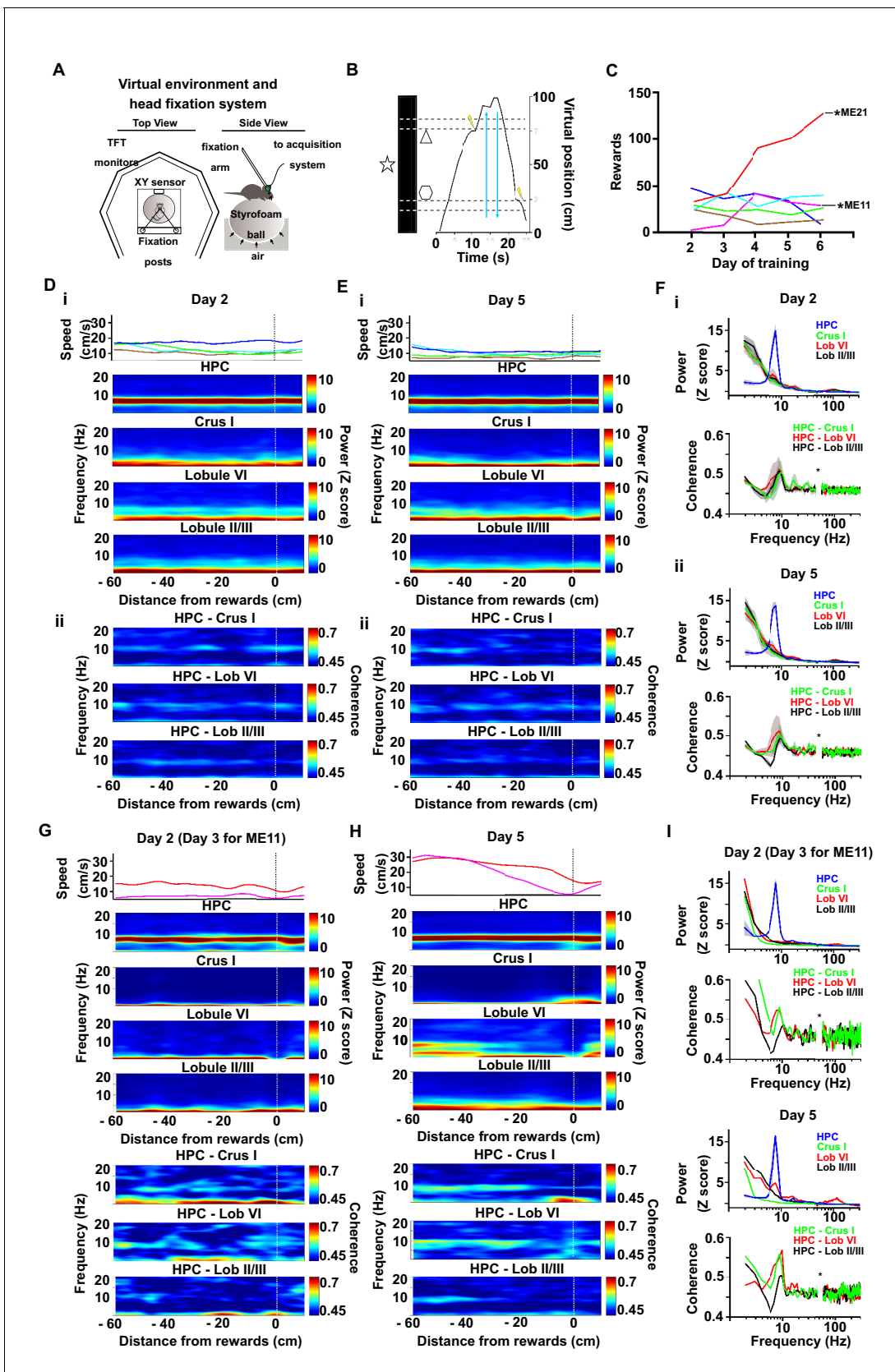


**Figure 4—figure supplement 4.** Cerebello-hippocampal coherence patterns during running or goal-directed movement in a virtual environment. (A) Schematic of the virtual reality system and recording setup. Head-fixed mice were trained to move an air-cushioned Styrofoam ball in order to navigate  
 Figure 4—figure supplement 4 continued on next page

*Figure 4—figure supplement 4 continued*

through a virtual environment displayed on six TFT monitors surrounding the animal. (B) Example recording of the virtual position as a mouse traversed a virtual linear track to receive rewards (MFB stimulation indicated by a lightning symbol,  $n = 6$ ). (C) Behavioral performance across training as illustrated by the mean number of rewards. Each mouse represented by a different line color. Two mice, ME21 and ME11, showed an increase in the number of rewards obtained over training days. (D) i, speed (top) and spectrograms (bottom; HPC,  $n = 6$ ; Crus I,  $n = 2$ ; lobule II/III,  $n = 5$ ; lobule VI,  $n = 3$ ) averaged by distance to reward from a session in early training day 2 (session 5); ii, coherograms for non learning mice averaged by distance to reward during early training day 2 (Crus I-HPC,  $n = 2$ ; lobule II/III-HPC,  $n = 5$ ; lobule VI-HPC,  $n = 3$ ). (E) same as D for late training day 5 (session 14). (F) i, power spectra (upper) and coherence (lower) for non-learner mice during early training day 2 pooled from  $-60$  to  $-20$  cm from reward. ii, power spectra (upper) and coherence (lower) for non-learner mice during late training day 5 pooled from  $-60$  to  $-20$  cm from reward. (G-I). Same as E-F but for the two mice that showed an increase in the number of rewards obtained over training (ME21 and ME11, Crus I,  $n = 1$ ; lobule II/III,  $n = 1$ ; lobule VI,  $n = 1$ ).

DOI: <https://doi.org/10.7554/eLife.41896.020>

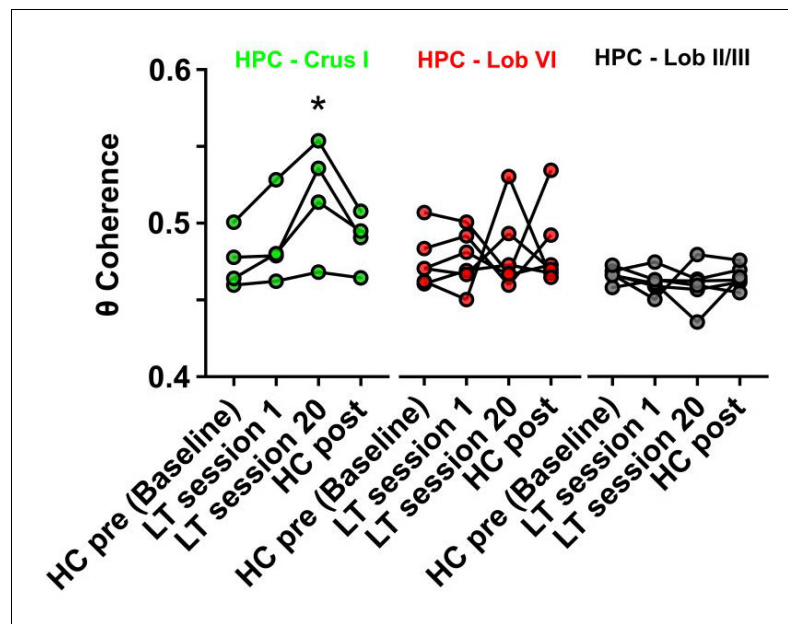


**Figure 5.** Hippocampal-Crus I theta coherence is dynamic. Comparisons of hippocampal-cerebellar theta coherence before and after acquisition of a goal-directed behavior in the linear track task. Levels of coherence during homecage active exploration before first session in the linear track were taken as a baseline. HPC-Crus I theta coherence became significantly different from baseline by session 20 in the linear track task and returned to baseline levels during a second homecage recording immediately following linear track session 20 ( $n = 4$ , repeated measures Friedman test with FDR correction, Friedman statistic = 11.1,  $p = 0.0009$ ; LT session 20 vs baseline,  $p = 0.0021$ ). No significant differences across conditions were observed for the other hippocampal-cerebellar combinations.

DOI: <https://doi.org/10.7554/eLife.41896.022>

**CHAPTER 2:**

Modulation of cerebellar oscillations and cerebello-hippocampal  
interaction across sleep states



## **Modulation of cerebellar oscillations and cerebello-hippocampal interaction across sleep states**

Torres-Herraez A\*, Watson TC\* and Rondi-Reig L

### **Abstract:**

During sleep the pattern of activity exhibited in multiple areas of the brain is known to be profoundly modulated. Moreover, different functional roles have been attributed to specific sleep states mainly involving sleep-dependent plasticity mechanisms across distributed neural networks. Little is known about how the cerebellar activity is modulated by sleep. This knowledge is important in order to fully understand its integration in functional networks with other brain areas. Therefore, we have recorded the local field potentials (LFPs) from the cerebellar cortex and the hippocampus in mice during natural sleep. We have characterized the main cerebellar oscillatory patterns arising during particular sleep states and we have found a characteristic infra-slow (< 1 Hz) oscillation during REM. We also recorded phasic events in the cerebellum during REM sleep which were phase locked to the infra-slow oscillations and were identified as putative pontine waves. Interestingly, an increase in theta coherence between the activity of cerebellar Crus I and hippocampus was observed during REM at preferred phases of the infra-slow oscillations suggesting potential functional implications in the coordination of these two structures during sleep. Finally, we have also recorded evoked activity in the cerebellum triggered by hippocampal sharp-wave ripples suggesting functional connectivity also from the hippocampus to the cerebellum.

### **Introduction:**

Different behavioural states are associated with global and local changes in neuronal activity and neuronal networks dynamics across the brain (Buzsaki, 2006). We can roughly separate the plethora of behaviours exhibited by animals and humans in two main states, wakefulness and sleep. Wakefulness is associated with the generation of voluntary movements and is characterized by high neocortical excitability, high responsiveness to internal and external stimuli and high levels of arousal. In contrast, sleep is characterised by high levels of immobility and low levels of responsiveness, arousal and overall neural excitability (see Scammell et al., 2017). Many important physiological processes are associated with sleep, including memory consolidation (Siegel, 2005; Stickgold, 2005) or homeostatic regulation of neuronal activity (Tononi and Cirelli, 2006). As a consequence, extensive efforts have been made to identify and characterize both the structures involved in controlling and regulating sleep and the impact these processes have on associated brain dynamics and physiology (Scammell et al., 2017).

Sleep can be further subdivided in two main states: non-REM and REM sleep, which have differing networks dynamics and are thought to subserve diverse functions (Saper et al., 2010; Brown et al., 2012). During sleep, both states alternate in predominance and frequency, which depends upon the stage of the cycle and the species (Siegel, 2005). During active wakefulness and REM sleep, the overall electroencephalogram (EEG) profiles are similar with a predominance of low amplitude and fast frequency oscillations, which represent high levels of asynchronous activity in the cortical neuronal populations (Ecker et al., 2010; Renart et al., 2010). Despite these similarities, major differences exist between wakefulness and REM sleep as muscle tone is strongly suppressed in the latter and only bursts of fast saccadic eye movements are expressed (Nir and Tononi, 2010). On the other hand, non-REM sleep and resting wakefulness are characterized by an EEG dominated by high amplitude, slow frequency activity (Steriade et al., 1993) and by the appearance of high amplitude events such as k-complexes (Roth et al., 1956) and sleep spindles (Steriade et al., 1986; De Gennaro and Ferrara, 2003). These events represent the rhythmic discharge of synchronized neuronal populations and tend to occur in preferred phases of the dominant slow wave oscillations (Siapas and Wilson, 1998; Clemens et al., 2007).

Because of their major role in generating and regulating sleep cycles (Scammell et al., 2017), the activity of different hypothalamic (see Saper et al., 2001) and brainstem nuclei (see Steriade and McCarley, 2013) has been extensively studied across the different behavioural states. Similarly, the interplay between thalamus, neocortex and hippocampus during sleep has also attracted considerable attention (e.g. Steriade et al., 1993; Urakami, 2008; Gardner et al., 2013; Latchoumane et al., 2017). However, our understanding of sleep-related neuronal dynamics in many other brain regions is currently lacking. Indeed, little is known about how cerebellar activity changes during sleep (see Canto et al., 2017 for a review). This is surprising given that cerebellar malfunction has been associated with changes in the wakefulness-sleep cycle (Cunchillos and De Andres, 1982) and with sleep disorders (DelRosso and Hoque, 2014). Furthermore, the cerebellum is known to participate in the acquisition of procedural memory (Molinari et al., 1997), a process which is modulated and enhanced by sleep (Stickgold, 2005). Moreover, the similarities on the overall brain activity between active wakefulness, when cerebellum has a major role in the control of voluntary movements, and REM sleep, characterized by the depressed muscle tone and the absence of voluntary movements, confer particular interest to the sleep related changes in the activity of this structure and its interaction with other brain regions.

Early studies in epileptic patients implanted with intra-cerebellar electrodes (Niedermeyer and Umematsu, 1974) and more recent work using non-invasive techniques (Kaufmann et al. (2006); Jahnke et al., 2012; Schabus et al., 2007) have shown state-dependent modulation of cerebellar activity during sleep in humans. During non-REM sleep, the cerebellum exhibited coordinated slow oscillations, which were preferentially

recorded in the vermis and fastigial nucleus (Niedermeyer and Umematsu, 1974; Dang-Vu et al., 2008), as well as correlated activity with neocortical K-complexes (Jahnke et al., 2012) and sleep spindles (Schabus et al., 2007). During REM, an increase in cerebellar activity was observed both in the vermis and the hemispheres (Braun, 1997), most likely reflecting increased activity in the mossy fibre-parallel fibre pathways. Similarly, single cell recording carried out in animal models also showed changes in firing rates and regularity of Purkinje cells in the cerebellar cortex and neurons from the deep cerebellar nuclei. During non-REM, no clear changes in the firing rates of these neurons were observed either in cats (Marchesi and Strata, 1970; Hobson and McCarley, 1972; McCarley and Hobson, 1972; Palmer, 1979) or monkeys (Mano, 1970). However, changes in the temporal organization of Purkinje cell simple spike firing was reported; with a reduced probability of short interspike intervals (McCarley and Hobson, 1972). Given the impact that the spatiotemporal organization of the Purkinje cell activity has on cerebellar function (see De Zeeuw et al., 2011), the observed changes may represent an important mechanism for cerebellar network activity modulation. In line with the observations in humans, during REM sleep, a significant increase in the firing rate of Purkinje cells was observed in the cerebellar cortex in cats (Marchesi and Strata, 1970; Hobson and McCarley, 1972) and monkeys (Mano, 1970). However, while in the cat both simple and complex spikes were up-regulated, in the monkey only simple spikes rate increased while it decreased for complex spikes. Interestingly, activity in the fastigial nuclei of cats, but not in the interpositus, also showed increased activity during REM with the appearance of rhythmic bursting activity which was unrelated to the eye movements (Palmer, 1970). Finally, the presence of phasic activity in the cerebellum of cats (Pellet et al., 1974; Pellet and Harlay, 1977) or rats (Marks et al., 1980), mainly during REM sleep epochs, has been associated with the transmission of ponto-geniculo-occipital waves (named p-waves in rodents) (Farber et al., 1980; Velluti et al., 1985).

P-waves are field potentials reflecting phasic high-frequency bursts in specific pontine nuclei (McCarley et al., 1978; Datta, 1997), which are then transmitted through an extended network, primarily including the thalamic lateral geniculate nuclei and the occipital cortex (Brooks and Bizzi, 1963; Sakai and Jouvet, 1980). They have been proposed to participate in the initiation and maintenance of REM sleep (Dement, 1973) and to have a role in higher-order functions associated to this state, such as memory and learning (Datta et al., 2004, 2005, 2008). Interestingly, in rats, direct projections from the P-waves generators to the hippocampus (Datta et al., 1998) seem to play a role in the regulation of theta frequency during REM (Karashima et al., 2007), which may subsequently effect the coordination of activity in the hippocampus and other regions activated by p-waves in order to favour synaptic plasticity (Nakao et al., 2007).

To date, no comprehensive study of the changes in the local field potentials (LFPs) from the cerebellum across different sleep states has been performed in mice. Similarly, no information about how the

cerebellum differentially engages with specific regions of the brain during different stages of sleep cycle is available. In this study, we investigated the dynamics of intrinsic cerebellar LFP activity and cerebello-hippocampal interactions 'offline' i.e. during sleep and found a characteristic infra-slow ( $<1\text{Hz}$ ) oscillatory profile as well as phasic activity in the cerebellar cortex during REM sleep. The phasic events were identified as putative pontine waves and were found to be phase locked to the infra-slow oscillations. Similarly, an increase in the level of theta coherence between the cerebellar Crus I region and the hippocampus was observed preferentially at the same phases of the infra-slow oscillations during which the phasic events occur pointing to a role in coordinating long-range functional networks during REM. Finally, we also found evoked activity in the cerebellum triggered by hippocampal sharp-waves ripples suggesting the existence of functional connectivity from the hippocampus to the cerebellum.

## **Results:**

### Infra-slow ( $< 1\text{Hz}$ ) oscillations are a signature of REM sleep in the cerebellum

We first recorded spontaneous LFPs from the hippocampus vermis of the anterior lobules II/III and the posterior lobule VI and in the hemispherical Crus I in freely behaving mice staying in their home-cages ( $n = 5$ ). Based on the animal speed, EMG amplitude and the activity in the hippocampus, we divided the recordings in periods of active wakefulness (awake), non-REM and REM sleep (Figure 1A, top plot; see material and methods). A visual inspection of the raw signals revealed clear differences in the patterns of activity across different states both in the hippocampus and in the cerebellar recordings, which indeed showed opposite profiles (Figure 1A). The hippocampus showed powerful but low amplitude theta activity (6-12 Hz) during awake and REM sleep and high amplitude slow oscillations in the delta range (1-4 Hz) during non-REM sleep. Conversely, in the cerebellum, high amplitude activity was observed during awake and mainly during REM sleep epochs. Indeed, the appearance of high amplitude infra-slow waves ( $< 1\text{ Hz}$ ) highly synchronized across all the cerebellar recordings was characteristic of this state (Figure 1B-C). During awake periods, infra-slow oscillations were also present but their amplitude was lower, individual cycles were hardly identified in the raw signal and they were less coordinated across cerebellar recordings (Figure 1B-C). During non-REM sleep, delta oscillations (1-4 Hz) were also observed in the cerebellum (Figure 1B-C). While in the example shown in Figure 1 they appeared to be stronger in the lobule VI, the average spectrogram showed no clear differences across regions. Another difference between awake and sleep in the cerebellar activity was found in the high frequency domain. During awake, prominent high gamma oscillations (100-160 Hz) were clearly observed in the cerebellar power spectra (Figure 1C), however, activity in this band was reduced during sleep and a prominent higher frequency oscillation with a peak at  $\sim 250\text{ Hz}$  appeared. This activity was present in both non-REM and REM sleep. However, the peak in the spectrogram was sharper and more pronounced during REM.

In summary, clear modulation of the cerebellar LFP is observed across natural sleep states in mice. In particular, during REM we have identified the appearance of high amplitude, infra-slow waves (<1 Hz), which found in all recording sites sampled in this study. These include vermal regions in the anterior and posterior cerebellum as well as the hemispheres, thus suggesting a large-scale, wide synchronization of all the cerebellar cortex during REM.

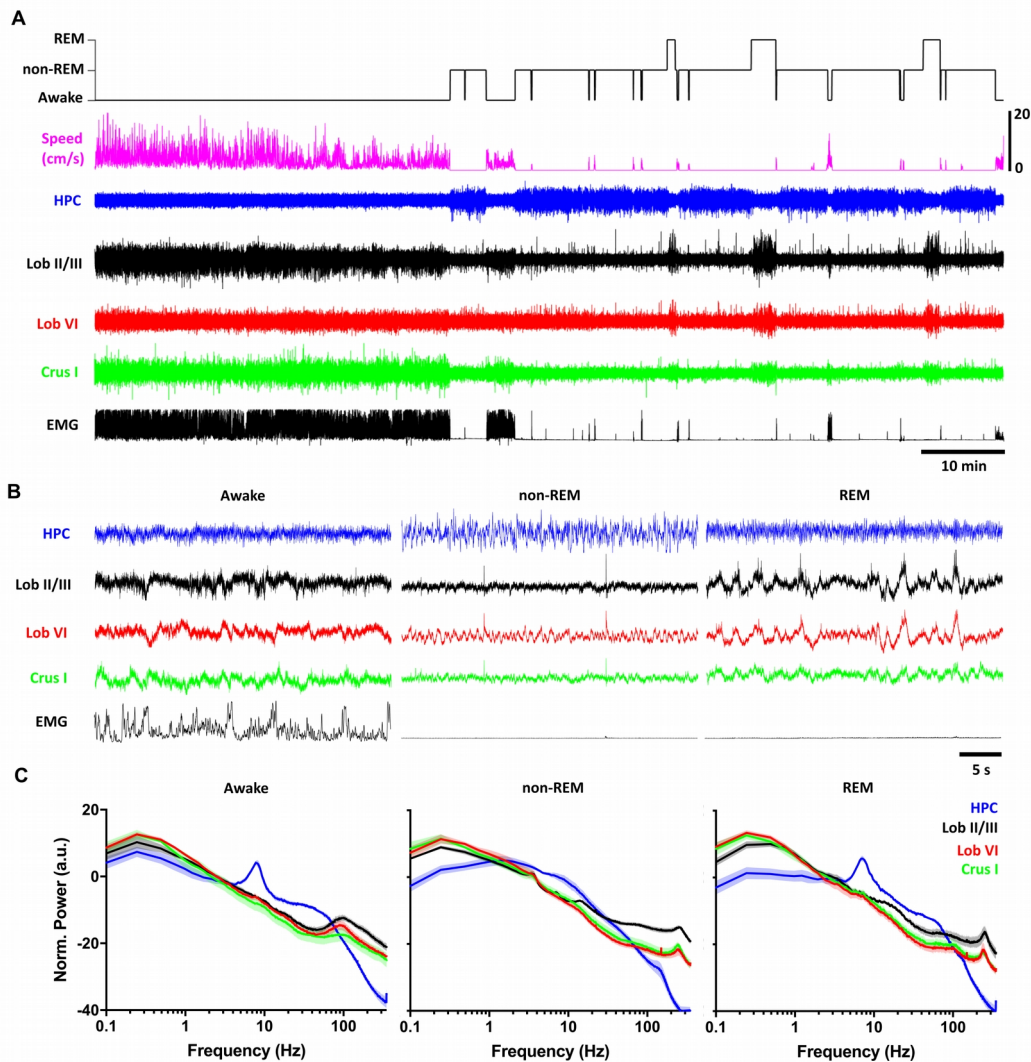


**Figure 1. The cerebellar cortical LFPs present sleep-state specific patterns of activity.** **A)** We recorded the LFPs from the hippocampus (HPC) and the cerebellar cortex in the Crus I, lobule VI (Lob VI) and lobules II/III (Lob II/III) in mice staying in their homecages for long periods during which they exhibited different behavioural states which we catalogued as awake, non-REM and REM sleep. In order to discriminate between these states we measured the instantaneous speed of the animals as well as the neck electromyogram (EMG). The hippocampal LFP presented high amplitude activity during non-REM sleep while in the cerebellum, the maximal amplitude was observed during awake and specially during REM sleep. **B)** A higher magnification of the activity patterns during awake, non-REM and REM sleep revealed that the high amplitude activity observed during non-REM sleep in the hippocampus was associated with slow phasic oscillations. In the cerebellum, the high amplitude activity observed during REM is related to infra-slow oscillations (< 1 Hz) which were coherently observed in all the cerebellar recordings. During awake, slow

oscillations were also observed but they were less organized and coherent across cerebellar regions. **C)** We computed the normalized power spectra for each of the behavioural states. During awake, a clear peak in theta coherence was observed in the hippocampus while in the cerebellum the dominant activity was found in the high gamma band between 100-160 Hz. During sleep, both non-REM and REM, the high frequency peak was sifted toward higher frequencies peaking at 250 Hz. During non-REM, the hippocampus exhibited an increased in the delta range (1-4 Hz) while the cerebellum presented activity in both the infra-slow and delta frequencies. During REM, the hippocampus presented again a clear peak in theta range while the cerebellum was dominated by the infra-slow oscillations.

#### Phasic events in the cerebellum are phase locked to the infra-slow cerebellar oscillations and to the hippocampal theta during REM

During sleep, we noticed the presence of phasic sharp potentials (PEs) in the cerebellar recordings (Figure 2A). They were observed in all the cerebellar recordings at similar times; however, the amplitude and waveform were variable between them and across animals. However, the average waveforms presented very similar profiles (Figure 2B) and thus waveform differences were likely due to the positioning of electrodes relative to signal sinks and sources in the cerebellum. Thus, for further analysis, in each individual we have selected the cerebellar region which captured the maximal amplitude of the PEs. They appeared sparsely during non-REM sleep (Figure 1B, central panel), however, they were mostly concentrated around the REM sleep epochs, when they often appeared in clusters (Figure 1B, right panel; Figure 2A). This was clearly observed in the normalized autocorrelograms of the detected PEs in non-REM and REM sleep which showed that the probability of finding two PEs closely in time is much higher during the later (Figure 2C). Moreover, the PEs during REM seemed to occur more often during the upright phase of the infra-slow oscillations (Figure 2A). This was confirmed by computing the distribution of occurrence of the PEs by the phase of these oscillations that were robustly and significantly different than the random distribution in all the individuals (Figure 2D, in red; all the individual p-values of Rayleigh test < 0.001). We found a mean preferred angle of  $350.6 \pm 2.248$  degrees, corresponding to the ascending phase near the peak of the oscillations. Given that the hippocampal activity exhibits strong theta activity during REM (Figure 1B-C; Figure 2A), we wondered if the PEs recorded in the cerebellum were also phase locked to the hippocampal theta phase. We thus first calculated the averaged triggered waveform in the hippocampus centred on the peak of the recorded PEs. This analysis showed that the PEs occurred at a consistent phase of the theta cycle, near the trough of the oscillations (Figure 2E). This was further confirmed by the significant phase-locking that was found when computing the distribution of cerebellar PEs by the phase of the hippocampal theta oscillations (Figure 2D, in blue) which revealed that the preferred phase locking angle was  $147.4 \pm 15.93$  degrees.

## Hippocampal theta frequency is modulated by cerebellar infra-slow oscillations during REM

We next investigated the potential interaction between the cerebellar infra-slow waves and the hippocampal theta rhythm. Therefore, we identified individual cycles of the cerebellar slow waves and computed the triggered spectrogram of the hippocampal activity centred at their peaks (Figure 2F). In order to avoid the potential distorting effect of different durations of the cycles, we constructed the spectrograms by phase of the slow waves rather than time. We found that the theta frequency of the hippocampus was modulated by the phase of the cerebellar infra-slow oscillations, with an increase of the rhythm, which was maximal at the peak of the cerebellar slow wave cycle (Figure 2F, preferred frequency in white). Given that

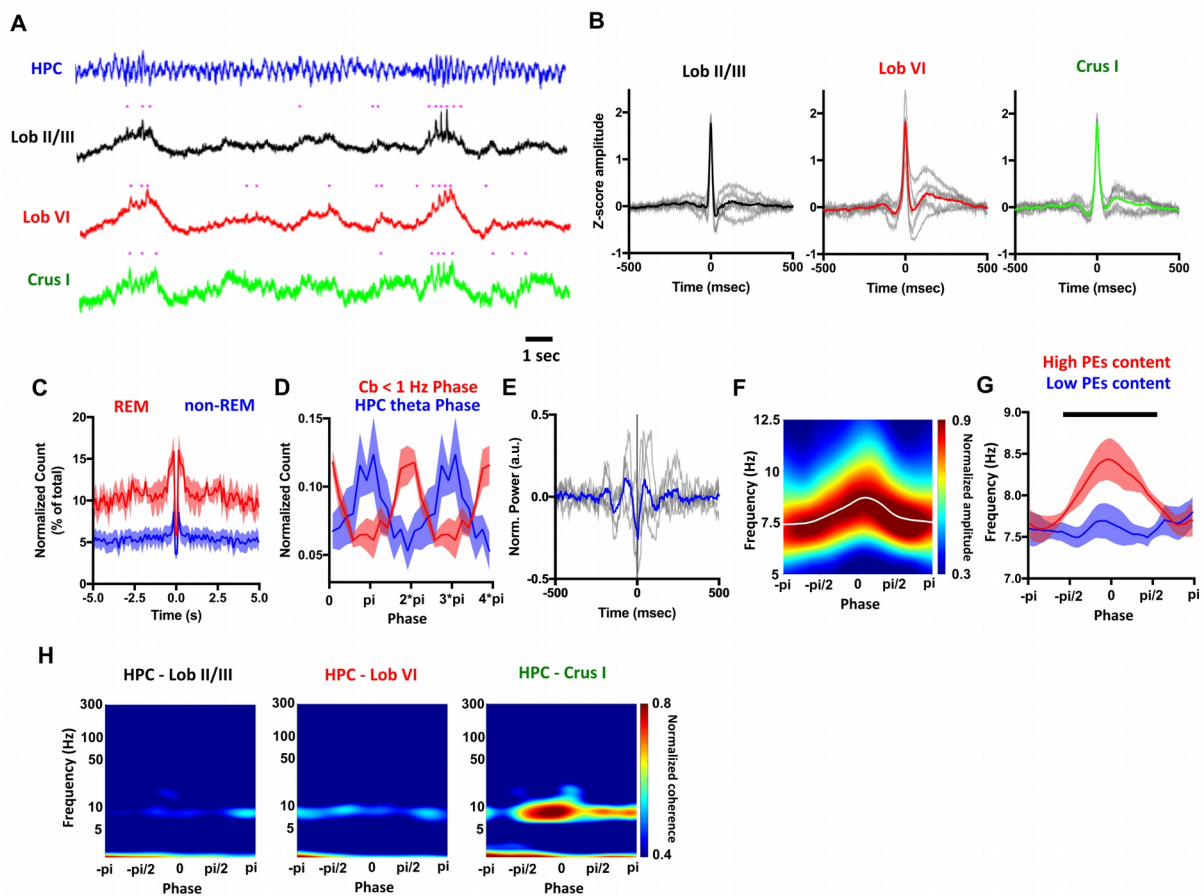


**Figure 2. Phasic events (PEs) occurred at preferred phases of the cerebellar infra-slow (< 1 Hz) oscillations during REM.** **A)** During REM, we also observed phasic potentials appearing in the cerebellar LFP recordings (purple points). We notice that they seemed to occur preferentially during the up-phases of the infra-slow oscillations. Moreover, in the hippocampus, a transient acceleration of the theta oscillations was apparent also during the up-phases of these oscillations. **B)** The PEs were recorded in all the individuals in all the cerebellar sites with similar waveform profiles. In light grey are the averaged waveforms from each of the 5 mouse while the thick coloured lines represent the mean across mice. **C)** The PEs were concentrated in the REM epochs when they also tended to appeared in clusters. These observations were confirmed in the autocorrelograms of REM and non-REM epochs. **D)** The normalized count of the PEs relative to the phase of the infra-slow oscillation revealed a robust and significant phase-locking (all the individuals had p-values < 0.001 in the Rayleigh test) with a preferred phase near the positive peak of the oscillations (mean preferred angle of

350.6 ± 2.248 degrees). They were also phase locked to the hippocampal theta phase but the preferred angle corresponded to the trough of the oscillations (mean preferred angle of 147.4 ± 15.93 degrees). **E)** The averaged PEs-triggered waveform from the hippocampal activity confirmed that these events are coordinated with the theta rhythm and preferentially occur at the trough of the cycle. **F)** We identify each infra-slow wave in the cerebellar cortex and obtained its instantaneous phase using the Hilbert transform. We then computed the averaged triggered spectrogram relative to the phase of the slow oscillation. We found a modulation of the hippocampal theta frequency by the phase of the infra-slow oscillation which was reflected as an acceleration peaking at the up-phase of the cerebellar activity. **G)** We separated the individual infra-slow waves in two groups depending on their density of PEs (high PEs content if more than two and low PEs content if two or less). We found that only the infra-slow waves with high PEs content modulated the hippocampal theta frequency. **H)** We calculated the triggered coherogram between the hippocampal and the cerebellar signals relative to the phase of the infra-slow oscillations and we found an increase in the theta coherence between Crus I and HPC which was maximal at phases near the peak of the cycle.

this was aligned with the preferred phase of occurrence of the PEs, which are phase-locked to the hippocampal theta (Figure 2D), we wondered whether the strength of the modulation was correlated with the presence and number of PEs occurring during the infra-slow wave. To test this hypothesis, we separated cycles with low PE content ( $\leq 2$ ; blue in Figure 2G) and those with a higher PE content ( $> 2$ ; red in Figure 2G). We found that the modulation of hippocampal theta occurred only when the oscillations occurred in the presence of many PEs (PE quantity x cerebellar <1 Hz phase repeated measures two-way ANOVA, quantity of PE effect,  $F(1,4) = 43.94$ ,  $p = 0.0027$ ; interaction effect  $F(47,188) = 4.678$ ,  $p\text{-value} < 0.0001$ ), suggesting that they are responsible for the observed increases in hippocampal oscillation frequency.

#### Hippocampal-cerebellar coherence is enhanced during the ascending phase of the cerebellar infra-slow oscillations during REM

We have recently reported that the cerebellum dynamically interacts with the hippocampus during different behavioural paradigms potentially through theta-band LFP coherence (Watson et al., 2019). We wondered if such interaction is also present during REM sleep and, if so, whether it was also modulated by the infra-slow cerebellar oscillations. Thus, we computed the triggered wavelet coherence between the hippocampus and each of the cerebellar recording sites centred on the peak of the infra-slow waves (Figure 2H). First, we have found that coherence in the theta band between the cerebellum and the hippocampus is also present during REM sleep. Secondly, the levels of theta coherence were significantly modulated by the phase of the infra-slow oscillations and this modulation was different across combinations (phase x cerebello-hippocampal combination repeated measures two-way ANOVA, phase effect  $F(39,156) = 1.564$ ,  $p = 0.0294$ ; interaction effect  $F(78, 312) = 1.505$ ,  $p = 0.0081$ ). Finally, a post-hoc multiple comparisons test confirmed that the level of coherence between the hippocampus and Crus I regions was modulated by the phase and it was enhanced in the ascending part of the slow-wave cycle, reaching significantly higher levels than the hippocampus-lobule II and the hippocampus-lobule VI recording combinations (False-discovery rate corrected  $p\text{-values} < 0.01$  for all comparisons between 296.50 and 26.25 degrees). Thus, our results suggest

an enhancement of the cerebello-hippocampal coordination, as indicated by theta coherence, specifically involving the Crus I. Furthermore, we reveal that the hippocampus – Crus I theta coherence increase is coincident with the maximal probability of appearance of phasic events in the cerebellum and with the acceleration of the hippocampal theta frequency.

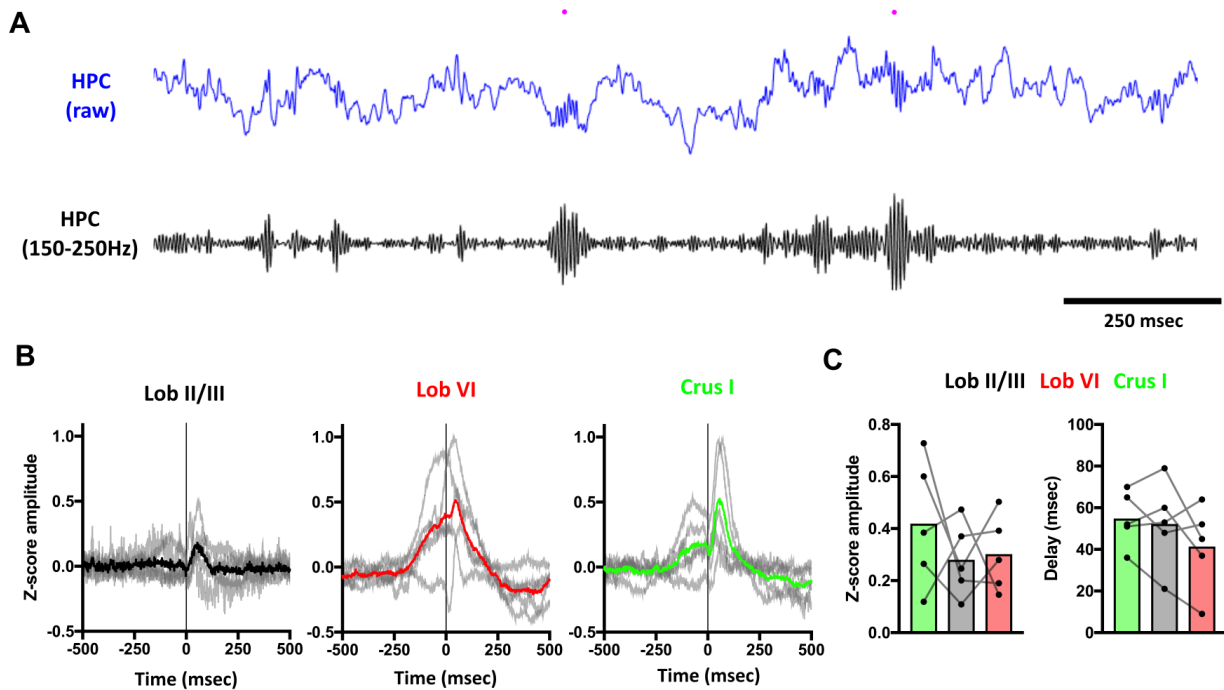


**Figure 3. Hippocampal sharp-waves ripples (SWR) triggered evoked activity in the cerebellum. A)** Example of the raw (blue) and filtered (150-250 Hz, black) hippocampal LFP during non-REM sleep. SWR were identified (purple dots) at the maximal value in the filtered signal. **B)** Averaged SWR-triggered waveforms from the cerebellar recordings. The zero represent the detected peak in the filtered signal. The light grey lines represent the mean for each individual and the solid coloured lines are the mean of all mice. Evoked field potentials were observed in all the cerebellar recordings. The averaged waveforms in lobule VI and Crus I revealed that the SWR occurred at the peak of cerebellar slow oscillations. **C)** We quantified the normalized amplitude of the responses measured as the onset-to-peak value as well as the latency of the onset of the evoked response. No significant differences between cerebellar recordings were observed for either of them.

### Hippocampal ripples triggered evoked potentials in the cerebellum

We have shown that during REM, the most dominant cerebellar LFP activity is coordinated with the most prominent hippocampal LFP activity (theta). However, during non-REM sleep, the hippocampal activity is characterized by the presence of sharp-waves ripples (SWR). Therefore, we next asked if cerebellar activity also correlates with hippocampal ripples during non-REM sleep? To address this question we first detected SWRs (Figure 3A) and then computed the cerebellar LFP triggered on SWR maximal amplitude (Figure 3B). Event related field potentials (ERPs) were clearly observed at all the cerebellar regions in most of the

individuals. The peak of these evoked potentials occurred at a mean latency of  $49.47 \pm 4.73$  msec following the SWR maximal amplitude. This value was lower when measuring the evoked wave onset rather than the peak ( $9.17 \pm 1.89$  msec). No statistical difference across cerebellar regions was observed in the amplitude of the ERP, measured as the onset-to-peak amplitude of the fields (Figure 3C, left panel; z-score amplitude in Crus I =  $0.419 \pm 0.110$ , lobule II/III =  $0.280 \pm 0.064$  and lobule VI =  $0.302 \pm 0.065$ ; repeated measurement one-way ANOVA,  $F(1.743, 6.971) = 0.6988$ , p-value = 0.51) most likely due to the large variability exhibited in the responses. Similarly, no differences were obtained for the latency either (Figure 3C, right panel; latency of the peak in Crus I =  $54.8 \pm 6.0$  msec; lobule II/III =  $52.2 \pm 9.4$  msec and lobule VI =  $41.4 \pm 9.2$  msec; repeated measurement one-way ANOVA,  $F(1.687, 6.748) = 1.999$ , p-value = 0.2079). Thus, we have recorded even-related-activity in the cerebellar cortex following the occurrence of hippocampal ripples during non-REM sleep.

Moreover, we noticed one major difference between the triggered activity observed in the different cerebellar locations. In lobule VI and Crus I, the average SWR-triggered waveforms revealed that the ERPs occurred on top of a slow wave oscillation while in the lobule II/III no clear oscillatory component was observed. These slow waves were more consistently recorded in the lobule VI (4 out of the 5 mice; Figure 3B, the light grey lines represent the SWR-triggered average for each individual).

## **Discussion**

To our knowledge, this is the first detailed description of the cerebellar cortex LFP activity in mice during natural sleep. We have found clear modulation of this activity by the sleep state and we have report for the first time the presence of infra-slow (<1Hz) oscillations in the cerebellar cortex during REM sleep. Moreover, we have found that the presence of putative pontine-waves (P-waves) in the cerebellar recordings is phase locked to this oscillations and that an increase in the theta coherence between the Crus I and the hippocampus is observed preferentially at the similar phases as the P-waves. This may subserve a mechanism for functional interaction during REM which may favour plasticity mechanisms in the circuit. Finally, we have also reported the presence of event related field potentials in the cerebellum following sharp-wave ripples (SWR) triggered in the hippocampus during non-REM sleep. Furthermore they occurred at specific phases of the slow oscillations in the cerebellum. This may be indicative of functional pathways between the hippocampus and the cerebellum.

Sleep-related changes in cerebellar activity have been already observed in humans (e.g., Niedermeyer and Umematsu, 1974; Kaufmann et al. (2006); Jahnke et al., 2012; Schabus et al., 2007), cats (e.g., Marchesi and Strata, 1970; Hobson and McCarley, 1972; McCarley and Hobson, 1972; Palmer, 1979), monkeys (Mano, 1970) and rats (Farber et al., 1980; Marks et al., 1980). However, these studies were focussed on recording cellular activity in restricted regions of the cerebellar cortex or the deep cerebellar nuclei and little

information is available regarding distributed cerebellar network activity across sleep states. Here we have recorded cerebellar cortex LFP in mice during natural sleep.

Cerebellar activity during active wakefulness is dominated by low amplitude high frequency oscillations in the high gamma band (100-160 Hz, peaking at approximately 120 Hz) embedded in high amplitude slow oscillations. High frequency activity (>150 Hz) has been described in the cerebellar cortex of cerebellar mutant mice (Cheron et al., 2004) and a mouse model for Angelman syndrome (Cheron et al., 2005) and is thought to be generated by Purkinje cell activity. Recently, its presence and its local origin have been confirmed in awake rats (de Solages et al., 2008). De Solages et al (2008) reported spectral peaks of around 250Hz during wakefulness in head fixed rats. This frequency is higher than what we observed during wake in freely moving mice but is similar to what we observed during sleep states, both in non-REM and REM (Figure 1). Thus, differences in observed oscillatory frequency may be related to the effect of movement restriction. These oscillations were sharper and more prominent during REM periods. However, the most distinctive cerebellar activity during REM sleep were the high amplitude infra-slow oscillations (<1 Hz). Slow activity around 1 Hz in the cerebellar cortex has been previously reported in anaesthetised rats (Ros et al., 2009; Rowland et al., 2010). They demonstrated that this activity is locally generated through cerebellar network dynamics but depends on the entrainment of neocortical slow waves. However, the neocortical slow oscillations are typical hallmarks of non-REM sleep (Steriade et al., 2001) and the cerebellar infra-slow waves that we describe here were characteristic of REM epochs. Therefore, we cannot assume that the infra-slow activity we observed are homologous to those described by Ros and colleagues, although they may share common local network mechanisms.

Another characteristic feature that we have observed in the cerebellum during sleep is the presence of phasic sharp potentials. They were disparately distributed during non-REM sleep and mostly concentrated during REM epochs. Phasic activity in the cerebellum of cats (Pellet et al., 1974; Pellet and Harlay, 1977) and rats (Marks et al., 1980) has been identified as propagated ponto-geniculate-occipital waves (P-waves; Farber et al., 1980; Velluti et al., 1985). P-waves have been found to follow the same distribution that we have observed for the phasic events, that is, mainly concentrated in REM epochs (Pellet et al., 1974; Pellet and Harlay, 1977; Marks et al., 1980). Indeed, they are considered as an electrophysiological signature of REM sleep. Secondly, Karashima and colleagues demonstrated that P-waves are phase-locked to the hippocampal theta rhythm during REM and modulate its frequency provoking an acceleration of the oscillatory cycles in cats (Karashima et al., 2002) and rats (Karashima et al., 2007). We too have found that the cerebellar phasic events are phase-locked to the hippocampal theta rhythm. Similarly, we also report here an acceleration of the hippocampal theta frequency that was modulated by the cerebellar infra-slow oscillations only when those had a high content of phasic events (>2 in a cycle). Thus, it is likely that the acceleration is related to these events themselves. The observed modulation of the hippocampal theta

frequency by the phase of the cerebellar infra-slow oscillations may be then provoked by the strong and robust phase-locking of the phasic events to these rhythm. Thus, the most parsimonious explanation is that the phasic events we observed in the cerebellum are propagated p-waves.

The phase locking of these putative P-waves to the cerebellar oscillations seems to favour the coincidence of epochs of high frequency theta in the hippocampus with the up phase of the infra-slow oscillations in the cerebellum. During the infra-slow oscillations recorded by Ros and colleagues and described above (Ros et al., 2009), high local excitability and synchronicity in the cerebellar network was observed during the up phases of the slow rhythms, as reflected by an increase of the multiunit activity mainly in the granule cell layer.

Assuming that the infra-slow activity that we have reported here during REM sleep share the same underlying mechanisms, this would infer that the epochs of hippocampal high frequency theta oscillation occur during periods of high cerebellar network excitability thus favouring the coordination of cerebellar and hippocampal activity during REM sleep. Indeed, the role of the P-waves in coordinating long-range network dynamics which may underlie sleep-dependent cognitive processes, including learning and memory, has been already investigated (Datta et al., 1998; Datta, 2000; Datta and O'Malley, 2013). They have demonstrated that the consolidation associated with REM sleep, at least in fear memory, depends on the presence and density of P-waves (Datta, 2000; Datta et al., 2004; Datta and O'Malley, 2013). Moreover, they showed that the mechanism underlying the p-wave-dependent consolidation of fear memory involves the expression of plasticity-related genes and proteins in the hippocampus, amygdala and hypothalamus (Saha and Datta, 2005; Datta et al., 2008, 2009). On the other hand, hippocampal-amygdala sleep-dependent theta activity synchronization during REM has been also identified as a mechanisms for fear memory consolidation (Totty et al., 2017). All together, these results support a main role of P-waves in coordinating distributed networks during REM mainly through synchronization of theta oscillations, which favour the induction of plasticity mechanisms. Our finding of enhanced theta coherence between the hippocampus and the cerebellar Crus I region specifically during the phases of the infra-slow wave cycles when the putative P-waves are concentrated suggests that a similar mechanism also applies for the cerebello-hippocampal network as we have previously described (Watson et al., 2019). Indeed, anatomical substrates which could support such functional interaction have been already described. The P-waves are generated in the pontine nuclei and they reach the cerebellum through the mossy fibres (Datta et al., 1998). Similarly, there are direct projections from the P-wave generators to the hippocampus, as well as a potential indirect pathway through the septum (Datta et al., 1998). Furthermore, we have recently shown that topographically restricted regions of the cerebellum project to the hippocampus through multiple di- and tri-synaptic pathways potentially involving the septum in mice (Watson et al., 2019) thus providing the neuronal architecture required for closed loop, bi-directional cerebello-hippocampal interactions.

We also report here that the sharp waves ripples (SWR) generated in the hippocampus during non-REM sleep induced event related potentials in the cerebellar cortex. Moreover, the SWR seemed to occur preferentially at the peak of slow-waves recorded in the cerebellum, mainly in the lobule VI. SWR are fast oscillations during which both CA3 and CA1 pyramidal cells fire synchronously (Buzsaki, 1986, Csicsvari et al., 2000). They are known to be coordinated with cortical spindles, which are themselves coordinated with the cortical slow oscillations (Siapas and Wilson, 1998) and this triple phase-locking is important for memory formation (Maingret et al., 2016; Latchoumane et al., 2017). Taken together, the SWR-triggered evoked potentials recorded in the cerebellar cortex and their coordination with the cerebellar slow oscillations clearly suggest the existence of functionally relevant pathways from the hippocampus to the cerebellum and their potential role in sleep-dependent memory processes during non-REM epochs. The cerebellar evoked activity had a short onset latency of  $\sim 9.17$  msec, which is in agreement with previous reports of di-synaptic cerebro-ponto-cerebellar pathways (e.g. Allen and Tsukahara, 1974; Proville et al., 2014) and thus, we propose that hippocampus-ponto-cerebellar connections underlie this interaction.

To summarize, we have revealed a novel infra-slow ( $< 1$  Hz) oscillatory activity in the cerebellum during REM sleep which is coordinated with the occurrence of putative pontine waves and a subsequent modulation of the hippocampal theta frequency. We have shown that this coordination may support enhanced coordination of the oscillatory activity in the theta range between the cerebellar Crus I region and the hippocampus. Such enhanced synchrony may subserve plasticity mechanisms in the cerebello-hippocampal circuit. Finally, we have also observed event related activity in the cerebellum following the occurrence of sharp-wave ripples in the hippocampus suggesting the existence of functional connectivity from the hippocampus to the cerebellum. In overall, our findings suggest that the cerebello-hippocampal network undergoes sleep-state related modulation emphasizing its functional relevance.

## **Material and Methods:**

### Mice

5 adult male C57BL6-J mice were used for this study (Janvier, France). Mice were housed individually under a 12 hr light/12 hr dark cycle (light cycle beginning at 8 am) and received food and water *ad libitum*. All behavioural experiments were performed in accordance with the official European guidelines for the care and use of laboratory animals (86/609/EEC) and in accordance with the Policies of the French Committee of Ethics (Decrees n° 87-848 and n° 2001-424). The animal housing facility of the laboratory where experiments were made is fully accredited by the French Direction of Veterinary Services (B-75-05-24, 18 May 2010). Surgeries and experiments were authorized by the French Direction of Veterinary Services (authorization number: 75-752).

## Surgery

Surgical and implant procedures have been already described in Watson et al., 2019. Briefly, surgical implantation was performed under constant isoflurane anaesthesia (1.5 %) combined with oxygen (1.5 L/min). Animals were placed in a stereotaxic frame device (David Kopf Instruments, USA) and an incision was performed in order to expose the scalp. Coordinates for implantation were calculated from bregma following the references given in Franklin and Paxinos, 2007. We targeted bilateral hippocampi (AP -2.2 mm, ML  $\pm$  2.0 mm, DV 1.0 mm), cerebellar lobule II/III (AP -5.52 mm, ML 0 mm, DV 1.8 mm), cerebellar lobule VI (AP -6.72 mm, ML 0 mm, DV 0.1 mm) and left cerebellar Crus I (AP -6.24 mm, ML 2.5 mm, DV 0.1 mm). Small craniotomies were performed over the targetted regions using a drill and the dura was carefully remove with a needle. Two wires of 140  $\mu$ m diameter teflon coated stainless-steel (A-M system, USA) were twisted together to create bipolar LFP recording electrodes (interpolar distance  $\sim$ 0.5 mm) and were implanted in the brain. Pairs of flexible stainless-steel wires were also sutured to the neck muscles to obtain EMG recordings (Cooner wire, USA). 3 mice were also implanted with bipolar stimulation electrodes (same as the LFP electrodes but with interpolar distance of  $\sim$ 140  $\mu$ m) in the left medial forebrain bundle (AP -1.4 mm, ML 1.2 mm, DV 4.8 mm) to serve as a reward signal in a set of experiments already published (Watson et al., 2019). All electrodes were attached to an electrode interface board (EIB-18, Neuralynx, USA) and the assembly was fixed to the skull using a combination of UV activated cement (SpeedCem, Henry Shein, UK), SuperBond (SunMedical, Japan) and dental cement (Simplex Rapid, Kemdent, UK). Four miniature screws (Antrin, USA) were also attached to the skull for additional support and to serve as recording ground. Animals were given a minimum of 5 days post-surgery recovery time before experiments commenced.

## Electrophysiological recordings

The EEGs, EMGs and LFP recordings were obtained via a unity-gain headstage preamplifier (HS-18) and a Digital Lynx SX system and Cheetah software (Neuralynx, USA). Signals were bandpass-filtered between 0.1 and 600 Hz and sampled at 1 kHz. Mouse position was tracked at 30 Hz using video tracker software and infra-red LEDs attached to the headstage (Neuralynx, USA).

## Histology

After completion of the experiments, mice were deeply anaesthetized with ketamine/xylazine solution (150 mg/Kg) and electrolytic lesions were created by passing a positive current through the electrodes (30  $\mu$ A, 10 s). The animals were then perfused transcardially with saline (0.9 %) followed by paraformaldehyde (4%). Once perfused, the electrode assemble was carefully removed, the brain extracted and post-fixed in paraformaldehyde (4%) for 24 hr and then embedded in agarose (3%). 50  $\mu$ m sagittal and coronal sections for the cerebellum and the hippocampus, respectively, were made using a vibratome. The sections were

mounted on gelatinized slides and stained with cresyl violet. The electrolytic lesions were then identified in order to reconstruct the recording locations using standard maps with reference to a stereotaxic atlas (Franklin and Paxinos, 2007).

### Behaviour and sleep scoring

The animals were recorded during the day (between 10 am and 6 pm) in their own home-cages (30 cm x 10 cm x 10 cm plastic box), with the lid removed and with the lights off for periods up to 4 hr. Animals exhibited different behavioural states that were scored off-line and included in four categories: active wakefulness, resting, non-REM sleep and REM sleep. The scoring was semi-automatically performed using multi-parameter thresholds based upon instantaneous speed, neck EMG (rectified, smoothed with 1 s window and z-scored) and theta/delta ratio in the hippocampal LFP (z-scored and calculated in 100 ms bins). Thus, epochs of more than 4 s with instantaneous speed above 3 cm/s were considered as active wakefulness, periods of less than 30 s where the speed stayed below 3 cm/s and were surrounded by active wakefulness epochs were considered as rest. Similarly, when the EMG recording was optimal, a manually selected threshold was also used to discriminate between rest and sleep epochs. We finally used manual thresholding in the theta/delta ratio to separate non-REM and REM sleep epochs. Only epochs of more than four seconds were selected for further analysis.

### Data preprocessing

All the data processing was performed in custom-made MATLAB scripts (Mathworks, USA). Raw signals were preprocessed by applying a notch filter to remove electrical line noise (filter centered to 50 Hz). Values were z-scored in order to reduce overall differences in amplitude in the signal recorded from different electrodes.

### Offline detection of ripples, slow oscillations and phasic events

Discrete sharp-waves ripples (SPW-r) were detected using criteria employed elsewhere (Maingret et al., 2016). The raw signal was then filtered using a zero-phase bandpass second order filter between 150-250 Hz, squared, smoothed (using xx running average) and z-scored. The SPW-r were defined as events in which the transformed signal remained above 2 z-scores for 30 to 100 ms with a peak above 5 z-scores.

The slow oscillations in the cerebellum were divided in individual cycles which were identified as follows: first the raw signal was filtered using a zero-phase bandpass second order filter between 0-1-Hz. The instantaneous phase was obtained by applying the Hilbert transform to the filtered signal. Each cycle was defined by the epoch between two negative peaks on the cosine of the instantaneous phase. Only cycles

which lasted between 750 ms and 3 s and presented amplitudes in the upper third of the amplitude distribution were further analysed.

For the detection of the phasic events (putative p-waves) in the cerebellum, we first filtered the signal using a zero-phase bandpass second order filter between 5-35 Hz, squared it and calculated the z-score of the ensemble of sleep epochs. A double threshold strategy was then applied to the transformed signal so that epochs separated for at least 50 ms with values above 1 z-score and a peak above 3 z-scores were considered as events.

### Spectral analysis

All the spectral analysis were performed employing fully-available toolboxes. For computing the overall spectral power and spectral coherence across sleep-states, a multi-taper Fourier analysis (Chronux toolbox) was computed with 4 s sliding windows in 1 s steps and using  $x$  tapers. The mean power spectrum and coherence was obtained for each behavioural state by averaging the spectrogram and coherogram from the identified epochs. In order to reduce the impact of the different durations for each state, we split the epochs to match with the minimal duration and then we averaged them. For computing the triggered spectrogram and coherograms we used the continuous wavelet transform and the wavelet coherence from the wavelet toolbox of MATLAB. We employed analytic Morse wavelets with 8 octaves with 48 voices per octave.

### Phase locking of the phasic events and slow-wave triggered spectrogram and coherogram

The cerebellar signals and hippocampal signals were filtered using a zero-phase bandpass second order filter between 0.1-1Hz and 6-12Hz, respectively. The instantaneous phase of the cerebellar infra-slow oscillations and the hippocampal theta oscillations were obtained then applying Hilbert transformed to the filtered signals. The phase locking of the detected cerebellar phasic events to these rhythms were tested using circular statistics toolbox and the significance was determined for Rayleigh test  $p$ -value  $< 0.05$ .

For computing the cerebellar slow-wave triggered spectrogram and coherogram, for each cerebellar slow-wave, the time-frequency series obtained as explained before was matched with the correspondent instantaneous phase of the cerebellar  $< 1$  Hz oscillations and then averaged by phase bins of  $xx$  degrees.

### Statistical analysis

Statistical analysis were conducted using MATLAB Statistical Toolbox and Prism (Graphpad, USA). Normality was assessed using a Shapiro-Wilk test. Parametric and non-parametric test were then used accordingly. Paired analysis were employed when possible.

## References:

- Allen, G. I., & Tsukahara, N. (1974). Cerebrocerebellar communication systems.. *Physiological Reviews*, 54(4), 957–1006. <https://doi.org/10.1152/physrev.1974.54.4.957>
- Braun, A. (1997). Regional cerebral blood flow throughout the sleep-wake cycle. An H2(15)O PET study. *Brain*, 120(7), 1173–1197. <https://doi.org/10.1093/brain/120.7.1173>
- Brooks, D. C., & Bizzi, E. (1963). Brain stem electrical activity during deep sleep. *Archives italiennes de biologie*, 101, 648–65.
- Brown, R. E., Basheer, R., McKenna, J. T., Strecker, R. E., & McCarley, R. W. (2012). Control of Sleep and Wakefulness. *Physiological Reviews*, 92(3), 1087–1187. <https://doi.org/10.1152/physrev.00032.2011>
- Buzsáki, G. (1986). Hippocampal sharp waves: Their origin and significance. *Brain Research*, 398(2), 242–252. [https://doi.org/10.1016/0006-8993\(86\)91483-6](https://doi.org/10.1016/0006-8993(86)91483-6)
- Buzsáki, G. (2006). *Rhythms of the brain*. Oxford, United Kingdom: Oxford University Press.
- Canto, C. B., Onuki, Y., Bruinsma, B., Van der Werf, Y. D., & De Zeeuw, C. I. (2017). The Sleeping Cerebellum. *Trends in Neurosciences*, 40(5), 309–323. <https://doi.org/10.1016/j.tins.2017.03.001>
- Cheron, G. (2004). Inactivation of Calcium-Binding Protein Genes Induces 160 Hz Oscillations in the Cerebellar Cortex of Alert Mice. *Journal of Neuroscience*, 24(2), 434–441. <https://doi.org/10.1523/jneurosci.3197-03.2004>
- Cheron, G., Servais, L., Wagstaff, J., & Dan, B. (2005). Fast cerebellar oscillation associated with ataxia in a mouse model of angelman syndrome. *Neuroscience*, 130(3), 631–637. <https://doi.org/10.1016/j.neuroscience.2004.09.013>
- Clemens, Z., Molle, M., Eross, L., Barsi, P., Halasz, P., & Born, J. (2007). Temporal coupling of parahippocampal ripples, sleep spindles and slow oscillations in humans. *Brain*, 130(11), 2868–2878. <https://doi.org/10.1093/brain/awm146>
- Csicsvari, J., Hirase, H., Mamiya, A., & Buzsáki, G. (2000). Ensemble Patterns of Hippocampal CA3-CA1 Neurons during Sharp Wave-Associated Population Events. *Neuron*, 28(2), 585–594. [https://doi.org/10.1016/s0896-6273\(00\)00135-5](https://doi.org/10.1016/s0896-6273(00)00135-5)
- Cunchillos, J., & De Andrés, I. (1982). Participation of the cerebellum in the regulation of the sleep-wakefulness cycle. Results in cerebellectomized cats. *Electroencephalography and Clinical Neurophysiology*, 53(5), 549–558. [https://doi.org/10.1016/0013-4694\(82\)90067-0](https://doi.org/10.1016/0013-4694(82)90067-0)
- Dang-Vu, T. T., Schabus, M., Desseilles, M., Albouy, G., Boly, M., Darsaud, A., . . . Maquet, P. (2008). Spontaneous neural activity during human slow wave sleep. *Proceedings of the National Academy of Sciences*, 105(39), 15160–15165. <https://doi.org/10.1073/pnas.0801819105>
- Datta, S. (1997). Cellular basis of pontine ponto-geniculo-occipital wave generation and modulation. *Cellular and Molecular Neurobiology*, 17(3), 341–365. <https://doi.org/10.1023/a:1026398402985>
- Datta, S. (2000). Avoidance Task Training Potentiates Phasic Pontine-Wave Density in the Rat: A Mechanism for Sleep-Dependent Plasticity. *The Journal of Neuroscience*, 20(22), 8607–8613. <https://doi.org/10.1523/jneurosci.20-22-08607.2000>

- Datta, S., Li, G., & Auerbach, S. (2008). Activation of phasic pontine-wave generator in the rat: a mechanism for expression of plasticity-related genes and proteins in the dorsal hippocampus and amygdala. *European Journal of Neuroscience*, 27(7), 1876–1892. <https://doi.org/10.1111/j.1460-9568.2008.06166.x>
- Datta, S., Mavanji, V., Ulloor, J., & Patterson, E. H. (2004). Activation of Phasic Pontine-Wave Generator Prevents Rapid Eye Movement Sleep Deprivation-Induced Learning Impairment in the Rat: A Mechanism for Sleep-Dependent Plasticity. *Journal of Neuroscience*, 24(6), 1416–1427. <https://doi.org/10.1523/jneurosci.4111-03.2004>
- Datta, S., & O'Malley, M. W. (2013). Fear Extinction Memory Consolidation Requires Potentiation of Pontine-Wave Activity during REM Sleep. *Journal of Neuroscience*, 33(10), 4561–4569. <https://doi.org/10.1523/jneurosci.5525-12.2013>
- Datta, S., Saha, S., Prutzman, S. L., Mullins, O. J., & Mavanji, V. (2005). Pontine-wave generator activation-dependent memory processing of avoidance learning involves the dorsal hippocampus in the rat. *Journal of Neuroscience Research*, 80(5), 727–737. <https://doi.org/10.1002/jnr.20501>
- Datta, S., Siwek, D. F., & Huang, M. P. (2009). Improvement of Two-Way Active Avoidance Memory Requires Protein Kinase A Activation and Brain-Derived Neurotrophic Factor Expression in the Dorsal Hippocampus. *Journal of Molecular Neuroscience*, 38(3), 257–264. <https://doi.org/10.1007/s12031-009-9206-7>
- Datta, S., Siwek, D. F., Patterson, E. H., & Cipolloni, P. B. (1998). Localization of pontine PGO wave generation sites and their anatomical projections in the rat. *Synapse*, 30, 409–423.
- De Gennaro, L., & Ferrara, M. (2003). Sleep spindles: an overview. *Sleep Medicine Reviews*, 7(5), 423–440. <https://doi.org/10.1053/smr.2002.0252>
- De Solages, C., Szapiro, G., Brunel, N., Hakim, V., Isope, P., Buisseret, P., . . . Léna, C. (2008). High-Frequency Organization and Synchrony of Activity in the Purkinje Cell Layer of the Cerebellum. *Neuron*, 58(5), 775–788. <https://doi.org/10.1016/j.neuron.2008.05.008>
- De Zeeuw, C. I., Hoebeek, F. E., Bosman, L. W. J., Schonewille, M., Witter, L., & Koekkoek, S. K. (2011). Spatiotemporal firing patterns in the cerebellum. *Nature Reviews Neuroscience*, 12(6), 327–344. <https://doi.org/10.1038/nrn3011>
- DelRosso, L. M., & Hoque, R. (2014). The Cerebellum and Sleep. *Neurologic Clinics*, 32(4), 893–900. <https://doi.org/10.1016/j.ncl.2014.07.003>
- Dement, W. C., Mitler, M. M., & Zarcone, V. P. (1973). Some Fundamental Considerations in the Study of Sleep. *Psychosomatics*, 14(2), 89–94. [https://doi.org/10.1016/s0033-3182\(73\)71361-x](https://doi.org/10.1016/s0033-3182(73)71361-x)
- Ecker, A. S., Berens, P., Keliris, G. A., Bethge, M., Logothetis, N. K., & Tolias, A. S. (2010). Decorrelated Neuronal Firing in Cortical Microcircuits. *Science*, 327(5965), 584–587. <https://doi.org/10.1126/science.1179867>
- Farber, J., Marks, G., & Roffwarg, H. (1980). Rapid eye movement sleep PGO-type waves are present in the dorsal pons of the albino rat. *Science*, 209(4456), 615–617. <https://doi.org/10.1126/science.6994229>

- Gardner, R. J., Hughes, S. W., & Jones, M. W. (2013). Differential Spike Timing and Phase Dynamics of Reticular Thalamic and Prefrontal Cortical Neuronal Populations during Sleep Spindles. *Journal of Neuroscience*, 33(47), 18469–18480. <https://doi.org/10.1523/jneurosci.2197-13.2013>
- Hobson, J., & McCarley, R. W. (1972). Spontaneous discharge rates of cat cerebellar purkinje cells in sleep and waking. *Electroencephalography and Clinical Neurophysiology*, 33(5), 457–469. [https://doi.org/10.1016/0013-4694\(72\)90210-6](https://doi.org/10.1016/0013-4694(72)90210-6)
- Jahnke, K., Von Wegner, F., Morzelewski, A., Borisov, S., Maischein, M., Steinmetz, H., & Laufs, H. (2012). To wake or not to wake? The two-sided nature of the human K-complex. *NeuroImage*, 59(2), 1631–1638. <https://doi.org/10.1016/j.neuroimage.2011.09.013>
- Karashima, A., Katayama, N., & Nakao, M. (2007). Phase-locking of spontaneous and tone-elicited pontine waves to hippocampal theta waves during REM sleep in rats. *Brain Research*, 1182, 73–81. <https://doi.org/10.1016/j.brainres.2007.08.060>
- Karashima, A., Nakamura, K., Sato, N., Nakao, M., Katayama, N., & Yamamoto, M. (2002). Phase-locking of spontaneous and elicited ponto-geniculo-occipital waves is associated with acceleration of hippocampal theta waves during rapid eye movement sleep in cats. *Brain Research*, 958(2), 347–358. [https://doi.org/10.1016/s0006-8993\(02\)03673-9](https://doi.org/10.1016/s0006-8993(02)03673-9)
- Kaufmann, C., Wehrle, R., Wetter, T. C., Holsboer, F., Auer, D. P., Pollmächer, T., & Czisch, M. (2005). Brain activation and hypothalamic functional connectivity during human non-rapid eye movement sleep: an EEG/fMRI study. *Brain*, 129(3), 655–667. <https://doi.org/10.1093/brain/awh686>
- Latchoumane, C. V., Ngo, H. V., Born, J., & Shin, H. (2017). Thalamic Spindles Promote Memory Formation during Sleep through Triple Phase-Locking of Cortical, Thalamic, and Hippocampal Rhythms. *Neuron*, 95(2), 424–435. <https://doi.org/10.1016/j.neuron.2017.06.025>
- Maingret, N., Girardeau, G., Todorova, R., Goutier, M., & Zugaro, M. (2016). Hippocampo-cortical coupling mediates memory consolidation during sleep. *Nature Neuroscience*, 19(7), 959–964. <https://doi.org/10.1038/nn.4304>
- Mano, N. (1970). Changes of Simple and Complex Spike Activity of Cerebellar Purkinje Cells with Sleep and Waking. *Science*, 170(3964), 1325–1327. <https://doi.org/10.1126/science.170.3964.1325>
- Marchesi, G. F., & Strata, P. (1970). Climbing fibers of cat cerebellum: modulation of activity during sleep. *Brain Research*, 17(1), 145–148. [https://doi.org/10.1016/0006-8993\(70\)90317-3](https://doi.org/10.1016/0006-8993(70)90317-3)
- Marks, G., Farber, J., Rubinstein, M., & Roffwarg, H. (1980). Demonstration of ponto-geniculo-occipital waves in the albino rat. *Experimental Neurology*, 69(3), 648–666. [https://doi.org/10.1016/0014-4886\(80\)90058-8](https://doi.org/10.1016/0014-4886(80)90058-8)
- McCarley, R., Nelson, J., & Hobson, J. (1978). Ponto-geniculo-occipital (PGO) burst neurons: correlative evidence for neuronal generators of PGO waves. *Science*, 201(4352), 269–272. <https://doi.org/10.1126/science.663656>
- McCarley, R. W., & Hobson, J. (1972). Simple spike firing patterns of cat cerebellar purkinje cells in sleep and waking. *Electroencephalography and Clinical Neurophysiology*, 33(5), 471–483. [https://doi.org/10.1016/0013-4694\(72\)90211-8](https://doi.org/10.1016/0013-4694(72)90211-8)

- Molinari, M., Leggio, M. G., Solida, A., Ciorra, R., Misciagna, S., Silverini, M. C., & Petrosini, L. (1997). Cerebellum and procedural learning: evidence from focal cerebellar lesions. *Brain*, *120*(10), 1753–1762. <https://doi.org/10.1093/brain/120.10.1753>
- Nakao, M., Karashima, A., & Katayama, N. (2007). Mathematical models of regulatory mechanisms of sleep-wake rhythms. *Cellular and Molecular Life Sciences*, *64*(10), 1236–1243. <https://doi.org/10.1007/s00018-007-6534-z>
- Niedermeyer, E., & Uematsu, S. (1974). Electroencephalographic recordings from deep cerebellar structures in patients with uncontrolled epileptic seizures. *Electroencephalography and Clinical Neurophysiology*, *37*(4), 355–365. [https://doi.org/10.1016/0013-4694\(74\)90111-4](https://doi.org/10.1016/0013-4694(74)90111-4)
- Nir, Y., & Tononi, G. (2010). Dreaming and the brain: from phenomenology to neurophysiology. *Trends in Cognitive Sciences*, *14*(2), 88–100. <https://doi.org/10.1016/j.tics.2009.12.001>
- Palmer, C. (1979). Interpositus and fastigial unit activity during sleep and waking in the cat. *Electroencephalography and Clinical Neurophysiology*, *46*(4), 357–370. [https://doi.org/10.1016/0013-4694\(79\)90137-8](https://doi.org/10.1016/0013-4694(79)90137-8)
- Pellet, J., & Harlay, F. (1977). [Relations between the unit activity of the vermis cerebelli and the phasic waves of the electrocerebellogram during sleep in chronic cats]. *Archives Italiennes de Biologie*, *115*, 108–135.
- Pellet, J., Tardy, M. F., Dubrocard, S., & Harlay, F. (1974). [Phasic electrical activity of the cerebellar cortex during sleep and wakefulness]. *Physiology & Behavior*, *12*(6), 939–949. [https://doi.org/10.1016/0031-9384\(74\)90141-3](https://doi.org/10.1016/0031-9384(74)90141-3)
- Proville, R. D., Spolidoro, M., Guyon, N., Dugué, G. P., Selimi, F., Isope, P., . . . Léna, C. (2014). Cerebellum involvement in cortical sensorimotor circuits for the control of voluntary movements. *Nature Neuroscience*, *17*(9), 1233–1239. <https://doi.org/10.1038/nn.3773>
- Renart, A., De la Rocha, J., Bartho, P., Hollender, L., Parga, N., Reyes, A., & Harris, K. D. (2010). The Asynchronous State in Cortical Circuits. *Science*, *327*(5965), 587–590. <https://doi.org/10.1126/science.1179850>
- Ros, H., Sachdev, R. N. S., Yu, Y., Sestan, N., & McCormick, D. A. (2009). Neocortical Networks Entrain Neuronal Circuits in Cerebellar Cortex. *Journal of Neuroscience*, *29*(33), 10309–10320. <https://doi.org/10.1523/jneurosci.2327-09.2009>
- Roth, M., Shaw, J., & Green, J. (1956). The form, voltage distribution and physiological significance of the K-complex. *Electroencephalography and Clinical Neurophysiology*, *8*(3), 385–402. [https://doi.org/10.1016/0013-4694\(56\)90004-9](https://doi.org/10.1016/0013-4694(56)90004-9)
- Rowland, N., Goldberg, J., & Jaeger, D. (2010). Cortico-cerebellar coherence and causal connectivity during slow-wave activity. *Neuroscience*, *166*(2), 698–711. <https://doi.org/10.1016/j.neuroscience.2009.12.048>
- Saha, S., & Datta, S. (2005). Two-way active avoidance training-specific increases in phosphorylated cAMP response element-binding protein in the dorsal hippocampus, amygdala, and hypothalamus. *European Journal of Neuroscience*, *21*(12), 3403–3414. <https://doi.org/10.1111/j.1460-9568.2005.04166.x>

- Sakai, K., & Jouvet, M. (1980). Brain stem PGO-on cells projecting directly to the cat dorsal lateral geniculate nucleus. *Brain Research*, 194(2), 500–505. [https://doi.org/10.1016/0006-8993\(80\)91231-7](https://doi.org/10.1016/0006-8993(80)91231-7)
- Saper, C. B., Chou, T. C., & Scammell, T. E. (2001). The sleep switch: hypothalamic control of sleep and wakefulness. *Trends in Neurosciences*, 24(12), 726–731. [https://doi.org/10.1016/s0166-2236\(00\)02002-6](https://doi.org/10.1016/s0166-2236(00)02002-6)
- Saper, C. B., Fuller, P. M., Pedersen, N. P., Lu, J., & Scammell, T. E. (2010). Sleep State Switching. *Neuron*, 68(6), 1023–1042. <https://doi.org/10.1016/j.neuron.2010.11.032>
- Scammell, T. E., Arrigoni, E., & Lipton, J. O. (2017). Neural Circuitry of Wakefulness and Sleep. *Neuron*, 93(4), 747–765. <https://doi.org/10.1016/j.neuron.2017.01.014>
- Schabus, M., Dang-Vu, T. T., Albouy, G., Balet, E., Boly, M., Carrier, J., . . . Maquet, P. (2007). Hemodynamic cerebral correlates of sleep spindles during human non-rapid eye movement sleep. *Proceedings of the National Academy of Sciences*, 104(32), 13164–13169. <https://doi.org/10.1073/pnas.0703084104>
- Siapas, A. G., & Wilson, M. A. (1998). Coordinated Interactions between Hippocampal Ripples and Cortical Spindles during Slow-Wave Sleep. *Neuron*, 21(5), 1123–1128. [https://doi.org/10.1016/s0896-6273\(00\)80629-7](https://doi.org/10.1016/s0896-6273(00)80629-7)
- Siegel, J. M. (2005). Clues to the functions of mammalian sleep. *Nature*, 437(7063), 1264–1271. <https://doi.org/10.1038/nature04285>
- Steriade, M., Domich, L., & Oakson, G. (1986). Reticularis thalami neurons revisited: activity changes during shifts in states of vigilance. *The Journal of Neuroscience*, 6(1), 68–81. <https://doi.org/10.1523/jneurosci.06-01-00068.1986>
- Steriade, M., Nunez, A., & Amzica, F. (1993). A novel slow (< 1 Hz) oscillation of neocortical neurons in vivo: depolarizing and hyperpolarizing components. *The Journal of Neuroscience*, 13(8), 3252–3265. <https://doi.org/10.1523/jneurosci.13-08-03252.1993>
- Steriade, M., Timofeev, I., & Grenier, F. (2001). Natural Waking and Sleep States: A View From Inside Neocortical Neurons. *Journal of Neurophysiology*, 85(5), 1969–1985. <https://doi.org/10.1152/jn.2001.85.5.1969>
- Steriade, M. M., & McCarley, R. W. (2013). *Brainstem control of wakefulness and sleep*. New York, EEUU: Springer Science+Business Media.
- Stickgold, R. (2005). Sleep-dependent memory consolidation. *Nature*, 437(7063), 1272–1278. <https://doi.org/10.1038/nature04286>
- Tononi, G., & Cirelli, C. (2006). Sleep function and synaptic homeostasis. *Sleep Medicine Reviews*, 10(1), 49–62. <https://doi.org/10.1016/j.smr.2005.05.002>
- Totty, M. S., Chesney, L. A., Geist, P. A., & Datta, S. (2017). Sleep-Dependent Oscillatory Synchronization: A Role in Fear Memory Consolidation. *Frontiers in Neural Circuits*, 11. <https://doi.org/10.3389/fncir.2017.00049>
- Urakami, Y. (2008). Relationships Between Sleep Spindles and Activities of Cerebral Cortex as Determined by Simultaneous EEG and MEG Recording. *Journal of Clinical Neurophysiology*, 25(1), 13–24. <https://doi.org/10.1097/wnp.0b013e318162a8a4>

Velluti, R., Yamuy, J., Hadjez, J., & Monti, J. M. (1985). Spontaneous cerebellar nuclei PGO-like waves in natural paradoxical sleep and under reserpine. *Electroencephalography and Clinical Neurophysiology*, *60*(3), 243–248. [https://doi.org/10.1016/0013-4694\(85\)90038-0](https://doi.org/10.1016/0013-4694(85)90038-0)

Watson\*, T. C., Obiang\*, P., Torres-Herraez\*, A., Watilliaux, A., Coulon, P., Rochefort, C., & Rondi-Reig, L. (2019). Anatomical and physiological foundations of cerebello-hippocampal interaction. *eLife*, *8*. <https://doi.org/10.7554/elife.41896>

# **DISCUSSION**



The existence of cerebello-hippocampal functional interaction has been suggested by numerous and compelling forms of evidence obtained from both behavioural and physiological studies in humans and animal models. In particular, it seems that this interaction plays an important role in spatial navigation processes (Burguière et al., 2005,2010; Rochefort et al., 2011; Lefort et al., 2019). In order to interact, the cerebellum and the hippocampus need to be engaged in long-range neuronal networks. However, the underlying neuroanatomical connectivity and electrophysiological mechanisms supporting the formation of such networks have remained elusive. Moreover, the dynamic modulation of this long-range cerebello-hippocampal network and its behavioural state/task dependence has not been addressed either. This knowledge is critical in order to fully understand the functional role of the cerebellum in these circuits, particularly considering the complex nature of the topographical and functional organization of this structure.

My PhD aimed to address these two fundamental questions about the anatomical and electrophysiological foundations of cerebello-hippocampal functional networks and the dynamic nature of their interaction depending on the behavioural states. To do so, we have employed a combination of 1) anatomical retrograde tracing studies and 2) simultaneous multisite electrophysiological recordings in behaving mice. The results that have been presented in the previous section of this dissertation demonstrated the existence of multiple topographically restricted cerebello-hippocampal anatomical pathways, which support dynamic coherent oscillatory activity within specific behavioural states suggesting their engagement in functional networks.

## 1. TOPOGRAPHICAL ORGANIZATION OF CEREBELLAR PROJECTIONS TO THE HIPPOCAMPUS:

### Timing of the retrograde labelling and number of relays between the cerebellum and the hippocampus

The employment of trans-synaptic retrograde tracers have the major advantage of allowing access to poly-synaptic pathways; however, it also makes the interpretation of the results particularly complicated - the timing and spread of the infection are critical factors. In our study, multiple survival times were used aiming to track each replication cycle and, as a consequence, each relay in the pathway. The initial uptake of the rabies virus and the infection of first order neurons usually requires long periods of 1-2 days while the infection of the subsequent relays follows regular replication periods of approximately 12 h (Ugolini, 2010; Coulon et al., 2011). However, slight variations in this timing may depend on the species or the characteristics of the pathways being traced (Ugolini, 2010; Ruigrok et al., 2016). Thus, in order to reduce the potential impact of these factors, the specific time points used in our study were based on previous reports of cerebello-cerebral connections in rodents (Suzuki et al., 2012; Jwair et al., 2017; Aoki et al., 2019). Moreover, we also co-injected cholera toxin  $\beta$ -subunit (CTb), a monosynaptic retrograde tracer, in order to positively identify the first-order relays and to measure the spreading of the virus in the injection sites (Prevosto et al., 2009).

The main results we obtained from our anatomical tracing study regarding the number of relays between cerebellum and hippocampus have been:

1) **The absence of monosynaptic projections from the cerebellum to the hippocampus.** Early studies in cats (Harper and Heath, 1973) and monkeys (Heath and Harper, 1974) proposed the existence of monosynaptic projections from the fastigial nucleus to the hippocampus based on the presence of short-latency responses or the appearance of degenerating axons after the stimulation or lesion of it. However, further anatomical support for such projection has not been found and latter studies failed to replicate the findings and reported latencies indicative of poly-synaptic pathways instead (Newman and Reza, 1979). In our study, the absence of rabies-positive or CTb-positive neurons in the deep cerebellar or vestibular nuclei after 30 h post-infection demonstrated the absence of cerebello-hippocampal monosynaptic pathways. However, our injection sites were restricted to the dorsal hippocampus, mainly in the septal pole and, in order to fully exclude the possibility of such connectivity, a systematic mapping across the septo-temporal and the dorso-ventral axes of the hippocampus may be employed.

2) **Di- and tri-synaptic pathways connecting the cerebellum and the hippocampus.** After 48 h post-infection we found few rabies-labeled neurons in the deep cerebellar and vestibular nuclei in the three mice analysed at that time point. There are multiple lines of evidence suggesting that these labeled cells represent second order neurons and not early third order populations. First, 48 h has been previously employed in other studies involving cerebello-cerebral connectivity in rodents and it was shown to be restricted to first and second order neurons (Suzuki et al., 2012; Jwair et al., 2017). Second, the staining observed in these neurons was comparably stronger than other second order labeled populations and extended to their full dendritic processes, an indication of advanced infection as the viral replication in the cell bodies precedes the transport to distal dendrites (Ugolini, 2008). Third, at 58 h, in the next time point analysed, we observed few rabies-positive Purkinje cells in the cerebellar cortex. Since this occurred in less than the 12 h required for a full cycle of replication and infection of the virus, it is not likely that the cerebellar labeled cells observed at 58 h represented a fourth infection cycle and, therefore, they may be part of cerebellar circuits projecting through di-synaptic pathways to the hippocampus. Moreover, among the structures labeled at 30 h, three are known to receive direct projection from the deep cerebellar nuclei in cat (Paul et al., 1973), rat (Teune et al., 2000), and the macaque (Haines et al., 1990): the medial septum, the hypothalamic nuclei (potentially including the supramammillary nucleus) and the raphe nuclei. Thus, these could represent the first-order relays in the di-synaptic pathways.

However, tri-synaptic pathways are also major cerebello-hippocampal connectivity as we observed strong and abundant labelling in the deep cerebellar and vestibular nuclei at 58 h and in the cerebellar cortex at 66 h, the last time-point that we analysed. It is unlikely that these populations represent an increase in the number of visualized neurons participating in the di-synaptic projections. This is mainly due to the fact that,

as mentioned before, the labeled neurons observed at 48 h and 58 h in the deep cerebellar nuclei and the cerebellar cortex, respectively, already presented features of advanced infection and were not intermingled with a bigger population of weakly labeled neurons. On the contrary, at 66 h we did observe Purkinje cells showing weak staining, most likely representing cells that were delayed in their infection cycle. However, in previous studies, timings of 66-70 h were strictly associated with third order neurons (Suzuki et al., 2012; Aoki et al., 2019). While this discrepancy may be due to the different species employed (mice in our study and rats in theirs), future experiments focussed on the identification of the relays in the potential di- and tri-synaptic pathways will help to clarify their contribution to cerebello-hippocampal connectivity. Moreover, while our injections were restricted to the dentate gyrus and the hippocampus proper, the hippocampal formation circuit is considered to start in the entorhinal cortex which conveys most of the cortical and subcortical inputs to the dentate gyrus and the hippocampus through the perforant pathways (Andersen et al., 2007). Thus, if some of the cerebellar pathways that we have identified follows these routes, the influence on hippocampal function may already be exerted at the level of the entorhinal cortex. Interestingly, in this region many neuronal populations involved in the spatial coding such as the grid cells (Hafting et al., 2005) or head direction cells (Sargolini et al., 2006) are found, which could be modulated and affected by the cerebellar activity as has been shown in hippocampal place cells (Rocheffort et al., 2011; Lefort et al., 2019).

Finally, regarding the length of the cerebello-hippocampal pathways, our finding of relatively short connectivity between the cerebellum and the hippocampus does not exclude the potential influence exerted through longer routes. For instance, those involving projections through thalamic nuclei to the posterior parietal cortex (Giannetti and Molinari, 2002) which then reach the hippocampus through the entorhinal cortex (Andersen et al., 2007), have been propose to be important in the role of the cerebellum in spatial cognition (see Rocheffort et al., 2013; Rondi-Reig et al., 2014).

#### Multiple olivo-cortico-nuclear complexes project to and converge in the dorsal hippocampus

The anatomical retrograde tracing study revealed topographically restricted clusters of Purkinje cells organized in bilateral parasagittal bands in the vermal lobule VI, the paravermal and hemispherical Crus I and the dorsal and ventral paraflocculus. This arrangement is in agreement with the longitudinal and transversal grid-like subdivision of the cerebellar cortex in functional microzones (Oscarsson, 1979) and suggests the involvement of disparate and discrete cortico-nuclear cerebellar circuits (Apps and Garwicz, 2005) in the cerebello-hippocampal projections.

These circuits may represent parallel cerebellar processing channels as they are known to receive information from different origins in the nervous system (Sugihara and Shinoda, 2004) and to project through discrete routes involving specific subdivisions of the deep cerebellar nuclei (Voogd et al., 2003). However, since the mossy fibres are known to spread in the transversal plane and contact granule cells from

multiple zones (Shinoda et al., 2000; Quy et al., 2011), we can not exclude the possibility of a common input from the mossy fibre system. Furthermore, given that the Crus I is a hemispheric prolongation of the caudal part of the lobule VI and the parallel fibres are known to spread several millimetres in the transverse plane (Pichitpornchai et al., 1994), we can not rule out the possibility that the clusters in these two locations may also share similar parallel fibres inputs. Indeed, although it is known that the main influence exerted by the granule cells is concentrated on the Purkinje cells located immediately above them (Bower and Woolston, 1983; Isope and Barbour, 2002), it has been recently shown that a given microzone is heavily contacted by a limited number of distal sites in the granule cell layer in a very stereotyped manner (Valera et al., 2016). All this prevents us from assuming a purely parallel organization of the processing carried out by the different cerebellar circuits projecting to the hippocampus and the potential connectivity between them may be mapped in the future to test such a hypothesis.

All the clusters appeared simultaneously in the cerebellar cortex after a single injection in the dorsal hippocampus. This suggests that cerebellar outputs either converge at the hippocampal level or within the intermediate structures. Taken together, our findings suggest that the role of the cerebellum regarding its integration in a functional network with the hippocampus is complex and involves the cooperation of multiple cerebellar microzones.

#### Anatomo-functional identity of the cerebellar microcircuits projecting to the hippocampus

The modular organization of the cerebellar cortex has been proposed as a useful framework to study its function (Cerminara and Apps, 2010; Glickstein et al., 2011; Ruigrok, 2011). Therefore, we also addressed the modular identity of the cerebellar circuits that we found to project to the hippocampus. To do so, we took advantage of the stereotyped and well studied Zebrin II expression pattern in the cerebellar cortex of the mouse (Sugihara and Nguyen Quy, 2007) and its close relationship to the modular organization (Voogd et al., 2003). The cluster of rabies-positive Purkinje cells we observed in lobule VI was identified as part of the A module. In the Crus I, the module involved in the paravermal cluster was the C2 while in the hemisphere it was the D2. The topographical organization of the paraflocculus, particularly the ventral part, is very complex (Voogd and Barmack, 2006) and in this study we did not address in detail the specific modules involved in the clusters labeled in those regions.

A single module can be further subdivided in several functional domains, which may correspond to specific lobules or group of lobules (see for instance the section by Lawrenson, Lumb and Apps in a recent consensus paper, Apps et al., 2018). Indeed, the association of specific lobules with functional subdivisions remains controversial. While functional imaging studies in humans performing specific tasks revealed differential clusters of cerebellar activation that, in many cases, overlapped with anatomically delimited lobules (Stoodley and Schmahmann, 2009; Igloi et al., 2015; see also Schmahmann, 2019), recent studies proposed the existence of functional gradients (Guell et al., 2018) or defined functional parcellations which

does not follow such delimitation when employing large batteries of multi-domain task (King et al., 2019). Despite of the absence of consensus, the clusters observed in our retrograde labelling study were clearly restricted to specific lobules and, therefore, our results suggest that those may represent functional subdivisions.

The vermal lobule VI is part of the so-called oculomotor cerebellum (Voogd and Barmack, 2006; Glickstein et al., 2011). As mentioned before, the cluster in this lobule is part of the module A or the group II of the olivocerebellar system, which are known to receive multi-modal sensory information from the superior colliculus and the vestibular nuclei both through the climbing fibres and the mossy fibres (Sugihara and Shinoda, 2004; Voogd and Barmack, 2006; Sugihara and Nguyen Quy, 2007). This region projects then through the caudal fastigial nucleus to multiple areas including the superior colliculus, the periaqueductal grey, raphe nuclei or the mesencephalic reticular formation (Voogd and Barmack, 2006). Functional studies of this area have revealed an association with the control of visually driven saccadic eye and head movements in primates (e.g., Kase et al., 1979; Noda et al., 1987; Ohtsuka and Noda., 1995) and humans (Nitschke et al., 2004). However, since mice are afoveate animals, the visually oriented or gaze-shifting movements of the eyes may not be as behaviourally relevant as they are in primates (Stahl, 2004). A more general functional interpretation is that this region is involved in the guidance of movement in a head-centred reference frame, which is obtained from the combination of the visual space imposed by the collicular projections (Basso and May, 2017) and the head-relative to body information obtained from the vestibular projections (Cullen, 2014). Such information may be particularly relevant in the process of self-location in the environment and the construction and maintenance of the hippocampal spatial map (Rocheffort et al., 2013; Rondi-Reig et al., 2014).

Not much information regarding the C2 module at the Crus I paravermis is available. It is mainly interconnected with the visuomotor system. It receives dense cortical projections from the motor, prefrontal and posterior parietal cortices as well as from the frontal eye fields after relaying in the Darkschewitsch nucleus (see Glickstein et al., 2011; Voogd, 2014). Its output routes through the nucleus interpositus posterior which also projects to the Darkschewitsch nucleus and to the superior colliculus which project back to the frontal eye field after thalamic relay (Glickstein et al., 2011; Voogd, 2014). Finally, it also projects through thalamic relay to the primary motor, premotor areas, posterior parietal and prefrontal cortices (Glickstein et al., 2011; Voogd, 2014). The functional role of this area has been related to the visuospatial adaptation and the visual and proprioceptive guidance of movements (Prevosto et al., 2009). Moreover, its functional connectivity with the parietal cortex (O'Reilly et al., 2010) is particularly relevant for our study as this structure has been proposed to integrate visuo-spatial-motor information (Snyder et al., 1998) and perform a transformation from egocentric-to-allothetic reference frame (Save and Poucet, 2009), having an important role in path-integration (Save et al., 2001) and planning of routes during goal-directed behaviours (Nitz, 2006; Calton and Taube, 2009).

The hemisphere of the Crus I, along with the Crus II, are the most expanded regions of the human cerebellum (Whiting and Barton, 2003; Balsters et al., 2010) and have been proposed to participate in a plethora of non-motor functions including working memory, language generation, visuo-motor integration or spatial processing (Stoodley and Schmahmann, 2009; Igloi et al., 2015; see also Schmahmann, 2019). Studies in primates shown that they are heavily interconnected with the cerebral cortex including high associative areas as the prefrontal cortex (Kelly and Strick, 2003) as well as primary motor, premotor, or posterior parietal areas (see Voogd, 2014). It also receives visual (Edge et al., 2003) and somatosensory information (Mihailoff et al., 1981). Indeed, it has been recently shown in rodents that sensory and motor information from the whiskers converge in the same area of the Crus I D2 module (Proville et al., 2014). This information is conveyed to the parvocellular red nucleus and to the reticular nuclei of the pons. This module projects to the dentate nucleus and establishes close loops with most of their cortical afferent areas through thalamic projections (see Strick et al., 2009). While many differences in the structure and function may be observed between the primate and the rodent cerebellar hemispheres, it has been recently shown that rodent Crus I is homologous to the primate and human Crus I and Crus II (Sugihara, 2017). Interestingly, in a recent report in mice it has been shown that Purkinje cells simple spikes activity in the Crus I represent the instantaneous phase of dorsal hippocampus and prefrontal cortex, as well as the phase differences between them (McAfee et al., 2019). This finding is particularly relevant for our work as prefrontal cortex and hippocampus are known to form functional networks involved in spatial navigation (Jones and Wilson, 2005; Gordon, 2011; Cholvin et al., 2018) and particularly during goal-directed navigation (Hirel et al., 2013; Igloi et al. 2015; Ito et al., 2015; Babayan et al., 2017).

Finally, the dorsal paraflocculus is also intimately related to the visual system (Giolli et al., 2001) and has been also involved in the visuo-motor coordination and visually guided reaching in primates (Kralj-Hans et al., 2006). On the other hand, the ventral paraflocculus is part of the vestibulo-cerebellum. It receives vestibular inputs along with multimodal information and may be implicated in the generation of head-direction signals (see Rondi-Reig et al., 2014).

## 2. MECHANISMS FOR CEREBELLO-HIPPOCAMPAL INTERACTION

### Synchronization of theta oscillations as a potential mechanism for interaction

During my PhD I have used the levels of synchronization between the oscillatory activity measured in the local field potentials (LFPs) from the hippocampus and different cerebellar locations as a proxy for functional interaction. This is based on the neuronal communication through neuronal coherence hypothesis (Fries, 2005), which is founded in the correlation between fluctuating changes in the excitability of local neuronal populations and the oscillatory profile of their LFPs. Thus, these oscillations affect both the output of the neuronal populations and also the sensitivity to a given input and, in consequence, the coordination of the oscillatory activity between two communicating structures allow for an efficient

transmission of the information (Buzsaki and Draguhn, 2004). Furthermore, the modulation of this coherence depending on the behavioural context or task demands may support flexible routing of information across networks (Akam and Kullmann, 2010). This hypothesis has been supported by multiple studies demonstrating that coherence at specific frequency bands in long-range neural networks occur in a behaviourally dependent manner in rodents (e.g., Jones and Wilson, 2005; Benchenane et al., 2010; Watson et al., 2014), primates (e.g., Courtemanche and Lamarre, 2005; Soteropoulos and Baker, 2006; Fries et al., 2009; Bosman et al., 2012) and humans (Anderson et al., 2010; Backus et al., 2016). Moreover, abnormal levels of coherence have been found in pathological conditions in humans such in Parkinson's disease (Brown, 2007; Sarnthein and Jeanmonod, 2007) or schizophrenia (Light et al., 2006; Uhlhaas and Singer, 2010).

In our studies we have found significant levels of coherence in the theta frequency range (6-12 Hz) between the cerebellum and the hippocampus. This coherence was dynamically modulated in a subregion-specific manner depending on the behavioural context, suggesting that it may represent a mechanism by which the two structures are functionally engaged upon requirement. In line with such hypothesis, theta rhythmicity has been proposed as a fundamental mechanism for facilitating the transfer of information across brain regions during sensory information processing (Buzsaki, 2002, 2005; Colgin, 2013). Moreover, in the hippocampus, it seems to represent a temporal framework that facilitates plasticity mechanisms (Buzsaki, 2002, 2005). Interestingly, we also observed theta coherence between the cerebellum and the hippocampus during REM sleep periods suggesting that such mechanism may be relevant for sleep dependent plasticity mechanisms (Buzsaki, 1996). Indeed, coherence during REM sleep was modulated by a cerebellar infra-slow rhythm (< 1Hz), which was also coordinated with the occurrence of putative pontine-waves which are involved in memory consolidation processes in the hippocampus, at least during fear conditioning (Datta, 2000; Datta et al., 2004; Datta and O'Malley, 2013).

Local theta oscillations have been observed in the granule cell layer of the cerebellum (D'Angelo et al., 2001; Solinas et al., 2007; Dugué et al., 2009). Furthermore, the inferior olive also present subthreshold oscillations in the theta range (Chorev et al., 2007) which is able to generate rhythmic climbing fibre discharges at frequency ranges up to 12 Hz (Eccles et al., 1967). Indeed, previous reports of coherence in the cerebello-cerebral systems were also found to be preferentially coordinated in the theta range. For instance, theta coherence has been described in rats between the cerebellum and the somatosensory cortex during free whisking (O'Connor et al., 2002), the prefrontal cortex during active exploration (Watson et al., 2014) or the supplementary motor area in anaesthetize animals (Rowland et al., 2010). In guinea pigs, theta coherence between the cerebellum and the prefrontal cortex has been found during the learning phase of eye-blink conditioning and the disruption of such coupling impaired the performance of the task (Chen et al., 2016). Particularly relevant for our study, theta coherence during eye-blink conditioning has

been also found between the cerebellum and the hippocampus in rabbits (Hoffmann and Berry, 2009; Wikgren et al., 2010).

Thus, our results suggest that the neural mechanisms underlying potential functional engagement between the cerebellum and the hippocampus in mice relies on the temporal and dynamic coordination of their theta frequency oscillations. However, since our cerebellar recordings targeted the cerebellar cortex, it is still not clear how exactly the coherence observed in our results is translated into meaningful messages in the deep cerebellar nuclei and their outputs. Watson and colleagues reported theta coherence between the fastigial nucleus and the prefrontal cortex in rats (Watson et al., 2014), suggesting that these oscillations may be transmitted to the deep cerebellar nuclei. Future experiments targeting simultaneously the cerebellar cortex, deep cerebellar nuclei and the hippocampus may help to clarify how the information is coordinated inside the cerebellar circuit in relationship to its target. Similarly, given that these pathways are poly-synaptic, a functional dissection of the role of the different intermediate structures in the information transfer across the cerebello-hippocampal network will be needed.

#### Cerebellar Crus I is involved in goal-directed navigation

In our studies we have demonstrated the existence of differential and dynamic coupling of the theta oscillatory activity between the hippocampus and multiple cerebellar locations upon behavioural demands. In particular, we have found that the higher levels of coherence were obtained between the hippocampus and the Crus I region specifically when the animals performed a goal-directed behaviour. Interestingly, this coherence increased in parallel with the acquisition of the behaviour during the learning phase and was not correlated with motor parameters such as the instantaneous speed. We also demonstrated that this coherence was sustained along the approaching trajectory towards the goal once the animals exhibited a clear goal-directed behaviour but not when they were still in the exploratory phase.

A first interpretation of these results is that the Crus I-hippocampal circuit was selectively engaged when the animals employed a goal-directed navigational strategy and it keeps track of the position of the animal with respect to the goal-location. Interestingly, as previously discussed, the modules identified in the Crus I regions projecting to the hippocampus are also involved in loops with parietal and prefrontal cortices (see Glickstein et al., 2011; Voogd, 2014). Both areas are known to be functionally engaged with the hippocampus during goal directed behaviour. The former seems to be involved in path-integration (Save et al., 2001) and the encoding of routes during a goal-directed behaviours (Nitz, 2006; Calton and Taube, 2009). The latter is related to the encoding and maintenance of the goal-locations both in rats (Hok et al., 2005) and humans (Spiers, 2008). It has been also proven that this is related to a working memory process (Yoon et al., 2008). In humans, Crus I has been found to be involved in working memory processes too (Stoodley and Schmahmann, 2009). Since all these regions are interconnected, we can assume that the Crus I may have access to the goal-location (encoded in the prefrontal cortex), the self-location (encoded in the

hippocampus) and the planned trajectory (encoded in the parietal cortex). The Crus I region may then integrate this information in the current multisensory and motor states in order to coordinate and adjust the trajectory towards the goal through forward and inverse models (Wolpert and Kawato, 1998; Kawato, 1999; Imamizu et al., 2003). Interestingly, the existence of internal models in the Crus I has been demonstrated in cats performing a visually driven goal directed reaching task (Cerminara et al., 2009).

While our results do not imply causality and, therefore, we cannot assume that the coordination between the Crus I and the hippocampus is needed for a correct behavioural performance, they clearly suggested the functional relevance of such connectivity. Indeed, intact cerebellar long-term plasticity seems to be required in order to perform accurate and efficient goal-directed behaviour in mice (Burguière et al., 2005, 2010). The observed increase in coherence in parallel with the acquisition of the goal-directed behaviour is in agreement with the involvement of plasticity mechanisms in the cerebello-hippocampal circuits. Moreover, our finding of increased Crus I-hippocampal theta coherence during REM sleep in concert with the occurrence of pontine waves also points to a potential role of sleep-dependent plasticity mechanisms. Future experiments addressing the causality of the Crus I-hippocampal coherence and the goal-directed behaviour by employing disruption or enhancement of the electrophysiological coupling between them both online (during the actual performance of the task) and offline (during sleep) may help to better understand the specific role of this functional connectivity. Similarly, the potential coordination of the Crus I with the different nodes of the goal-directed navigation networks may be tested through simultaneous recordings in the different structures. The finding of Purkinje cell simple spikes activity in the Crus I encoding the phase differences in the theta rhythm from prefrontal cortex and dorsal hippocampus (McAfee et al., 2019) clearly suggests that this region may represent an important node in a large neuronal network involved in goal directed navigation.

#### Evidence of a cerebello-hippocampal loop

Finally, it has been proposed that the fundamental organization of the cerebello-cerebral circuits follows the formation of close loops with the cerebellar regions projecting to specific cerebral areas receiving inputs from them (Dum and Strick, 2003; Kelly and Strick, 2003; Strick et al., 2009). For instance, this has been found to be true for cerebellar circuits with the motor cortex, the prefrontal cortex (Kelly and Strick, 2003) or the striatum (Bostan and Strick, 2010). Therefore, one important question that needs to be addressed is the potential existence of hippocampal projections back to the cerebellum to close the loop. Early electrophysiological mapping studies already suggested the existence of hippocampo-cerebellar pathways to the vermal lobule VI in cats (Newman and Reza, 1979) and rats (Saint-Cyr and Woodward, 1980). However, the anatomical substrate of these pathways remains unknown. While our anatomical tracing study has only addressed the organization of the cerebellar projections to the hippocampus and, in

consequence, it does not shed light in to this fundamental question, we too have found electrophysiological evidence suggesting the existence of hippocampo-cerebellar connectivity.

The most direct evidence in our results was the recording of evoked potentials in the cerebellar cortex after the detection of sharp-wave ripples (SWR) in the hippocampus during non-REM sleep. The SWR are local fast oscillations generated in the hippocampus during which the pyramidal cells in CA1 and CA3 regions fire synchronously (Buzsaki, 1986, Csicsvari et al., 2000). Therefore, the presence of evoked field potentials appearing shortly after the occurrence of a SWR may reflect a population response to the synchronous activation of hippocampal outputs reaching the cerebellum. In agreement with such a hypothesis, similar responses to the ones reported in our work has been observed in the anterior cingulate cortex and have been associated with increases of certain neuronal populations firing (Wang and Ikemoto, 2016). The latency of the onset of the cerebellar evoked activity ( $\sim 9.17$  msec) was in agreement with previous reports of di-synaptic pathways described in the cerebro-ponto-cerebellar circuits (e.g., Allen and Tsukahara, 1974; Proville et al., 2014) thus suggesting the involvement of the mossy fibre input. A potential influence through the inferior olive-climbing fibres system may also be possible although it would require an additional relay (hippocampus-mesodiencephalic nuclei-inferior olive). Future experiments recording the activity of Purkinje cells in response to SWR may help to clarify the involvement of the mossy and the climbing fibres systems.

Other indirect evidences for the hippocampal-cerebellar circuits can be also inferred from our studies. First, we reported the existence of Purkinje cells whose firing is significantly phase-locked to the hippocampal theta phase. Given the high frequency basal firing rates of the Purkinje cells and the relatively sparse distribution of these cells in the cerebellar cortex, it is unlikely that such influence is directed from the cerebellum to the hippocampus. Therefore, the observed phase-locking may be indicative of the entraining of the cerebellar circuit by the hippocampal oscillations, further suggesting hippocampo-cerebellar connectivity. Following the same logic, as discussed before, generation of theta oscillations in the cerebellar circuits is often ascribed to the granule cell layer and is largely influenced by their mossy fibres synaptic inputs (Gandolfi et al., 2013). It is then conceivable that the coherent theta oscillations that we observed may depend on the arrival of mossy fibre inputs entrained by the hippocampal rhythm. In order to determine univocally the directionality of the cerebello-hippocampal coherence, occlusion experiments transiently disrupting the deep cerebellar nuclei or other intermediate structures in the cerebello-hippocampal pathway may be appropriate.

### 3. CONCLUSIONS AND FUTURE PERSPECTIVES

The results obtained during my PhD have demonstrated the existence of relatively direct connectivity between restricted regions of the cerebellum and the hippocampus, which are able to support dynamic and differential coupling of the theta oscillations in both structures during awake and sleep states. In particular,

the Crus I hemispherical region seems to be functionally engaged with the hippocampus during goal-directed behaviour.

In the discussion I have already mentioned multiple future experiments that may be needed to clarify the role of the identified cerebello-hippocampal circuits in larger functional neuronal networks. The main questions to be addressed are, in my opinion, the following:

**1) Identification of the specific anatomical pathways.** While our study has identified the specific cerebellar regions projecting to the hippocampus, the methods employed were not tailored for a proper identification of the intermediate relays. This knowledge is fundamental in order to understand the functional role of the cerebellum and to integrate our new findings within the larger brain network. Future experiments should then be conducted employing state-of-the-art tracing techniques which may allow identification of each intermediate structure. For instance, the use of modified rabies virus deficient for the envelope glycoprotein limits their spreading to a monosynaptic relay (Wickersham et al., 2007). However, selective injection of this protein allow for a novel replication and infection cycle reaching a following relay (for instance, see Xu et al., 2016). Employing this technique would allow us to track all the pathway from the hippocampus back to the cerebellum.

**2) Causal demonstration of the cerebello-hippocampal interaction and understanding how local neuronal populations in the cerebellum and the hippocampus are mutually affected.** Our recordings of the local field potential activity were particularly useful for the identification of general mechanisms of coordination between the cerebellum and the hippocampus. However, while extensively used and accepted, the coherence measurements do not offer a causal demonstration of interaction nor inform about what is the specific modulation of the local neuronal activity. The multiple demonstrations of abnormal hippocampal neuronal population activity in cerebellar mutants (Rocheffort et al., 2011; Lefort et al., 2019) make clear that a deeper understanding of the cerebellar role in shaping and modulating hippocampal activity is needed. An interesting approach to address this fundamental questions is the employment of optogenetic tools which allow tight temporal control of specific neuronal populations. Indeed, a mutant mouse expressing channelrhodopsin II under the control of the L7 promotor, which is expressed exclusively in the cerebellar Purkinje cells, is already available (Chaumont et al., 2013). Employing selective optogenetic activation in this mice in combination with hippocampal recordings might be a good strategy in order to study the specific modulation of hippocampal network activity upon manipulation of the cerebellar circuits.

**3) Anatomical mapping of hippocampal projections to the cerebellum.** Our study has demonstrated the existence of anatomical substrate for previously proposed cerebello-hippocampal pathways based on electrophysiological observations. Similarly, multiple indirect forms of evidence from others (Newman and Reza, 1979; Saint-Cyr and Woodward, 1980) and even our own observations also suggest the existence of hippocampal-cerebellar pathways. Clarifying if the cerebello-hippocampal circuits are organize in close

loops and how the information is transferred in one or the other direction depending on the behavioural state may be particularly useful for understanding the functional network in which they may be embedded. Applying a similar tracing strategy to the one employed in our work but injecting the rabies virus in to the cerebellar cortex may be the best option to start.

# **REFERENCES**



- ADRIAN, E. D. (1943). AFFERENT AREAS IN THE CEREBELLUM CONNECTED WITH THE LIMBS. *Brain*, 66(4), 289–315. <https://doi.org/10.1093/brain/66.4.289>
- Akam, T., & Kullmann, D. M. (2010). Oscillations and Filtering Networks Support Flexible Routing of Information. *Neuron*, 67(2), 308–320. <https://doi.org/10.1016/j.neuron.2010.06.019>
- Albus, J. S. (1971). A theory of cerebellar function. *Mathematical Biosciences*, 10(1-2), 25–61. [https://doi.org/10.1016/0025-5564\(71\)90051-4](https://doi.org/10.1016/0025-5564(71)90051-4)
- Allen, G. I., & Tsukahara, N. (1974). Cerebrocerebellar communication systems.. *Physiological Reviews*, 54(4), 957–1006. <https://doi.org/10.1152/physrev.1974.54.4.957>
- Alstermark, B., & Ekerot, C. (2013). The lateral reticular nucleus: a precerebellar centre providing the cerebellum with overview and integration of motor functions at systems level. A new hypothesis. *The Journal of Physiology*, 591(22), 5453–5458. <https://doi.org/10.1113/jphysiol.2013.256669>
- Amaral, D. G. (1993). Emerging principles of intrinsic hippocampal organization. *Current Opinion in Neurobiology*, 3, 225–229.
- Anand, B. K., Malhotra, C. L., Singh, B., & Dua, S. (1959). CEREBELLAR PROJECTIONS TO LIMBIC SYSTEM. *Journal of Neurophysiology*, 22(4), 451–457. <https://doi.org/10.1152/jn.1959.22.4.451>
- Andersen, P., Morris, R., Amaral, D., & O'Keefe, J. (2007). *The Hippocampus Book*. New York, EEUU: Oxford University Press.
- Anderson, J. S., Druzgal, T. J., Lopez-Larson, M., Jeong, E., Desai, K., & Yurgelun-Todd, D. (2010). Network anticorrelations, global regression, and phase-shifted soft tissue correction. *Human Brain Mapping*, 32(6), 919–934. <https://doi.org/10.1002/hbm.21079>
- Andreasen, N. C., Paradiso, S., & O'Leary, D. S. (1998). "Cognitive Dysmetria" as an Integrative Theory of Schizophrenia: A Dysfunction in Cortical-Subcortical-Cerebellar Circuitry? *Schizophrenia Bulletin*, 24(2), 203–218. <https://doi.org/10.1093/oxfordjournals.schbul.a033321>
- Angaut, P., Alvarado-Mallart, R. M., & Sotelo, C. (1985). Compensatory climbing fiber innervation after unilateral pedunculotomy in the newborn rat: Origin and topographic organization. *The Journal of Comparative Neurology*, 236(2), 161–178. <https://doi.org/10.1002/cne.902360203>
- Angaut, P., Cicerata, F., & Serapide, M. (1987). The Dentatorubral Projection. An Autoradiography Study in Rats. *Brain, Behavior and Evolution*, 30(5-6), 272–281. <https://doi.org/10.1159/000118651>
- Ankri, L., Husson, Z., Pietrajtis, K., Proville, R., Léna, C., Yarom, Y., . . . Uusisaari, M. Y. (2015). A novel inhibitory nucleo-cortical circuit controls cerebellar Golgi cell activity. *eLife*, 4. <https://doi.org/10.7554/elife.06262>
- Annand, B. K., Malhotra, C. L., Singh, B., & Dua, S. (1959). Cerebellar projections to limbic system. *Journal of Neurophysiology*, 22(4), 451–457.
- Aoki, S., Coulon, P., & Ruigrok, T. J. H. (2017). Multizonal Cerebellar Influence Over Sensorimotor Areas of the Rat Cerebral Cortex. *Cerebral Cortex*, 29(2), 598–614. <https://doi.org/10.1093/cercor/bhx343>

Apps, R., & Garwicz, M. (2005). Anatomical and physiological foundations of cerebellar information processing. *Nature Reviews Neuroscience*, 6(4), 297–311. <https://doi.org/10.1038/nrn1646>

Apps, R., & Hawkes, R. (2009). Cerebellar cortical organization: a one-map hypothesis. *Nature Reviews Neuroscience*, 10(9), 670–681. <https://doi.org/10.1038/nrn2698>

Apps, R., Hawkes, R., Aoki, S., Bengtsson, F., Brown, A. M., Chen, G., . . . Ruigrok, T. J. H. (2018). Cerebellar Modules and Their Role as Operational Cerebellar Processing Units. *The Cerebellum*, 17(5), 654–682. <https://doi.org/10.1007/s12311-018-0952-3>

- B -

Babayán, B. M., Watilliaux, A., Viejo, G., Paradis, A., Girard, B., & Rondi-Reig, L. (2017). A hippocampo-cerebellar centred network for the learning and execution of sequence-based navigation. *Scientific Reports*, 7(1). <https://doi.org/10.1038/s41598-017-18004-7>

Backus, A. R., Bosch, S. E., Ekman, M., Grabovetsky, A. V., & Doeller, C. F. (2016). Mnemonic convergence in the human hippocampus. *Nature Communications*, 7(1). <https://doi.org/10.1038/ncomms11991>

Badura, A., Verpeut, J. L., Metzger, J. W., Pereira, T. D., Pisano, T. J., Deverett, B., . . . Wang, S. S. (2018). Normal cognitive and social development require posterior cerebellar activity. *eLife*, 7. <https://doi.org/10.7554/elife.36401>

Bagnall, M. W., Zingg, B., Sakatos, A., Moghadam, S. H., Zeilhofer, H. U., & Lac, S. (2009). Glycinergic Projection Neurons of the Cerebellum. *Journal of Neuroscience*, 29(32), 10104–10110. <https://doi.org/10.1523/jneurosci.2087-09.2009>

Balsters, J., Cussans, E., Diedrichsen, J., Phillips, K., Preuss, T., Rilling, J., & Ramnani, N. (2010). Evolution of the cerebellar cortex: The selective expansion of prefrontal-projecting cerebellar lobules. *NeuroImage*, 49(3), 2045–2052. <https://doi.org/10.1016/j.neuroimage.2009.10.045>

Barili, P., Bronzetti, E., Ricci, A., Zaccheo, D., & Amenta, F. (2000). Microanatomical localization of dopamine receptor protein immunoreactivity in the rat cerebellar cortex. *Brain Research*, 854(1-2), 130–138. [https://doi.org/10.1016/s0006-8993\(99\)02306-9](https://doi.org/10.1016/s0006-8993(99)02306-9)

Barmack, N. H., & Yakhnitsa, V. (2008). Functions of Interneurons in Mouse Cerebellum. *Journal of Neuroscience*, 28(5), 1140–1152. <https://doi.org/10.1523/jneurosci.3942-07.2008>

Basso, M. A., & May, P. J. (2017). Circuits for Action and Cognition: A View from the Superior Colliculus. *Annual Review of Vision Science*, 3(1), 197–226. <https://doi.org/10.1146/annurev-vision-102016-061234>

Beier, K., Steinberg, E., DeLoach, K., Xie, S., Miyamichi, K., Schwarz, L., . . . Luo, L. (2015). Circuit Architecture of VTA Dopamine Neurons Revealed by Systematic Input-Output Mapping. *Cell*, 162(3), 622–634. <https://doi.org/10.1016/j.cell.2015.07.015>

Benchenane, K., Peyrache, A., Khamassi, M., Tierney, P. L., Gioanni, Y., Battaglia, F. P., & Wiener, S. I. (2010). Coherent Theta Oscillations and Reorganization of Spike Timing in the Hippocampal- Prefrontal Network upon Learning. *Neuron*, 66(6), 921–936. <https://doi.org/10.1016/j.neuron.2010.05.013>

- Bengtsson, F., & Jorntell, H. (2009). Sensory transmission in cerebellar granule cells relies on similarly coded mossy fiber inputs. *Proceedings of the National Academy of Sciences*, *106*(7), 2389–2394. <https://doi.org/10.1073/pnas.0808428106>
- Biswas, M. S., Luo, Y., Sarpong, G. A., & Sugihara, I. (2019). Divergent projections of single pontocerebellar axons to multiple cerebellar lobules in the mouse. *Journal of Comparative Neurology*, *527*(12), 1966–1985. <https://doi.org/10.1002/cne.24662>
- Blenkinsop, T. A. (2006). Block of Inferior Olive Gap Junctional Coupling Decreases Purkinje Cell Complex Spike Synchrony and Rhythmicity. *Journal of Neuroscience*, *26*(6), 1739–1748. <https://doi.org/10.1523/jneurosci.3677-05.2006>
- Blot, A., & Barbour, B. (2013). Analysis of the study of the cerebellar pinceau by Korn and Axelrad. *BioRxiv*, . <https://doi.org/10.1101/001123>
- Boccaro, C. N., Sargolini, F., Thoresen, V. H., Solstad, T., Witter, M. P., Moser, E. I., & Moser, M. (2010). Grid cells in pre- and parasubiculum. *Nature Neuroscience*, *13*(8), 987–994. <https://doi.org/10.1038/nn.2602>
- Bosman, C., Schoffelen, J., Brunet, N., Oostenveld, R., Bastos, A., Womelsdorf, T., . . . Fries, P. (2012). Attentional Stimulus Selection through Selective Synchronization between Monkey Visual Areas. *Neuron*, *75*(5), 875–888. <https://doi.org/10.1016/j.neuron.2012.06.037>
- Bosman, L. W. J., Koekkoek, S. K. E., Shapiro, J., Rijken, B. F. M., Zandstra, F., Van Der Ende, B., . . . De Zeeuw, C. I. (2010). Encoding of whisker input by cerebellar Purkinje cells. *The Journal of Physiology*, *588*(19), 3757–3783. <https://doi.org/10.1113/jphysiol.2010.195180>
- Bostan, A. C., Dum, R. P., & Strick, P. L. (2010). The basal ganglia communicate with the cerebellum. *Proceedings of the National Academy of Sciences*, *107*(18), 8452–8456. <https://doi.org/10.1073/pnas.1000496107>
- Bostan, A. C., Dum, R. P., & Strick, P. L. (2013). Cerebellar networks with the cerebral cortex and basal ganglia. *Trends in Cognitive Sciences*, *17*(5), 241–254. <https://doi.org/10.1016/j.tics.2013.03.003>
- Bostan, A. C., & Strick, P. L. (2018). The basal ganglia and the cerebellum: nodes in an integrated network. *Nature Reviews Neuroscience*, *19*(6), 338–350. <https://doi.org/10.1038/s41583-018-0002-7>
- Bower, J. M., Beermann, D. H., Gibson, J. M., Shambes, G. M., & Welker, W. (1981). Principles of Organization of a Cerebro-Cerebellar Circuit. *Brain, Behavior and Evolution*, *18*(1-2), 1–18. <https://doi.org/10.1159/000121772>
- Bower, J. M., & Woolston, D. C. (1983). Congruence of spatial organization of tactile projections to granule cell and Purkinje cell layers of cerebellar hemispheres of the albino rat: vertical organization of cerebellar cortex. *Journal of Neurophysiology*, *49*(3), 745–766. <https://doi.org/10.1152/jn.1983.49.3.745>
- BRAITENBERG, V. (1961). Functional Interpretation of Cerebellar Histology. *Nature*, *190*(4775), 539–540. <https://doi.org/10.1038/190539b0>
- Braitenberg, V., & Atwood, R. P. (1958). Morphological observations on the cerebellar cortex. *The Journal of Comparative Neurology*, *109*(1), 1–33. <https://doi.org/10.1002/cne.901090102>

- Brochu, G., Maler, L., & Hawkes, R. (1990). Zebrin II: A polypeptide antigen expressed selectively by purkinje cells reveals compartments in rat and fish cerebellum. *The Journal of Comparative Neurology*, 291(4), 538–552. <https://doi.org/10.1002/cne.902910405>
- BRODAL, P. (1978). THE CORTICOPONTINE PROJECTION IN THE RHESUS MONKEY ORIGIN AND PRINCIPLES OF ORGANIZATION. *Brain*, 101(2), 251–283. <https://doi.org/10.1093/brain/101.2.251>
- Brodal, P. (1979). The pontocerebellar projection in the rhesus monkey: An experimental study with retrograde axonal transport of horseradish peroxidase. *Neuroscience*, 4(2), 193–208. [https://doi.org/10.1016/0306-4522\(79\)90082-4](https://doi.org/10.1016/0306-4522(79)90082-4)
- Brown, A. M., Arancillo, M., Lin, T., Catt, D. R., Zhou, J., Lackey, E. P., . . . Sillitoe, R. V. (2019). Molecular layer interneurons shape the spike activity of cerebellar Purkinje cells. *Scientific Reports*, 9(1). <https://doi.org/10.1038/s41598-018-38264-1>
- Brown, I. E. (2001). Congruence of mossy fiber and climbing fiber tactile projections in the lateral hemispheres of the rat cerebellum. *Journal of Comparative Neurology*, 429(1).
- Brown, I. E., & Bower, J. M. (2002). The Influence of Somatosensory Cortex on Climbing Fiber Responses in the Lateral Hemispheres of the Rat Cerebellum after Peripheral Tactile Stimulation. *The Journal of Neuroscience*, 22(15), 6819–6829. <https://doi.org/10.1523/jneurosci.22-15-06819.2002>
- Brown, J. T., Chan-Palay, V., & Palay, S. L. (1977). A study of afferent input to the inferior olivary complex in the rat by retrograde axonal transport of horseradish peroxidase. *The Journal of Comparative Neurology*, 176(1), 1–22. <https://doi.org/10.1002/cne.901760102>
- Burguiere, E., Arabo, A., Jarlier, F., De Zeeuw, C. I., & Rondi-Reig, L. (2010). Role of the Cerebellar Cortex in Conditioned Goal-Directed Behavior. *Journal of Neuroscience*, 30(40), 13265–13271. <https://doi.org/10.1523/jneurosci.2190-10.2010>
- Burguière, E., Arleo, A., Hojjati, M., Elgersma, Y., Zeeuw, C. I. D., Berthoz, A., & Rondi-Reig, L. (2005). Spatial navigation impairment in mice lacking cerebellar LTD: a motor adaptation deficit? *Nature Neuroscience*, 8(10), 1292–1294. <https://doi.org/10.1038/nn1532>
- Burwell, R. D., & Amaral, D. G. (1998). Cortical afferents of the perirhinal, postrhinal, and entorhinal cortices of the rat. *Journal of Comparative Neurology*, 398(2).
- Butler, A. B., & Hodos, W. (2005). Comparative Vertebrate Neuroanatomy. *John Wiley & Sons*, . <https://doi.org/10.1002/0471733849>
- Buzsáki, G. (2004). Neuronal Oscillations in Cortical Networks. *Science*, 304(5679), 1926–1929. <https://doi.org/10.1126/science.1099745>
- Buzsáki, G. (1986). Hippocampal sharp waves: Their origin and significance. *Brain Research*, 398(2), 242–252. [https://doi.org/10.1016/0006-8993\(86\)91483-6](https://doi.org/10.1016/0006-8993(86)91483-6)
- Buzsáki, G. (1996). The Hippocampo-Neocortical Dialogue. *Cerebral Cortex*, 6(2), 81–92. <https://doi.org/10.1093/cercor/6.2.81>
- Buzsáki, G. (2002). Theta Oscillations in the Hippocampus. *Neuron*, 33(3), 325–340. [https://doi.org/10.1016/s0896-6273\(02\)00586-x](https://doi.org/10.1016/s0896-6273(02)00586-x)

- Buzsáki, G. (2005). Theta rhythm of navigation: Link between path integration and landmark navigation, episodic and semantic memory. *Hippocampus*, 15(7), 827–840. <https://doi.org/10.1002/hipo.20113>
- Buzsáki, G. (2006). *Rhythms of the Brain*. New York, EEUU: Oxford University Press.
- C -
- Calton, J. L., & Taube, J. S. (2009). Where am I and how will I get there from here? A role for posterior parietal cortex in the integration of spatial information and route planning. *Neurobiology of Learning and Memory*, 91(2), 186–196. <https://doi.org/10.1016/j.nlm.2008.09.015>
- Canto, C. B., Onuki, Y., Bruinsma, B., Van der Werf, Y. D., & De Zeeuw, C. I. (2017). The Sleeping Cerebellum. *Trends in Neurosciences*, 40(5), 309–323. <https://doi.org/10.1016/j.tins.2017.03.001>
- Carta, I., Chen, C. H., Schott, A. L., Dorizan, S., & Khodakhah, K. (2019). Cerebellar modulation of the reward circuitry and social behavior. *Science*, 363(6424). <https://doi.org/10.1126/science.aav0581>
- Cerminara, N. L., & Apps, R. (2010). Behavioural Significance of Cerebellar Modules. *The Cerebellum*, 10(3), 484–494. <https://doi.org/10.1007/s12311-010-0209-2>
- Cerminara, N. L., Apps, R., & Marple-Horvat, D. E. (2009). An internal model of a moving visual target in the lateral cerebellum. *The Journal of Physiology*, 587(2), 429–442. <https://doi.org/10.1113/jphysiol.2008.163337>
- Cerminara, N. L., Lang, E. J., Sillitoe, R. V., & Apps, R. (2015). Redefining the cerebellar cortex as an assembly of non-uniform Purkinje cell microcircuits. *Nature Reviews Neuroscience*, 16(2), 79–93. <https://doi.org/10.1038/nrn3886>
- Cesana, E., Pietrajtis, K., Bidoret, C., Isope, P., D'Angelo, E., Dieudonne, S., & Forti, L. (2013). Granule Cell Ascending Axon Excitatory Synapses onto Golgi Cells Implement a Potent Feedback Circuit in the Cerebellar Granular Layer. *Journal of Neuroscience*, 33(30), 12430–12446. <https://doi.org/10.1523/jneurosci.4897-11.2013>
- Chabrol, F. P., Arenz, A., Wiechert, M. T., Margrie, T. W., & DiGregorio, D. A. (2015). Synaptic diversity enables temporal coding of coincident multisensory inputs in single neurons. *Nature Neuroscience*, 18(5), 718–727. <https://doi.org/10.1038/nn.3974>
- Chan Palay, V. (1977). *Cerebellar Dentate Nucleus: Organization, cytology and Transmitters*. New York, EEUU: Springer-Verlag Berlin Heidelberg.
- Chan-Palay, V. (1973). Neuronal circuitry in the nucleus lateralis of the cerebellum. *Zeitschrift für Anatomie und Entwicklungsgeschichte*, 142(3), 259–265. <https://doi.org/10.1007/bf00519132>
- Chaumont, J., Guyon, N., Valera, A. M., Dugue, G. P., Popa, D., Marcaggi, P., . . . Isope, P. (2013). Clusters of cerebellar Purkinje cells control their afferent climbing fiber discharge. *Proceedings of the National Academy of Sciences*, 110(40), 16223–16228. <https://doi.org/10.1073/pnas.1302310110>
- Chen, C. H., Fremont, R., Arteaga-Bracho, E. E., & Khodakhah, K. (2014). Short latency cerebellar modulation of the basal ganglia. *Nature Neuroscience*, 17(12), 1767–1775. <https://doi.org/10.1038/nn.3868>

- Chen, G., Manson, D., Cacucci, F., & Wills, T. (2016). Absence of Visual Input Results in the Disruption of Grid Cell Firing in the Mouse. *Current Biology*, *26*(17), 2335–2342. <https://doi.org/10.1016/j.cub.2016.06.043>
- Chen, L. L., Lin, L., Green, E. J., Barnes, C. A., & McNaughton, B. L. (1994). Head-direction cells in the rat posterior cortex. *Experimental Brain Research*, *101*(1), 8–23. <https://doi.org/10.1007/bf00243212>
- Cheron, G., Servais, L., Wagstaff, J., & Dan, B. (2005). Fast cerebellar oscillation associated with ataxia in a mouse model of angelman syndrome. *Neuroscience*, *130*(3), 631–637. <https://doi.org/10.1016/j.neuroscience.2004.09.013>
- Choe, K. Y., Sanchez, C. F., Harris, N. G., Otis, T. S., & Mathews, P. J. (2018). Optogenetic fMRI and electrophysiological identification of region-specific connectivity between the cerebellar cortex and forebrain. *NeuroImage*, *173*, 370–383. <https://doi.org/10.1016/j.neuroimage.2018.02.047>
- Cholvin, T., Hok, V., Giorgi, L., Chaillan, F., & Poucet, B. (2017). Ventral midline thalamus is necessary for hippocampal place field stability and cell firing modulation. *The Journal of Neuroscience*, , 2039–17. <https://doi.org/10.1523/jneurosci.2039-17.2017>
- Chorev, E., Yarom, Y., & Lampl, I. (2007). Rhythmic Episodes of Subthreshold Membrane Potential Oscillations in the Rat Inferior Olive Nuclei In Vivo. *Journal of Neuroscience*, *27*(19), 5043–5052. <https://doi.org/10.1523/jneurosci.5187-06.2007>
- Clascá, F., Rubio-Garrido, P., & Jabaudon, D. (2012). Unveiling the diversity of thalamocortical neuron subtypes. *European Journal of Neuroscience*, *35*(10), 1524–1532. <https://doi.org/10.1111/j.1460-9568.2012.08033.x>
- Cohen, D., & Yarom, Y. (2000). Cerebellar On-Beam and Lateral Inhibition: Two Functionally Distinct Circuits. *Journal of Neurophysiology*, *83*(4), 1932–1940. <https://doi.org/10.1152/jn.2000.83.4.1932>
- Colgin, L. L. (2013). Mechanisms and Functions of Theta Rhythms. *Annual Review of Neuroscience*, *36*(1), 295–312. <https://doi.org/10.1146/annurev-neuro-062012-170330>
- Coulon, P., Bras, H., & Vinay, L. (2011). Characterization of last-order premotor interneurons by transneuronal tracing with rabies virus in the neonatal mouse spinal cord. *The Journal of Comparative Neurology*, *519*(17), 3470–3487. <https://doi.org/10.1002/cne.22717>
- Courtemanche, R., Chabaud, P., & Lamarre, Y. (2009). Synchronization in primate cerebellar granule cell layer local field potentials: Basic anisotropy and dynamic changes during active expectancy. *Frontiers in Cellular Neuroscience*, *3*. <https://doi.org/10.3389/neuro.03.006.2009>
- Courtemanche, R., & Lamarre, Y. (2005). Local Field Potential Oscillations in Primate Cerebellar Cortex: Synchronization With Cerebral Cortex During Active and Passive Expectancy. *Journal of Neurophysiology*, *93*(4), 2039–2052. <https://doi.org/10.1152/jn.00080.2004>
- Courtemanche, R., Robinson, J. C., & Aponte, D. I. (2013). Linking oscillations in cerebellar circuits. *Frontiers in Neural Circuits*, *7*. <https://doi.org/10.3389/fncir.2013.00125>
- Csicsvari, J., Hirase, H., Mamiya, A., & Buzsáki, G. (2000). Ensemble Patterns of Hippocampal CA3-CA1 Neurons during Sharp Wave–Associated Population Events. *Neuron*, *28*(2), 585–594. [https://doi.org/10.1016/s0896-6273\(00\)00135-5](https://doi.org/10.1016/s0896-6273(00)00135-5)

- Cullen, K. E. (2014). The neural encoding of self-generated and externally applied movement: implications for the perception of self-motion and spatial memory. *Frontiers in Integrative Neuroscience*, 7. <https://doi.org/10.3389/fnint.2013.00108>
- Cunchillos, J., & De Andrés, I. (1982). Participation of the cerebellum in the regulation of the sleep-wakefulness cycle. Results in cerebellectomized cats. *Electroencephalography and Clinical Neurophysiology*, 53(5), 549–558. [https://doi.org/10.1016/0013-4694\(82\)90067-0](https://doi.org/10.1016/0013-4694(82)90067-0)
- D -
- D'Angelo, E. (2014). The Organization of Plasticity in the Cerebellar Cortex: From Synapses to Control. *Progress in Brain Research*, , 31–58. <https://doi.org/10.1016/b978-0-444-63356-9.00002-9>
- D'Angelo, E., Nieuwenhuis, T., Maffei, A., Armano, S., Rossi, P., Taglietti, V., . . . Naldi, G. (2001). Theta-Frequency Bursting and Resonance in Cerebellar Granule Cells: Experimental Evidence and Modeling of a Slow K<sup>+</sup>-Dependent Mechanism. *The Journal of Neuroscience*, 21(3), 759–770. <https://doi.org/10.1523/jneurosci.21-03-00759.2001>
- Datta, S. (2000). Avoidance Task Training Potentiates Phasic Pontine-Wave Density in the Rat: A Mechanism for Sleep-Dependent Plasticity. *The Journal of Neuroscience*, 20(22), 8607–8613. <https://doi.org/10.1523/jneurosci.20-22-08607.2000>
- Datta, S. (2004). Activation of Phasic Pontine-Wave Generator Prevents Rapid Eye Movement Sleep Deprivation-Induced Learning Impairment in the Rat: A Mechanism for Sleep-Dependent Plasticity. *Journal of Neuroscience*, 24(6), 1416–1427. <https://doi.org/10.1523/jneurosci.4111-03.2004>
- Datta, S., & O'Malley, M. W. (2013). Fear Extinction Memory Consolidation Requires Potentiation of Pontine-Wave Activity during REM Sleep. *Journal of Neuroscience*, 33(10), 4561–4569. <https://doi.org/10.1523/jneurosci.5525-12.2013>
- De Andrés, I. (2011). Functional anatomy of non-REM sleep. *Frontiers in Neurology*, 2. <https://doi.org/10.3389/fneur.2011.00070>
- De Solages, C., Szapiro, G., Brunel, N., Hakim, V., Isope, P., Buisseret, P., . . . Léna, C. (2008). High-Frequency Organization and Synchrony of Activity in the Purkinje Cell Layer of the Cerebellum. *Neuron*, 58(5), 775–788. <https://doi.org/10.1016/j.neuron.2008.05.008>
- De Zeeuw, C. (1998). Microcircuitry and function of the inferior olive. *Trends in Neurosciences*, 21(9), 391–400. [https://doi.org/10.1016/s0166-2236\(98\)01310-1](https://doi.org/10.1016/s0166-2236(98)01310-1)
- De Zeeuw, C. I., Hansel, C., Bian, F., Koekkoek, S. K., Van Alphen, A. M., Linden, D. J., & Oberdick, J. (1998). Expression of a Protein Kinase C Inhibitor in Purkinje Cells Blocks Cerebellar LTD and Adaptation of the Vestibulo-Ocular Reflex. *Neuron*, 20(3), 495–508. [https://doi.org/10.1016/s0896-6273\(00\)80990-3](https://doi.org/10.1016/s0896-6273(00)80990-3)
- De Zeeuw, C. I., Hoebeek, F. E., & Schonewille, M. (2008). Causes and Consequences of Oscillations in the Cerebellar Cortex. *Neuron*, 58(5), 655–658. <https://doi.org/10.1016/j.neuron.2008.05.019>
- DelRosso, L. M., & Hoque, R. (2014). The Cerebellum and Sleep. *Neurologic Clinics*, 32(4), 893–900. <https://doi.org/10.1016/j.ncl.2014.07.003>

- Deschênes, M., Bourassa, J., & Parent, A. (1996). Striatal and cortical projections of single neurons from the central lateral thalamic nucleus in the rat. *Neuroscience*, *72*(3), 679–687.  
[https://doi.org/10.1016/0306-4522\(96\)00001-2](https://doi.org/10.1016/0306-4522(96)00001-2)
- DiGregorio, D. A., Nusser, Z., & Silver, R. (2002). Spillover of Glutamate onto Synaptic AMPA Receptors Enhances Fast Transmission at a Cerebellar Synapse. *Neuron*, *35*(3), 521–533.  
[https://doi.org/10.1016/s0896-6273\(02\)00787-0](https://doi.org/10.1016/s0896-6273(02)00787-0)
- Dizon, M. J., & Khodakhah, K. (2011). The Role of Interneurons in Shaping Purkinje Cell Responses in the Cerebellar Cortex. *Journal of Neuroscience*, *31*(29), 10463–10473.  
<https://doi.org/10.1523/jneurosci.1350-11.2011>
- Dolorfo, C. L., & Amaral, D. G. (1998). Entorhinal cortex of the rat: Topographic organization of the cells of origin of the perforant path projection to the dentate gyrus. *Journal of Comparative Neurology*, *398*(1).
- Doya, K. (2000). Complementary roles of basal ganglia and cerebellum in learning and motor control. *Current Opinion in Neurobiology*, *10*(6), 732–739. [https://doi.org/10.1016/s0959-4388\(00\)00153-7](https://doi.org/10.1016/s0959-4388(00)00153-7)
- Dugué, G. P., Brunel, N., Hakim, V., Schwartz, E., Chat, M., Lévesque, M., . . . Dieudonné, S. (2009). Electrical Coupling Mediates Tunable Low-Frequency Oscillations and Resonance in the Cerebellar Golgi Cell Network. *Neuron*, *61*(1), 126–139. <https://doi.org/10.1016/j.neuron.2008.11.028>
- Dum, R. P., & Strick, P. L. (2003). An Unfolded Map of the Cerebellar Dentate Nucleus and its Projections to the Cerebral Cortex. *Journal of Neurophysiology*, *89*(1), 634–639.  
<https://doi.org/10.1152/jn.00626.2002>
- Dumoulin, A., Triller, A., & Dieudonné, S. (2001). IPSC Kinetics at Identified GABAergic and Mixed GABAergic and Glycinergic Synapses onto Cerebellar Golgi Cells. *The Journal of Neuroscience*, *21*(16), 6045–6057.
- E -
- Eccles, J. C., Ito, M., & Szentagothai, J. (1967). *The Cerebellum as a Neuronal Machine*. Berlin: Springer Berlin Heidelberg.
- Eccles, J. C., Llinás, R., & Sasaki, K. (1966). The excitatory synaptic action of climbing fibres on the Purkinje cells of the cerebellum. *The Journal of Physiology*, *182*, 268–296.
- Edge, A. L., Marple-Horvat, D. E., & Apps, R. (2003). Lateral cerebellum: functional localization within crus I and correspondence to cortical zones. *European Journal of Neuroscience*, *18*(6), 1468–1485.  
<https://doi.org/10.1046/j.1460-9568.2003.02873.x>
- Eichenbaum, H. (2000). A cortical–hippocampal system for declarative memory. *Nature Reviews Neuroscience*, *1*(1), 41–50. <https://doi.org/10.1038/35036213>
- Eichenbaum, H. (2004). Hippocampus. *Neuron*, *44*(1), 109–120.  
<https://doi.org/10.1016/j.neuron.2004.08.028>
- Ekerot, C. (1990). The lateral reticular nucleus in the cat. *Experimental Brain Research*, *79*(1), 120–128.  
<https://doi.org/10.1007/bf00228880>

- Ekerot, C., & Jörntell, H. (2001). Parallel fibre receptive fields of Purkinje cells and interneurons are climbing fibre-specific. *European Journal of Neuroscience*, *13*(7), 1303–1310. <https://doi.org/10.1046/j.0953-816x.2001.01499.x>
- Ekerot, C., & Jörntell, H. (2003). Parallel fiber receptive fields: a key to understanding cerebellar operation and learning. *The Cerebellum*, *2*(2), 101–109. <https://doi.org/10.1080/14734220309411>
- Etienne, A. S., & Jeffery, K. J. (2004). Path integration in mammals. *Hippocampus*, *14*(2), 180–192. <https://doi.org/10.1002/hipo.10173>
- Evarts, E. V., & Thach, W. T. (1969). Motor Mechanisms of the CNS: Cerebrocerebellar Interrelations. *Annual Review of Physiology*, *31*(1), 451–498. <https://doi.org/10.1146/annurev.ph.31.030169.002315>
- F -
- Fanselow, M. S., & Dong, H. (2010). Are the Dorsal and Ventral Hippocampus Functionally Distinct Structures? *Neuron*, *65*(1), 7–19. <https://doi.org/10.1016/j.neuron.2009.11.031>
- Fries, P. (2005). A mechanism for cognitive dynamics: neuronal communication through neuronal coherence. *Trends in Cognitive Sciences*, *9*(10), 474–480. <https://doi.org/10.1016/j.tics.2005.08.011>
- Fries, P. (2009). Neuronal Gamma-Band Synchronization as a Fundamental Process in Cortical Computation. *Annual Review of Neuroscience*, *32*(1), 209–224. <https://doi.org/10.1146/annurev.neuro.051508.135603>
- Fyhn, M. (2004). Spatial Representation in the Entorhinal Cortex. *Science*, *305*(5688), 1258–1264. <https://doi.org/10.1126/science.1099901>
- Fyhn, M., Hafting, T., Treves, A., Moser, M., & Moser, E. I. (2007). Hippocampal remapping and grid realignment in entorhinal cortex. *Nature*, *446*(7132), 190–194. <https://doi.org/10.1038/nature05601>
- G -
- Gandolfi, D., Lombardo, P., Mapelli, J., Solinas, S., & D'Angelo, E. (2013). Theta-Frequency Resonance at the Cerebellum Input Stage Improves Spike Timing on the Millisecond Time-Scale. *Frontiers in Neural Circuits*, *7*. <https://doi.org/10.3389/fncir.2013.00064>
- Gao, W., Chen, G., Reinert, K. C., & Ebner, T. J. (2006). Cerebellar Cortical Molecular Layer Inhibition Is Organized in Parasagittal Zones. *Journal of Neuroscience*, *26*(32), 8377–8387. <https://doi.org/10.1523/jneurosci.2434-06.2006>
- Gao, Z., Proietti-Onori, M., Lin, Z., Ten Brinke, M., Boele, H., Potters, J., . . . De Zeeuw, C. (2016). Excitatory Cerebellar Nucleocortical Circuit Provides Internal Amplification during Associative Conditioning. *Neuron*, *89*(3), 645–657. <https://doi.org/10.1016/j.neuron.2016.01.008>
- Gao, Z., Van Beugen, B. J., & De Zeeuw, C. I. (2012). Distributed synergistic plasticity and cerebellar learning. *Nature Reviews Neuroscience*, *13*(9), 619–635. <https://doi.org/10.1038/nrn3312>
- Garwicz, M., Ekerot, C., & Schouenborg, J. (1992). Distribution of Cutaneous Nociceptive and Tactile Climbing Fibre Input to Sagittal Zones in Cat Cerebellar Anterior Lobe. *European Journal of Neuroscience*, *4*(4), 289–295. <https://doi.org/10.1111/j.1460-9568.1992.tb00876.x>

- Gauck, V., & Jaeger, D. (2000). The Control of Rate and Timing of Spikes in the Deep Cerebellar Nuclei by Inhibition. *The Journal of Neuroscience*, 20(8), 3006–3016. <https://doi.org/10.1523/jneurosci.20-08-03006.2000>
- Ghez, C. (1991). *The Cerebellum*. New York, EEUU: Appleton and Lange.
- Giannetti, S., & Molinari, M. (2002). Cerebellar input to the posterior parietal cortex in the rat. *Brain Research Bulletin*, 58(5), 481–489. [https://doi.org/10.1016/s0361-9230\(02\)00815-8](https://doi.org/10.1016/s0361-9230(02)00815-8)
- GIOLLI, R. A., GREGORY, K. M., SUZUKI, D. A., BLANKS, R. H., LUI, F., & BETELAK, K. F. (2001). Cortical and subcortical afferents to the nucleus reticularis tegmenti pontis and basal pontine nuclei in the macaque monkey. *Visual Neuroscience*, 18(5), 725–740. <https://doi.org/10.1017/s0952523801185068>
- Giovannucci, A., Badura, A., Deverett, B., Najafi, F., Pereira, T. D., Gao, Z., . . . Wang, S. S. (2017). Cerebellar granule cells acquire a widespread predictive feedback signal during motor learning. *Nature Neuroscience*, 20(5), 727–734. <https://doi.org/10.1038/nn.4531>
- Glickstein, M., Sultan, F., & Voogd, J. (2011). Functional localization in the cerebellum. *Cortex*, 47(1), 59–80. <https://doi.org/10.1016/j.cortex.2009.09.001>
- Goodlett, C. R., Hamre, K. M., & West, J. R. (1992). Dissociation of spatial navigation and visual guidance performance in Purkinje cell degeneration (pcd) mutant mice. *Behavioural Brain Research*, 47(2), 129–141. [https://doi.org/10.1016/s0166-4328\(05\)80119-6](https://doi.org/10.1016/s0166-4328(05)80119-6)
- Goodridge, J. P., Dudchenko, P. A., Worboys, K. A., Golob, E. J., & Taube, J. S. (1998). Cue control and head direction cells. *Behavioral Neuroscience*, 112(4), 749–761. <https://doi.org/10.1037/0735-7044.112.4.749>
- Gordon, J. A. (2011). Oscillations and hippocampal–prefrontal synchrony. *Current Opinion in Neurobiology*, 21(3), 486–491. <https://doi.org/10.1016/j.conb.2011.02.012>
- Gornati, S. V., Schäfer, C. B., Eelkman Rooda, O. H., Nigg, A. L., De Zeeuw, C. I., & Hoebeek, F. E. (2018). Differentiating Cerebellar Impact on Thalamic Nuclei. *Cell Reports*, 23(9), 2690–2704. <https://doi.org/10.1016/j.celrep.2018.04.098>
- Gould, B. B. (1979). The organization of afferents to the cerebellar cortex in the cat: Projections from the deep cerebellar nuclei. *The Journal of Comparative Neurology*, 184(1), 27–42. <https://doi.org/10.1002/cne.901840103>
- Gould, B. B., & Graybiel, A. M. (1976). Afferents to the cerebellar cortex in the cat: evidence for an intrinsic pathway leading from the deep nuclei to the cortex. *Brain Research*, 110(3), 601–611. [https://doi.org/10.1016/0006-8993\(76\)90869-6](https://doi.org/10.1016/0006-8993(76)90869-6)
- Green, J. D., & Morin, F. (1953). Hypothalamic electrical activity and hypothalamo-cortical relationship. *American Journal of Physiology*, 172, 175–186.
- Grieves, R. M., & Jeffery, K. J. (2017). The representation of space in the brain. *Behavioural Processes*, 135, 113–131. <https://doi.org/10.1016/j.beproc.2016.12.012>
- Guell, X., Schmahmann, J. D., Gabrieli, J. D., & Ghosh, S. S. (2018). Functional gradients of the cerebellum. *eLife*, 7. <https://doi.org/10.7554/elife.36652>

Gundappa-Sulur, G., De Schutter, E., & Bower, J. M. (1999). Ascending granule cell axon: An important component of cerebellar cortical circuitry. *Journal of Comparative Neurology*, 48(4).

- H -

Hafting, T., Fyhn, M., Molden, S., Moser, M., & Moser, E. I. (2005). Microstructure of a spatial map in the entorhinal cortex. *Nature*, 436(7052), 801–806. <https://doi.org/10.1038/nature03721>

Haines, D. E., May, P. J., & Dietrichs, E. (1990). Neuronal connections between the cerebellar nuclei and hypothalamus in *Macaca fascicularis*: Cerebello-visceral circuits. *The Journal of Comparative Neurology*, 299(1), 106–122. <https://doi.org/10.1002/cne.902990108>

Ham, J. J., & Yeo, C. H. (1992). Somatosensory Trigeminal Projections to the Inferior Olive, Cerebellum and other Precerebellar Nuclei in Rabbits. *European Journal of Neuroscience*, 4(4), 302–317. <https://doi.org/10.1111/j.1460-9568.1992.tb00878.x>

Hamori, J., Mezey, E., & Szentagothai, J. (1981). Electron microscopic identification of cerebellar nucleo-cortical mossy terminals in the rat. *Experimental Brain Research*, 44(1). <https://doi.org/10.1007/bf00238753>

Hariri, A. R. (2019). The Emerging Importance of the Cerebellum in Broad Risk for Psychopathology. *Neuron*, 102(1), 17–20. <https://doi.org/10.1016/j.neuron.2019.02.031>

Harper, J. W., & Heath, R. G. (1973). Anatomic connections of the fastigial nucleus to the rostral forebrain in the cat. *Experimental Neurology*, 39(2), 285–292. [https://doi.org/10.1016/0014-4886\(73\)90231-8](https://doi.org/10.1016/0014-4886(73)90231-8)

Hartley, T., Lever, C., Burgess, N., & O'Keefe, J. (2014). Space in the brain: how the hippocampal formation supports spatial cognition. *Philosophical Transactions of the Royal Society B: Biological Sciences*, 369(1635), 20120510. <https://doi.org/10.1098/rstb.2012.0510>

HARVEY, R., & NAPPER, R. (1991). Quantitative studies on the mammalian cerebellum. *Progress in Neurobiology*, 36(6), 437–463. [https://doi.org/10.1016/0301-0082\(91\)90012-p](https://doi.org/10.1016/0301-0082(91)90012-p)

Harvey, R. J., & Napper, R. M. A. (1988). Quantitative study of granule and Purkinje cells in the cerebellar cortex of the rat. *The Journal of Comparative Neurology*, 274(2), 151–157. <https://doi.org/10.1002/cne.902740202>

Hashimoto, M., & Mikoshiba, K. (2003). Mediolateral Compartmentalization of the Cerebellum Is Determined on the “Birth Date” of Purkinje Cells. *The Journal of Neuroscience*, 23(36), 11342–11351. <https://doi.org/10.1523/jneurosci.23-36-11342.2003>

Hashimoto, Y., Karube, F., Yanagawa, Y., Fujiyama, F., & Kano, M. (2018). Supramammillary Nucleus Afferents to the Dentate Gyrus Co-release Glutamate and GABA and Potentiate Granule Cell Output. *Cell Reports*, 25(10), 2704–2715. <https://doi.org/10.1016/j.celrep.2018.11.016>

Hausser, M. (2004). The Beat Goes On: Spontaneous Firing in Mammalian Neuronal Microcircuits. *Journal of Neuroscience*, 24(42), 9215–9219. <https://doi.org/10.1523/jneurosci.3375-04.2004>

Hawkes, R. (2014). Purkinje cell stripes and long-term depression at the parallel fiber-Purkinje cell synapse. *Frontiers in Systems Neuroscience*, 8. <https://doi.org/10.3389/fnsys.2014.00041>

- Hawkes, R., & Leclerc, N. (1989). Purkinje cell axon collateral distribution reflect the chemical compartmentation of the rat cerebellar cortex. *Brain Research*, 476(2), 279–290. [https://doi.org/10.1016/0006-8993\(89\)91248-1](https://doi.org/10.1016/0006-8993(89)91248-1)
- Heath, R. G., & Harper, J. W. (1974). Ascending projections of the cerebellar fastigial nucleus to the hippocampus, amygdala, and other temporal lobe sites: Evoked potential and histological studies in monkeys and cats. *Experimental Neurology*, 45(2), 268–287. [https://doi.org/10.1016/0014-4886\(74\)90118-6](https://doi.org/10.1016/0014-4886(74)90118-6)
- Heck, D. H., Thach, W. T., & Keating, J. G. (2007). On-beam synchrony in the cerebellum as the mechanism for the timing and coordination of movement. *Proceedings of the National Academy of Sciences*, 104(18), 7658–7663. <https://doi.org/10.1073/pnas.0609966104>
- Herculano-Houzel, S. (2010). Coordinated scaling of cortical and cerebellar numbers of neurons. *Frontiers in Neuroanatomy*, . <https://doi.org/10.3389/fnana.2010.00012>
- Hirel, J., Gaussier, P., Quoy, M., Banquet, J., Save, E., & Poucet, B. (2013). The hippocampo-cortical loop: Spatio-temporal learning and goal-oriented planning in navigation. *Neural Networks*, 43, 8–21. <https://doi.org/10.1016/j.neunet.2013.01.023>
- Hoche, F., Guell, X., Vangel, M. G., Sherman, J. C., & Schmahmann, J. D. (2017). The cerebellar cognitive affective/Schmahmann syndrome scale. *Brain*, 141(1), 248–270. <https://doi.org/10.1093/brain/awx317>
- Hoebeek, F. E., Witter, L., Ruigrok, T. J. H., & De Zeeuw, C. I. (2010). Differential olivo-cerebellar cortical control of rebound activity in the cerebellar nuclei. *Proceedings of the National Academy of Sciences*, 107(18), 8410–8415. <https://doi.org/10.1073/pnas.0907118107>
- Hoffmann, L. C., & Berry, S. D. (2009). Cerebellar theta oscillations are synchronized during hippocampal theta-contingent trace conditioning. *Proceedings of the National Academy of Sciences*, 106(50), 21371–21376. <https://doi.org/10.1073/pnas.0908403106>
- Hok, V., Save, E., Lenck-Santini, P. P., & Poucet, B. (2005). Coding for spatial goals in the prelimbic/infralimbic area of the rat frontal cortex. *Proceedings of the National Academy of Sciences*, 102(12), 4602–4607. <https://doi.org/10.1073/pnas.0407332102>
- HOLMES, G. (1917). THE SYMPTOMS OF ACUTE CEREBELLAR INJURIES DUE TO GUNSHOT INJURIES. *Brain*, 40(4), 461–535. <https://doi.org/10.1093/brain/40.4.461>
- Hoshi, E., Tremblay, L., Féger, J., Carras, P. L., & Strick, P. L. (2005). The cerebellum communicates with the basal ganglia. *Nature Neuroscience*, 8(11), 1491–1493. <https://doi.org/10.1038/nn1544>
- Houck, B. D., & Person, A. L. (2015). Cerebellar premotor output neurons collateralize to innervate the cerebellar cortex. *Journal of Comparative Neurology*, 523(15), 2254–2271. <https://doi.org/10.1002/cne.23787>
- Huang, C., Sugino, K., Shima, Y., Guo, C., Bai, S., Mensh, B. D., . . . Hantman, A. W. (2013). Convergence of pontine and proprioceptive streams onto multimodal cerebellar granule cells. *eLife*, 2. <https://doi.org/10.7554/elife.00400>
- Hull, C., & Regehr, W. (2012). Identification of an Inhibitory Circuit that Regulates Cerebellar Golgi Cell Activity. *Neuron*, 73(1), 149–158. <https://doi.org/10.1016/j.neuron.2011.10.030>

- Humphrey, D. R., Gold, R., & Reed, D. J. (1984). Sizes, laminar and topographic origins of cortical projections to the major divisions of the red nucleus in the monkey. *The Journal of Comparative Neurology*, 225(1), 75–94. <https://doi.org/10.1002/cne.902250109>
- Humphrey, D. R., & Rietz, R. R. (1976). Cells of origin of corticorubral projections from the arm area of primate motor cortex and their synaptic actions in the red nucleus. *Brain Research*, 110(1), 162–169. [https://doi.org/10.1016/0006-8993\(76\)90217-1](https://doi.org/10.1016/0006-8993(76)90217-1)
- Häusser, M., & Clark, B. A. (1997). Tonic Synaptic Inhibition Modulates Neuronal Output Pattern and Spatiotemporal Synaptic Integration. *Neuron*, 19(3), 665–678. [https://doi.org/10.1016/s0896-6273\(00\)80379-7](https://doi.org/10.1016/s0896-6273(00)80379-7)
- I -
- Ichinohe, N., Mori, F., & Shoumura, K. (2000). A di-synaptic projection from the lateral cerebellar nucleus to the laterodorsal part of the striatum via the central lateral nucleus of the thalamus in the rat. *Brain Research*, 880(1-2), 191–197. [https://doi.org/10.1016/s0006-8993\(00\)02744-x](https://doi.org/10.1016/s0006-8993(00)02744-x)
- Igloi, K., Zaoui, M., Berthoz, A., & Rondi-Reig, L. (2009). Sequential egocentric strategy is acquired as early as allocentric strategy: Parallel acquisition of these two navigation strategies. *Hippocampus*, 19(12), 1199–1211. <https://doi.org/10.1002/hipo.20595>
- Iglói, K., Doeller, C. F., Paradis, A., Benchenane, K., Berthoz, A., Burgess, N., & Rondi-Reig, L. (2015). Interaction Between Hippocampus and Cerebellum Crus I in Sequence-Based but not Place-Based Navigation. *Cerebral Cortex*, 25(11), 4146–4154. <https://doi.org/10.1093/cercor/bhu132>
- Ikai, Y., Takada, M., Shinonaga, Y., & Mizuno, N. (1992). Dopaminergic and non-dopaminergic neurons in the ventral tegmental area of the rat project, respectively, to the cerebellar cortex and deep cerebellar nuclei. *Neuroscience*, 51(3), 719–728. [https://doi.org/10.1016/0306-4522\(92\)90310-x](https://doi.org/10.1016/0306-4522(92)90310-x)
- Imamizu, H., Higuchi, S., Toda, A., & Kawato, M. (2007). Reorganization of Brain Activity for Multiple Internal Models After Short But Intensive Training. *Cortex*, 43(3), 338–349. [https://doi.org/10.1016/s0010-9452\(08\)70459-3](https://doi.org/10.1016/s0010-9452(08)70459-3)
- Isope, P., & Barbour, B. (2002). Faculty of 1000 evaluation for Properties of unitary granule cell->Purkinje cell synapses in adult rat cerebellar slices.. *F1000 - Post-publication peer review of the biomedical literature*, . <https://doi.org/10.3410/f.1010825.167958>
- ISOPE, P., DIEUDONNE, S., & BARBOUR, B. (2002). Temporal Organization of Activity in the Cerebellar Cortex: A Manifesto for Synchrony. *Annals of the New York Academy of Sciences*, 978(1 THE CEREBELLUM), 164–174. <https://doi.org/10.1111/j.1749-6632.2002.tb07564.x>
- Ito, H. T., Zhang, S., Witter, M. P., Moser, E. I., & Moser, M. (2015). A prefrontal–thalamo–hippocampal circuit for goal-directed spatial navigation. *Nature*, 522(7554), 50–55. <https://doi.org/10.1038/nature14396>
- Ito, M., & Kano, M. (1982). Long-lasting depression of parallel fiber-Purkinje cell transmission induced by conjunctive stimulation of parallel fibers and climbing fibers in the cerebellar cortex. *Neuroscience Letters*, 33(3), 253–258. [https://doi.org/10.1016/0304-3940\(82\)90380-9](https://doi.org/10.1016/0304-3940(82)90380-9)

Ito, M., Sakurai, M., & Tongroach, P. (1982). Climbing fibre induced depression of both mossy fibre responsiveness and glutamate sensitivity of cerebellar Purkinje cells. *The Journal of Physiology*, 324(1), 113–134. <https://doi.org/10.1113/jphysiol.1982.sp014103>

- J -

Jacob, P., Capitano, F., Poucet, B., Save, E., & Sargolini, F. (2019). Path integration maintains spatial periodicity of grid cell firing in a 1D circular track. *Nature Communications*, 10(1). <https://doi.org/10.1038/s41467-019-08795-w>

Jakab, R. L., & Hamori, J. (1988). Quantitative morphology and synaptology of cerebellar glomeruli in the rat. *Anatomy and Embryology*, 179(1), 81–88. <https://doi.org/10.1007/bf00305102>

Jansen, J., & Brodal, A. (1940). Experimental studies on the intrinsic fibers of the cerebellum. II. The cortico-nuclear projection. *The Journal of Comparative Neurology*, 73(2), 267–321. <https://doi.org/10.1002/cne.900730204>

Ji, Z., & Hawkes, R. (1994). Topography of purkinje cell compartments and mossy fiber terminal fields in lobules ii and iii of the rat cerebellar cortex: Spinocerebellar and cuneocerebellar projections. *Neuroscience*, 61(4), 935–954. [https://doi.org/10.1016/0306-4522\(94\)90414-6](https://doi.org/10.1016/0306-4522(94)90414-6)

Jones, E. G. (1985). *The Thalamus*. New York, EEUU: Plenum Press.

Jones, M. W., & Wilson, M. A. (2005). Theta Rhythms Coordinate Hippocampal–Prefrontal Interactions in a Spatial Memory Task. *PLoS Biology*, 3(12), 402. <https://doi.org/10.1371/journal.pbio.0030402>

Jwair, S., Coulon, P., & Ruigrok, T. J. H. (2017). Disynaptic Subthalamic Input to the Posterior Cerebellum in Rat. *Frontiers in Neuroanatomy*, 11. <https://doi.org/10.3389/fnana.2017.00013>

- K -

Takegawa, W., Katoh, A., Narumi, S., Miura, E., Motohashi, J., Takahashi, A., . . . Matsuda, S. (2018). Optogenetic Control of Synaptic AMPA Receptor Endocytosis Reveals Roles of LTD in Motor Learning. *Neuron*, 99(5), 985–998. <https://doi.org/10.1016/j.neuron.2018.07.034>

Kanichay, R. T., & Silver, R. A. (2008). Synaptic and Cellular Properties of the Feedforward Inhibitory Circuit within the Input Layer of the Cerebellar Cortex. *Journal of Neuroscience*, 28(36), 8955–8967. <https://doi.org/10.1523/jneurosci.5469-07.2008>

Karashima, A., Katayama, N., & Nakao, M. (2007). Phase-locking of spontaneous and tone-elicited pontine waves to hippocampal theta waves during REM sleep in rats. *Brain Research*, 1182, 73–81. <https://doi.org/10.1016/j.brainres.2007.08.060>

Karashima, A., Nakamura, K., Sato, N., Nakao, M., Katayama, N., & Yamamoto, M. (2002). Phase-locking of spontaneous and elicited ponto–geniculo–occipital waves is associated with acceleration of hippocampal theta waves during rapid eye movement sleep in cats. *Brain Research*, 958(2), 347–358. [https://doi.org/10.1016/s0006-8993\(02\)03673-9](https://doi.org/10.1016/s0006-8993(02)03673-9)

Kase, M., Noda, H., Suzuki, D., & Miller, D. (1979). Target velocity signals of visual tracking in vermal Purkinje cells of the monkey. *Science*, 205(4407), 717–720. <https://doi.org/10.1126/science.111350>

- Katoh, A., Shin, S., Kimpo, R. R., Rinaldi, J. M., & Raymond, J. L. (2015). Purkinje cell responses during visually and vestibularly driven smooth eye movements in mice. *Brain and Behavior*, *5*(3). <https://doi.org/10.1002/brb3.310>
- Kawato, M. (1999). Internal models for motor control and trajectory planning. *Current Opinion in Neurobiology*, *9*(6), 718–727. [https://doi.org/10.1016/s0959-4388\(99\)00028-8](https://doi.org/10.1016/s0959-4388(99)00028-8)
- Kelly, R. M., & Strick, P. L. (2003). Cerebellar Loops with Motor Cortex and Prefrontal Cortex of a Nonhuman Primate. *The Journal of Neuroscience*, *23*(23), 8432–8444. <https://doi.org/10.1523/jneurosci.23-23-08432.2003>
- Khosrovani, S., Van Der Giessen, R. S., De Zeeuw, C. I., & De Jeu, M. T. G. (2007). In vivo mouse inferior olive neurons exhibit heterogeneous subthreshold oscillations and spiking patterns. *Proceedings of the National Academy of Sciences*, *104*(40), 15911–15916. <https://doi.org/10.1073/pnas.0702727104>
- King, M., Hernandez-Castillo, C. R., Poldrack, R. A., Ivry, R. B., & Diedrichsen, J. (2019). Functional boundaries in the human cerebellum revealed by a multi-domain task battery. *Nature Neuroscience*, . <https://doi.org/10.1038/s41593-019-0436-x>
- Kleinfeld, D., Deschênes, M., & Ulanovsky, N. (2016). Whisking, Sniffing, and the Hippocampal  $\theta$ -Rhythm: A Tale of Two Oscillators. *PLOS Biology*, *14*(2(e1002385)). <https://doi.org/10.1371/journal.pbio.1002385>
- Kloosterman, F., Van Haeften, T., Witter, M. P., & Lopes da Silva, F. H. (2003). Electrophysiological characterization of interlaminar entorhinal connections: an essential link for re-entrance in the hippocampal-entorhinal system. *European Journal of Neuroscience*, *18*(11), 3037–3052. <https://doi.org/10.1111/j.1460-9568.2003.03046.x>
- Knogler, L. D., Markov, D. A., Dragomir, E. I., Štih, V., & Portugues, R. (2017). Sensorimotor Representations in Cerebellar Granule Cells in Larval Zebrafish Are Dense, Spatially Organized, and Non-temporally Patterned. *Current Biology*, *27*(9), 1288–1302. <https://doi.org/10.1016/j.cub.2017.03.029>
- Korbo, L., Andersen, B. B., Ladefoged, O., & Møller, A. (1993). Total numbers of various cell types in rat cerebellar cortex estimated using an unbiased stereological method. *Brain Research*, *609*(1-2), 262–268. [https://doi.org/10.1016/0006-8993\(93\)90881-m](https://doi.org/10.1016/0006-8993(93)90881-m)
- Korn, H., & Axelrad, H. (1980). Electrical Inhibition of Purkinje Cells in the Cerebellum of the Rat. *Proceedings of the National Academy of Sciences of the United States of America*, *77*(10), 6244–6247.
- Koziol, L. F., Budding, D., Andreasen, N., D'Arrigo, S., Bulgheroni, S., Imamizu, H., . . . Yamazaki, T. (2013). Consensus Paper: The Cerebellum's Role in Movement and Cognition. *The Cerebellum*, *13*(1), 151–177. <https://doi.org/10.1007/s12311-013-0511-x>
- Kralj-Hans, I., Baizer, J. S., Swales, C., & Glickstein, M. (2006). Independent roles for the dorsal paraflocculus and vermal lobule VII of the cerebellum in visuomotor coordination. *Experimental Brain Research*, *177*(2), 209–222. <https://doi.org/10.1007/s00221-006-0661-x>
- Krook-Magnuson, E., Szabo, G. G., Armstrong, C., Oijala, M., & Soltesz, I. (2014). Cerebellar Directed Optogenetic Intervention Inhibits Spontaneous Hippocampal Seizures in a Mouse Model of Temporal Lobe Epilepsy. *eNeuro*, *1*(1). <https://doi.org/10.1523/eneuro.0005-14.2014>

- Kuramoto, E., Furuta, T., Nakamura, K. C., Unzai, T., Hioki, H., & Kaneko, T. (2009). Two Types of Thalamocortical Projections from the Motor Thalamic Nuclei of the Rat: A Single Neuron-Tracing Study Using Viral Vectors. *Cerebral Cortex*, *19*(9), 2065–2077. <https://doi.org/10.1093/cercor/bhn231>
- Kuramoto, E., Ohno, S., Furuta, T., Unzai, T., Tanaka, Y. R., Hioki, H., & Kaneko, T. (2013). Ventral Medial Nucleus Neurons Send Thalamocortical Afferents More Widely and More Preferentially to Layer 1 than Neurons of the Ventral Anterior–Ventral Lateral Nuclear Complex in the Rat. *Cerebral Cortex*, *25*(1), 221–235. <https://doi.org/10.1093/cercor/bht216>
- Köhler, C. (1985). Intrinsic projections of the retrohippocampal region in the rat brain. I. The subicular complex. *Journal of Comparative Neurology*, *236*(4), 504–522. <https://doi.org/10.1002/cne.902360407>
- L -
- Lalonde, R., Lamarre, Y., & Smith, A. M. (1988). Does the mutant mouse lurcher have deficits in spatially oriented behaviours? *Brain Research*, *455*, 24–30.
- Lang, E. J., Sugihara, I., & Llinás, R. (1996). GABAergic Modulation of Complex Spike Activity by the Cerebellar Nucleoolivary Pathway in Rat. *Journal of Neurophysiology*, *76*(1), 255–275.
- Larriva-Sahd, J. A. (2014). Some predictions of Rafael Lorente de Nó 80 years later. *Frontiers in Neuroanatomy*, *8*. <https://doi.org/10.3389/fnana.2014.00147>
- Larsell, O., & Jansen, J. (1970). *The Comparative Anatomy and Histology of the Cerebellum: From Monotremes Through Apes*. Minnesota, EEUU: University of Minnesota Press.
- Latchoumane, C. V., Ngo, H. V., Born, J., & Shin, H. (2017). Thalamic Spindles Promote Memory Formation during Sleep through Triple Phase-Locking of Cortical, Thalamic, and Hippocampal Rhythms. *Neuron*, *95*(2), 424–435. <https://doi.org/10.1016/j.neuron.2017.06.025>
- Leergaard, T. B. (2007). Topography of the complete corticopontine projection: From experiments to principal maps. *Frontiers in Neuroscience*, *1*(1), 211–223. <https://doi.org/10.3389/neuro.01.1.1.016.2007>
- Lefort, J. M., Vincent, J., Tallot, L., Jarlier, F., De Zeeuw, C. I., Rondi-Reig, L., & Rochefort, C. (2019). Impaired cerebellar Purkinje cell potentiation generates unstable spatial map orientation and inaccurate navigation. *Nature Communications*, *10*(1). <https://doi.org/10.1038/s41467-019-09958-5>
- Leznik, E., Makarenko, V., & Llinás, R. (2002). Electrotonically Mediated Oscillatory Patterns in Neuronal Ensembles: An In Vitro Voltage-Dependent Dye-Imaging Study in the Inferior Olive. *The Journal of Neuroscience*, *22*(7), 2804–2815. <https://doi.org/10.1523/jneurosci.22-07-02804.2002>
- Light, G. A., Hsu, J. L., Hsieh, M. H., Meyer-Gomes, K., Sprock, J., Swerdlow, N. R., & Braff, D. L. (2006). Gamma Band Oscillations Reveal Neural Network Cortical Coherence Dysfunction in Schizophrenia Patients. *Biological Psychiatry*, *60*(11), 1231–1240. <https://doi.org/10.1016/j.biopsych.2006.03.055>
- Limperopoulos, C., Chilingaryan, G., Sullivan, N., Guizard, N., Robertson, R. L., & Du Plessis, A. J. (2012). Injury to the Premature Cerebellum: Outcome is Related to Remote Cortical Development. *Cerebral Cortex*, *24*(3), 728–736. <https://doi.org/10.1093/cercor/bhs354>

- Llinás, R., Walton, K., Hillman, D., & Sotelo, C. (1975). Inferior olive: its role in motor learning. *Science*, *190*(4220), 1230–1231. <https://doi.org/10.1126/science.128123>
- Llinás, R. (1980). Electrophysiological properties of in vitro Purkinje cell dendrites in mammalian cerebellar slices. *The Journal of Physiology*, *305*, 197–213.
- Llinás, R. (1982). General Discussion: Radial Connectivity in the Cerebellar Cortex: A Novel View Regarding the Functional Organization of the Molecular Layer. *The Cerebellum—New Vistas*, , 189–194. [https://doi.org/10.1007/978-3-642-68560-6\\_10](https://doi.org/10.1007/978-3-642-68560-6_10)
- Llinás, R. R. (2014). The olivo-cerebellar system: a key to understanding the functional significance of intrinsic oscillatory brain properties. *Frontiers in Neural Circuits*, *7*. <https://doi.org/10.3389/fncir.2013.00096>
- Locke, T. M., Soden, M. E., Miller, S. M., Hunker, A., Knakal, C., Licholai, J. A., . . . Carlson, E. S. (2018). Dopamine D1 Receptor–Positive Neurons in the Lateral Nucleus of the Cerebellum Contribute to Cognitive Behavior. *Biological Psychiatry*, *84*(6), 401–412. <https://doi.org/10.1016/j.biopsych.2018.01.019>
- Loewenstein, Y., Mahon, S., Chadderton, P., Kitamura, K., Sompolinsky, H., Yarom, Y., & Häusser, M. (2005). Bistability of cerebellar Purkinje cells modulated by sensory stimulation. *Nature Neuroscience*, *8*(2), 202–211. <https://doi.org/10.1038/nn1393>
- Lorente De Nó, R. (1934). Studies on the structure of the cerebral cortex. II. Continuation of the study of the ammonic system. *Journal für Psychologie und Neurologie*, *46*, 113–177.
- Lübbert, M., Goral, R. O., Keine, C., Thomas, C., Guerrero-Given, D., Putzke, T., . . . Young, S. M. (2019). CaV2.1  $\alpha$ 1 Subunit Expression Regulates Presynaptic CaV2.1 Abundance and Synaptic Strength at a Central Synapse. *Neuron*, *101*(2), 260–273. <https://doi.org/10.1016/j.neuron.2018.11.028>
- M -
- Mano, N. (1970). Changes of Simple and Complex Spike Activity of Cerebellar Purkinje Cells with Sleep and Waking. *Science*, *170*(3964), 1325–1327. <https://doi.org/10.1126/science.170.3964.1325>
- Mapelli, L., Pagani, M., Garrido, J. A., & D’Angelo, E. (2015). Integrated plasticity at inhibitory and excitatory synapses in the cerebellar circuit. *Frontiers in Cellular Neuroscience*, *9*. <https://doi.org/10.3389/fncel.2015.00169>
- Marr, D. (1969). A theory of cerebellar cortex. *The Journal of Physiology*, *202*(2), 437–470. <https://doi.org/10.1113/jphysiol.1969.sp008820>
- Marshall, L., & Born, J. (2007). The contribution of sleep to hippocampus-dependent memory consolidation. *Trends in Cognitive Sciences*, *11*(10), 442–450. <https://doi.org/10.1016/j.tics.2007.09.001>
- Maruta, J., Hensbroek, R. A., & Simpson, J. I. (2007). Intraburst and Interburst Signaling by Climbing Fibers. *Journal of Neuroscience*, *27*(42), 11263–11270. <https://doi.org/10.1523/jneurosci.2559-07.2007>
- McAfee, S. S., Liu, Y., Sillitoe, R. V., & Heck, D. H. (2019). Cerebellar Lobulus Simplex and Crus I Differentially Represent Phase and Phase Difference of Prefrontal Cortical and Hippocampal Oscillations. *Cell Reports*, *27*(8), 2328–2334. <https://doi.org/10.1016/j.celrep.2019.04.085>

- McNaughton, B. L., Battaglia, F. P., Jensen, O., Moser, E. I., & Moser, M. (2006). Path integration and the neural basis of the 'cognitive map'. *Nature Reviews Neuroscience*, 7(8), 663–678. <https://doi.org/10.1038/nrn1932>
- Middleton, F., & Strick, P. (1994). Anatomical evidence for cerebellar and basal ganglia involvement in higher cognitive function. *Science*, 266(5184), 458–461. <https://doi.org/10.1126/science.7939688>
- Middleton, F. A., & Strick, P. L. (1998). Cerebellar output: motor and cognitive channels. *Trends in Cognitive Sciences*, 2(9), 348–354. [https://doi.org/10.1016/s1364-6613\(98\)01220-0](https://doi.org/10.1016/s1364-6613(98)01220-0)
- Middleton, S. J., Racca, C., Cunningham, M. O., Traub, R. D., Monyer, H., Knöpfel, T., . . . Whittington, M. A. (2008). High-Frequency Network Oscillations in Cerebellar Cortex. *Neuron*, 58(5), 763–774. <https://doi.org/10.1016/j.neuron.2008.03.030>
- Mihailoff, G. A., Burne, R. A., Azizi, S. A., Norell, G., & Woodward, D. J. (1981). The pontocerebellar system in the rat: An HRP study. II. Hemispherical components. *The Journal of Comparative Neurology*, 197(4), 559–577. <https://doi.org/10.1002/cne.901970403>
- Mizumori, S., & Williams, J. (1993). Directionally selective mnemonic properties of neurons in the lateral dorsal nucleus of the thalamus of rats. *The Journal of Neuroscience*, 13(9), 4015–4028. <https://doi.org/10.1523/jneurosci.13-09-04015.1993>
- Moberget, T., Alnæs, D., Kaufmann, T., Doan, N. T., Córdova-Palomera, A., Norbom, L. B., . . . Westlye, L. T. (2019). Cerebellar Gray Matter Volume Is Associated With Cognitive Function and Psychopathology in Adolescence. *Biological Psychiatry*, 86(1), 65–75. <https://doi.org/10.1016/j.biopsych.2019.01.019>
- Morris, R. (1984). Developments of a water-maze procedure for studying spatial learning in the rat. *Journal of Neuroscience Methods*, 11(1), 47–60. [https://doi.org/10.1016/0165-0270\(84\)90007-4](https://doi.org/10.1016/0165-0270(84)90007-4)
- Moser, E., & Moser, M. (1998). Functional differentiation in the hippocampus. *Hippocampus*, 8(16).
- Moser, E., Moser, M., & Andersen, P. (1993). Spatial learning impairment parallels the magnitude of dorsal hippocampal lesions, but is hardly present following ventral lesions. *The Journal of Neuroscience*, 13(9), 3916–3925. <https://doi.org/10.1523/jneurosci.13-09-03916.1993>
- Moser, E. I., Moser, M., & McNaughton, B. L. (2017). Spatial representation in the hippocampal formation: a history. *Nature Neuroscience*, 20(11), 1448–1464. <https://doi.org/10.1038/nn.4653>
- Muller, R., & Kubie, J. (1987). The effects of changes in the environment on the spatial firing of hippocampal complex-spike cells. *The Journal of Neuroscience*, 7(7), 1951–1968. <https://doi.org/10.1523/jneurosci.07-07-01951.1987>
- N -
- Naber, P. A., Lopes da Silva, F. H., & Witter, M. P. (2001). Reciprocal connections between the entorhinal cortex and hippocampal fields CA1 and the subiculum are in register with the projections from CA1 to the subiculum. *Hippocampus*, 11(2), 99–104. <https://doi.org/10.1002/hipo.1028>
- Nadel, L. (1968). Dorsal and ventral hippocampal lesions and behavior. *Physiology & Behavior*, 3(6), 891–900. [https://doi.org/10.1016/0031-9384\(68\)90174-1](https://doi.org/10.1016/0031-9384(68)90174-1)

- Newman, P. P., & Reza, H. (1979). Functional relationships between the hippocampus and the cerebellum: an electrophysiological study of the cat. *Journal of Physiology*, *287*, 405–426.
- Nitschke, M. F., Binkofski, F., Buccino, G., Posse, S., Erdmann, C., Kömpf, D., . . . Heide, W. (2004). Activation of cerebellar hemispheres in spatial memorization of saccadic eye movements: An fMRI study. *Human Brain Mapping*, *22*(2), 155–164. <https://doi.org/10.1002/hbm.20025>
- Nitz, D. A. (2006). Tracking Route Progression in the Posterior Parietal Cortex. *Neuron*, *49*(5), 747–756. <https://doi.org/10.1016/j.neuron.2006.01.037>
- Noda, H., & Fujikado, T. (1987). Involvement of Purkinje cells in evoking saccadic eye movements by microstimulation of the posterior cerebellar vermis of monkeys. *Journal of Neurophysiology*, *57*(5), 1247–1261. <https://doi.org/10.1152/jn.1987.57.5.1247>
- O -
- O'Connor, S. M., Berg, R. W., & Kleinfeld, D. (2002). Coherent Electrical Activity Between Vibrissa Sensory Areas of Cerebellum and Neocortex Is Enhanced During Free Whisking. *Journal of Neurophysiology*, *87*(4), 2137–2148. <https://doi.org/10.1152/jn.00229.2001>
- O'Keefe, J., & Dostrovsky, J. (1971). The hippocampus as a spatial map. Preliminary evidence from unit activity in the freely-moving rat. *Brain Research*, *34*(1), 171–175. [https://doi.org/10.1016/0006-8993\(71\)90358-1](https://doi.org/10.1016/0006-8993(71)90358-1)
- O'Keefe, J., & Nadel, L. (1978). *The Hippocampus as a Cognitive Map*. Oxford, EEUU: Oxford University Press.
- O'Reilly, J. X., Beckmann, C. F., Tomassini, V., Ramnani, N., & Johansen-Berg, H. (2009). Distinct and Overlapping Functional Zones in the Cerebellum Defined by Resting State Functional Connectivity. *Cerebral Cortex*, *20*(4), 953–965. <https://doi.org/10.1093/cercor/bhp157>
- Ohmae, S., & Medina, J. F. (2015). Climbing fibers encode a temporal-difference prediction error during cerebellar learning in mice. *Nature Neuroscience*, *18*(12), 1798–1803. <https://doi.org/10.1038/nn.4167>
- Ohtsuka, K., & Noda, H. (1995). Discharge properties of Purkinje cells in the oculomotor vermis during visually guided saccades in the macaque monkey. *Journal of Neurophysiology*, *74*(5), 1828–1840. <https://doi.org/10.1152/jn.1995.74.5.1828>
- Oostland, M., & Van Hooft, J. (2013). The role of serotonin in cerebellar development. *Neuroscience*, *248*, 201–212. <https://doi.org/10.1016/j.neuroscience.2013.05.029>
- Orduz, D., & Llano, I. (2007). Recurrent axon collaterals underlie facilitating synapses between cerebellar Purkinje cells. *Proceedings of the National Academy of Sciences*, *104*(45), 17831–17836. <https://doi.org/10.1073/pnas.0707489104>
- Oscarsson, O. (1979). Functional units of the cerebellum - sagittal zones and microzones. *Trends in Neurosciences*, *2*, 143–145. [https://doi.org/10.1016/0166-2236\(79\)90057-2](https://doi.org/10.1016/0166-2236(79)90057-2)
- Ozden, I., Sullivan, M. R., Lee, H. M., & Wang, S. S. (2009). Reliable Coding Emerges from Coactivation of Climbing Fibers in Microbands of Cerebellar Purkinje Neurons. *Journal of Neuroscience*, *29*(34), 10463–10473. <https://doi.org/10.1523/jneurosci.0967-09.2009>

Ozol, K., Hayden, J. M., Oberdick, J., & Hawkes, R. (1999). Transverse zones in the vermis of the mouse cerebellum. *Journal of Comparative Neurology*, 412(1), 95–111.

- P -

Palay, S. L., & Chan-Palay, V. (1974). *Cerebellar Cortex: Cytology and Organization*. New York, EEUU: Springer Berlin Heidelberg.

Parent, A., & Hazrati, L. (1995). Functional anatomy of the basal ganglia. II. The place of subthalamic nucleus and external pallidum in basal ganglia circuitry. *Brain Research Reviews*, 20(1), 128–154. [https://doi.org/10.1016/0165-0173\(94\)00008-d](https://doi.org/10.1016/0165-0173(94)00008-d)

Paul, S. M., Heath, R. G., & Ellison, J. P. (1973). Histochemical demonstration of a direct pathway from the fastigial nucleus to the septal region. *Experimental Neurology*, 40(3), 798–805. [https://doi.org/10.1016/0014-4886\(73\)90113-1](https://doi.org/10.1016/0014-4886(73)90113-1)

Peter, S., Ten Brinke, M. M., Stedehouder, J., Reinelt, C. M., Wu, B., Zhou, H., . . . De Zeeuw, C. I. (2016). Dysfunctional cerebellar Purkinje cells contribute to autism-like behaviour in Shank2-deficient mice. *Nature Communications*, 7(1). <https://doi.org/10.1038/ncomms12627>

Petrosini, L., Leggio, M. G., & Molinari, M. (1998). THE CEREBELLUM IN THE SPATIAL PROBLEM SOLVING: A CO-STAR OR A GUEST STAR? *Progress in Neurobiology*, 56, 191–210.

Pichitpornchai, C., Rawson, J. A., & Rees, S. (1994). Morphology of parallel fibres in the cerebellar cortex of the rat: An experimental light and electron microscopic study with biocytin. *The Journal of Comparative Neurology*, 342(2), 206–220. <https://doi.org/10.1002/cne.903420205>

Pijpers, A., & Ruigrok, T. J. (2006a). Organization of pontocerebellar projections to identified climbing fiber zones in the rat. *The Journal of Comparative Neurology*, 496(4), 513–528. <https://doi.org/10.1002/cne.20940>

Pijpers, A., & Ruigrok, T. J. (2006b). Organization of pontocerebellar projections to identified climbing fiber zones in the rat. *The Journal of Comparative Neurology*, 496(4), 513–528. <https://doi.org/10.1002/cne.20940>

Popa, D., Spolidoro, M., Proville, R. D., Guyon, N., Belliveau, L., & Lena, C. (2013). Functional Role of the Cerebellum in Gamma-Band Synchronization of the Sensory and Motor Cortices. *Journal of Neuroscience*, 33(15), 6552–6556. <https://doi.org/10.1523/jneurosci.5521-12.2013>

Poucet, B., Chaillan, F., Truchet, B., Save, E., Sargolini, F., & Hok, V. (2015). Is there a pilot in the brain? Contribution of the self-positioning system to spatial navigation. *Frontiers in Behavioral Neuroscience*, 9. <https://doi.org/10.3389/fnbeh.2015.00292>

Poucet, B., Sargolini, F., Song, E. Y., Hangya, B., Fox, S., & Muller, R. U. (2014). Independence of landmark and self-motion-guided navigation: a different role for grid cells. *Philosophical Transactions of the Royal Society B: Biological Sciences*, 369(1635), 20130370. <https://doi.org/10.1098/rstb.2013.0370>

Prevosto, V., & Sommer, M. A. (2013). Cognitive control of movement via the cerebellar-recipient thalamus. *Frontiers in Systems Neuroscience*, 7. <https://doi.org/10.3389/fnsys.2013.00056>

- Proville, R. D., Spolidoro, M., Guyon, N., Dugué, G. P., Selimi, F., Isope, P., . . . Léna, C. (2014). Cerebellum involvement in cortical sensorimotor circuits for the control of voluntary movements. *Nature Neuroscience*, 17(9), 1233–1239. <https://doi.org/10.1038/nn.3773>
- Pérez-Escobar, J. A., Kornienko, O., Latuske, P., Kohler, L., & Allen, K. (2016). Visual landmarks sharpen grid cell metric and confer context specificity to neurons of the medial entorhinal cortex. *eLife*, 5. <https://doi.org/10.7554/elife.16937>
- R -
- Ramnani, N. (2006). The primate cortico-cerebellar system: anatomy and function. *Nature Reviews Neuroscience*, 7(7), 511–522. <https://doi.org/10.1038/nrn1953>
- Ramón y Cajal, S. (1911). *Histologie du système nerveux de l'homme et des vertébrés*. Paris, Maloine: Tome II.
- Reeber, S. L., White, J. J., George-Jones, N. A., & Sillitoe, R. V. (2013). Architecture and development of olivocerebellar circuit topography. *Frontiers in Neural Circuits*, 6. <https://doi.org/10.3389/fncir.2012.00115>
- Reinoso-Suaáñez, F. (1992). Considerations on thalamic and pontine sleep mechanisms. in *Fundamental Neurobiology*. ed Velluti R., editor, , 59–71.
- Rennó-Costa, C., & Tort, A. B. (2017). Place and Grid Cells in a Loop: Implications for Memory Function and Spatial Coding. *The Journal of Neuroscience*, 37(34), 8062–8076. <https://doi.org/10.1523/jneurosci.3490-16.2017>
- Rocheffort, C., Arabo, A., Andre, M., Poucet, B., Save, E., & Rondi-Reig, L. (2011). Cerebellum Shapes Hippocampal Spatial Code. *Science*, 334(6054), 385–389. <https://doi.org/10.1126/science.1207403>
- Rocheffort, C., Lefort, J., & Rondi-Reig, L. (2013). The cerebellum: a new key structure in the navigation system. *Frontiers in Neural Circuits*, 7. <https://doi.org/10.3389/fncir.2013.00035>
- Rokni, D., Llinás, R., & Yarom, Y. (2008). The morpho/functional discrepancy in the cerebellar cortex: Looks alone are deceptive. *frontiers in Neuroscience*, 2(2), 192–198. <https://doi.org/10.3389/neuro.01.036.2008>
- Romer, A. L., Knodt, A. R., Houts, R., Brigidi, B. D., Moffitt, T. E., Caspi, A., & Hariri, A. R. (2018). Structural alterations within cerebellar circuitry are associated with general liability for common mental disorders. *Molecular Psychiatry*, 23(4), 1084–1090. <https://doi.org/10.1038/mp.2017.57>
- Rondi-Reig, L., & Burguière, E. (2005). Is the cerebellum ready for navigation? *Progress in Brain Research*, , 199–212. [https://doi.org/10.1016/s0079-6123\(04\)48017-0](https://doi.org/10.1016/s0079-6123(04)48017-0)
- Rondi-Reig, L., Le Marec, N., Caston, J., & Mariani, J. (2002). The role of climbing and parallel fibers inputs to cerebellar cortex in navigation. *Behavioural Brain Research*, 132(1), 11–18. [https://doi.org/10.1016/s0166-4328\(01\)00381-3](https://doi.org/10.1016/s0166-4328(01)00381-3)
- Rondi-Reig, L., Paradis, A., Lefort, J. M., Babayan, B. M., & Tobin, C. (2014). How the cerebellum may monitor sensory information for spatial representation. *Frontiers in Systems Neuroscience*, 8. <https://doi.org/10.3389/fnsys.2014.00205>

- Ros, H., Sachdev, R. N. S., Yu, Y., Sestan, N., & McCormick, D. A. (2009). Neocortical Networks Entrain Neuronal Circuits in Cerebellar Cortex. *Journal of Neuroscience*, *29*(33), 10309–10320. <https://doi.org/10.1523/jneurosci.2327-09.2009>
- Rosenblatt, F. (1958). The perceptron: A probabilistic model for information storage and organization in the brain.. *Psychological Review*, *65*(6), 386–408. <https://doi.org/10.1037/h0042519>
- Rowland, D. C., Weible, A. P., Wickersham, I. R., Wu, H., Mayford, M., Witter, M. P., & Kentros, C. G. (2013). Transgenically Targeted Rabies Virus Demonstrates a Major Monosynaptic Projection from Hippocampal Area CA2 to Medial Entorhinal Layer II Neurons. *Journal of Neuroscience*, *33*(37), 14889–14898. <https://doi.org/10.1523/jneurosci.1046-13.2013>
- Ruigrok, T. J. H. (2010). Ins and Outs of Cerebellar Modules. *The Cerebellum*, *10*(3), 464–474. <https://doi.org/10.1007/s12311-010-0164-y>
- Ruigrok, T. J. H., Van Touw, S., & Coulon, P. (2016). Caveats in Transneuronal Tracing with Unmodified Rabies Virus: An Evaluation of Aberrant Results Using a Nearly Perfect Tracing Technique. *Frontiers in Neural Circuits*, *10*. <https://doi.org/10.3389/fncir.2016.00046>
- S -
- Saint-Cyr, J., & Woodward, D. (1980). A Topographic analysis of limbic and somatic inputs to the cerebellar cortex in the rat. *Experimental Brain Research*, *40*(1). <https://doi.org/10.1007/bf00236658>
- Santamaria, F., Tripp, P. G., & Bower, J. M. (2007). Feedforward Inhibition Controls the Spread of Granule Cell–Induced Purkinje Cell Activity in the Cerebellar Cortex. *Journal of Neurophysiology*, *97*(1), 248–263. <https://doi.org/10.1152/jn.01098.2005>
- Sargolini, F. (2006). Conjunctive Representation of Position, Direction, and Velocity in Entorhinal Cortex. *Science*, *312*(5774), 758–762. <https://doi.org/10.1126/science.1125572>
- Sarnthein, J., & Jeanmonod, D. (2007). High Thalamocortical Theta Coherence in Patients with Parkinson's Disease. *Journal of Neuroscience*, *27*(1), 124–131. <https://doi.org/10.1523/jneurosci.2411-06.2007>
- Save, E., Cressant, A., Thinus-Blanc, C., & Poucet, B. (1998). Spatial Firing of Hippocampal Place Cells in Blind Rats. *The Journal of Neuroscience*, *18*(5), 1818–1826. <https://doi.org/10.1523/jneurosci.18-05-01818.1998>
- Save, E., Nerad, L. N., & Poucet, B. (2000). Contribution of multiple sensory information to place field stability in hippocampal place cells. *Hippocampus*, *10*(1).
- Save, E., Guazzelli, A., & Poucet, B. (2001). Dissociation of the effects of bilateral lesions of the dorsal hippocampus and parietal cortex on path integration in the rat.. *Behavioral Neuroscience*, *115*(6), 1212–1223. <https://doi.org/10.1037/0735-7044.115.6.1212>
- Save, E., & Poucet, B. (2009). Role of the parietal cortex in long-term representation of spatial information in the rat. *Neurobiology of Learning and Memory*, *91*(2), 172–178. <https://doi.org/10.1016/j.nlm.2008.08.005>
- Schell, G., & Strick, P. (1984). The origin of thalamic inputs to the arcuate premotor and supplementary motor areas. *The Journal of Neuroscience*, *4*(2), 539–560. <https://doi.org/10.1523/jneurosci.04-02-00539.1984>

- Schilling, K., Oberdick, J., Rossi, F., & Baader, S. L. (2008). Besides Purkinje cells and granule neurons: an appraisal of the cell biology of the interneurons of the cerebellar cortex. *Histochemistry and Cell Biology*, 130(4), 601–615. <https://doi.org/10.1007/s00418-008-0483-y>
- Schmahmann, J., MacMore, J., & Vangel, M. (2009). Cerebellar stroke without motor deficit: clinical evidence for motor and non-motor domains within the human cerebellum. *Neuroscience*, 162(3), 852–861. <https://doi.org/10.1016/j.neuroscience.2009.06.023>
- Schmahmann, J. D. (1998). The cerebellar cognitive affective syndrome. *Brain*, 121, 561–579.
- Schmahmann, J. D. (2010). The Role of the Cerebellum in Cognition and Emotion: Personal Reflections Since 1982 on the Dysmetria of Thought Hypothesis, and Its Historical Evolution from Theory to Therapy. *Neuropsychology Review*, 20(3), 236–260. <https://doi.org/10.1007/s11065-010-9142-x>
- Schmahmann, J. D. (2019). The cerebellum and cognition. *Neuroscience Letters*, 688, 62–75. <https://doi.org/10.1016/j.neulet.2018.07.005>
- Schonewille, M., Belmeguenai, A., Koekkoek, S., Houtman, S., Boele, H., Van Beugen, B., . . . De Zeeuw, C. (2010). Purkinje Cell-Specific Knockout of the Protein Phosphatase PP2B Impairs Potentiation and Cerebellar Motor Learning. *Neuron*, 67(4), 618–628. <https://doi.org/10.1016/j.neuron.2010.07.009>
- Schonewille, M., Gao, Z., Boele, H., Vinueza Veloz, M., Amerika, W., Šimek, A., . . . De Zeeuw, C. (2011). Reevaluating the Role of LTD in Cerebellar Motor Learning. *Neuron*, 70(1), 43–50. <https://doi.org/10.1016/j.neuron.2011.02.044>
- SCOTT, T. G. (1963). A Unique Pattern of Localization within the Cerebellum. *Nature*, 200(4908), 793. <https://doi.org/10.1038/200793a0>
- Scoville, W. B., & Milner, B. (1957). LOSS OF RECENT MEMORY AFTER BILATERAL HIPPOCAMPAL LESIONS. *Journal of Neurosurgery and Psychiatry*, 20(11).
- Serapide, M. F., Pantó, M. R., Zappalá, A., & Cicirata, F. (2001). Multiple zonal projections of the basilar pontine nuclei to the cerebellar cortex of the rat. *Journal of Comparative Neurology*, 430(4).
- Shambes, G. M., Gibson, J. M., & Welker, W. (1978). Fractured Somatotopy in Granule Cell Tactile Areas of Rat Cerebellar Hemispheres Revealed by Micromapping; pp. 94–105. *Brain, Behavior and Evolution*, 15(2), 94–105. <https://doi.org/10.1159/000123774>
- Shin, S., Hoebeek, F. E., Schonewille, M., De Zeeuw, C. I., Aertsen, A., & De Schutter, E. (2007). Regular Patterns in Cerebellar Purkinje Cell Simple Spike Trains. *PLoS ONE*, 2(5(e485)). <https://doi.org/10.1371/journal.pone.0000485>
- Shinoda, Y., Sugiuchi, Y., Futami, T., & Izawa, R. (1992). Axon collaterals of mossy fibers from the pontine nucleus in the cerebellar dentate nucleus. *Journal of Neurophysiology*, 67(3), 547–560. <https://doi.org/10.1152/jn.1992.67.3.547>
- Shinoda, Y., Tanaka, T., Tominaga-Yoshino, K., & Ogura, A. (2010). Persistent Synapse Loss Induced by Repetitive LTD in Developing Rat Hippocampal Neurons. *PLoS ONE*, 5(4(e10390)). <https://doi.org/10.1371/journal.pone.0010390>
- Sillitoe, R. V., Chung, S., Fritschy, J., Hoy, M., & Hawkes, R. (2008). Golgi Cell Dendrites Are Restricted by Purkinje Cell Stripe Boundaries in the Adult Mouse Cerebellar Cortex. *Journal of Neuroscience*, 28(11), 2820–2826. <https://doi.org/10.1523/jneurosci.4145-07.2008>

- Simpson, J. I., Wylie, D. R. W., & De Zeeuw, C. (1996). More on climbing fiber signals and their consequence(s). *Behavioral and Brain Sciences*, 19(03), 496–498. <https://doi.org/10.1017/s0140525x00081991>
- Snider, R. S., & Maiti, A. (1976). Cerebellar contributions to the papez circuit. *Journal of Neuroscience Research*, 2(2), 133–146. <https://doi.org/10.1002/jnr.490020204>
- Snider, R. S., & Stowell, A. (1944). RECEIVING AREAS OF THE TACTILE, AUDITORY, AND VISUAL SYSTEMS IN THE CEREBELLUM. *Journal of Neurophysiology*, 7(6), 331–357. <https://doi.org/10.1152/jn.1944.7.6.331>
- Snyder, L. H., Grieve, K. L., Brotchie, P., & Andersen, R. A. (1998). Separate body- and world-referenced representations of visual space in parietal cortex. *Nature*, 394(6696), 887–891. <https://doi.org/10.1038/29777>
- Solinas, S. (2007). Fast-reset of pacemaking and theta-frequency resonance patterns in cerebellar golgi cells: Simulations of their impact in vivo. *Frontiers in Cellular Neuroscience*, 1. <https://doi.org/10.3389/neuro.03.004.2007>
- Sotelo, C. (2008). Viewing the Cerebellum through the Eyes of Ramón Y Cajal. *The Cerebellum*, 7(4), 517–522. <https://doi.org/10.1007/s12311-008-0078-0>
- Soteropoulos, D. S., & Baker, S. N. (2006). Cortico-Cerebellar Coherence During a Precision Grip Task in the Monkey. *Journal of Neurophysiology*, 95(2), 1194–1206. <https://doi.org/10.1152/jn.00935.2005>
- Spiers, H. J. (2008). Keeping the goal in mind: Prefrontal contributions to spatial navigation. *Neuropsychologia*, 46(7), 2106–2108. <https://doi.org/10.1016/j.neuropsychologia.2008.01.028>
- Stackman, R. W., & Taube, J. S. (1998). Firing Properties of Rat Lateral Mammillary Single Units: Head Direction, Head Pitch, and Angular Head Velocity. *The Journal of Neuroscience*, 18(21), 9020–9037. <https://doi.org/10.1523/jneurosci.18-21-09020.1998>
- Stackman, R. W., Golob, E. J., Bassett, J. P., & Taube, J. S. (2003). Passive Transport Disrupts Directional Path Integration by Rat Head Direction Cells. *Journal of Neurophysiology*, 90(5), 2862–2874. <https://doi.org/10.1152/jn.00346.2003>
- Stahl, J. S. (2004). Using eye movements to assess brain function in mice. *Vision Research*, 44(28), 3401–3410. <https://doi.org/10.1016/j.visres.2004.09.011>
- Steinbusch, H., Verhofstad, A., & Joosten, H. (1978). Localization of serotonin in the central nervous system by immunohistochemistry: Description of a specific and sensitive technique and some applications. *Neuroscience*, 3(9), 811–819. [https://doi.org/10.1016/0306-4522\(78\)90033-7](https://doi.org/10.1016/0306-4522(78)90033-7)
- Stensola, H., Stensola, T., Solstad, T., Frøland, K., Moser, M., & Moser, E. I. (2012). The entorhinal grid map is discretized. *Nature*, 492(7427), 72–78. <https://doi.org/10.1038/nature11649>
- Stevens, R., & Cowey, A. (1973). Effects of dorsal and ventral hippocampal lesions on spontaneous alternation, learned alternation and probability learning in rats. *Brain Research*, 52, 203–224. [https://doi.org/10.1016/0006-8993\(73\)90659-8](https://doi.org/10.1016/0006-8993(73)90659-8)

- Stoodley, C., & Schmahmann, J. (2009). Functional topography in the human cerebellum: A meta-analysis of neuroimaging studies. *NeuroImage*, *44*(2), 489–501. <https://doi.org/10.1016/j.neuroimage.2008.08.039>
- Stoodley, C. J., D’Mello, A. M., Ellegood, J., Jakkamsetti, V., Liu, P., Nebel, M. B., . . . Tsai, P. T. (2017). Altered cerebellar connectivity in autism and cerebellar-mediated rescue of autism-related behaviors in mice. *Nature Neuroscience*, *20*(12), 1744–1751. <https://doi.org/10.1038/s41593-017-0004-1>
- Strange, B. A., Witter, M. P., Lein, E. S., & Moser, E. I. (2014). Functional organization of the hippocampal longitudinal axis. *Nature Reviews Neuroscience*, *15*(10), 655–669. <https://doi.org/10.1038/nrn3785>
- Strick, P. L., Dum, R. P., & Fiez, J. A. (2009). Cerebellum and Nonmotor Function. *Annual Review of Neuroscience*, *32*(1), 413–434. <https://doi.org/10.1146/annurev.neuro.31.060407.125606>
- Sugihara, I. (2017). Crus I in the Rodent Cerebellum: Its Homology to Crus I and II in the Primate Cerebellum and Its Anatomical Uniqueness Among Neighboring Lobules. *The Cerebellum*, *17*(1), 49–55. <https://doi.org/10.1007/s12311-017-0911-4>
- Sugihara, I., Fujita, H., Na, J., Quy, P. N., Li, B., & Ikeda, D. (2009). Projection of reconstructed single purkinje cell axons in relation to the cortical and nuclear aldolase C compartments of the rat cerebellum. *The Journal of Comparative Neurology*, *512*(2), 282–304. <https://doi.org/10.1002/cne.21889>
- Sugihara, I., & Quy, P. N. (2006). Identification of aldolase C compartments in the mouse cerebellar cortex by olivocerebellar labeling. *The Journal of Comparative Neurology*, *500*(6), 1076–1092. <https://doi.org/10.1002/cne.21219>
- Sugihara, I., & Shinoda, Y. (2004). Molecular, Topographic, and Functional Organization of the Cerebellar Cortex: A Study with Combined Aldolase C and Olivocerebellar Labeling. *Journal of Neuroscience*, *24*(40), 8771–8785. <https://doi.org/10.1523/jneurosci.1961-04.2004>
- Sugihara, I., & Shinoda, Y. (2007). Molecular, Topographic, and Functional Organization of the Cerebellar Nuclei: Analysis by Three-Dimensional Mapping of the Olivonuclear Projection and Aldolase C Labeling. *Journal of Neuroscience*, *27*(36), 9696–9710. <https://doi.org/10.1523/jneurosci.1579-07.2007>
- Sugihara, I., Wu, H., & Shinoda, Y. (2001). The Entire Trajectories of Single Olivocerebellar Axons in the Cerebellar Cortex and their Contribution to Cerebellar Compartmentalization. *The Journal of Neuroscience*, *21*(19), 7715–7723. <https://doi.org/10.1523/jneurosci.21-19-07715.2001>
- Sultan, F., & Bower, J. M. (1998). Quantitative Golgi study of the rat cerebellar molecular layer interneurons using principal component analysis. *Journal of Comparative Neurology*, *393*(3).
- Suzuki, L., Coulon, P., Sabel-Goedknegt, E. H., & Ruigrok, T. J. H. (2012). Organization of Cerebral Projections to Identified Cerebellar Zones in the Posterior Cerebellum of the Rat. *Journal of Neuroscience*, *32*(32), 10854–10869. <https://doi.org/10.1523/jneurosci.0857-12.2012>
- Swanson, L. W., & Cowan, W. M. (1979). The connections of the septal region in the rat. *The Journal of Comparative Neurology*, *186*(4), 621–655. <https://doi.org/10.1002/cne.901860408>
- Szapiro, G., & Barbour, B. (2007). Multiple climbing fibers signal to molecular layer interneurons exclusively via glutamate spillover. *Nature Neuroscience*, *10*(6), 735–742. <https://doi.org/10.1038/nn1907>

- T -

- Taube, J. (1995). Head direction cells recorded in the anterior thalamic nuclei of freely moving rats. *The Journal of Neuroscience*, 15(1), 70–86. <https://doi.org/10.1523/jneurosci.15-01-00070.1995>
- Taube, J., Muller, R., & Ranck, J. (1990). Head-direction cells recorded from the postsubiculum in freely moving rats. II. Effects of environmental manipulations. *The Journal of Neuroscience*, 10(2), 436–447. <https://doi.org/10.1523/jneurosci.10-02-00436.1990>
- Taube, J. S. (2007). The Head Direction Signal: Origins and Sensory-Motor Integration. *Annual Review of Neuroscience*, 30(1), 181–207. <https://doi.org/10.1146/annurev.neuro.29.051605.112854>
- Teune, T., Van der Burg, J., Van der Moer, J., Voogd, J., & Ruigrok, T. (2000). Topography of cerebellar nuclear projections to the brain stem in the rat. *Progress in Brain Research*, , 141–172. [https://doi.org/10.1016/s0079-6123\(00\)24014-4](https://doi.org/10.1016/s0079-6123(00)24014-4)
- Teune, T. M., Van der Burg, J., De Zeeuw, C. I., Voogd, J., & Ruigrok, T. J. H. (1998). Single Purkinje cell can innervate multiple classes of projection neurons in the cerebellar nuclei of the rat: A light microscopic and ultrastructural triple-tracer study in the rat. *Journal of Comparative Neurology*, 392(2).
- Thompson, L., & Best, P. (1990). Long-term stability of the place-field activity of single units recorded from the dorsal hippocampus of freely behaving rats. *Brain Research*, 509(2), 299–308. [https://doi.org/10.1016/0006-8993\(90\)90555-p](https://doi.org/10.1016/0006-8993(90)90555-p)
- Tolbert, D., Bantli, H., & Bloedel, J. (1976). Anatomical and physiological evidence for a cerebellar nucleo-cortical projection in the cat. *Neuroscience*, 1(3), 205–217. [https://doi.org/10.1016/0306-4522\(76\)90078-6](https://doi.org/10.1016/0306-4522(76)90078-6)
- Trott, J. R., Apps, R., & Armstrong, D. M. (1998a). Zonal organization of cortico-nuclear and nucleo-cortical projections of the paramedian lobule of the cat cerebellum. 1. The C 1 zone. *Experimental Brain Research*, 118(3), 298–315. <https://doi.org/10.1007/s002210050285>
- Trott, J. R., Apps, R., & Armstrong, D. M. (1998b). Zonal organization of cortico-nuclear and nucleo-cortical projections of the paramedian lobule of the cat cerebellum. 2. The C 2 zone. *Experimental Brain Research*, 118(3), 316–330. <https://doi.org/10.1007/s002210050286>
- U -
- Ugolini, G. (2008). Use of rabies virus as a transneuronal tracer of neuronal connections: Implications for the understanding of rabies pathogenesis. *Developments in biologicals*, 131, 493–506.
- Ugolini, G. (2010). Advances in viral transneuronal tracing. *Journal of Neuroscience Methods*, 194(1), 2–20. <https://doi.org/10.1016/j.jneumeth.2009.12.001>
- Uhlhaas, P. J., & Singer, W. (2010). Abnormal neural oscillations and synchrony in schizophrenia. *Nature Reviews Neuroscience*, 11(2), 100–113. <https://doi.org/10.1038/nrn2774>
- Uusisaari, M., & Knöpfel, T. (2009). GlyT2+ Neurons in the Lateral Cerebellar Nucleus. *The Cerebellum*, 9(1), 42–55. <https://doi.org/10.1007/s12311-009-0137-1>

Uusisaari, M., & Knöpfel, T. (2010). Functional Classification of Neurons in the Mouse Lateral Cerebellar Nuclei. *The Cerebellum*, 10(4), 637–646. <https://doi.org/10.1007/s12311-010-0240-3>

Uusisaari, M. Y., & Knöpfel, T. (2012). Diversity of Neuronal Elements and Circuitry in the Cerebellar Nuclei. *The Cerebellum*, 11(2), 420–421. <https://doi.org/10.1007/s12311-011-0350-6>

- V -

Valera, A. M., Binda, F., Pawlowski, S. A., Dupont, J., Casella, J., Rothstein, J. D., . . . Isope, P. (2016). Stereotyped spatial patterns of functional synaptic connectivity in the cerebellar cortex. *eLife*, 5. <https://doi.org/10.7554/elife.09862>

Voogd, J. (1969). in *Neurobiology of Cerebellar Evolution and Development* (Llinás R., ed.). *AMA-ERF Institute for Biomedical Research*, , 493–541.

Voogd, J. (2003). The human cerebellum. *Journal of Chemical Neuroanatomy*, 26(4), 243–252. <https://doi.org/10.1016/j.jchemneu.2003.07.005>

Voogd, J. (2014). What we do not know about cerebellar systems neuroscience. *Frontiers in Systems Neuroscience*, 8. <https://doi.org/10.3389/fnsys.2014.00227>

Voogd, J., & Barmack, N. H. (2006). Oculomotor cerebellum. *Progress in Brain Research*, , 231–268. [https://doi.org/10.1016/s0079-6123\(05\)51008-2](https://doi.org/10.1016/s0079-6123(05)51008-2)

Voogd, J., & Bigaré, F. (1980). Topographical distribution of olivary and cortico nuclear fibers in th cerebellum: a review.. In: *J. Courville, C. Montigni, Y. Lamarre, editors. The inferior olvary nucleus anatomy and physiology. New York: Raven*, , 207–234.

Voogd, J., Pardoe, J., Ruigrok, T. J. H., & Apps, R. (2003). The Distribution of Climbing and Mossy Fiber Collateral Branches from the Copula Pyramidis and the Paramedian Lobule: Congruence of Climbing Fiber Cortical Zones and the Pattern of Zebrin Banding within the Rat Cerebellum. *The Journal of Neuroscience*, 23(11), 4645–4656. <https://doi.org/10.1523/jneurosci.23-11-04645.2003>

Voogd, J., & Ruigrok, T. J. H. (2004). The organization of the corticonuclear and olivocerebellar climbing fiber projections to the rat cerebellar vermis: The congruence of projection zones and the zebrin pattern. *Journal of Neurocytology*, 33(1), 5–21. <https://doi.org/10.1023/b:neur.0000029645.72074.2b>

- W -

Wagner, M. J., Kim, T. H., Kadmon, J., Nguyen, N. D., Ganguli, S., Schnitzer, M. J., & Luo, L. (2019). Shared Cortex-Cerebellum Dynamics in the Execution and Learning of a Motor Task. *Cell*, 177(3), 669–682. <https://doi.org/10.1016/j.cell.2019.02.019>

Wagner, M. J., Kim, T. H., Savall, J., Schnitzer, M. J., & Luo, L. (2017). Cerebellar granule cells encode the expectation of reward. *Nature*, 544(7648), 96–100. <https://doi.org/10.1038/nature21726>

Walter, J. T., Alviña, K., Womack, M. D., Chevez, C., & Khodakhah, K. (2006). Decreases in the precision of Purkinje cell pacemaking cause cerebellar dysfunction and ataxia. *Nature Neuroscience*, 9(3), 389–397. <https://doi.org/10.1038/nn1648>

- Walter, J. T., Dizon, M., & Khodakhah, K. (2009). The Functional Equivalence of Ascending and Parallel Fiber Inputs in Cerebellar Computation. *Journal of Neuroscience*, 29(26), 8462–8473. <https://doi.org/10.1523/jneurosci.5718-08.2009>
- Wang, D. V., & Ikemoto, S. (2016). Coordinated Interaction between Hippocampal Sharp-Wave Ripples and Anterior Cingulate Unit Activity. *Journal of Neuroscience*, 36(41), 10663–10672. <https://doi.org/10.1523/jneurosci.1042-16.2016>
- Watson, T. C., Becker, N., Apps, R., & Jones, M. W. (2014). Back to front: cerebellar connections and interactions with the prefrontal cortex. *Frontiers in Systems Neuroscience*, 8. <https://doi.org/10.3389/fnsys.2014.00004>
- Watson, T. C., Jones, M. W., & Apps, R. (2009). Electrophysiological mapping of novel prefrontal - cerebellar pathways. *Frontiers in Integrative Neuroscience*, 3. <https://doi.org/10.3389/neuro.07.018.2009>
- Welsh, J. P., Lang, E. J., Sugihara, I., & Llinás, R. (1995). Dynamic organization of motor control within the olivocerebellar system. *Nature*, 374(6521), 453–457. <https://doi.org/10.1038/374453a0>
- Whiteside, J. A., & Snider, R. S. (1953). RELATION OF CEREBELLUM TO UPPER BRAIN STEM. *Journal of Neurophysiology*, 16(4), 397–413. <https://doi.org/10.1152/jn.1953.16.4.397>
- Whiting, B., & Barton, R. (2003). The evolution of the cortico-cerebellar complex in primates: anatomical connections predict patterns of correlated evolution. *Journal of Human Evolution*, 44(1), 3–10. [https://doi.org/10.1016/s0047-2484\(02\)00162-8](https://doi.org/10.1016/s0047-2484(02)00162-8)
- Wickersham, I. R., Finke, S., Conzelmann, K., & Callaway, E. M. (2006). Retrograde neuronal tracing with a deletion-mutant rabies virus. *Nature Methods*, 4(1), 47–49. <https://doi.org/10.1038/nmeth999>
- Wiesendanger, R., & Wiesendanger, M. (1982a). The corticopontine system in the rat. I. Mapping of corticopontine neurons. *The Journal of Comparative Neurology*, 208(3), 215–226. <https://doi.org/10.1002/cne.902080302>
- Wiesendanger, R., & Wiesendanger, M. (1982b). The corticopontine system in the rat. II. The projection pattern. *The Journal of Comparative Neurology*, 208(3), 227–238. <https://doi.org/10.1002/cne.902080303>
- Wikgren, J., Nokia, M., & Penttonen, M. (2010). Hippocampo–cerebellar theta band phase synchrony in rabbits. *Neuroscience*, 165(4), 1538–1545. <https://doi.org/10.1016/j.neuroscience.2009.11.044>
- Witter, L., Rudolph, S., Pressler, R. T., Lahlaf, S. I., & Regehr, W. G. (2016). Purkinje Cell Collaterals Enable Output Signals from the Cerebellar Cortex to Feed Back to Purkinje Cells and Interneurons. *Neuron*, 91(2), 312–319. <https://doi.org/10.1016/j.neuron.2016.05.037>
- Witter, M. P., Canto, C. B., Couey, J. J., Koganezawa, N., & O'Reilly, K. C. (2014). Architecture of spatial circuits in the hippocampal region. *Philosophical Transactions of the Royal Society B: Biological Sciences*, 369(1635), 20120515. <https://doi.org/10.1098/rstb.2012.0515>
- Wolpert, D., & Kawato, M. (1998). Multiple paired forward and inverse models for motor control. *Neural Networks*, 11(7-8), 1317–1329. [https://doi.org/10.1016/s0893-6080\(98\)00066-5](https://doi.org/10.1016/s0893-6080(98)00066-5)

Wu, H. S., Sugihara, I., & Shinoda, Y. (1999). Projection patterns of single mossy fibers originating from the lateral reticular nucleus in the rat cerebellar cortex and nuclei. *Journal of Comparative Neurology*, 411(1).

Wulff, P., Schonewille, M., Renzi, M., Viltono, L., Sassoè-Pognetto, M., Badura, A., . . . De Zeeuw, C. I. (2009). Synaptic inhibition of Purkinje cells mediates consolidation of vestibulo-cerebellar motor learning. *Nature Neuroscience*, 12(8), 1042–1049. <https://doi.org/10.1038/nn.2348>

- X -

Xiao, J., Cerminara, N. L., Kotsurovskyy, Y., Aoki, H., Burroughs, A., Wise, A. K., . . . Lang, E. J. (2014). Systematic Regional Variations in Purkinje Cell Spiking Patterns. *PLoS ONE*, 9(8:e105633). <https://doi.org/10.1371/journal.pone.0105633>

Xu, C., Krabbe, S., Gründemann, J., Botta, P., Fadok, J. P., Osakada, F., . . . Lüthi, A. (2016). Distinct Hippocampal Pathways Mediate Dissociable Roles of Context in Memory Retrieval. *Cell*, 167(4), 961–972. <https://doi.org/10.1016/j.cell.2016.09.051>

- Y -

Yaginuma, H., & Matsushita, M. (1986). Spinocerebellar projection fields in the horizontal plane of lobules of the cerebellar anterior lobe in the cat: an anterograde wheat germ agglutinin-horseradish peroxidase study. *Brain Research*, 365(2), 345–349. [https://doi.org/10.1016/0006-8993\(86\)91647-1](https://doi.org/10.1016/0006-8993(86)91647-1)

Yamaguchi, K., Itohara, S., & Ito, M. (2016). Reassessment of long-term depression in cerebellar Purkinje cells in mice carrying mutated GluA2 C terminus. *Proceedings of the National Academy of Sciences*, 113(36), 10192–10197. <https://doi.org/10.1073/pnas.1609957113>

Yamazaki, T., & Lennon, W. (2019). Revisiting a theory of cerebellar cortex. *Neuroscience Research*, . <https://doi.org/10.1016/j.neures.2019.03.001>

Yoon, T., Okada, J., Jung, M. W., & Kim, J. J. (2008). Prefrontal cortex and hippocampus subserve different components of working memory in rats. *Learning & Memory*, 15(3), 97–105. <https://doi.org/10.1101/lm.850808>

- Z -

Zeeuw, C. I., & Berrebi, A. S. (1995). Postsynaptic Targets of Purkinje Cell Terminals in the Cerebellar and Vestibular Nuclei of the Rat. *European Journal of Neuroscience*, 7(11), 2322–2333. <https://doi.org/10.1111/j.1460-9568.1995.tb00653.x>

Zhang, C., Zhou, P., & Yuan, T. (2016). The cholinergic system in the cerebellum: from structure to function. *Reviews in the Neurosciences*, 27(8). <https://doi.org/10.1515/revneuro-2016-0008>

Zhang, S., Schönfeld, F., Wiskott, L., & Manahan-Vaughan, D. (2014). Spatial representations of place cells in darkness are supported by path integration and border information. *Frontiers in Behavioral Neuroscience*, 8. <https://doi.org/10.3389/fnbeh.2014.00222>

Zhou, H., Lin, Z., Voges, K., Ju, C., Gao, Z., Bosman, L. W., . . . Schonewille, M. (2014). Cerebellar modules operate at different frequencies. *eLife*, 3. <https://doi.org/10.7554/elife.02536>



# **APPENDIX**



**INDEX OF FIGURES:**



Figure 1. Cajal’s illustrations of his studies to unravel the circuitry of the cerebellum .....	15
Figure 2. Fundamental organization of the cerebellum .....	20
Figure 3. Fundamental architecture of the cerebellar circuit .....	23
Figure 4. Purkinje cell morphology and connectivity .....	25
Figure 5. Granule cell morphology and connectivity .....	27
Figure 6. Topographic organization of the climbing and mossy fibres .....	29
Figure 7. Partial overlap between mossy fibres and climbing fibres in the cerebellar cortex .....	30
Figure 8. Receptive fields in the cerebellum .....	31
Figure 9. Overlap of mossy and climbing fibres receptive fields .....	32
Figure 10. Loops with the deep cerebellar nuclei .....	34
Figure 11. First experiments leading to the beam hypothesis .....	36
Figure 12. Marr-Albus-Ito model .....	38
Figure 13. Hotspots of distal granule cell connectivity .....	39
Figure 14. Simple and complex spikes patterns .....	41
Figure 15. Read-out of patterns in cerebellar nuclei .....	43
Figure 16. Oscillations in the cerebellar circuits .....	45
Figure 17. Synergistic plasticity in the cerebellar circuit .....	46
Figure 18. Cerebral inputs to the cerebellum .....	51
Figure 19. Cerebellar projections to the cerebrum .....	54
Figure 20. Cerebro-cerebellar loops .....	55
Figure 21. Recent methodological approaches for demonstrating the functional relevance of the anatomical cerebello-cerebral pathways .....	57
Figure 22. The Cerebellar Cognitive Affective Syndrome (CCAS) .....	59
Figure 23. Fundamental anatomy and connectivity of the hippocampal formation .....	67
Figure 24. Septo-temporal anatomical-functional topography .....	69

Figure 25. Main spatial coding cell populations in the hippocampal formation ..... 71

Figure 26. Distributed spatial coding network in the brain ..... 72

Figure 27. Closed-loop optogenetic cerebellar stimulation inhibits spontaneous hippocampal seizures.....75

Figure 28. Hippocampal-dependent navigation impairments in two cerebellar mutant mice with plasticity deficits ..... 77

**RESUMÉ ÉTENDU EN FRANÇAIS:**



Le cervelet est bien connu dans la communauté scientifique par son implication dans le domaine moteur avec des rôles importants dans la coordination et le contrôle précis des mouvements volontaires ainsi que dans l'apprentissage et l'adaptation moteurs. Cependant, le cervelet est interconnecté de manière abondante et bidirectionnelle avec la majeure partie du cortex cérébral, y compris les zones motrices et sensorielles principales, mais également les zones associatives élevées, telles que le cortex préfrontal ou pariétal (voir Strick et al., 2009). Grâce à cette connectivité, le cervelet est engagé dans de multiples réseaux anatomiques et fonctionnels avec le cerveau et participe à une pléthore de fonctions motrices et cognitives (voir Schmahmann, 2019).

L'équipe de Laure Rondi Reig a récemment mis en évidence l'implication du cervelet dans la cognition spatiale et la navigation spatiale. De même, ces études suggèrent fortement que le cervelet interagit avec l'hippocampe dans un réseau fonctionnel. Chez l'homme, des études d'imagerie fonctionnelle réalisées chez des individus naviguant dans un environnement virtuel ont montré une co-activation du cervelet et de l'hippocampe lorsqu'ils utilisaient une stratégie de navigation basée sur la séquence (Igloi et al., 2015). Chez les souris également, la navigation par séquence dirigée vers un but a révélé des réseaux étendus dominés par une activité hautement corrélée entre l'hippocampe et le cervelet (Babayán et al., 2017). Dans un modèle de souris transgéniques caractérisé par le manque de plasticité à long terme spécifiquement dans les synapses entre les fibres parallèles et les cellules de Purkinje dans le cervelet, il a été constaté que les mutants présentaient un déficit dans l'optimisation des trajectoires pendant la navigation dirigée vers un but dans une tâche dépendant de l'hippocampe quand ils devaient s'appuyer sur la mémoire spatiale mais pas quand ils pouvaient utiliser des points de repère externes afin de guider leur cheminement (Burguière et al., 2005). De plus, dans une autre étude utilisant le même modèle de souris, une perturbation globale du code de position de l'hippocampe a été observée lorsque les animaux devaient se fier exclusivement aux informations d'auto-mouvement, alors qu'ils étaient inchangés lorsqu'ils pouvaient utiliser des points de repère externes pour s'orienter (Rochefort et al., 2011). Également, une étude récente réalisée dans une lignée mutante différente, dépourvue de formes synaptiques et intrinsèques de potentialisation à long terme dans les cellules de Purkinje, a révélé aussi des altérations du code de lieu de l'hippocampe avec une population très instable de cellules de lieu qui présente une rotation cohérente de la carte du lieu dès la re-exposition à un environnement familier en présence de points de repère externes, mais pas pendant la navigation par auto-mouvement (Lefort et al., 2019). En résumé, un grand nombre de preuves suggère que le cervelet et l'hippocampe interagissent en tant qu'éléments d'un réseau fonctionnel impliqués dans l'utilisation et la stabilisation du code de lieu de l'hippocampe au cours de la navigation spatiale.

Cependant, malgré la robustesse de ces évidences, nous ne disposons pas à ce jour d'informations sur le substrat anatomique de cette interaction, ni sur les mécanismes physiologiques qui la sous-tendent. Ces informations sont essentielles pour bien comprendre le rôle du cervelet dans ces fonctions et ont été au centre de ma thèse. En particulier, j'ai tenté de répondre à quatre questions principales concernant la

connectivité et l'interaction présumées cérébello-hippocampe: 1) est-ce qu'il y a des voies courtes (di- ou tri-synaptiques) reliant le cervelet à l'hippocampe?, 2) si oui, quelles zones spécifiques dans le cervelet sont impliqués dans de telles projections?, 3) quels sont les mécanismes physiologiques qui soutiennent l'interaction fonctionnelle entre les deux régions? et 4) quelle est la dynamique d'une telle interaction en fonction de l'état comportemental? Afin de répondre à ces questions, nous avons utilisé une combinaison d'approches techniques comprenant des études anatomiques de traçages trans-synaptiques rétrogrades avec le virus de la rage et des enregistrements électrophysiologiques extracellulaires simultanés dans le cervelet et l'hippocampe des souris engagé dans plusieurs états comportementaux.

En ce qui concerne la connectivité anatomique, en injectant le virus de la rage dans l'hippocampe dorsal et en testant plusieurs périodes de survie pouvant être associées aux relais ultérieurs de la voie, nous avons révélé l'apparition de clusters de cellules de Purkinje restreintes de manière topographique dans le cortex cérébelleux qui projettent à travers des voies parallèles di- et/ou tri-synaptiques vers l'hippocampe: un cluster paravermique et un autre hémisphérique dans le Crus I, un cluster dans le vermal lobule VI et les paraflocculus dorsal et ventral. Ces populations étaient organisées en bandes parasagittales longitudinales et projettent à travers des sous-régions spécifiques de noyaux cérébelleux profonds suggérant l'implication de zones ou de modules cérébelleux spécifiques. L'organisation topographique du cervelet dans une grille de lobules transversaux et de modules sagittaux a des implications fonctionnelles importantes car elle est liée au type spécifique d'informations intégrées et traitées par le circuit cérébelleux et, par conséquent, nous avons voulu identifier les modules impliqués dans les projections cérébelleuses à l'hippocampe. À cette fin, nous avons combiné les injections du virus de la rage avec le patron d'expression de la molécule Zebrin II, connue pour être exprimée en bandes parasagittales, qui peuvent servir de points de repère pour les différents modules cérébelleux (Sugihara et Nguyen Quy, 2007). En utilisant cette stratégie, nous avons identifié le module A pour le cluster dans le lobule VI et les modules C2 et D2 pour les clusters paravermique et hémisphérique dans le Crus I, respectivement. Le module A du lobule VI fait partie du cervelet oculomoteur. Il reçoit des informations sensorielles multimodales du collicule supérieur et des noyaux vestibulaires et se projette à travers le noyau fastigial caudal vers le collicule supérieur, la substance grise périaqueducale, les noyaux de raphe ou la formation réticulaire mésencéphalique (Voogd et Barmack, 2006). Il est impliqué dans le contrôle des mouvements saccadés oculaires et de la tête (voir Cerminara et Apps, 2010) et peut être impliqué dans le guidage des mouvements dans un cadre de référence centré sur la tête, une information qui peut être particulièrement utile dans le processus d'auto-localisation dans l'environnement ainsi que la construction et la maintenance de la carte spatiale de l'hippocampe (voir Rochefort et al., 2013 et Rondi-Reig et al., 2014). Le module C2 au niveau de Crus I est principalement interconnecté de manière bidirectionnelle avec le système visuo-moteur, comprenant à la fois les zones motrices principales et les zones associatives élevées telles que le cortex préfrontal et pariétal postérieur (Voogd, 2014). Le rôle fonctionnel de cette zone a été lié à l'adaptation visuo-spatiale et au guidage visuel et

proprioceptif des mouvements (Prevosto et al., 2009) qui peuvent être importants pour les mécanismes d'intégration de chemins. Enfin, il a été proposé que le Crus I hémisphérique chez l'homme participe à une multitude de fonctions non motrices, notamment la mémoire de travail, la génération de langage, l'intégration visuomotrice ou le traitement spatial (voir Schmahmann, 2019). Chez les primates, il est fortement interconnecté avec le cortex cérébral, y compris les zones associatives élevées comme le cortex préfrontal (Kelly et Strick, 2003), ainsi que les zones motrices primaires, prémotrices ou pariétales postérieures (voir Voogd, 2014). Il reçoit également des informations visuelles (Edge et al., 2003) et somatosensorielles (Mihailoff et al., 1981). En effet, il a été récemment montré chez les rongeurs que les informations sensorielles et motrices des vibrisses convergent dans la même zone du module D2 dans le Crus I (Proville et al., 2014). Ce module se projette sur le noyau denté et établit des boucles avec la plupart de leurs zones afférentes corticales par le biais de projections thalamiques (voir Strick et al., 2009). Dans un rapport récent chez la souris, il a été démontré que l'activité des cellules de Purkinje dans le Crus I représentant la phase instantanée de l'hippocampe dorsal et du cortex préfrontal, ainsi que leurs différences de phase (McAfee et al., 2019). Cette découverte est particulièrement pertinente, car le cortex préfrontal et l'hippocampe forment des réseaux fonctionnels impliqués dans la navigation spatiale (Jones et Wilson, 2005) et en particulier lors de la navigation dirigée vers un but (Igloi et al. 2015; Babayan et al., 2017).

Guidés par ces découvertes anatomiques, nous avons implanté chez des souris des électrodes bipolaires bilatérales dans l'hippocampe et dans trois régions du cervelet: le lobule VI, le Crus I et le lobule II / III (une région contrôle non anatomiquement connectée). Nous avons simultanément enregistré l'activité oscillatoire extracellulaire reflétée dans les potentiels de champ locaux d'animaux engagés dans différents paradigmes comportementaux: exploration d'un environnement familier (leur home-cages), comportement orienté vers un but dans une track linéaire et à travers les états de sommeil. Nous avons mesuré les niveaux de cohérence ou de synchronie des oscillations de ces deux structures en tant que proxy pour l'interaction fonctionnelle. Ceci est basé sur l'hypothèse de la communication neuronale par cohérence neuronale (Fries, 2005) qui est fondée sur la corrélation entre les variations fluctuantes de l'excitabilité des populations neuronales locales et le profil oscillant de leurs potentiels de champ locaux. Ainsi, ces oscillations affectent à la fois la sortie des populations neuronales et également la sensibilité à une entrée donnée et, par conséquent, la coordination de l'activité oscillatoire entre deux structures communicantes permet une transmission efficace de l'information. En outre, la modulation de cette cohérence en fonction du contexte comportemental où des exigences de la tâche peut permettre un routage flexible des informations sur des réseaux (Akam et Kullmann, 2010). À travers les différents paradigmes comportementaux, nous avons systématiquement trouvé une cohérence cérébello-hippocampique limitée au rythme thêta (6-12 Hz). De plus, cette cohérence était modulée dynamiquement d'une manière spécifique pour chaque sous-région en fonction du contexte comportemental, ce qui suggère qu'elle peut représenter un mécanisme par lequel les

deux structures sont fonctionnellement engagées à la demande. Il est intéressant de noter que la rythmicité thêta a été proposée comme mécanisme fondamental facilitant le transfert d'informations entre les régions du cerveau lors du traitement d'informations sensorielles (Buzsaki, 2002, 2005). Des rapports antérieurs sur la cohérence thêta cérébello-hippocampique ont été découverts lors du conditionnement du clignement des yeux chez le lapin (Hoffmann et Berry, 2009; Wikgren et al., 2010).

Pendant le mouvement actif dans leurs home-cages, la cohérence entre l'hippocampe et le lobule VI était significativement plus forte que celle avec la région contrôle lobule II/III. Le niveau de cohérence lobule VI-hippocampe était maintenu stable entre les différents paradigmes comportementaux, ce qui concorde avec un rôle dans le traitement visuel et la génération de comportements d'orientation requis indépendamment du comportement spécifique. Par ailleurs, le niveau de cohérence avec le Crus I était très dynamique et montrait une augmentation significative lors de l'acquisition d'un comportement dirigée vers un but dans le track linéaire, où les animaux devaient courir entre deux emplacements cibles afin de maximiser le nombre de récompenses reçues dans une session. En effet, au début de l'entraînement, lorsque les animaux ont présenté un comportement exploratoire, la cohérence est restée à des niveaux similaires à ceux observés lors des enregistrements dans leurs home-cages. Cependant, la cohérence a augmenté parallèlement à l'amélioration des performances dans la tâche, atteignant des niveaux nettement supérieurs à ceux du contrôle à la fin de l'entraînement, lorsque les animaux manifestaient un comportement clairement orienté vers un but. De plus, cette cohérence a été maintenue lors de l'approche du but sur toute la trajectoire linéaire et n'a pas été corrélée avec des paramètres moteurs tels que la vitesse instantanée suggérant que le circuit du Crus I-hippocampe est sélectivement engagé lorsque les animaux utilisent une stratégie de navigation dirigée vers un but et surveille la position de l'animal par rapport à l'emplacement de l'objectif.

Enfin, pendant le sommeil, nous avons identifié une activité oscillatoire ultra-lente (<1Hz) caractéristique des époques REM, observée dans tous les sites cérébelleux échantillonnés. Ces oscillations ont été accompagnées de l'apparition d'événements phasiques qui se sont concentrés préférentiellement au sommet des ondes ultra-lentes et qui ont été associés à une accélération du rythme thêta de l'hippocampe. Ces caractéristiques suggèrent que les événements phasiques que nous avons observés sont des ondes pontiques propagées (Marks et al., 1980; Karashima et al., 2007). Il est intéressant de noter que la cohérence thêta entre Crus I et l'hippocampe était également présente pendant le sommeil paradoxal et était coordonnée par la phase des oscillations ultra-lentes. Il est maximal au sommet des vagues, lorsque les ondes pontiques putatives sont concentrées et lorsque le thêta de l'hippocampe présente une fréquence plus élevée. Les ondes pontiques étaient auparavant associées aux processus de consolidation de la mémoire dans l'hippocampe (Datta, 2000; Datta et al., 2004; Datta et O'Malley, 2013) et leur coordination par les oscillations ultra-lentes cérébelleuses accompagnées d'une cohérence thêta accrue suggère que cela peut représenter un mécanisme important pour la plasticité liée au sommeil. De plus, pendant le sommeil non paradoxal, nous avons observé les potentiels évoqués dans le cortex cérébelleux après la détection de

sharp-wave ripples dans l'hippocampe, ce qui pourrait refléter une réponse de la population à l'activation synchrone des sorties de l'hippocampe atteignant le cervelet, suggérant que la connectivité entre les deux structures est bidirectionnel et peut être organisé en boucle.

En résumé, les résultats obtenus au cours de ma thèse confirmaient l'existence de voies di- et tri-synaptiques discrètes et parallèles entre des zones topographiquement restreintes du cortex cérébelleux et l'hippocampe dorsal chez la souris. De plus, nous avons identifié le couplage oscillatoire thêta comme un mécanisme potentiel d'interaction fonctionnelle dans le réseau cérébello-hippocampique, qui peut être particulièrement actif lors de la navigation orientée vers un but. Enfin, la présence de cohérence cérébello-hippocampique pendant le sommeil paradoxal suggère que le réseau est modulé par une plasticité synaptique dépendante du sommeil qui semble être organisée par un rythme ultra-lent cérébelleux.

